Imperial College London

An integrated experimental and modelling approach for the study of apoptosis in GS-NS0 cell cultures

Chonlatep Usaku

Submitted to Department of Chemical Engineering in fulfilment of the requirements for the degree of Doctor of Philosophy

*The copyright of this thesis rests with the author and is made available under a Creative Commons Attribution Non-Commercial No Derivatives licence. Researchers are free to copy, distribute or transmit the thesis on the condition that they attribute it, that they do not use it for commercial purposes and that they do not alter, transform or build upon it. For any reuse or redistribution, researchers must make clear to others the licence terms of this work.

Abstract

Mammalian cell cultures are nowadays adopted as industrial platforms for monoclonal antibody (mAb) manufacture. Although improving product quality and expression stability becomes predominant these days, enhancement in mAb production still remains one of the greatest challenges facing the industrial biotechnology community. One of reasons behind this is the synthesis of mAb is restricted by the decline phase occurring in the mammalian cell cultures as a result of cell death. Prolongation of culture viability via suppression of cell death appears as a potential strategy to improve mAb production and productivity. Understanding of cell death in the mammalian cell cultures is, therefore, crucial to the improvement of the strategy toward mAb production and productivity enhancement.

Apoptosis, or programmed cell death, is found to be the major cause of culture viability loss in the mammalian cell cultures. It is a highly-organised physiological process of cell death that can be triggered through activation of the genetic programme underlying a signal cascade that governs particular morphological and physiological changes in response to extracellular and intracellular stimuli. In order to devise strategies to optimise degrees of apoptosis in the mammalian cell cultures, understanding of apoptosis is inevitable. However, to establish the understanding of apoptosis is an extremely challenging task given the complexity arising from the dynamic nature of apoptosis and its association with internal and external milieu, including other cellular processes and environmental conditions.

This thesis presents a combined experimental and modelling approach for a study of apoptosis in GS-NS0 cell cultures, aiming to identify relevant metabolic stresses, evaluate their impact on apoptosis induction, and investigate kinetics of apoptosis in response to the identified stresses. The novelty of this study is a systemic view of apoptosis where apoptosis is studied

in accordance with dynamic changes in culturing conditions, as well as cell proliferation and metabolic activities. Batch culture experiments of GS-NS0 cell line demonstrate interplay between apoptosis and other cellular processes, including cell cycle progression and metabolism. In addition, the batch cultures allow evaluating impact of metabolic stresses and culture conditions on induction of apoptosis. Fed-batch culture experiments help validate links between apoptosis and metabolic stresses as suggested based on the batch cultures, and also shed some light on feeding strategies for a delay in apoptosis induction. The first-principles mathematical model for apoptosis in the GS-NS0 cell cultures demonstrates a good reproduction of the experimental data. Model analysis reveals model characteristics through global parameter sensitivities and helps guide further model modification toward development of a predictive apoptosis mathematical model.

Declaration of Originality

I hereby declare that the work presented in this thesis is genuine. It was originally conducted by the author, unless explicitly acknowledged. To the best of my knowledge, the thesis has not been submitted and/or accepted for the award of a degree in any other Institution or University. The thesis contains no material previously published by other persons, unless it is acknowledged in accordance with the standard referencing practices.

Acknowledgements

This study was conducted during the years of 2010 to 2014 at Biological System Engineering Laboratory (BSEL), Department of Chemical Engineering, Imperial College London.

First of all, I am deeply grateful to Royal Thai Government for financial support during my studies (2009-2014). Without this, I would not have had an opportunity to study abroad, where experiences I have gained are far beyond monetary worth.

I would like to express my warmest gratitude to Professor Athanasios Mantalaris, my main supervisor, for his patient guidance and constructive critiques of this work. Thanks to academic and financial support he has provided, I have earned so much experiences from collaborative meetings, international conferences and publication. Without him, I would not have been this far and this thesis would hardly have been completed. I would also like to show my appreciation to Professor Stratos Pistikopoulos, my co-supervisor, for his advice in mathematical modelling and his help in preparation for publication.

I would like to give very special thanks to Dr. D. G. García Münzer for his great collaboration and companionship throughout my PhD years. Thanks to his expertise in cell cycle, my research on apoptosis is complemented. I would also like to extend my thanks to Dr. Alexandros Kyparissidis for his help in cell cultures and model analysis during the first years of my PhD study.

This thesis would hardly have been possible unless I have gained great support from my colleagues; Dr. Eirini Velliou for her advice in preparation for conference abstracts and thesis writing-up, and Dr. Spyridon E Vernardis, Mr. Mark Allenby and Mr. Naveed Tariq for their help in proofreading and editing this thesis. I would also like to thanks members in the

BSEL group for their support during my experimentation and their warmest friendships. I want to extend my thanks to all of my friends who are always there for me and tirelessly encourage me in everything I have desired to achieve throughout my life.

Finally, I want to express my gratitude to my family for being my spiritual anchor when things become difficult for me. I want to extend my gratitude to myself for being able to complete all experiments and modelling, and ultimately this thesis.

Table of Contents

Nomenclature **XI**

List of Figures **XVI**

List of Tables **XXV**

List of Publications **XXIX**

Chapter 1: Introduction **1**

1.1. Motivation **2**

1.2. Thesis structure **5**

Chapter 2: Literature Review **7**

2.1 Cell biology **8**

2.1.1 An overview of mAb synthesis-associated cellular processes 8

2.2 Apoptosis **17**

2.2.1 Apoptosis pathways 17

2.2.2 The ER stress-associated apoptotic pathway 24

2.3 Mammalian Cell Cultures for production of mAbs **27**

2.3.1 Mammalian cell lines 28

2.3.2 Glutamine synthetase (GS) expression systems 29

2.3.3 Modes of mammalian cell cultures 31

2.3.4 Limitations of mammalian cell cultures 33

2.4 Temperature effects on culture performance **34**

2.4.1 Hypothermic conditions 35

2.4.2 Hyperthermic conditions 39

2.4.3 Temperature shift effects on culture performance 43

2.5 Cellular responses to nutrient composition shifts **46**

2.5.1 Glucose and glutamine initial concentrations 47

2.5.2 Lactate and ammonia initial concentrations 50

2.6 Strategies to enhance therapeutic protein production **52**

2.6.1 Control of cell proliferation 53

2.6.2 Suppression of apoptosis 54

2.6.3 Impact of apoptosis inhibition on productivity and final titre 55

2.6.4 Apoptosis inhibition and cell cycle arrest 57

2.6.5 Apoptosis inhibition and product quality 58
2.6.6 Protein expression and unfolded protein response 59
2.6.7 Relationships between cell cycle as well as apoptosis, and metabolism 61
2.7 Mathematical model development 65
2.7.1 An overview of mathematical model development 65
2.7.2 Model classification 66
2.7.3 Computational tools for model analysis 69
2.7.4 Frameworks for predictive mathematical model development 74
2.8 Mathematical models for cell growth, metabolism and death 76
2.8.1 Unstructured models for cell growth and metabolism 77
2.8.2 Detailed cell growth and metabolism models 82
2.8.3 Unstructured cell death kinetics 85
2.9 Mathematical model description for apoptosis 87
2.9.1 Mathematical models for apoptotic pathways 87
2.9.2 Mathematical models for apoptosis in the mammalian cell cultures 92

Chapter 3: Thesis Goal 94

3.1 Research gaps 95
3.2 Thesis goal 97

Chapter 4: Materials & Methods 99

4.1 Mammalian cell cultures 100
4.1.1 Cell line 100
4.1.2 Medium preparation 100
4.1.3 Cryopreservation and cell expansion 101
4.1.4 Culture condition 101
4.1.5 Experiments 102
4.1.6 Sample collection 103
4.2 Cell analysis 103
4.2.1 Cell density and viability 103
4.2.2 Apoptotic cell quantification 104
4.2.3 Cell cycle analysis 107
4.2.4 The profiling of cyclins and Ki-67 proliferation marker 108
4.2.5 Gene expression measurements 110
4.3 Extracellular metabolite quantification 114

4.3.1 Nutrient and metabolite quantification 114
4.3.2 Amino acid quantification 115
4.3.3 cB72.3 mAb quantification 118
4.3.4 cB72.3 mAb quality assessment 119
4.4 Data analysis 120
4.4.1 The estimation of cell culture descriptive parameters 120
4.4.2 Statistical Analysis 121
Chapter 5: A Map of the Dynamic Interplay between Cell Cycle and Apoptosis, and Metabolism 127
5.1 Background 128
5.1.1 Introduction 128
5.1.2 Objectives 131
5.2 Methodology 131
5.3 Results 132
5.3.1 Cell growth and metabolic profiles 132
5.3.2 Amino acid profiles 136
5.3.3 Cell cycle and apoptosis 144
5.3.4 Pro-apoptotic and anti-apoptotic gene expressions 145
5.4 Discussion 149
5.4.1 Extracellular metabolite levels and its effect on cellular activities 149
5.4.2 The genetic control of cell cycle and apoptosis linked to metabolic stresses 153
5.5 Conclusions 155
Chapter 6: The Impact of Temperature, Medium Composition and Nutrient Addition, on Apoptosis 157
6.1 Background 158
6.1.1 Introduction 158
6.1.2 Objectives 161
6.2 Methodology 161
6.2.1 Temperature fluctuations 161
6.2.2 Medium composition 162
6.2.3 Nutrient additions 163
6.3 Results & Discussion 165

6.3.1 Temperature fluctuations 165
6.3.2 Medium composition 173
6.3.3 Nutrient additions 183
6.4 Conclusions 198

Chapter 7: An Experimentally-Validated Mathematical Model of Apoptosis 200

7.1 Background 201
7.1.1 Introduction 201
7.1.2 Objectives 204
7.2 Methodology 205
7.2.1 The proposed model development framework 205
7.2.2 Model construction 206
7.2.3 Parameter values 228
7.2.4 Model analysis 231
7.3 Results & Discussion 235
7.3.1 Batch and Fed-batch simulations 235
7.3.2 Parameter sensitivities 246
7.4 Conclusions 260

Chapter 8: Overall Conclusions and Future Research Directions 262

8.1 Overall conclusions 263
8.1.1 Summary of results 263
8.1.2 Main conclusions 266
8.2 Recommendations for future work 268
8.2.1 Experimental investigations 268
8.2.2 Mathematical modelling and its applications 270

Bibliography 272

Appendix A: Supplementary Materials for Chapter 4 313

Appendix B: Supplementary Materials for Chapter 5, 6&7 330

V	The total volume of the system (L)
F_{in}	The total flowrate of feeding streams (L/hr)
F_{out}	The total flowrate of outlet streams (L/hr)
$F_{in,\ glc}$, $F_{in,\ glu}$, $F_{in,\ asp}$, $F_{in,\ asn}$, $F_{in,\ arg}$	The flowrates of fed glucose, glutamate, aspartate, asparagine and arginine, respectively (L/hr)
X_v	The viable cell concentration (cells/mL)
X_{ad}	The ESA cell concentration (cells/mL)
X_{nd}	The concentration of dead cells from other pathways than apoptosis (cells/mL)
X_d	The dead cell concentration (cells/mL)
μ_{ad}	The specific rate of ESA death (hr^{-1})
μ_{nd}	The specific rate of cell death via other pathways than apoptosis (hr^{-1})
k_d	The degradation rate (hr^{-1})
X_t	The total cell concentration (cells/mL)
Glc	The extracellular concentration of glucose (mM)
Glu	The extracellular concentration of glutamate (mM)
$\mu_{max,\ glc}$	The glucose-associated maximum specific growth rate (hr^{-1})
$\mu_{max,\ glu}$	The glutamate-associated maximum specific growth rates (hr^{-1})
K_{glc} and K_{glu}	The glucose and glutamate limiting constants (mM)
$\mu_{max,\ ad}$	The maximum specific rate of ESA death rate (hr^{-1})
Casp3	The concentration of active caspase-3 molecule (mM)
K_{casp3}	The Monod constant for ESA (mM)
$\mu_{max,\ d}$	The maximum specific rate of LSA or dead cells (hr^{-1})
$\mu_{max,\ nd}$	The maximum specific rate of cell death via other pathways than apoptosis (hr^{-1})
Lac	The extracellular lactate concentration (mM)
K_{lac}	The Monod constant for lactate limitation effect (mM)
Glc_{in}	The concentration of fed glucose (mM)
Q_{glc}	The specific glucose utilisation rate ($mmol.cells^{-1}.hr^{-1}$)
$Y_{x,\ glc}$	The yield of cells over glucose (cells/mmol)
m_{glc}	The glucose-associated maintenance energy constant ($mmol.cells^{-1}.hr^{-1}$)

$Km_{glc, asp}$, $Km_{lac, asp}$	The Monod constant for aspartate-associated glucose and lactate limiting effects, respectively (mM)
$Q_{lac, pro}$, $Q_{lac, con}$	The specific lactate production and consumption rates, respectively (mmol $cells^{-1}$ hr^{-1})
$Y_{lac, glc}$	The yield of lactate over glucose (mmol/mmol)
$k_{lac, con}$	The specific lactate consumption constant ($mmol.cells^{-1}.hr^{-1}$)
Glu_{in}	The concentration of fed glutamate (mM)
Q_{glu}, Q_{asp}, $Q_{arg,}$ $Q_{ala, con}$, $Q_{gln, con}$	The specific glutamate, aspartate, arginine, alanine and glutamine utilisation rates, respectively ($mmol.cells^{-1}.hr^{-1}$)
$Q_{ala, pro}$, $Q_{gln, pro}$	The specific alanine and glutamine production rates, respectively ($mmol.cells^{-1}.hr^{-1}$)
$f_{glu, asp}$, $f_{glu, arg}$, $f_{glu, ala}$ $f_{glu, gln}$	The yield of glutamate over aspartate, arginine, alanine and glutamine, respectively (mmol/mmol)
$Y_{x, glu}$	The yield of cells over glutamate (cells/mmol)
m_{glu}	The glutamate-associated maintenance energy constant ($mmol.cells^{-1}.hr^{-1}$)
$Km_{glu, glu}$	The Monod constant for glutamate-associated glutamate limiting effect (mM)
Asp	The extracellular concentration of aspartate (mM)
Asp_{in}	The concentration of fed aspartate (mM)
Q_{asn}	The specific asparagine utilisation rates ($mmol.cells^{-1}.hr^{-1}$)
$f_{asp, asn}$	The yield of aspartate over asparagine (mmol/mmol)
$Y_{x, asp}$	The yield of cells over aspartate (cells/mmol)
m_{asp}	The aspartate-associated maintenance energy constant ($mmol.cells^{-1}.hr^{-1}$)
$Km_{asp, asp}$	The Monod constant for aspartate-associated aspartate limiting effect (mM)
Asn	The extracellular concentration of asparagine (mM)
Asn_{in}	The concentration of fed asparagine (mM)
$Y_{x, asn}$	The yield of cells over asparagine (cells/mmol)
m_{asn}	The asparagine-associated maintenance energy constant ($mmol.cells^{-1}.hr^{-1}$)
$Km_{asn, asp}$	The Monod constant for asparagine-associated aspartate limiting effect (mM)

Arg	The extracellular concentration of arginine (mM)
Arg_{in}	The concentration of fed arginine (mM)
Q_{arg}	The specific arginine utilisation rates ($mmol.cells^{-1}.hr^{-1}$)
$Y_{x,\ arg}$	The yield of cells over arginine (cells/mmol)
m_{arg}	The arginine-associated maintenance energy constant ($mmol.cells^{-1}.hr^{-1}$)
$Km_{arg,\ arg}$	The Monod constant for arginine-associated arginine limiting effect (mM)
Ala	The extracellular concentration of alanine (mM)
$Y_{ala,\ glu}$	The yield of alanine over glutamate (mmol/mmol)
$Y_{x,\ ala}$	The yield of cells over alanine (cells/mmol)
m_{ala}	The alanine-associated maintenance energy constant ($mmol.cells^{-1}.hr^{-1}$)
$Km_{ala,\ glu}$	Monod constant for alanine-associated glutamate limiting effect (mM)
Gln	The extracellular concentration of glutamine (mM)
$Y_{gln,\ glu}$	The yield of glutamine over glutamate (mmol/mmol)
$Y_{x,\ gln}$	The yield of cells over alanine (cells/mmol)
m_{ala}	The alanine-associated maintenance energy constant ($mmol.cells^{-1}.hr^{-1}$)
$Km_{ala,\ glu}$	The Monod constant for alanine-associated glutamate limiting effect (mM)
Leu	The extracellular concentration of leucine (mM)
Q_{leu}	The specific leucine utilisation rates ($mmol.cells^{-1}.hr^{-1}$)
$Y_{x,\ leu}$	The yield of cells over leucine (cells/mmol)
m_{leu}	The leucine associated maintenance energy constant ($mmol.cells^{-1}.hr^{-1}$)
$Km_{arg,\ arg}$	The Monod constant for leucine -associated leucine limiting effect (mM)
Ab	The extracellular concentration of mAb (mg/L)
Q_{ab}	The specific mAb prediction rate ($mg.cells^{-1}.hr^{-1}$)
α_{ab}	The constant for the mAb synthesis rate ($mg.cells^{-1}.hr^{-1}$)
$Km_{ab,\ aa}$	The Monod constant for amino acid-limiting effect on mAb synthesis (mM)

$mRNA_{atf5}$	The relative fold change of *atf5* expression (-)
$\beta_{mRNAatf5}$	The maximal fold change of *atf5* expression (hr^{-1})
$Km_{asp, atf5}$, $Km_{ab, atf5}$	The Monod constants for *atf5* associated-aspartate (mM) and mAb (mg/L) limiting effect, respectively
$\alpha_{mRNAatf5}$	The mRNA degradation rate of *atf5* (hr^{-1})
$mRNA_{trp53bp2}$	The relative fold change of *trp53bp2* expression (-)
$\beta_{mRNAtrp53bp2}$	The maximal fold change of *trp53bp2* expression (hr^{-1})
$Km_{glu, trp53bp2}$, $Km_{lac, trp53bp2}$	The Monod constants for *trp53bp2* associated-glutamate and lactate limiting effect, respectively (mM)
$\alpha_{mRNAtrp53bp2}$	The mRNA degradation rate of *trp53bp2* (hr^{-1})
$mRNA_{casp8}$	The relative fold change of *casp8* expression (-)
$\beta_{mRNAcasp8}$	The maximal fold change of *casp8* expression (hr^{-1})
$Km_{glu, casp8}$	The Monod constant for *casp8* associated-glutamate limiting effect (mM)
$\alpha_{mRNAcasp8}$	The mRNA degradation rate of *casp8* (hr^{-1})
$mRNA_{bcl2}$	The relative fold change of *bcl-2* expression (-)
$\beta_{mRNAbcl2}$	The maximal fold change of *bcl-2* expression (hr^{-1})
$Km_{trp53bp2, bcl-2}$, $Km_{atf5, bcl-2}$	The Monod constants for *trp53bp2* and *atf5* limiting effects, respectively, on *bcl-2* expression (-)
$\alpha_{mRNAbcl2}$	The mRNA degradation rate of *bcl-2* (hr^{-1})
$mRNA_{bax}$	The relative fold change of *bax* expression (-)
$\beta_{mRNAbax}$	The maximal fold change of *bax* expression (hr^{-1})
$Km_{bcl-2, bax}$ $Km_{trp53bp2, bax}$	The Monod constants for *bcl-2* and *trp53bp2* limiting effects, respectively, on *bax* expression (-)
$\alpha_{mRNAbax}$	The mRNA degradation rate of *bax* (hr^{-1})
$mRNA_{casp3}$	The relative fold change of *casp3* expression (-)
$\beta_{mRNAcasp3}$	The maximal fold change of *casp3* expression (hr^{-1})
$Km_{casp3, iC3}$ *casp3*	The Monod constant for caspase 3 limiting effect, respectively, on expression (mM)
$\alpha_{mRNAcasp3}$	The mRNA degradation rate of *casp3* (hr^{-1})
iCasp3	The concentration of procaspases-3 (mM)
Casp3,	The concentration of Caspases-3 (mM)
Bax_4	The concentration of active bax (mM)
Casp8	The concentration of caspase-8 (mM)

β_{iC3}	The maximal procaspase-3 translation rate based on the expression of *casp3* ($mmol.hr^{-1}$)
k_{C3}, k_{C8}	The rate constants for active bax and caspase-8, respectively, associated-caspase-3 activation ($L.mmol^{-1}.hr^{-1}$)
Kb_{iC3}	The Monod constant for $mRNA_{casp3}$ limiting effect on the translation of procaspase-3 (-)
iBax, Bcl2	The concentration of inactive Bax and Bcl-2, respectively (mM)
β_{ibax}	The maximal inactive Bax translation rate based on the expression of *bax* ($mmol.hr^{-1}$)
k_{bax}, $k_{_bax}$	The rate constants for the Bax tetramerization ($L^3.mmol^{-3}.hr^{-1}$) and the inhibitive binding of Bcl-2 to active Bax ($L.mmol^{-1}.hr^{-1}$), respectively
Kb_{ibax}	The Monod constant for $mRNA_{bax}$ limiting effect on the translation of inactive Bax (-)
β_{bcl2}	The maximal Bcl-2 translation rate based on the expression of *bcl2* ($mmol.hr^{-1}$)
Kb_{bcl2}	The Monod constant for $mRNA_{bcl2}$ limiting effect on Bcl-2 translation
β_{casp8}	The maximal caspase-8 translation rate based on the expression of *casp8* ($mmol.hr^{-1}$)
Kb_{C8}	The Monod constant for $mRNA_{casp8}$ limiting effect on the translation of caspase-8 (-)

List of Figures

Figure 2.1.1	An overview of cell metabolism; catabolism and anabolism. Adapted from (O'Connor and Adams, 2010).	**7**
Figure 2.1.2	An overview of transcription and translation in eukaryotic cells. Adapted from (O'Connor and Adams, 2010).	**9**
Figure 2.1.3	Alternative splicing. Adapted from (Clancy, 2008b).	**10**
Figure 2.1.4	The breakdown of glucose into CO_2 and H_2O via three pathways of catabolism in eukaryotic cells: Glycolysis, Citric acid cycle (TCA cycle), and Oxidative phosphorylation. Adapted from (O'Connor and Adams, 2010).	**13**
Figure 2.1.5	The structure of IgG antibody. Adapted from (http://www.jenabioscience.com).	**14**
Figure 2.1.6	Cell cycle and DNA content according to each phase in the cycle. Adapted from (O'Connor, 2008).	**16**
Figure 2.2.1	Apoptotic pathways: the death-receptor pathway and the mitochondrial pathway. Adapted from (Hengartner, 2000).	**18**
Figure 2.2.2	The association of *atf5* and *trp53bp2* genes with the apoptotic pathways.	**22**
Figure 2.2.3	The upstream signalling of ER-stress associated pathways. Adapted from (Logue et al., 2013).	**24**
Figure 2.2.4	Caspase activation through the ER-stress associated pathway. Adapted from (Szegezdi et al., 2006).	**25**
Figure 2.4.1	Literature review for the temperature effect on cellular activities in the mammalian cell cultures.	**34**
Figure 2.4.2	The role of HSPs in the apoptotic pathways, Adapted from (Lanneau et al., 2008).	**41**
Figure 2.5.1	Literature review for the effect of initial concentration of nutrients and metabolites on cellular activities in the mammalian cell cultures.	**47**

Figure 2.6.1	Literature review for the effect of cell proliferation control and suppression of apoptosis, which are accounted as strategies for enhancement of desired biologics production, on cellular activities in the mammalian cell cultures.	**53**
Figure 2.7.1	Model classification. Adapted from (Ramkrishna, 1979, Sidoli et al., 2004).	**67**
Figure 2.7.2	The framework for predictive mathematical model development proposed by (Kontoravdi et al., 2010).	**75**
Figure 2.9.1	Two models of the Bcl-2 family member interaction. The difference between (A) and (B) is the auto-activation of active bax. Adapted from (Cui et al., 2008).	**88**
Figure 4.2.1	Cell count example (viable/dead).	**104**
Figure 4.3.1	The chromatogram of the standard of 19 amino acids.	**117**
Figure 4.4.1	The F-distribution with 3 and 10 degrees of freedom. The vertical line at around F=3.71 indicates the F-critical value at $\alpha = 0.05$. The shaded area is *p*-value indicating the likelihood of getting an F-statistic being equal to or larger than the observed F-statistic. In this case, the observed F-statistic is equal to the F-critical, therefore, *p*-value = 0.05 which is equal to α. If the observed F-statistic is larger than the F-critical, then *p*-value is less than α and the null hypothesis is rejected. Adapted from (Seltman, 2012).	**124**
Figure 5.3.1	Cell growth, dead and extracellular nutrient level profiles of the batch culture of GS-NS0: (A) viable cell concentration; (A.1) on linear scale Y-axis and (A.2) on base 10 logarithmic scale Y-axis; (B) Late stage apoptotic (LSA) cell fraction and viability; (C) glutamate and ammonium; (D) glucose and lactate and (E) Extracellular c72.3 mAb titer. I indicates early-exponential phase, II indicates exponential phase, III indicates stationary phase and IV indicate death phase. The normal vertical lines indicate each culture phase boundary (n=3, error bar = SD).	**133-134**

Figure 5.3.2 The assessment of produced mAb quality: (A) protein gel electrophoresis and (B) the comparison between mAb quantified by the HPLC technique and the ELISA technique. r_p represents the Pearson correlation coefficient. **135**

Figure 5.3.3 A metabolic network of relevant amino acids and reactions involved in the TCA. Modified from (Nelson and Cox 2004; Sellick et al. 2011). **138**

Figure 5.3.4 Extracellular amino acid concentrations in the batch culture of GS-NS0: A) aspartate and glutamate; B) asparagine and arginine; C) serine and alanine; D) leucine and lysine E) valine and isoleucine; F) cysteine and proline; G) tryptophan and histidine; H) methionine and tyrosine; I) threonine and phenylalanine; and J) glycine. (n=3, error bar = SD). **140-142**

Figure 5.3.5 Cell culture dependent metabolic networks: A) early and exponential phases; and B) stationary phase. Notation: solid arrows show the supported direction by the results, dashed arrows show the proposed direction. **143**

Figure 5.3.6 Cell cycle distribution and early stage apoptotic cell fraction in the batch culture of GS-NS0: A) cell cycle distribution; and B) early stage apoptotic cells. **146**

Figure 5.3.7 Relative expressions of key apoptotic and cell cycle-related genes: A) *trp53bp2* and *bax*; B) *casp3* and *casp8*; C) *atf5*; D) *bcl-2* and *p21*. Notation: relative gene expression quantification normalized to *gapdh* (housekeeping gene) and with respect to time 0 hour. **147**

Figure 5.3.8 Map of events occurring in each phase of the GS-NS0 culture. **148**

Figure 6.2.1 Two different schemes of nutrient additions in the fed-batch cultures: (A) F1 (glucose, glutamate, aspartate, asparagine and arginine); and (B) F2 (glucose and glutamate). The concentration of each feeding nutrient stock solution is as follows: 200 g/L (1.1 M) of glucose; 7.5 g/L (50mM) of glutamate; 5 g/L (37.5 mM) of aspartate; 10 g/L of **164**

(76 mM) asparagine; and 10 g/L (57.5 mM) arginine.

Figure 6.3.1 The profiles of A) cell density and viability; B) % ESA; and C) % LSA VS. % dead cells, in the temperature shift experiment. The vertical dot line represents the temperature shift. The arrows indicate the corresponding axes to the data (n=3, error bar = SD). r_p represents the Pearson correlation coefficient. **166**

Figure 6.3.2 The metabolic and mAb profiles and in the batch cultures with the temperature shifts: A) glutamate and mAb concentrations; B) specific glucose consumption rates; C) specific lactate generation rates; and D) specific mAb productivity. The vertical dot line represents the temperature shift. The arrows indicate the corresponding axes to the data (n=3, error bar = SD). **169**

Figure 6.3.3 The cell cycle analysis: A) cell fraction in G_1/G_0 lumped phase; B) cell fraction in G_2/M lumped phase; and C) cyclin D1 profile with glutamate concentration. The vertical dot line represents the temperature shift. The arrows indicate the corresponding axes to the data (n=3, error bar = SD). **170**

Figure 6.3.4 Cell proliferation profiles in the medium blend experiment: A) viable cell density and viability; and B) apoptotic & Ki-67 positive (proliferative) cell fraction. FM is fresh medium and the arrows indicate the corresponding axes to the data (n=3, error bar = SD). **176**

Figure 6.3.5 Nutrient, metabolite and mAb concentration profiles in the medium blend experiment: A) glucose and lactate; B) glutamate; C) normalised mAb; and D) measured mAb. The normalised mAb represents "measured mAb at a given time – measured mAb at t = 0 hour". FM is fresh medium and the arrows indicate the corresponding axes to the data (n=3, error bar = SD). **178**

Figure 6.3.6 The expressions of genes related to apoptosis and cell cycle in in the medium blend experiment: A) *atf5*; B) *bcl-2*; C) *p21*; D) *trp53bp2*; E) *casp8*; and F) *casp3*. The relative fold change represents the gene **179**

expression normalised to 0 hr and the housekeeping gene, *gapdh* (see Appendix A). "*" indicates p<0.05 and the corresponding *p*-values are showed in Appendix B.3, (n=3, error bar = SD).

Figure 6.3.7 Scatter plots between *bcl-2* and cyclins in the medium shift experiment: A) *bcl-2* and cyclin D1 expressions; B) *bcl-2* and cyclin E1 expressions; and C) *bcl-2* and cyclin B1 expressions. FM is fresh medium and the dash dot lines represent the basal expressions. All relative expressions were normalised to time 0 hour (n=3, error bar = SD). r_p and r_s represent the Pearson and Spearman, respectively, correlation coefficients. **180**

Figure 6.3.8 Cell growth and ESA cell profiles in the batch & fed-batch cultures: A) viable cell concentration; B) viability; and C) %ESA cells. F1 and F2 represent the feeding strategies as described in section 6.2.3. (n=3, error bar = SD). **187**

Figure 6.3.9 The concentration profiles of A) glucose; B) lactate; C) consumed serine; D) glutamate; E) aspartate; F) alanine; G) leucine; and H) mAb in the batch & fed-batch cultures. F1 and F2 represent the feeding strategies as described in section 6.2.3. (n=3, error bar = SD). **188-189**

Figure 6.3.10 Cell cycle profiles in in the batch & fed-batch cultures: A) G_1/G_0 lumped; B) S; and C) G_2/M lumped phases. The relative change in cell fraction was the cell fractions that were normalised to the time 24 hours of cultures. F1 and F2 represent the feeding strategies as described in section 6.2.3. (n=3, error bar = SD). **193**

Figure 6.3.11 The expression profiles of apoptosis-associated genes in the batch & fed-batch cultures: A) *atf5*; B) *bcl-2*; C) *p21*; D) *bax*; E) *trp53bp2*; F) *casp8*; and G) *casp3*. The gene expressions were normalised to time 0 hour and a housekeeping gene (*gapdh*). F1 and F2 represent the feeding strategies as described in section 6.2.3. "*" indicates *p*<0.05 and the corresponding *p*-values are showed in Appendix B.3, (n=3, error bar = SD). **194-195**

Figure 7.2.1 The proposed framework for the development of mathematical model for the culture of GS-NS0 in this study. **205**

Figure 7.2.2 The flowchart of cell population kinetics in the cultures of GS-NS0 cells. It was herein postulated based on the experimental observation and used as a basis for the construction of cell growth mathematical sub-model. **208**

Figure 7.2.3 The network of enzymatic reactions among nutrients, metabolites and amino acids. This network was herein postulated based on the experimental observation and used as a basis for the construction of the unstructured sub-model for glucose and amino acid metabolism in the GS-NS0 cultures. **212**

Figure 7.2.4 The transcriptional and translational regulatory network of apoptosis with links to metabolic stresses in the cultures of GS-NS0. This was herein proposed in accordance with previous reports as well as the herein experimental observation. This was used as a basis for the construction of the apoptosis structured sub-model. **220**

Figure 7.3.1 Model simulation results for (A) viable cell concentration; (B) ESA cell concentration; and (C) viability. The left column represents the batch data and the right column represents the fed-batch data. r_p stands for the Pearson correlation coefficient, *p*-value indicates the probability that the identified correlation might not be existing, and Adjusted R^2 indicates goodness of fit. **237**

Figure 7.3.2 Model simulation results (A) glucose; (B) lactate; and (C) glutamate concentrations. The left column represents the batch data and the right column represents the fed-batch data. r_p stands for the Pearson correlation coefficient, *p*-value indicates the probability that the identified correlation might not be existing, and Adjusted R^2 indicates goodness of fit. **238**

Figure 7.3.3 Model simulation results for (A) aspartate; (B) asparagine; and (C) arginine concentrations. The left column represents the batch data and the right column represents the fed-batch data. r_p stands for the **239**

Pearson correlation coefficient, *p*-value indicates the probability that the identified correlation might not be existing, and Adjusted R^2 indicates goodness of fit.

Figure 7.3.4 Model simulation results (A) alanine; (B) leucine; and (C) mAb concentrations. The left column represents the batch data and the right column represents the fed-batch data. r_p stands for the Pearson correlation coefficient, *p*-value indicates the probability that the identified correlation might not be existing, and Adjusted R^2 indicates goodness of fit. **240**

Figure 7.3.5 Model simulation results for (A) *atf5*; (B) *bcl-2*; (C) *trp53bp2*; (D) *casp8*; and (E) *casp3* expressions. The left column represents the batch data and the right column represents the fed-batch data. r_p stands for the Pearson correlation coefficient, *p*-value indicates the probability that the identified correlation might not be existing, and Adjusted R^2 indicates goodness of fit. **241-242**

Figure 7.3.6 Model simulation results based on the set of optimal parameter values providing the minimum percentage error for (A) viable cell concentration; (B) ESA cell concentration; (C) viability; and (D) mAb concentration in the batch culture. r_p stands for the Pearson correlation coefficient, *p*-value indicates the probability that the identified correlation might not be existing, and Adjusted R^2 indicates goodness of fit. **245**

Figure A.1.1 Side scatter (SSC) VS. Forward scatter (FSC) diagram of an unstained sample with a gate to include viable and dead cell populations. **313**

Figure A.1.2 The histograms of the single stained samples: (A) Annexin V FITC; and (B) PI. **314**

Figure A.1.3 The workflow of the quantification of apoptotic population fractions: (A) the first gate applied to the double stained sample; (B) the dot pot of FSC width versus area to differentiate between populations by diameter size; (C) and (D) quad gates used to separate the four **315**

populations.

Figure A.2.1 DNA analysis with gates (A) the dot plot of SSC versus FSC and (B) the histogram showing the events against 561 nm fluorescence intensity. **316**

Figure A.2.2 Watson Algorithm (Watson et al., 1987) used to quantify the fraction of each sub-populations; G_1/G_0, S and G_2/M. **317**

Figure A.3.1 Data analysis for cyclin quantification. Adapted from (García Münzer, 2014). **319**

Figure A.4.1 The amplification plot and the threshold cycle (C_T) value; (A) the linear scale, and (B) the logarithm scale of the net fluorescence intensity. For example, The C_T value is around 27 cycles at the threshold value = 2.4712. **320**

Figure A.5.1 The plot of the amino acid concentrations versus the corresponding areas under peaks. The linear lines represent the correlations between the concentrations and the areas. **323**

Figure A.6.1 The calibration curve for mAb quantification. **326**

Figure A.7.1 The estimation of specific consumption rates (slope) of aspartate in each phase of a culture replicate; (I) early exponential, (II) exponential, (III) stationary and (IV) death phases. **327**

Figure B.2.1 Lactate and glucose metabolism in the temperature shift experiment: A) lactate and glucose concentration profiles; and B) lactate yields over glucose. The vertical dot line represents the temperature shifts, the arrows indicate the corresponding axes to the data (n=3, error bar = SD). **332**

Figure B.2.2 Scatter plots between *p21* and cyclins in the medium shift experiment: A) *p21* and cyclin D1 expressions; B) *p21* and cyclin E1 expressions; and C) *p21* and cyclin B1 expressions. FM is fresh medium and the dash dot lines represent the basal expressions. All relative expressions were normalised to time 0 hour (n=3, error bar = SD). **333**

Figure B.2.3 Scatter plots between *trp53bp2* and cyclins in the medium shift experiment: A) *trp53bp2* and cyclin D1 expressions; B) *trp53bp2* and cyclin E1 expressions; and C) *trp53bp2* and cyclin B1 expressions. FM is fresh medium and the dash dot lines represent the basal expressions. All relative expressions were normalised to time 0 hour (n=3, error bar = SD). **334**

Figure B.2.4 The concentration profiles of glutamine in the batch & fed-batch cultures. F1 and F2 represent the feeding strategies as described in section 6.2.3. (n=3, error bar = SD). **335**

List of Tables

Table 2.2.1	Target genes of p53 transcription factor.	**21**
Table 2.7.1	Existing kinetics describing relations between substrates and rates of reactions.	**65**
Table 2.8.1	Equations for the specific growth rate, the specific utilisation rate of substrates, the specific production rate of metabolic by-products, and the antibody synthesis rate. Adapted from (Pörtner and Schäfer, 1996).	**79-80**
Table 2.8.2	Models for specific cell death rate. Adapted from (Pörtner et al., 1996).	**86**
Table 4.1.1	Medium preparation.	**100**
Table 4.2.1	Apoptotic cell analysis.	**106**
Table 4.2.2	Primer sequences used in this study.	**111**
Table 4.3.1	The procedure for the pre-column derivatization.	**115**
Table 4.3.2	The composition of mobile phases (1 L).	**116**
Table 4.3.3	The fraction of mobile phase B in the total flowrate of the eluting mobile phase.	**116**
Table 5.3.1	Calculated specific consumption/production rates and yields.	**144**
Table 7.2.1	The preliminary values of model parameters and their references.	**228**
Table 7.3.1	The total sensitivity indices (TSIs) with respect to the viable cell concentration (X_V). The GSA was performed with ±25% simultaneous variation of all parameter values and 100,000 Sobol's sequences. Coloured cells are the parameter sensitivities being over the threshold (≥ 0.1).	**247**
Table 7.3.2	The total sensitivity indices (TSIs) with respect to the ESA cell concentration (X_{ad}). The GSA was performed with ±25% simultaneous variation of all parameter values and 100,000 Sobol's sequences. Coloured cells are the parameter sensitivities being over	**249**

the threshold (≥ 0.1).

Table 7.3.3 The total sensitivity indices (TSIs) with respect to the dead cell concentration (X_d). The GSA was performed with ±25% simultaneous variation of all parameter values and 100,000 Sobol's sequences. Coloured cells are the parameter sensitivities being over the threshold (≥ 0.1). **250**

Table 7.3.4 The total sensitivity indices (TSIs) with respect to the mAb titre (Ab). The GSA was performed with ±25% simultaneous variation of all parameter values and 100,000 Sobol's sequences. Coloured cells are the parameter sensitivities being over the S_{tot} threshold (≥ 0.1). **251**

Table 7.3.5 The total sensitivity indices (TSIs) with respect to the viable cell concentration: A) ±25% simultaneous variation of metabolism sub-model parameter values while 5% simultaneous variation of the reaming parameter values; and B) ±50% simultaneous variation of apoptosis sub-model parameter values while 5% simultaneous variation of the reaming parameter values. The analysis was performed with 60,000 simulations. Coloured cells are the parameter sensitivities being over the S_{tot} threshold (≥ 0.1). **254**

Table 7.3.6 The total sensitivity indices (TSIs) with respect to the ESA cell concentration: A) ±25% simultaneous variation of metabolism sub-model parameter values while 5% simultaneous variation of the reaming parameter values; and B) ±50% simultaneous variation of apoptosis sub-model parameter values while 5% simultaneous variation of the reaming parameter values. The analysis was performed with 60,000 simulations. Coloured cells are the parameter sensitivities being over the S_{tot} threshold (≥ 0.1). **255**

Table 7.3.7 The total sensitivity indices (TSIs) with respect to the dead cell concentration: A) ±25% simultaneous variation of metabolism sub-model parameter values while 5% simultaneous variation of the reaming parameter values; and B) ±50% simultaneous variation of apoptosis sub-model parameter values while 5% simultaneous **256**

variation of the reaming parameter values. The analysis was performed with 60,000 simulations. Coloured cells are the parameter sensitivities being over the S_{tot} threshold (≥ 0.1).

Table 7.3.8 The total sensitivity indices (TSIs) with respect to the mAb concentration: A) ±25% simultaneous variation of metabolism sub-model parameter values while 5% simultaneous variation of the reaming parameter values; and B) ±50% simultaneous variation of apoptosis sub-model parameter values while 5% simultaneous variation of the reaming parameter values. The analysis was performed with 60,000 simulations. Coloured cells are the parameter sensitivities being over the S_{tot} threshold (≥ 0.1). **257**

Table 7.3.9 Significant and insignificant parameters with respect to the corresponding model variables. The parameter significance was judged based on S_{tot} values being larger than 0.1. The S_{tot} was achieved from the further evaluation of parameter sensitivities as discussed earlier. **259**

Table A.3.1 Flow cytometers laser wavelength and filter configurations. **318**

Table A.4.1 The estimation of $\Delta\Delta C_T$ value of *atf5* gene at time = 23 hours of a culture replicate. **321**

Table A.4.2 The estimation of average *atf5* expression relative fold changes for all culture replicates at time = 23 hr. **322**

Table A.5.1 A series of amino acid standard dilutions. **324**

Table A.5.2 The linear correlations between the areas under the peaks and the concentrations of corresponding amino acids, where [Amino acid Conc.] = A × [Peak area] + B. **325**

Table A.6.1 A series of mAb standard dilutions. **326**

Table A.7.1 The average values of the specific consumption rate of aspartate ($\mu mol.10^{-6}$ cell. day^{-1}) from all culture replicates and its standard deviation values. **328**

Table A.8.1 p21 expression in the batch culture. **328**

Table A.8.2	F-statistic calculation.	**329**
Table B.1.1	Batch culture raw data of mAb quantification.	**330**
Table B.1.2	F1 Fed-Batch culture raw data of mAb quantification.	**330**
Table B.1.3	F2 Fed-Batch culture raw data of mAb quantification.	**331**
Table B.3.1	*p*-values from the statistical analysis in Figure 6.3.6.	**336**
Table B.3.2	*p*-values from the statistical analysis in Figure 6.3.11.	**336**
Table B.4.1	An optimal values of model parameters determined using the quasi-Monte Carlo algorithm with the minimisation of the total percentage error.	**337**

List of Publications

Refereed journal publication(s)

- D.G. García Münzer, M. Ivarsson b, **C. Usaku**, T. Habicherb, M. Soos, M. Morbidelli, E.N. Pistikopoulos, A. Mantalaris (2015), An unstructured model of metabolic and temperature dependent cell cycle arrest in hybridoma batch and fed-batch cultures, Biochemical Engineering Journal 93(0): 260-273.

Conference Proceeding(s)

- **C. Usaku**, D. G. Munzer, E. N. Pistikopoulos, A. Mantalaris (2013), Cell cycle and apoptosis: a map for the GS-NS0 cell line at the genetic level and the link to environmental stress, BMC Proceedings, 2013. 7(Suppl 6): p. P54.

Conference presentation(s)

- **C. Usaku**, C. A. Chua, S. Harun, E.N. Pistikopoulos, A. Mantalaris (2014), Toward Model-based Optimisation for Designing Glucose and Amino Acid Feeding Strategies to Supress Apoptosis in GS-NS0 Culture Producing Monoclonal Antibody, ESBES-IFIBIOP, Lille, France, 7-10 September 2014.
- **C. Usaku**, E. N. Pistikopoulos, A. Mantalaris (2014), Mathematical Modelling of Apoptosis for GS-NS0 Cell Culture Secreting Monoclonal Antibody: Linking Gene to Growth, Metabolism and Metabolic Stress, Metabolic Engineering X, Vancouver, Canada, 15-19 June 2014.
- **C. Usaku**, E. N. Pistikopoulos, A. Mantalaris (2014), Model-based optimization toward cell death suppression in a fed-batch culture of GS-NS0 cell line for production of antibody, Cell Culture Engineering XIV, Quebec city, Canada, 4-9 May 2014.
- **C. Usaku**, D. G. Munzer, E. N. Pistikopoulos, A. Mantalaris (2013), Cell cycle and apoptosis: a map for the GS-NS0 cell line at the genetic level and the link to

environmental stress, The European Society for Animal Cell Technology (23rd ESACT meeting), Lille, France, 23-26 June 2013.

Manuscripts in Preparation

- **C. Usaku,** D. G. Munzer, E. N. Pistikopoulos, A. Mantalaris, An integrated model of cell cycle, apoptosis and metabolism for GS-NS0 cell culture Systems, (Biotechnology and Bioengineering).
- **C. Usaku**, D. G. Munzer, A. Gauthier, E. N. Pistikopoulos, A. Mantalaris, The impact of culture temperature fluctuations, medium composition and nutrient additions on cell cycle and apoptosis in GS-NS0 cell cultures, (Biotechnology and Bioengineering).
- **C. Usaku**, D. G. Munzer, E. N. Pistikopoulos, A. Mantalaris, A mathematical model for apoptosis in GS-NS0 cell cultures, (Biochemical Engineering Journal).

Chapter 1

Introduction

1.1 Motivation

Mammalian cell culture systems are the reliable platforms for the manufacture of monoclonal antibodies (mAbs), one of the most important bio-therapeutics. Given the continuously increasing global demand for mAbs (Buss et al., 2012, Elvin et al., 2013), attention is drawn to optimisation of the mammalian cell culture systems toward improved mAb productivity as well as product quality (Torkashvand et al., 2015). Currently, improvement of mAb production becomes relatively mature; as high as 10 g/L of mAbs can be achieved from fed-batch cultures of mammalian cells, and research on mAb-producing cell culture systems has started to focus on shortening times spent for process development and improving product quality as well as expression stability (Li et al., 2010, Ho et al., 2013). However, given the steady increase in global demand for mAbs, further enhancing the mAb production/productivity in order to reduce the manufacturing cost remains one of greatest challenges facing the biotechnology community (Xing et al., 2012, Nasseri et al., 2014, Kang et al., 2014).

The cellular mAb synthesis is subject to a number of factors, nevertheless, its strong association with metabolic stresses is predominant in batch and fed-batch cultures, which are widely utilised for large-scale mAb production (Whitford, 2006). These metabolic stresses, which include nutrient exhaustion as well as toxic metabolite accumulation, affect the cell cycle at the centre of growth, productivity and cell death - lowering the culture lifespan and the final mAb titre. An insight into the interrelationship between the metabolic stresses, and cell proliferation as well as death is therefore required in order to develop strategies for the improvement of the mAb-production platforms toward the optimisation of mAb production/productivity.

Apoptosis, or programmed cell death, is believed to be the main cause of viability loss in mammalian cell cultures (Goswami et al., 1999, DiStefano et al., 1996, Browne and Al-Rubeai, 2011a, Singh et al., 1994). The induction of apoptosis is strongly subject to the metabolic stresses, including deprivation of nutrients (Simpson et al., 1998, Moley and Mueckler, 2000, Browne and Al-Rubeai, 2011b) and accumulation of toxic metabolites (Mastrangelo et al., 2000b, Figueroa et al., 2001). Moreover, there is strong interplay between the onset of apoptosis and cell cycle progression (Simpson et al., 1999b, Tey and Al-Rubeai, 2005, Mazel et al., 1996), and its impact on mAb production/productivity (Ibarra et al., 2003, Tey and Al-Rubeai, 2005). The onset of apoptosis was also found to be affected by culture conditions, such as culture temperature (Moore et al., 1997, Shi et al., 2005, Swiderek and Al-Rubeai, 2007) and the addition of nutrients during the culture period (DiStefano et al., 1996, Zhou et al., 1997a). These established facts attest the major involvement of apoptosis in the mammalian cell cultures, representing a mechanism of cell death as well as its links to environmental as well as physiological conditions. Given that prolonged culture viability is preferable due to the detrimental effects of cell death on mAb production and product quality (Yoon et al., 2003b, Majid et al., 2007, Tey et al., 2000a), understanding of apoptosis kinetics in association with the metabolic stresses is potentially the key to develop strategies to achieve longer culture viability, and thus higher mAb production/productivity as well as better product quality.

Apoptosis is however a highly complex cellular processes, which can be triggered through several pathways involving a number of apoptotic factors formed into regulatory networks governing apoptosis in response to both intracellular and extracellular apoptotic signals (Majors et al., 2007, Hengartner, 2000). Adding to its complexity, apoptosis has strong links to other cellular processes, as discussed above. Therefore, it is difficult to gain clear understanding of apoptosis kinetics by solely relying on *in-vitro* investigation. Using

mathematical modelling; mathematical equations relate culturing conditions including temperature, nutrient feeding strategies as well as medium composition, to cellular activities including growth, death (apoptosis), metabolism and product (mAb) synthesis, complements the understanding of apoptosis obtained from the experimental study. The systematic and quantitative nature of mathematical modelling enables us to simulate changes in variables of interest over time, and thus quantitatively explore and/or predict effects of the changes in these variables on cellular activities (Augusto et al., 2008). In addition, given its capability to simulate and predict dynamics of cell behaviour under different culturing conditions, mathematical modelling can be exploited for experimental planning (i.e. design of experiment), and thus reduce a number of possible trial and error experiments. It can also be used to guide process design, scaling up, optimisation as well as control of bioreactors when it comes to the development of large-scale mAb production platforms (Augusto et al., 2008). Therefore, it is essential to conduct *in-silico* study together with experimental investigation to establish insights into apoptosis kinetics. This approach is potentially one of the most effective approaches to study apoptosis.

The constructed mathematical model can be valid only for the system as well as the experimental conditions that the mathematical model is constructed based on. For example, different culture performances (growth, metabolism and death) are commonly seen among cultures of different lines of a mammalian cell host (i.e. NS0 cell lines), and thus the model constructed based on a line of the host might not be valid for other lines of the same cell host. Given that mathematical models are constructed based on existing general and relevant molecular biology together with experimental observation, they can be therefore refined, which might involve re-estimating parameter values and modifying model equations based on the experimental data from other culture systems and experimental conditions different from ones

used for the model construction. In this way, the model validity can be extended for the different culture systems and different culturing conditions.

1.2 Thesis structure

The outline of this thesis is as follow:

Chapter 1 describes the brief background and motivation behind the thesis. The structure of the thesis is also included in this chapter.

Chapter 2 presents a literature review. The review includes relevant molecular biology as well as apoptosis. An overview of mammalian cell cultures for the production of mAbs as well as factors that affect culture performance are also included. The effects of culture conditions, including culture temperature, medium contents and addition of nutrients, are discussed here. This chapter also provides a detailed review of apoptosis inhibition and cell cycle regulation–associated strategies for the improvement of mammalian cell cultures toward a higher production of bio-therapeutics. Finally, the frameworks for model development as well as model analysis are also summarised here. Additionally, existing mathematical models for the mammalian cell cultures as well as apoptosis are presented.

Chapter 3 lists research gaps identified from the literature review in Chapter 2. Given the identified research gaps, the research goal of the thesis is also introduced in this chapter.

Chapter 4 describes materials and methods applied in this study. The procedures for the cultures of GS-NS0 cell line, including medium preparation, cryopreservation and cell expansion, are described. The experimental conditions, including batch and fed-batch modes of cultures, are also elucidated. The procedures for analytical techniques, which include cell analysis and extracellular metabolite measurements, are also briefly summarised. The summary

of experimental data analysis as well as the method for statistical analysis are also included in this chapter. Appendix A includes the supplementary details of the analytical technique procedures as well as the calculation examples for the data analysis.

Chapter 5 presents the study of apoptosis in the batch culture of GS-NS0 cell line. This chapter reveals the effect of identified metabolic stresses - inherently occurring in the batch culture - upon the induction of apoptosis. In addition, metabolic shifts in response to the metabolic stresses are also elucidated. A map of cell cycle, apoptosis and metabolism for the batch culture of GS-NS0 cell line is herein presented.

Chapter 6 focuses on the study of culture condition effects on the induction of apoptosis. This chapter presents the effect of temperature shifts on the onset of apoptosis, cell proliferation, and mAb productivity. In addition, the effects of different medium blends on transcriptional control of apoptosis as well as the regulation of cell cycle progression are discussed. In this chapter, metabolic shifts and apoptosis induction as a result of the addition of nutrients are explored. Supplementary results are included in Appendix B.

Chapter 7 presents the mathematical model for apoptosis in the culture of GS-NS0 cells. This chapter illustrates mathematical model expressions constructed based on the observed phenomena discussed in Chapter 5 & 6. The model reproducibility with the preliminary set of parameter estimates is discussed here. In addition, model characteristics and further improvements suggested by model analysis are also described in this chapter.

Chapter 8 provides the main conclusion and the possible future research direction based on what was achieved in this study.

Chapter 2

Literature Review

2.1 Cell biology

2.1.1 An overview of mAb synthesis-associated cellular processes

Synthesis of mAb involves cellular metabolism. There are two cellular processes involved: catabolism and anabolism (Alberts et al., 2002), as shown in Figure 2.2.1. The former is where basic building blocks, including amino acids and nucleotides, as well as cellular energy, such as adenosine triphosphate (ATP) nutrients, are produced through the breakdown of macro-molecules, such as glucose. The latter involves synthesising macromolecules including proteins, by utilising the cellular energy and the basic building blocks obtained from the catabolism.

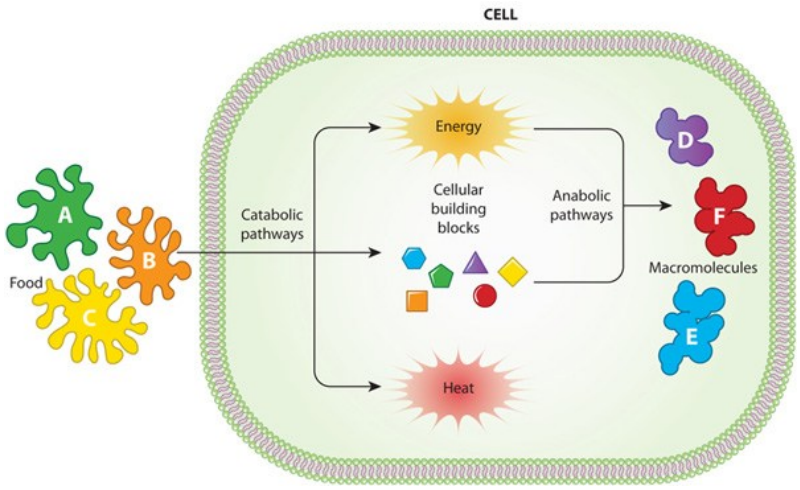


Figure 2.1.1 An overview of cell metabolism; catabolism and anabolism. Adapted from (O'Connor and Adams, 2010).

Controlling these metabolic activities is the central dogma, which involves cellular processes at transcriptional and translational levels. These processes are whereby regulatory molecules, including proteins and enzymes, are synthesised in response to external and internal stimuli and in turn translocated throughout the entire cellular system to manipulate cellular

biochemical activities (Shuler and Kargi, 2002). The stimuli are basically connected to changes in intracellular and extracellular conditions, such as the presence/absence of nutrients and heat shock (O'Connor and Adams, 2010).

Transcription and translation processes

The type of protein present in a cell and its amount are basically controlled by transcription and translation processes whereby proteins are synthesised. It begins from deoxyribonucleic acids (DNAs) where genetic information is stably stored as a sequence of three-letter long codes forming from four types of nucleobases: A (Adenine), G (Guanine), C (Cytosine) and T (Thymine) or U (Urasil) in ribonucleic acids (RNAs). Then the genetic information is transcribed into RNA molecules, which in turn serve as templates for protein synthesis. The process where information flows from DNA to RNA is called "transcription" and the process where information flows from RNA to protein is called "translation" (O'Connor and Adams, 2010).

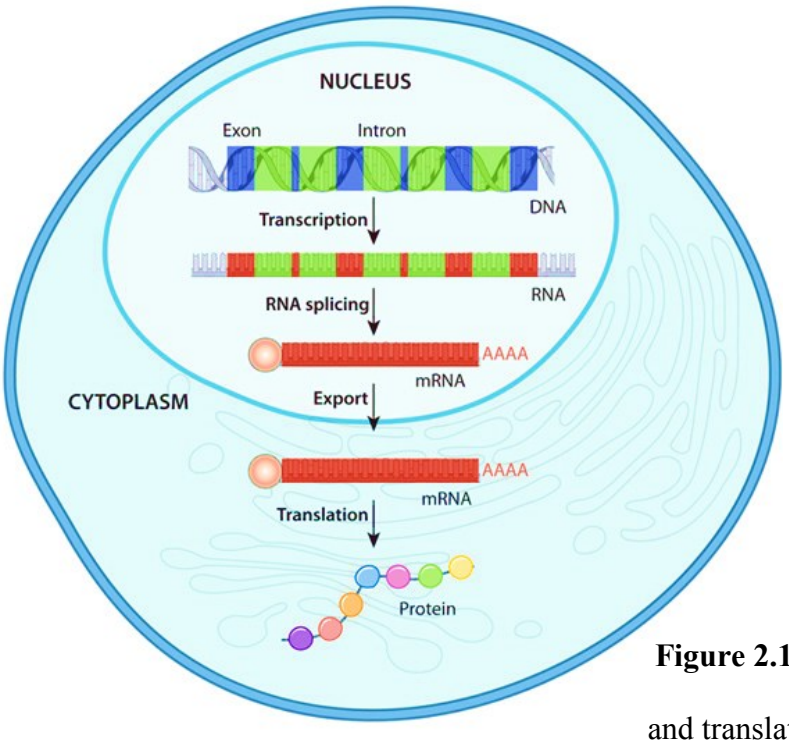


Figure 2.1.2 An overview of transcription and translation in eukaryotic cells. Adapted from (O'Connor and Adams, 2010).

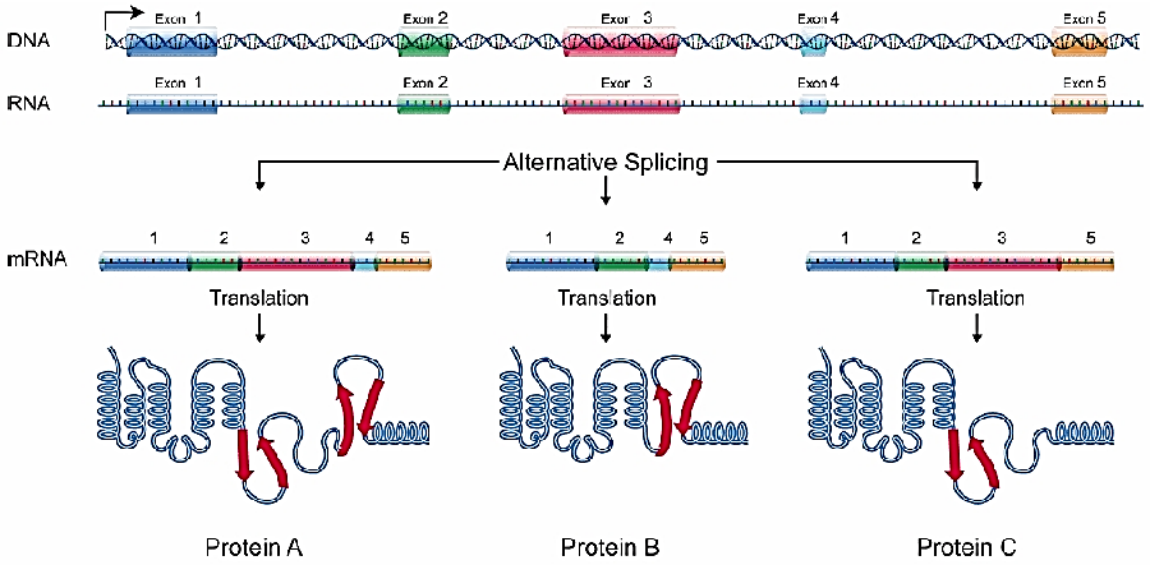


Figure 2.1.3 Alternative splicing. Adapted from (Clancy, 2008b).

DNA molecules have two strands bound with each other forming double helix chains. One strand is used at a time as a template for transcription. The template strand is called "the noncoding strand" while the coding strand refers to the strand not serving as a template for transcription but having the same sequence as the single-stranded RNA produced from transcription. However, there are times that both strands serve as templates given that they are at the same time transcripted in a different direction. The process of transcription starts once RNA polymerase, an enzyme that catalyses the synthesis of RNA, binds to a region on the DNA template strand, called promoter. The activity of RNA polymerase; whether it proceeds to transcription, is basically controlled by regulatory proteins acting in accordance with intracellular and extracellular stimuli. These proteins can be "activators" or "repressors". When these proteins bind to regions on the template strand, the former helps facilitate the activity of RNA polymerase while the latter inhibits the transcription. When transcription is initiated, the DNA double helix unwinds as the RNA polymerase adds nucleobases onto the RNA chain according to the nucleobases it reads on the template strand. The transcription terminates differently depending the type of RNA polymerase used in the process. The termination of

transcription can rely on either factors that helps unwind the bond between DNA and RNA or a termination sequence on the template strand, i.e. a stop codon (Clancy, 2008a, O'Connor and Adams, 2010).

The single-stranded RNA obtained from the transcription process is called the "precursor messenger RNA" (pre-mRNA) which is premature and contains sequences that will not be used for protein synthesis. "Introns" are the sequences that are removed from the pre-mRNA while "exons" are the sequences that remain in the pre-mRNA (Figure 2.1.2). The process of removing introns and chaining exons is called "splicing". Splicing occurs in many steps involving cleavage of the pre-mRNA at splice sites (conserved sequences at the two ends of introns), the attachment onto a complementary sequence within introns of small nuclear ribonucleoproteins (snRNPs) that catalyse the process, and introns looping out as well as covalently bonding between adjacent exons. Given that there are a large number of introns and exons in a single pre-mRNA molecule, different forms of mature messenger RNAs (mRNAs) arising from various combinations of exons can be achieved through splicing. This is so-called "alternative splicing" as can be seen in Figure 2.1.3 (Clancy, 2008b). Two forms of IgM immunoglobulin molecules, for example, are encoded by two different forms of mRNA molecules obtained through splicing though only a gene underlies the synthesis of these two mRNA molecules (Early et al., 1980).

It is worth noting here that not all RNA molecules after transcription become mRNA molecules which are later used for protein synthesis. Those RNA molecules not converted into mRNA molecules are called non-coding RNAs (ncRNAs). The ncRNA molecules include key RNA molecules, such as transfer RNAs (tRNAs) and ribosomal RNAs (rRNAs) used in translation, and microRNAs which play a role in regulating splicing and post-transcriptional regulation. It was suggested that there are thousands of ncRNAs existing, most of which have functionality while some of which might be non-functional (van Bakel et al., 2010).

mRNA molecules after splicing and before being transported to cytoplasm are modified through adding the 5-prime end cap and the polyA tail (4 adenosine molecules) as can be seen in Figure 2.1.2. The mature mRNA then undergoes the translation process, which involves complex molecules arising from ribosomes or rRNAs, initiation factors and decoders or tRNAs. These tRNA molecules have genetic codes corresponding to the codes on mRNA molecules, which are so-called anticodons. The tRNA molecules also carry amino acids corresponding to the codons. These amino acids are basically building blocks of protein molecules. The protein synthesis happens when amino acids are linearly bonded to yield a long-chain polypeptide. This process can selectively take place in either cytoplasm or rough endoplasmic reticulum (RER) where a larger number of ribosomal units are attached on its surface (Alberts et al., 2002).

The synthesised polypeptides chains or proteins need to be folded and modified before they become functional. There are a number of types of post-translational modification (PTM) which have difference characteristics and occur at different places inside cells. Protein folding and assembly normally take place at Endoplasmic Reticulum (ER). Only properly folded and assembled proteins are transported to Golgi Apparatus while unfolded or misfolded ones are detained in the ER (Lodish H, 2000). Therefore, overexpression of protein synthesis (Kober et al., 2012) as well as misfolding of synthesised proteins can potentially lead to the ER stress, in turn activating cellular responses in order to alleviate the stress including cell death (Sano and Reed, 2013, Reynaud, 2010).

Catabolism

There is a series of three main pathways underlying how sugar molecules, such as glucose, are broken down into smaller molecules. As illustrated in Figure 2.1.4, the cytoplasmic glucose is passed through the first pathway, glycolysis, in which the glucose is split into two

molecules of pyruvates. With a sufficient supply of oxygen, the pyruvate is transferred to the mitochondrion and is converted into a molecule of Acetyl CoA, containing two carbon atoms, before entering into the eight-stage citric acid cycle or TCA cycle (O'Connor and Adams, 2010).

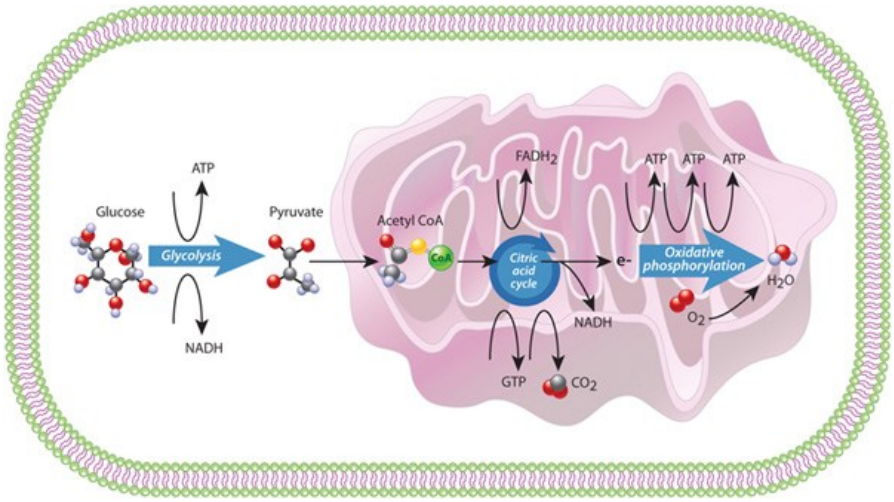


Figure 2.1.4 The breakdown of glucose into CO_2 and H_2O via three pathways of catabolism in eukaryotic cells: Glycolysis, Citric acid cycle (TCA cycle), and Oxidative phosphorylation. Adapted from (O'Connor and Adams, 2010).

Glycolysis and TCA cycle generate energy-containing molecules: ATPs, as well as electron carriers: NADH, $FADH_2$ and GTP. The electron carriers are then entered into the inner mitochondrial membrane where the final catabolic pathway, called the electron transport chain, takes place. Here, with the aid of transmembrane protein complexes, electrons are transferred from the electron carriers, across the membrane, to oxygen molecules (O_2) which in turn form molecules of water (H_2O). The difference of hydrogen ion concentration across the membrane causes the gradient of electrostatic potential inducing electron transferring. Every single electron transferred across the membrane, three molecules of ATP are achieved. It is worth noting that lack of O_2 availability can result in incomplete oxidation of pyruvate molecules. This generates several products other than CO_2. Lactate, for example, could be obtained via

glycolysis when there is need for cellular energy without sufficient supply of O_2 (O'Connor and Adams, 2010).

The structure of an antibody

Antibodies are protein molecules secreted from B lymphocyte cells to recognise antigenic determinants before disabling them via binding interactions. There are five classes, or isotypes, of antibodies: IgA, IgG, IgM, IgE and IgD. IgG is the most common one found in blood and extracellular fluid.

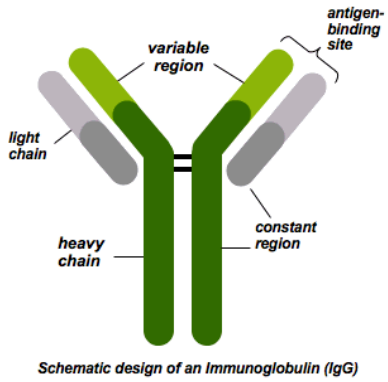


Figure 2.1.5 The structure of IgG antibody. Adapted from (http://www.jenabioscience.com).

Figure 2.1.5 illustrates the general structure of an antibody. The Y-shape structure is structured from two identical long-chain polypeptides (or called heavy chains) and two identical short-chain polypeptides (or called light chains). The two identical top ends of the antibody are where antigens bind to antibodies, or antigen-binding sites. These sites are so variable that a number of different binding sites exist to specifically capture various types of antigens. An antigen binding site contains a variable region and a constant region. It is relatively stable compared to the variable region (Alberts et al., 2002).

B lymphocyte cells can produce a number of molecules of antibodies which have an identical antigen binding site. These cells are therefore utilised to produce antibodies which have a single specificity to an antigen, called monoclonal antibodies (mAbs). By fusing a B lymphocyte cell (extracted from a mammal immune system) with a cancer cell (i.e. a myeloma cell), a resulting cell, so-called "hybridoma", which inherits characteristics of unlimited lifetime and antibody secretion from the B lymphocyte cell and cancer cells, can be achieved (Kohler and Milstein, 1975). This cell becomes a basis for the mAb production platform.

Glycosylation

After the translational process, proteins or antibodies are required to be structurally modified to generate their bioactivities, or so-called "the post-translational process". N-linked glycosylation is one of the post-translational modification processes, where an oligosaccharide side chain (N-acetyl-glucosamine, or NAG) is covalently linked to a polypeptide chain at asparagine building block before further modifications.

The process initially takes place at the ER. Here, a branch of oligosaccharide chains with 14 sugar molecules is covalently attached to asparagine building blocks in polypeptide chains. Then, the attached oligosaccharide chains are trimmed by several specific enzymes to gradually eliminate the 14 sugar molecules. This process ends at Golgi apparatus. Finally, additional sugars or amino-sugar molecules are added to enable the polypeptide chains to have bioactive structures (Shuler and Kargi, 2002).

It is worth discussing that eukaryotic cell-based antibody producing platforms do not always produce humanlike, N-linked glycosylation antibodies. The secreted antibodies with non-human like N-linked glycosylation patterns may lack desired bioactivity. Consequently, they could not reach antigenic targets and they may initiate unwanted responses from immune systems (Shuler and Kargi, 2002). The type of antibody producing platforms or cell hosts can indicate how human like N-linked glycosylation pattern is. Moreover, a number of culture conditions can affect glycosylation profiles (Rodrigues et al., 2010).

Cell cycle

Cell cycle is a basic physiological process that represents how cells divide and are increased in numbers through cell division. There are five phases in cell cycle progression as can be seen from Figure 2.1.6. The phase where cells perform normal physiological activities

and grow, called G_1 phase. However, in this phase cells can enter a state where the progress of cell growth as well as their physiological activities are halted. This is called G_0 phase. In this phase, cells can either resume their proliferation states as well as normal physiological activities, or undergo programmed cell death, subject to signals, such as nutrient availability. It can takes about 9 hours in G_1 phase for cells with a high growth rate (Alberts et al., 2002).

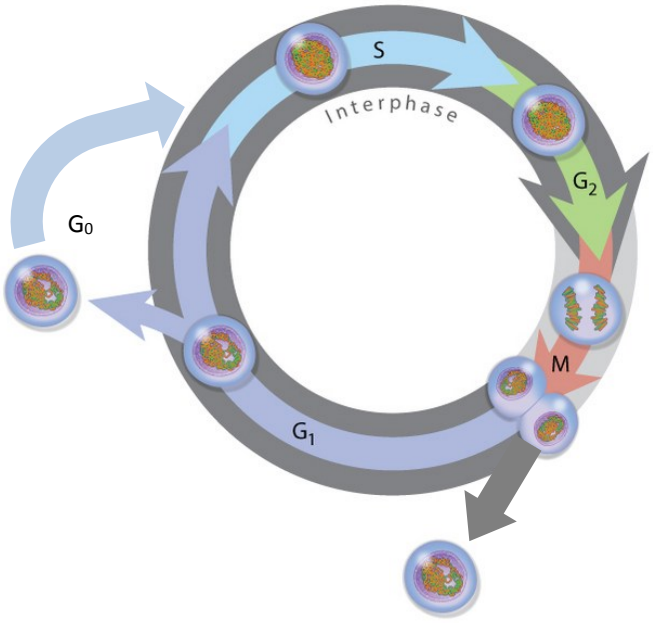


Figure 2.1.6 Cell cycle and DNA content according to each phase in the cycle. Adapted from (O'Connor, 2008).

Cells later undergo the synthesis phase, or S phase, where cells prepare to undergo cell division, or G_2 phase, and mitosis, or M phase, when receiving mitogenic signals. DNA molecules in the nucleus begin to duplicate in S phase (Figure 2.1.6). In typical animal cells, it takes around 10-12 hours in S phase, and much shorter (4.5 hours) for G_2 phase. G_1, S and G_2 phases can be all termed "interphase". Cells perform complete cell division and end the cell cycle at M phase where cells break down nucleuses and form two identical daughter cells, having identical genetic information (Alberts et al., 2002).

Cell death

Generally, cell death can be classified into two types according to causes and physiological processes underlying cell death: necrosis and apoptosis. Through signal transduction cascades, apoptosis allows cells to programme themselves to die in response to lethal signals. In contrast, cells die via necrosis as a result of severe culture conditions. Necrotic cells typically become swollen and are finally broken down to release intracellular contents (Arden and Betenbaugh, 2004).

It was established that more than four-fifths of cell deaths in a serum-free culture of Chinese Hamster Ovary (CHO) cells are caused by apoptosis (Goswami et al., 1999). This directly affects the number of viable cells as well as production of bio-therapeutics, such as mAb. In the next section, apoptosis is reviewed given its significant influence on the mammalian cell cultures for the production of bio-therapeutic proteins.

2.2 Apoptosis

2.2.1 Apoptosis pathways

There are two main apoptotic pathways: the death-receptor pathway or the extrinsic pathway, and the mitochondrial pathway or the intrinsic pathway (Hengartner, 2000). As shown in Figure 2.2.1, apoptosis can be initiated through the two pathways in response to intracellular and extracellular lethal signals. Caspase-3, an aspartate-specific cysteine protease, is the final executor of apoptosis. As a result of activation of caspase-3, apoptosis can ultimately happen. The activation of caspase-3 is also where the two pathways execute apoptosis. The inactive form of caspase molecules is called “procaspases”, which requires proteolytic cleavage to become active (Arden and Betenbaugh, 2004). In addition to caspase-3, caspase-6 and

caspase-7 are believed to be among final executioners of apoptosis in the apoptotic pathways (Majors et al., 2007).

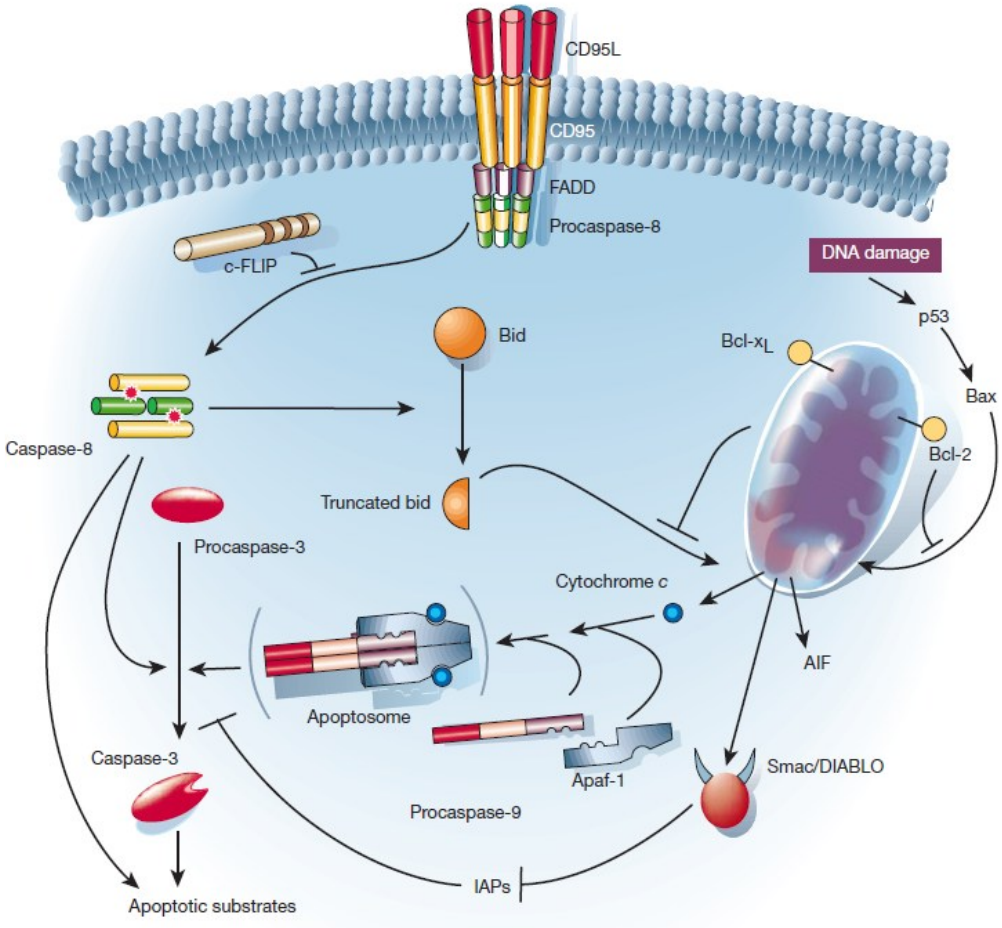


Figure 2.2.1 Apoptotic pathways: the death-receptor pathway and the mitochondrial pathway. Adapted from (Hengartner, 2000).

The death-receptor pathway is triggered by extracellular lethal signals. The signals are transduced through interactions between death receptors and death ligands, as can be seen in Figure 2.2.1. CD95 is for example one of the death receptors belonging to the tumour necrosis factor super-family (Arden and Betenbaugh, 2004). The death receptors lie across the cell membrane and become activated when binding to ligands. The recruitment of a protein FADD (Fas-associated death domain) is triggered by the activation of the death receptor. Procaspase-8 molecules, an initiator of apoptosis, are bound to FADD, forming a complex where (active)

caspase-8 molecules are then released. However, the activation of caspase-8 can be inhibited by the recruitment of c-FLIP molecules, an anti-apoptotic protein (Sprick and Walczak, 2004).

As illustrated in Figure 2.2.1, mitochondria are central to signal transduction in the intrinsic pathway. Pro-apoptotic proteins in this pathway can be divided into two groups: one residing in cytoplasm, such as Bax and Bad, and the other residing in the space between outer and inner mitochondrial membranes, such as cytochrome c and Smac/DIABLO. Under exposure to internal and/or external apoptotic signals, there is a morphological change in the structure of the outer mitochondrial membrane, which is associated with Bax molecules, as can be seen in Figure 2.2.1. This change affects integrity of the mitochondrial membrane and formation of transport channels; including the mitochondrial permeability transition pore (PTP) and voltage-dependent anion channels (VDAC), whereby release of pro-apoptotic proteins residing inside the mitochondria, especially cytochrome c, is triggered (Majors et al., 2007). Release of cytochrome c is a necessary event for activation of caspase-9. Apoptosome is a complex molecule that is composed of cytochrome c, procaspase-9 and apoptosis protein activation factor-1 (Apaf-1). It activates caspase-9, which in turn triggers activation of caspase-3 (Hengartner, 2000).

In the mitochondria-meditated apoptotic pathway, proteins in the Bcl-2 family play important roles in controlling the progression of apoptosis. These proteins can be categorised into three specific groups: anti-apoptotic members, such as Bcl-2 and Bcl-xL; pro-apoptotic members; Bax and Bak; and pro-apoptotic BH3-only members, such as Bid, Bad and Bim (Arden and Betenbaugh, 2004, Krampe and Al-Rubeai, 2010). Bcl-2 and Bcl-xL are essential survival factors that hinder pro-apoptotic effects of active Bax molecules on release of pro-apoptotic factors from mitochondria, as shown in Figure 2.2.1. They were found to suppress Bax and Bid translocation to the outer mitochondrial membrane, and thus limit the morphological change in mitochondrial membrane, which is required for the activation of

caspase-9 (Majors et al., 2007). Bid is essentially a link between the extrinsic and intrinsic pathways, where death signals from the ligand-receptors interactions can be transduced to the mitochondria-meditated apoptotic pathway. Activation of caspase-8 can induce Bid to become activated (truncated Bid). The truncated Bids then activate Bax molecules (Figure 2.2.1), which in turn induce the mitochondria-associated apoptosis (Hengartner, 2000).

It is worth discussing about the role of the pro-apoptotic BH3 proteins, including Bad, Bim, Noxa and Puma, which can be activated in accordance with cellular stresses, including DNA damage, shear stress and toxins, through several pathways (Majors et al., 2007). The role of Bad is to promote apoptosis via binding with Bcl-x_L on the mitochondrial membrane. However, when Bad is phosphorylated, it loses its ability to bind the anti-apoptotic proteins. Phosphorylation of Bad was found to be associated with Protein kinase B (Akt), which plays key roles in many pathways underlying cellular processes including cellular survival, cell cycle and metabolism. Despite under exposure of cellular stresses due to nutrient deprivation, UV-radiation, serum/growth factor withdrawal, and DNA damage, activation of Akt can phosphorylate Bad molecules, and ultimately inhibit apoptosis induction (Peso et al., 1997, Brognard et al., 2001, Hirai and Wang, 2001, Hwang and Lee, 2009). Jun N-terminal kinases (JNK) family, a group of cellular stress (UV radiation, heat and osmotic shock)-activated protein kinase enzymes, was also found to regulate apoptosis through interactions with the BH3-only proteins. In addition to caspase-8 activation, the tBid can be achieved through the activation of JNK, in turn promoting release of Smac/DIABLO and ultimately apoptosis via activation of caspase-9. JNK can also phosphorylate Bad, but at a different site to that by Akt. The phosphorylated Bad by JNK binds to Bcl-2, resulting in the inhibition of Bcl-2 activities (Dhanasekaran and Reddy, 2008).

As can be seen from Figure 2.2.1, p53; a tumour suppressor as well as a sequence-specific transcription factor, plays a role in the apoptotic pathway. It has been reported to play

important roles in growth arrest, cellular repair, and especially apoptosis through activation of the pro-apoptotic proteins. In general, p53 activities were reported to be controlled by a number of kinases underlying p53 phosphorylation required for its activation, and MDM2, the key antagonist of p53 found to normally mono-ubiquitinates p53 in order to stabilise its activities and to facilitate the degradation of p53 (Moll and Petrenko, 2003, Amaral et al., 2010). The cellular stresses (i.e. DNA damage) activate p53 (through stress kinases) and, at the same time, suppresses MDM2 activities, making p53 more vulnerable to be activated through kinase-associated phosphorylation. The activated p53 has been reported to induce apoptosis in several ways. One of them is to directly induce homo-oligomerisation of Bax as well as Bak molecules required for the activation of these molecules. These active molecules in turn translocate onto the mitochondrial membrane and induce the release of cytochrome c, and ultimately the intrinsic pathway. In addition, the activated 53 can also directly bind to Bcl-2 and Bcl-x_L to neutralise their anti-apoptotic effects (Speidel, 2010, Hengartner, 2000, Amaral et al., 2010).

Table 2.2.1 Target genes of p53 transcription factor.

p53 transcriptional targets	Roles	references
Bcl-2 family		
bax	+	[1], [2]
puma	+	[1]
noxa	+	[1]
bid	+	[1], [2]
bcl-2	-	[2]
bcl-x_L	-	[2]
Death Receptor		
DR5	-	[1], [2]
CD95, Fas or APO-1	-	[1], [2]
Adapters		
apaf-1	+	[1]
surviving	-	[2]
Caspases		
casp8	+	[3]

+; up-regulation, -; down-regulation, [1] ;(Schuler and Green, 2005), [2] ;(Speidel, 2010) and [3] (Liedtke et al., 2003).

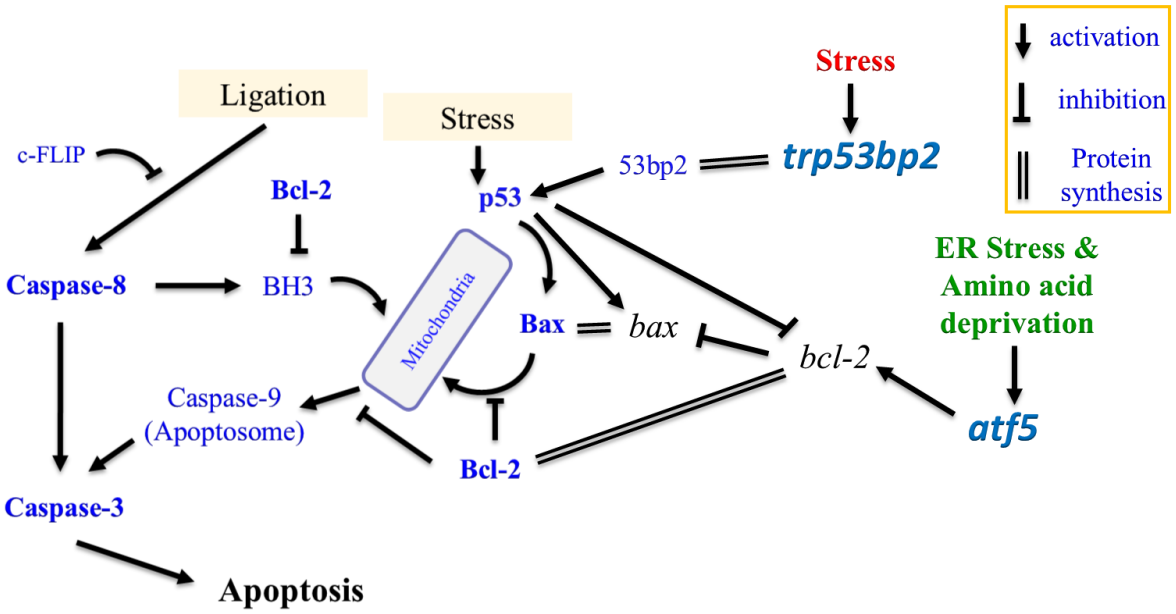


Figure 2.2.2 The association of *atf5* and *trp53bp2* genes with the apoptotic pathways.

In addition to the transcription-independent pro-apoptotic function, the activated p53 can basically regulate apoptosis predominately through transcriptional activities (Amaral et al., 2010). There are a number of transcriptional targets of p53 as can be seen from Table 2.2.1. Among those are genes representing the BH3 pro-apoptotic proteins including *bax*, *noxa* and *puma*. In addition, p53 can also up-regulate the death receptor pathway associated genes including *CD95*, *Fas* and *casp8*. In addition to the transcriptional targets of p53 as shown in Table 2.2.1, there are a number of genes that were found to be relevant to the transcription-independent pro-apoptotic function of p53. The genes of activating transcription factor 5 (*atf5*) and transformation related protein 53 binding protein 2 (*trp53bp2*) were among those, which were reported to be significantly up-regulated during the culture of a mammalian cell line and their unregulated levels were suggested to be linked with cellular stresses (Browne and Al-Rubeai, 2011b). As can be seen from Figure 2.2.2, the level of *atf5* expression was believed to be dependent on the ER stress as well as amino acid deprivation (Watatani et al., 2007, Zhou et al., 2008) while *trp53bp2* expression was suggested to be associated with cellular stresses (Browne and Al-Rubeai, 2011b). The up-regulation of *atf5* activates *bcl-2* (gene) expression

(Dluzen et al., 2011), providing a link to the apoptotic pathway via down-regulation of *bax* (gene) and Bcl-2 and Bax expression (Paul-Samojedny et al., 2005). 53BP2, the p53 binging protein 2 encoded by *trp53bp2*, was found to induce apoptosis through binding to p53 as well as Bcl-2 (Naumovski and Cleary, 1996, Samuels-Lev et al., 2001, Kobayashi et al., 2005). Given the targets of p53 (Table 2.2.1) and 53BP2, a link between *trp53bp2* and the apoptosis pathway could be drawn (Figure 2.2.2).

In addition to the apoptosis-associated role, p53 can also play regulatory roles in many cellular processes. Among those is control of cell cycle progression, where p53 was found to target one of important cell cycle regulator genes; CDKN1A (*p21*) encoding p21 protein (cyclin-dependent kinase inhibitor 1) (Li et al., 1994). This protein underlies cell growth arrest through directly interactions with cyclin-CDK complexes, in turn inhibiting the activity of these complexes required for the cell cycle phase transition (Goubin and Ducommun, 1995, Cazzalini et al., 2010). It was reported that p53 activation in response to DNA damage meditates the activity of p21, which then inhibits the activity of cyclin E/CDK2 complex, required for the G_1 to S cell cycle phase transition, and ultimately causing cell cycle arrest at G_1 phase (El-Deiry et al., 1994). In addition, p21 activation in response to cellular stresses was also found to regulate the G_2 cell cycle phase checkpoint through suppressing the activation of cyclin A/CDK1/2 complexes as well as cyclin B1-CDK1 complex, leading to cell cycle arrest at this phase (Charrier-Savournin et al., 2004). Both p53 and p21 expression levels were found to be up-regulated by the exposure to hypothermia (Kaija et al., 2015) and hyperthermia (Ohtsubo et al., 2000, Abe, 2001), suggesting the regulatory role of p53/p21 pathway in apoptosis and cell cycle progression in response to the temperature-associated stress. Given its impact on cell cycle regulation, it was suggested that p53 could also provide the anti-apoptotic effect through the p21-associated pathway in response to cellular stresses, despite p21 being

also found to be associated with a number of pathways underlying cellular processes other than cell cycle arrest (Cazzalini et al., 2010).

2.2.2 The ER stress-associated apoptotic pathway

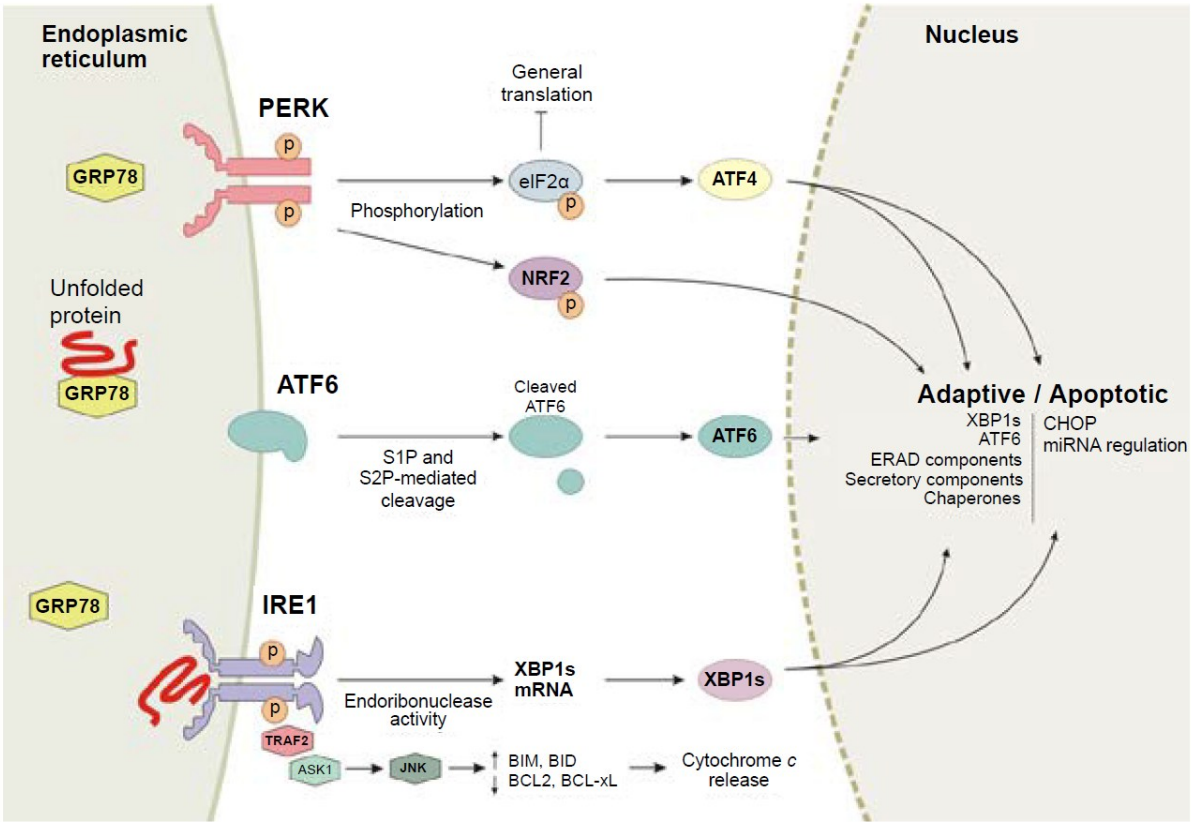


Figure 2.2.3 The upstream signalling of ER-stress associated pathways. Adapted from (Logue et al., 2013).

In addition to the two apoptotic pathways as discussed above, apoptosis can be induced by the ER-associated stress. This typically arises from increased protein synthesis as well as misfolding of proteins to the extent that protein chaperones (the protein folding assistants) cannot manage, though it can be developed from other factors (Tabas and Ron, 2011). In response to the ER stress, cells develop the unfolded protein response (UPR) in order to manage the accumulation of unfolded proteins within the ER lumen to relieve the stress (Logue et al., 2013). The UPR basically relies on activation of three upstream factors, including protein

kinase RNA (PKR)-like ER kinase (PERK), activating transcription factor 6 (ATF6), and inositol-requiring enzyme 1 (IRE1). These three proteins sense the ER stress (due to unfolded/misfolded protein accumulation), and later become active (via detaching the GRP78 (or BIP) chaperone protein) and proceed the UPR via their own pathways. The pathways are illustrated in Figure 2.2.3.

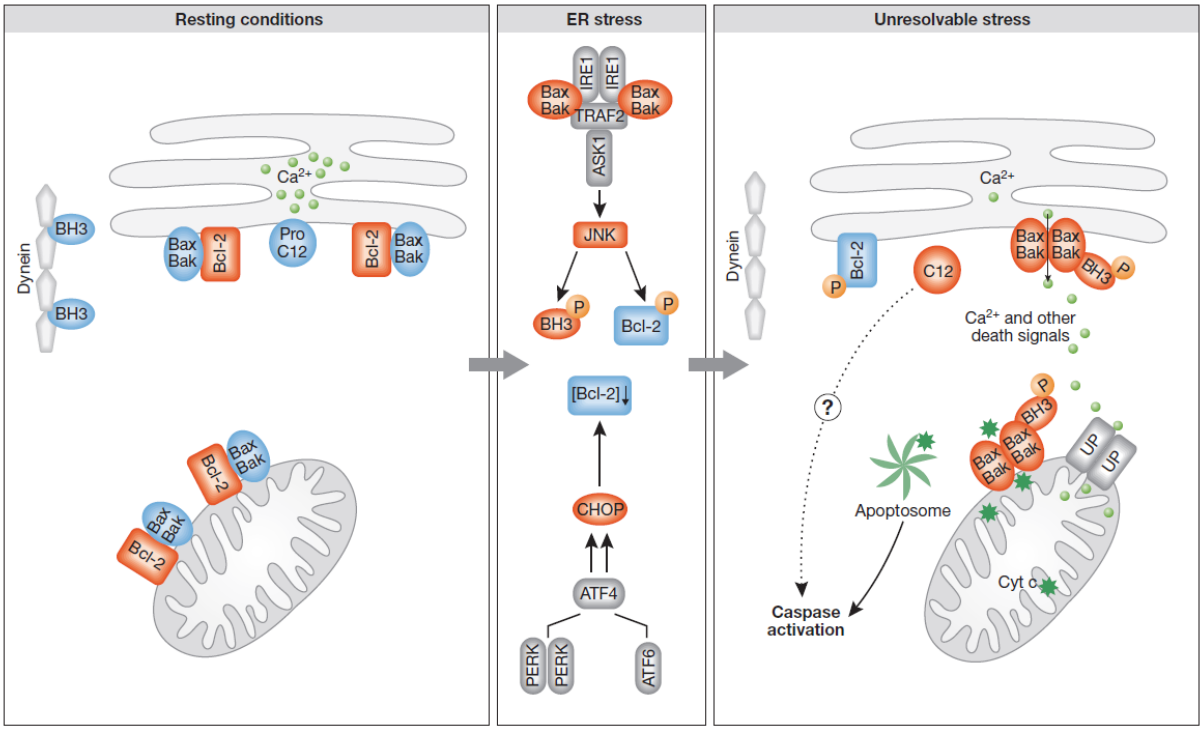


Figure 2.2.4 Caspase activation through the ER-stress associated pathway. Adapted from (Szegezdi et al., 2006).

As can be seen from Figure 2.2.3, the active IRE1 promotes splicing of the transcription factor called XBP-1 in response to unfolded protein accumulation. This form of XBP-1 (spliced) can activate transcription of various proteins underlying cellular activities required to restore ER homeostasis (i.e. ER chaperone, ER associated degradation, secretory pathway-associated species as well as transcription factors: pro-apoptotic CHOP and XBP-1 itself) (Logue et al., 2013). Due to the dissociation of GRP78, PERK undergoes dimerization and autophosphorylation to become active. The active PERK then phosphorylates eIF2α which can

in turn inhibit translation. The active eIF2α also activates ATF4 which later translocates to the nuclease and triggers transcription of various proteins underlying amino acid biosynthesis, chaperones, secretory pathways and pro-apoptotic CHOP. It is worth noting here that eIF2 was reported to also affect the ATF5 mRNA level (Zhou et al., 2008). ATF6 becomes active in response to the ER stress through translocation to Golgi apparatus and cleavage by two proteases: S1P and S2P. The active ATF6 then translocates to the nuclease and drives transcription of proteins; including chaperones, ER degradation (EDEM1), CHOP and XBP1, providing pro-survival impact in response to the ER stress (Szegezdi et al., 2006, Logue et al., 2013). It is worth noting that these three pathways take place selectively and in different timing; for example the simultaneous activation of the three pathways is not necessary to always take place in response to the severe ER stress (Tabas and Ron, 2011).

The UPR appears to be a pro-survival mechanism in response to the ER stress given its activation targets, however, UPR can change from pro-survival to pro-apoptotic under exposure to a persistent and severe ER stress (Logue et al., 2013). Central to the ER-stress associated apoptotic pathway is release of calcium ions (Ca^{2+}) from the ER, causing change in cytoplasmic Ca^{2+} levels, which in turn triggers apoptosis via activation of caspase-12, the mitochondrial apoptotic species, and ultimately activation of caspase-3 (Majors et al., 2007). The link between the upstream signalling of UPR-associated pathway and the release of Ca^{2+} is the activity of the Bcl-2 protein family, which can be controlled in accordance with the activation of UPR-associated pathways. CHOP (known as a growth arrest and DNA damage associated gene) and TRAF2 (TNF receptor associated factor 2) were reported to activate apoptosis in response to the ER stress. CHOP, activated by the UPR-associated pathways, was found to down-regulate Bcl-2, making its concentration reduced (Szegezdi et al., 2006). As can be seen in Figure 2.2.4, activation of IRE1 recruits TRAF2, triggers phosphorylation involving ASK1, and in turn activates JNK that can phosphorylate Bcl-2 as well as Bcl-xL. The

phosphorylated Bcl-2 by JNK loses the anti-apoptotic ability (McCullough et al., 2001). Pro-apoptotic effects can also be achieved through the phosphorylated Bid and Bim by JNK (Szegezdi et al., 2006). As can be seen from Figure 2.2.4, without exposure to the ER stress, Bax and Bak are bound to Bcl-2, which is their inactive state; while the activation of Bim (BH3) is suppressed by attaching to cytoskeletal dynein. Once Bcl-2 and Bim are phosphorylated by JNK (as well as Bcl-2 is down-regulated by CHOP), Bcl-2 is unable to inhibit the Bax and Bak activity. In the meantime, Bim translocates to Bax and Bak and helps promote their pro-apoptotic activities. This pro-apoptotic activities of Bax and Bak enable the ER Ca^{2+} flux to be uncontrolled, ultimately causing the induction of apoptosis (Szegezdi et al., 2006).

2.3 Mammalian Cell Cultures for production of mAbs

Mammalian cell culture systems are widely utilised for manufacture of bio-therapeutics, including production of mAb, given the fact that mammalian cell hosts have potential to synthesise therapeutic proteins possessing the pattern of post-translational modifications compatible with the human immune system (Werner et al., 1998). Over the last decade, there has been a steadily constant increase in global demand for mAb; almost 30 types of mAbs were commercialised with the total sale value of 18.5 billion dollars in 2010 and the sale is also expected to be continuously increasing within the next few years (Buss et al., 2012, Elvin et al., 2013). This is greatly contributed to therapeutic capability of mAbs to efficiently treat chronic diseases, such as cancers (Buss et al., 2012). The increase in demand for mAbs draws attention to improve performance of mammalian cell culture systems toward a higher quantity as well as a better quality of mAb produced.

2.3.1 Mammalian cell lines

Emergence of hybrid cells (i.e. hybridoma cells) paves the way for production of mAbs. The production of mAbs was initially achieved by *in vivo* cultures of the hybridoma cell line, which is derived from fusion of a mouse myeloma cell and spleen cells from an immunised BALB/c mouse (Kohler and Milstein, 1975). Later, *in vitro* cultures of hybridoma cell lines were developed, where cell growth as well as mAb titre were improved. However, the relatively low affinity of mAbs was often obtained in the *in vitro* cultures (Moroney and Plückthun, 2005). Humanised mAbs can be also achieved from a hybridoma cell line that is derived from transgenic mouse spleen cells or primary human B cells (Davis et al., 1999). NS0 and Sp2/0 cell lines are also the results of the hybridoma technology. These cell lines basically share the same origin, which is a BALB/c mouse plasmacytoma cell and spleen cells.

In addition to the hybridoma technology, there are other technologies for the development of cell hosts for mAb production. Chinese hamster's ovary cells or CHO cells are derived from a Chinese hamster's ovary biopsy. These cells have become a common platform for production of mAbs since its biological characteristics are well understood. In addition, human cell lines were utilised in order to obtain mAbs with human-like glycosylation as well as other posttranslational modification patterns. For example, HEK-293 is derived from a human embryonic kidney while PER.C6 originates from a human retinal cell.

The mammalian cell lines share similar characteristics, which show that they are suitable for bio-therapeutic production applications. These include capability to grow in a non-aggregated condition (i.e. in a suspension culture), capability to generate desired posttranslational modifications, capability to robustly grow and achieve a high level of final mAb titre, and capability to adapt themselves to various culture conditions (Whitford, 2006, Chu and Robinson, 2001). It is worth mentioning that there is difference in metabolic activities

as well as characteristics among these cell lines, although these cell lines are derived from a similar origin (i.e. between NS0 and Sp2/0 cell lines).

2.3.2 Glutamine synthetase (GS) expression systems

Glucose and glutamine are generally limiting substrates providing carbon as well as nitrogen sources for cell growth and bio-synthesis. Glutamine, in addition to providing a nitrogen source, is essentially required for anaplerotic activities in order to support the cellular energy production (i.e. in TCA cycle). Glutamine is a non-essential amino acid; therefore, it can be synthesised by cells. The enzyme that catalyses the reversible synthesis of glutamine is GS. The mechanism of this reaction involves hydrolysis of ATP and phosphorylation of glutamate by the enzyme-associated intermediate before being combined with ammonia to form glutamine (Barnes et al., 2000b).

The development of the GS expression system is based on the fact that cells with a very low expression level of endogenous GS need 1) an external source of glutamine or 2) an enhanced GS reaction activity by exogenous GS in order to survive and perform normal cellular activities. The selection of cells can be achieved through incorporating the GS gene in a plasmid vector containing heterologous protein expression, and then culturing the cells with transfection of the plasmid vector in glutamine-free media. Surviving cells in glutamine-free media represent ones that successfully take up the plasmid, which can be also inferred that they are capable to express the heterologous protein (Cockett et al., 1990, Bebbington et al., 1992, Barnes et al., 2000b). Methionine sulfoximine (MSX) can be used for the further selection of cells that express a high level of GS, given that MSX specifically and irreversibly inhibits GS (Brown et al., 1992, Bebbington et al., 1992). The low concentration of MSX was used; 10-100 μM for GS-NS0 cells and 250-500 μM for GS-CHO cells, in order to insert a reasonable level of GS inhibition, allowing to select cells with a relatively higher expression of GS gene.

Given that the GS gene is incorporated within the same plasmid vector as the heterologous protein gene, the high-expression GS cells achieved through the selection by the addition of MSX should simultaneously express a high level of the heterologous protein, allowing us to achieve the increase in production/productivity of the heterologous protein (Barnes et al., 2000b).

It is worth noting here that the presence of MSX can also affect cellular processes apart from the activities of GS. It was reported that cell growth and nitrogen assimilation, and thus cellular protein and nitrogen contents, were reduced in marine microalga *Chlorella autotrophica* due to the presence of MSX at 5 mM (Ahmad and Hellebust, 1985). In addition, MSX was found to increase the activities of ornithine decarboxylase (ODC), which is the key enzyme catalysing the rate-limiting reaction required for polyamine synthesis (Di Giacomo et al., 1997). The polyamines play essential roles in fundamental cellular processes; including DNA stabilisation, transcription, translation and semiconservative DNA replication. Moreover, the cell fate was found to be subject to the polyamine levels; apoptosis can be induced by a prolonged decrease in the polyamine levels under an exposure to oxidative stresses while increased polyamine levels due to ODC overexpression can trigger apoptosis (Pendeville et al., 2001). Therefore, these effects of MSX have to be taken into account when MSX is added into the cultures to achieve the GS inhibition.

The GS system is commonly used in CHO cells and NS0 cells. NS0 cells typically have as low endogenous GS level as phenotypical GS minus; therefore, they are favoured over CHO cells though the GS system has been extensively applied in CHO cells. As above discussed, the level of MSX used in the selection process of NS0 cells is much less than that of CHO cells. Compared to other systems (i.e. DHFR system), the GS system typically requires fewer copies of the plasmid vector (4-10 copies) in order to achieve stable and high production of the heterologous protein. In the GS system, glutamine can be intracellularly synthesised. Ammonia

is depleted in the synthesis process, providing a significant side benefit to the culture system where deleterious effects of toxic metabolite, especially due to ammonia accumulation can be avoided.

2.3.3 Modes of mammalian cell cultures

Given that microbial fermentation has long been established, modes of operation applied in cultures of a variety of mammalian cell lines basically originate from those used for microbial fermentation. This section reviews the most common modes of mammalian cell cultures that are industrially utilised for manufacture of bio-therapeutic proteins.

Batch culture

It is a basic and discontinuous mode of cell cultures. This mode allows cells to grow without an addition of nutrients as well as removal of metabolic by-products during cultivation. Cell growth as well as metabolism, thus, are limited to the level of nutrients at the beginning of cultures. Given that cell proliferation can suffer from osmotic impacts as well as toxic by-product accumulation, the initial concentration of substrates is typically set at a relatively low level. Consequently, batch cultures usually achieve a relatively low cell concentration, and thus limited final titre of secreted proteins (in the range of 1-50 mg/L). However, this mode is widely utilised for the production of therapeutic proteins because of its simple configuration and operation (Ve´liz et al., 2008).

Fed-batch culture

It is basically the batch culture with feeding stream(s) of nutrient(s). Therefore, a relatively higher cell concentration as well as final secreted protein titre can be achieved (more than 10 g/L of secreted proteins can be achieved (Robinson et al., 1994, Whitford, 2006, Pybus et al., 2014)). In addition, given that operation and configuration of fed-batch cultures are

relative moderate, this mode becomes the most common platform for manufacture of therapeutic proteins (Chu and Robinson, 2001). Prolonged culture viability achieved in the fed-batch cultures leads to a longer culture lifetime. This causes secreted proteins to stay in the culture for a longer time, and these proteins can be negatively affected by proteases and glycosidases released from lysed cells or dead cells (Goochee and Monica, 1990). In addition, a higher level of metabolic by-products, such as ammonia and lactate, is obtained in the fed-batch culture. This can negatively affect both the quality and quantity of secreted proteins.

Continuous culture

It is cell cultures with continuous feeding stream(s) of nutrient(s) and continuous removal stream(s) of cell suspension. The flowrate of inlet and outlet streams has to be equal to each other so that culture volume remains constant and the cultivation is allowed to reach a steady state, where cellular and metabolic activities are measured. However, given that cells are continuously removed, a relatively lower cell concentration, and thus a lower secretion of therapeutic proteins, are achieved in this mode of cultures. Given its relatively more complicated configuration and relatively lower production of heterologous proteins, this mode is still not mature as compared to batch and fed-batch modes of culture.

Perfusion culture

It is an improved version of the continuous model of cell cultures. Cells are separated from the outlet stream(s) and returned to the culture, allowing maintaining a high level of cell concentration, and thus a high level of protein secretion. To date, this mode of cell cultures achieves the highest production and productivity of secreted proteins and is becoming more popular, both experimental and industrial scales. However, despite its advantages over other modes of cultures, its configuration as well as operation are highly complicated, making it

difficult to be practically applied for large scale production of therapeutic proteins (Ve´liz et al., 2008).

2.3.4 Limitations of mammalian cell cultures

Compared to cultures of prokaryotic cells; such as algae as well as bacterial systems, as well as some eukaryotic systems; including yeast and fungi, to handle cultivation of mammalian cells is far more challenging, given that mammalian cells contain more complex intracellular structures as well as more intricate biochemical reactions involved. Hauser and Wagner (1997) pinpointed key characteristics of mammalian cell cultures for production of biopharmaceuticals as compared to those of prokaryotic cells as well as yeast and fungi as follows:

- ✓ Lower cell growth rates.
- ✓ Lower rates of production of desired products.
- ✓ More sensitive to chemical milieus; such as levels of nutrient supply, metabolites, growth factors, etc.
- ✓ More fragile to physical milieus due to having no cell wall.

Given the above list, behaviour of mammalian cells, and thus culture performance, highly depend on cultivation conditions. The following is the most important parameters that significantly affect culture performance;

- ➢ Initial concentrations of compositions in culture medium, including sugar(s), amino acids, inorganic ions and other growth factors.
- ➢ Dissolved oxygen, both its concentration and how it is supplied in the culture.
- ➢ Levels of toxic metabolite accumulation, especially lactate and ammonia.
- ➢ Sheer stress, temperature, pH as well as osmotic pressure.
- ➢ Feeding strategy for the fed-batch system.
- ➢ The number of viable cells and the secreted protein concentration.

The effect of these culture parameters on cellular activities as well as culture performance can also differ among cultures of different lines of mammalian cells. Given the cell line specific manner, to establish a generalisation for optimal culture parameters and operating conditions is one of the greatest challenges facing biotechnology community.

2.4 Temperature effects on culture performance

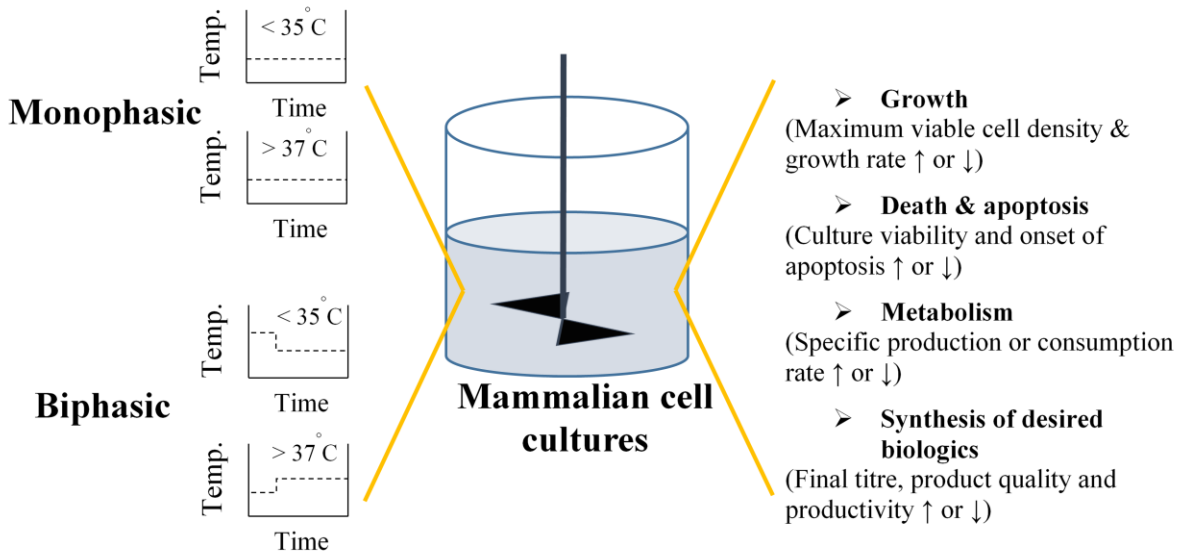


Figure 2.4.1 Literature review for the temperature effect on cellular activities in the mammalian cell cultures.

Culture temperature is one of the most important operating culture parameters. Given that culture temperature can be promptly measured and real-time manipulated during the cultivation, it draws attention to investigation of its impact on culture performance and identification of an optimal culture temperature profile for production of therapeutic proteins. The literature survey in this section focuses on impact of culture temperature on cellular activities. As illustrated in Figure 2.4.1, the effect of hypothermia (<35°C), hyperthermia (>37°C) and biphasic temperature profiles where temperature is shifted to hypothermia or

hyperthermia on especially cell metabolism (synthesis of desired biologics), cell cycle progression and apoptosis induction is reviewed.

2.4.1 Hypothermic conditions

37°C is the physiological temperature level where cellular systems perform their normal activities. However, growing cells at temperature levels lower than the physiological one, or hypothermia (<35°C), appears to influence cell proliferation and viability, and thus final titre and productivity of secreted proteins. It was reported that culture viability was prolonged when growing hybridoma cell lines under hypothermic conditions, despite achieving lower final mAb titre as well as productivity as compared to the cultures at 37°C (Reuveny et al., 1986, Sureshkumar and Mutharasan, 1991, Barnabé and Butler, 1994). The similar effects of hypothermia were also observed in the cultures of other mammalian cell lines under sub-physiological temperatures. A lower maximum cell density, prolonged culture viability as well as no significant improvement in productivity were achieved in the cultures of BHK cell (Weidemann et al., 1994), CHO cell (Yoon et al., 2003a, Yoon et al., 2006), GS-NS0 cell (Swiderek and Al-Rubeai, 2007) and the human host cell F2N78 (Seo et al., 2013). However, in the culture of GS-NS0 cells, hypothermia (33°C) did not affect the maximum cell density as well as the specific productivity, compared to the control culture (37°C).

On the contrary, increases in specific productivity of secreted proteins were observed in mammalian cell cultures under hypothermic conditions, although inhibition of cell growth and culture viability prolongation were still observed. The culture of CHO cell lines under hypothermia conditions (< 35°C) demonstrated a higher level of specific productivity while cell proliferation was arrested (Fogolín et al., 2004, Fox et al., 2005, Furukawa and Ohsuye, 1998, Shi et al., 2005, Rodriguez et al., 2005, Vergara et al., 2014). By adapting CHO cells for hypothermic conditions (30°C, 33°C and 35°C) before experiments at the corresponding

hypothermic temperatures, increases in specific productivity were achieved, however, volumetric productivity was lower than the culture at 37°C due to lower maximum cell concentrations (Trummer et al., 2006).

It was suggested that production of desired proteins and their mRNA levels could be correlated. Furukawa and Ohsuye (1998) observed an increase in both the secreted protein-associated mRNA level and production of the secreted protein in the hypothermic culture. Yoon et al. (2003) and Fox et al. (2005) also agreed on the correlation between the mRNA level and the level of desired protein production, given that they observed an increase in erythropoietin (EPO) and interferon–γ, respectively, productivity with an increase in its protein-associated mRNA levels (Fox et al., 2005, Yoon et al., 2003b). However, later Marchant et al. (2008) proved that the correlation does not hold true for the cultures of GS-NS0 and GS-CHO cell lines, given that cB72.3 mAb productivity did not increase as its corresponding mRNA level was found increased by temperature shifts to 32°C (Marchant et al., 2008).

The effect of hypothermia on control of cell cycle progression was also investigated so that detailed mechanistic explanations behind observed changes in cell proliferation as well as synthesis of desired proteins could be revealed. Yoon et al. (2003) and Trummer et al. (2006) suggested that CHO cells were arrested at G_1/G_0 phase in response to hypothermia, causing a lower specific growth rate as well as prolonged culture viability. This is in good agreement with the observation made by Bloemkolk et al. (1992), showing that the hybridoma cell line S4B6 spent longer time in G_1 cell cycle phase due to the hypothermic condition (34°C). Given that there was no significant difference in productivity as compared to the culture at 37°C, they suggested that arrested cells at G_1 phase may not benefit mAb secretion (Bloemkolk et al., 1992). Later, Shi et al. (2005) demonstrated that circa 50% of CHO cells were arrested at G_2/M phase rather than G_1/G_0 phase in the culture at 30°C (Shi et al., 2005). The culture of GS-NS0

cell line under a strong hypothermic condition (22°C) showed a sudden increase in cell fraction at G_2 phase as well as an elevated level of *Cdc2* (G_2/M regulator) gene expression, suggesting cell cycle arrest at G_2 phase (Swiderek and Al-Rubeai, 2007). However, Fox et al. (2005) observed an increase in cell fraction at S phase with an increase in specific productivity, suggesting that the productivity might not be associated with cell proliferation arrest, but actively proliferating states. This was later supported by further analysis of experimental data performed by Chong et al. (2008), showing that there was a correlation between cell fraction at S phase and specific productivity (Chong et al., 2008).

Relationships between apoptosis and hypothermia were established. A significant lower degree of apoptosis was achieved when growing the CHO cell line producing antibody-IL-2 fusion protein at 30°C. In addition, this hypothermic culture showed a delay in the onset of apoptosis for 48 hours (Shi et al., 2005). It also reported that hypothermic conditions (at 22°C and 34°C) enabled GS-NS0 cells to suppress apoptosis, as indicated by the fraction of apoptotic cells in the culture at 22°C after 120 hours of the culture being equal to that of the culture at 34°C after 72 hours and that of 37°C after 48 hours of the cultures (Swiderek and Al-Rubeai, 2007). However, this might be because the cultures under hypothermic conditions experienced nutrient deprivation at a later time than the culture at 37°C as a result of decreases in specific nutrient consumption. The culture of the human host cell line demonstrated that culture viability was preserved in the culture at 33°C while the culture at 37°C rather allowed cells to die faster (Seo et al., 2013).

Hypothermia was found to affect cell metabolism, as indicated by changes in the specific rates of consumption/production of metabolites and nutrients, including glucose, lactate, ammonia and key amino acids. Generally, there was a reduction in glucose consumption rates, and thus lactate production rates, in cultures under hypothermic temperatures of hybridoma cell lines (Reuveny et al., 1986, Sureshkumar and Mutharasan,

1991, Barnabé and Butler, 1994), BHK cell line (Weidemann et al., 1994), CHO cell line (Trummer et al., 2006), GS-NS0 cell line (Swiderek and Al-Rubeai, 2007) and human cell line, F2N78 (Seo et al., 2013). Sureshkumar and Mutharasan (1991) reported that there was also a decrease in the yield of lactate over glucose in the hybridoma cell culture at hypothermic temperatures. However, Barnabé and Butler (1994) demonstrated that the yield of lactate over glucose in the culture of another hybridoma cell line did not significantly change with decreases in culture temperature, suggesting that glucose metabolic pathway could not be influenced by hypothermic conditions. The effect of hypothermia on glutamine consumption rates, and thus production of ammonia was found to be variable. Barnabé and Butler (1994) showed that specific rates of glutamine consumption as well as ammonia production rates decreased in the culture of hybridoma cell line at hypothermic temperatures. However, the specific rate of glutamine consumption was found to be increased as the temperature decreased in the CHO cell culture, although the specific rate of ammonia was reduced. It was suggested that glutamine consumption might be substituted for a decrease in glucose utilisation in hypothermic conditions (Trummer et al., 2006). Seo et al. (2013) reported that there was no significant difference of the specific utilisation rate of glutamine (and so the specific generation rate of ammonia) between the cultures at 37°C and at 33°C. Recently, it was suggested that hypothermia affects cell metabolism at the transcriptional processes, given that there was a significant change in expression of metabolic pathway-associated genes (i.e. glycolysis and pentose phosphate pathway-associated genes) in the cultures of CHO and GS-NS0 cell lines (Baik et al., 2006, Swiderek and Al-Rubeai, 2007).

Hypothermia was generally found to preserve the quality of secreted bio-therapeutic proteins in mammalian cell cultures. The quality of secreted proteins was found to benefit from hypothermic conditions indicated by the preserved degrees of sialylation in the cultures of CHO cell lines (Yoon et al., 2003b, Kaufmann et al., 2001), and the reduced degree of secreted

protein aggregation in the culture of the CHO cell line producing *β*-interferon (Rodriguez et al., 2005). However, in the culture of the human host cell line F2N78 at a hypothermic condition did not significantly affect the glycosylation pattern of produced mAb, compared to the control (Seo et al., 2013). Contrary to results from other studies, Epo-Fc sialylation in the cultures of CHO cell line at 30°C and 33°C was found to be worse compared to the control culture (Trummer et al., 2006).

2.4.2 Hyperthermic conditions

Given that hyperthermia (> 37°C) is basically the opposite condition to hypothermia, it can be hypothesised that hyperthermia has the opposite impact on culture performance to that of hypothermia. The specific consumption rate of glucose, and thus the production rate of lactate, were found to be enhanced in the mild hyperthermic cultures of hybridoma cell lines (Sureshkumar and Mutharasan, 1991, Barnabé and Butler, 1994) and CHO cell line (Trummer et al., 2006). The specific glutamine consumption rates, and thus the production rates of ammonia, were also increased in the culture under hyperthermic conditions (Barnabé and Butler, 1994, Trummer et al., 2006). Compared to the cultures at 37°C, the hyperthermic cultures resulted in a lower maximum cell density, causing increases in specific productivity with a lower final titre of secreted proteins (Sureshkumar and Mutharasan, 1991, Barnabé and Butler, 1994). However, the cultures of another hybridoma cell line and a CHO cell line at a hyperthermic temperature showed reductions in productivity, despite a lower maximum cell concentration. It was also suggested that hyperthermia has no significant effect on cell cycle progression, given that there was no significant change in cell cycle population distribution profiles, compared to the control cultures (at 37°C) (Bloemkolk et al., 1992, Trummer et al., 2006). In addition, it appeared that hyperthermia had no significant effect on sialylation in the culture of CHO cell line (Trummer et al., 2006).

The impact of hyperthermia on cellular activities at a transcriptional level was studied. The level of DNA synthesis was increased in the hyperthermic culture of human bone marrow-derived stromal cells (BMSCs), suggesting a faster progression of cell proliferation. However, under the same condition, growth of human osblast-like osteosarcoma-derived MG-63 cells was arrested (Shui and Scutt, 2001). In addition, the level of cyclin D1, which plays a regulatory role in progression of cell cycle through controlling G_1 checkpoint, was elevated as the culture temperature increased, suggesting that the hyperthermia-associated acceleration of cell proliferation involves induction of cyclin D1 synthesis (Han et al., 2002). Anti-apoptotic pathways were suggested to be a cellular mechanism in response to hyperthermia (Park et al., 2005). It was later suggested that anti-apoptotic pathways could be initiated but it might not be the reason why a lower maximum cell density was achieved as a result of hyperthermia, given that apoptotic markers, including the activation of caspase-3 as well as DNA fragmentation, were not clearly detected in the culture at 39°C (Sugimoto et al., 2012).

It is worth noting that the concentration of Ca^{2+} in cytosol can be affected by either hypothermia or hyperthermia, and this could underlie the effect of these conditions on apoptosis induction. It was reported that elevated cytosolic Ca^{2+} levels could be achieved by the heat stress (Li et al., 2014, Gu et al., 2015). This could be because the heat stress activates STIM1, which acts as a ER Ca^{2+} sensor, and this protein then forms a plasma membrane and ER-associated pore (together with a plasma membrane pore-forming protein, Orai) facilitating ion transport, leading to Ca^{2+} influx (Xiao et al., 2011). The unbalanced level of cytosolic Ca^{2+} due to the Ca^{2+} influx could ultimately induce apoptosis through the ER-stress associated pathway (Li et al., 2014) as well as the mitochondrial apoptotic pathways (Gu et al., 2015), as previously discussed in Section 2.2.2. Given that STIM1 was found to be temperature-sensitive, hypothermia could also affect the activity of STIM1, resulting in disturbed cytosolic Ca^{2+} levels. It was reported that hypothermia decreased the store-operated Ca^{2+} entry, which

can be inferred that the activity of STIM1 could be slowed down by reduced temperature (Thompson et al., 2009). The change in cytosolic Ca^{2+} level due to hypothermia could trigger apoptosis, depending on the degree of hypothermia and cellular systems since there are studies showing an inhibitive effect of mild hypothermia on apoptosis while there are studies reporting that severe hypothermia could induce the cold stress and lead to apoptosis induction (Neutelings et al., 2013, Alva et al., 2013). In addition to alteration in the Ca^{2+} level, hyperthermia is reported to promote the production of reactive oxygen species (ROS), which also underlies apoptosis induction. In contrast, hypothermia decreases the production of ROS, which might explain its anti-apoptotic effect (Hsu et al., 2011, Neutelings et al., 2013).

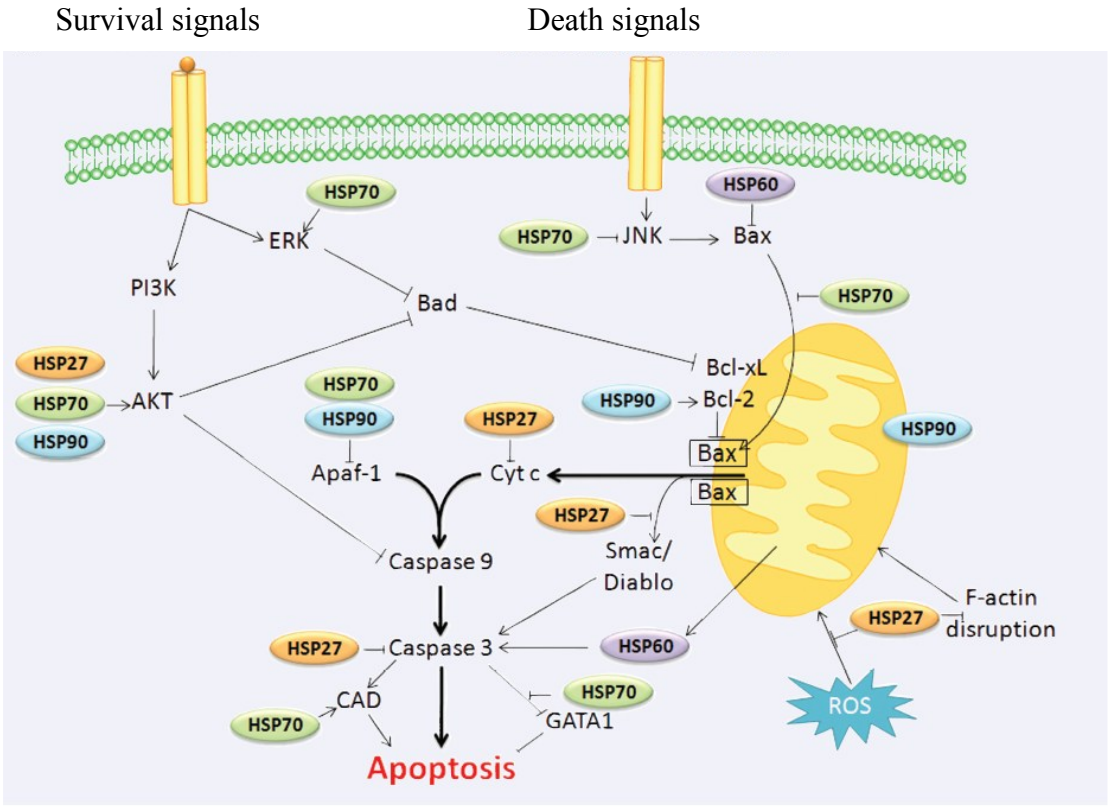


Figure 2.4.2 The role of HSPs in the apoptotic pathways, Adapted from (Lanneau et al., 2008).

Hypothermia and hyperthermia were also reported to activate proteins that act in response to cellular stress as a result of temperature change; cold shock proteins (CSPs) and

heat shock proteins (HSPs). CIRP and RBM3 are among CSPs that have been extensively studied. Their roles mainly involve regulation of transcription and translation in response to cold stress. CIRP was reported to be one of the components underlying growth arrest due to hypothermia. In addition, the binding of CIRP to RNA molecules under exposure to cellular stresses appeared to improve translation efficiency and the stability of RNA (Kumar et al., 2007). RBM3 was reported to regulate protein synthesis in response to the cold stress through interactions with ribosomal subunits as well as microRNAs (Dresios et al., 2005, Kumar et al., 2007). Both CIRP and RBM3 were reported to inhibit apoptosis (Kita et al., 2002, Sakurai et al., 2006) and this could contribute to the observed apoptosis inhibition due to hypothermia.

There are various members of HSPs. They can be divided into two main groups according to the molecule size: high molecular weight (i.e. HSP90, HSP70 and HSP60) and small molecular weight (i.e. HSP27) (Lanneau et al., 2008). Given a large number of HSPs, HSPs involve in a number of cellular functions through taking part in many signalling pathways. The basic role of HSPs involves protein folding where HSPs serve as chaperones. They help prevent aggregation arising from denatured proteins due to heat shock, guide the protein folding process, and prevent misfolding (Sonna et al., 2002). They were reported to have direct interactions with components in several signalling pathways, including apoptosis (Lanneau et al., 2008). Some of HSPs are anti-apoptotic factors while some might also act as pro-apoptotic species (Garrido et al., 2001). Their relevance to apoptosis occurs at upstream, downstream, and mitochondrial levels (Lanneau et al., 2008).

HSP70 is among those HSPs reported to act as an anti-apoptotic factor in response to cellular stresses. As can be seen from Figure 2.4.2, HSP70 plays the anti-apoptotic role in upstream signalling of apoptosis through regulating activities of JNK, Akt, p53, ERK and Bid (Lanneau et al., 2008). However, it was also found to inhibit nuclear factor-kappaB (NF-κB, a pro-survival factor) and in turn favour the death receptor apoptosis pathway (Ran et al., 2004).

At the downstream of apoptosis pathways, HSP70 was found to prevent bax translocation to the mitochondrial, which in turn inhibits activation of mitochondrial apoptosis pathway (Stankiewicz et al., 2005). In addition, activation of Apaf-1, and later recruitment of pro-caspase-9, can be blocked by HSP70 (Beere et al., 2000). CAD (a DNA fragmentation regulator) and GATA1 (a survival factor) were also inhibited by HSP70. As can be seen from Figure 2.4.2, HSP90 was also found to regulate activation of Akt, Apaf-1, NF-κB, p53, Bcl-2 and JNK, resulting in apoptosis inhibition (Lanneau et al., 2008). The anti-apoptotic effect of HSP27 involves its interaction with Akt. HSP27 was also reported to inhibit the mitochondrial pathway by interacting with cytochrome c and in turn preventing activation of caspase-9 and caspase-3 (Bruey et al., 2000, Pandey et al., 2000). In addition, reactive oxygen species can be inhibited by HSP27. HSP60 is normally bound by two molecules of HSP10 and serves as a chaperone. However, it was reported that HSP60 and HSP10 help activation of caspase-3 (Xanthoudakis et al., 1999) in apoptosis as can be seen from Figure 2.4.2. They were also found to play anti-apoptotic role given the recent studies showing that overexpression of HSP60 and/or HSP10 resulted in apoptosis inhibition (Lin et al., 2001b) and HSP60 can bind to Bax and inhibit its translocation to mitochondrial to induce apoptosis (Lanneau et al., 2008). The role of HSP60 in apoptosis remains inconclusive given evidence that HSP60 can help either promote or inhibit apoptosis.

2.4.3 Temperature shift effects on culture performance

Shifts to hypothermic temperatures

As discussed earlier, the maximum cell concentration was decreased in the hypothermic cultures, and therefore volumetric productivity of secreted proteins was not enhanced despite increased specific productivity. It was hypothesised that lowering culture temperature (to < 35°C) during the mid-exponential phase of the cultures (temperature shift), where cells are in a

proliferative state, could derive benefits from a high level of cell density, and thus could improve volumetric productivity. Generally, temperature shifts to hypothermic levels improved specific productivity as a result of prolonged culture viability and a lower maximum cell concentration as compared to the control culture (at 37°C). These effects was seen mainly in the cultures of CHO cell lines with temperature shifts to hypothermic levels (Furukawa and Ohsuye, 1999, Kaufmann et al., 1999, Fox et al., 2004, Hendrick et al., 2001, Rodriguez et al., 2005, Oguchi et al., 2006, Bollati-Fogolín et al., 2005). Furukawa and Ohsuye (1999) and Rodriguez et al. (2005) pointed out that, compared to the monophasic hypothermic cultures, final secreted protein titre as well as the maximum cell density were higher, though culture viability was not prolonged. Only analysis performed by Fox et al. (2004) showed that the biphasic CHO cell culture with a temperature shift to 32°C at an optimal culture time point achieved 90% and 40% higher volumetric productivity of interferon–γ as compared to the monophasic culture at 37°C and 32°C, respectively.

In some cases, lowering temperature during the exponential phase of cell growth did not result in higher productivity of secreted proteins, despite achieving growth arrest as well as prolonged culture viability. This phenomenon was observed in the biphasic cultures of hybridoma cell line (Barnabé and Butler, 1994), BHK cell line (Weidemann et al., 1994) as well as GS expression systems (Marchant et al., 2008). There was no significant difference of cell density, viability as well as final mAb titre between the culture at 33°C and the culture of hybridoma cell line with a temperature shift to 33°C (Barnabé and Butler, 1994). Marchant et al. (2008) showed that in addition to final mAb titre, there was no improvement in volumetric productivity of mAb, compared to the culture at 37°C.

Most of cultures with a temperature shift to hypothermic levels showed the same effects on metabolic activities. Generally, the temperature shift to hypothermic levels resulted in reductions in specific consumption rates of glucose, as well as production rates of lactate, as

compared to the culture at 37°C (Weidemann et al., 1994, Barnabé and Butler, 1994, Moore et al., 1997, Furukawa and Ohsuye, 1999, Marchant et al., 2008). Furukawa and Ohsuye (1999) showed that more glucose was consumed in the culture with a temperature shift to 32°C, as compared to the culture at 32°C. However, given that a higher level of cell density was achieved, the specific glucose consumption rate might be equal to that of the culture at 32°C. In addition, Marchant et al. (2008) showed that lactate generation was not affected by the decrease in specific glucose consumption rates as a result of a temperature shift to 32°C. This might suggest that the effect of temperature shift to hypothermic levels is cell-line dependent.

Effects of temperature shift to hypothermic levels on cell cycle, cell death and product quality were also studied. An increase in cell fraction at G_1/G_0 phase was observed in the biphasic cultures with temperature shifts to hypothermic levels of CHO cell lines (Moore et al., 1997, Kaufmann et al., 1999, Hendrick et al., 2001) and GS expression systems (Marchant et al., 2008), suggesting growth arrest at G_1/G_0 phase given a lower level of cell density as compared to the culture at 37°C. It was suggested that cell cycle arrest at G_1/G_0 could be a mechanism to delay apoptosis, given that apoptosis was delayed for 4 days after the temperature shift in the CHO cell culture. This could be because less toxic metabolites were produced due to the temperature shift (Moore et al., 1997). Like the monophasic hypothermic cultures, the biphasic cultures with a temperature shift to hypothermic levels did not negatively affect product quality. There was no deleterious effect on secreted protein bioactivity (Furukawa and Ohsuye, 1999); the pattern of glycosylation as well as the degree of sialylation (Bollati-Fogolín et al., 2005); the quality of N-glycosylation structures (Hendrick et al., 2001); and the degree of aggregation (Rodriguez et al., 2005).

The shift to hyperthermic temperatures

The concept of the temperature shifts to hypothermic levels was applied to hyperthermic cultures in an attempt to improve the yield of secreted protein while maintaining a high cell density/viability. Given that the highest level of cell density and the highest specific mAb productivity was obtained in the hybridoma cell culture at 33°C and 39°C, respectively, the temperature shift from 33°C to 39°C effect was studied. However, no significant increase in final mAb titre was observed. This might be because temperature difference of 6°C inserted excessive stresses to the extent that cells could not manage to adapt themselves for the new temperature condition (Sureshkumar and Mutharasan, 1991). Contrary to this result, a temperature shift to 39°C in the hybridoma cell culture increased final mAb titre (by 53%, compared to that of 37°C), although volumetric productivity was not significantly improved due to a lower cell concentration (compared to that of 37°C). In addition, the temperature shift to 39°C improved the specific rates of nutrient utilisation as well as the lactate specific production rate. It is worth mentioning that the glutamine degradation rate was higher when shifting temperature to a higher level (Barnabé and Butler, 1994).

2.5 Cellular responses to nutrient content shifts

One of the most influential parameters in cultures of mammalian cell lines is initial concentrations of nutrients (glucose and glutamine) as well as metabolic by-products (lactate and ammonia). This is because cell growth and metabolism are highly dependent on initial supply of nutrients as well as presence of metabolites at the beginning of the cultures. This section aims to discuss possible effects of nutrient and metabolite initial concentrations on culture performance as well as cellular activities. As described in Figure 2.5.1, the effect of

initial glucose, glutamine, lactate and ammonia on cell growth, metabolism and apoptosis is reviewed.

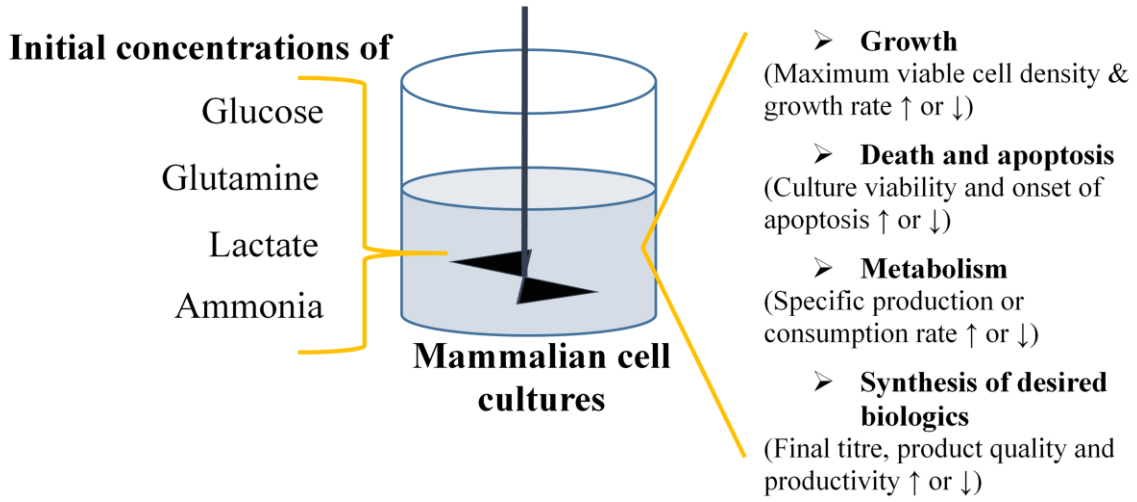


Figure 2.5.1 Literature review for the effect of initial concentration of nutrients and metabolites on cellular activities in the mammalian cell cultures.

2.5.1 Glucose and glutamine initial concentrations

It was established that the maximum cell density depends on initial glucose concentrations given that elevated levels (in the observed range) of glucose enhanced the specific growth rate in the culture of CHO cell line (Takagi et al., 2001). The maximum cell density also increased as the glucose concentration increased in the culture of hybridoma cell line (Miller et al., 1988a). In addition, both maintaining glucose concentration as low as 0.2 g/L in the culture of hybridoma cell line, and growing a CHO cell line with a low concentration of glucose (1 g/L) did not improve the maximum cell density (Sugiura, 1992, Kurokawa et al., 1994). Effects of initial glutamine concentration on cell growth were found to be similar to those of glucose. Higher levels of initial glutamine increased cell growth in the culture of hybridoma cell lines (Schneider and Lavoix, 1990, Dalili et al., 1990, Jeong and Wang, 1995), CHO cell lines (Takagi et al., 2001, Rajendra et al., 2011) and a HEK-293E cell line (Rajendra

et al., 2011). However, Miller et al. (1988) reported that there was a slight change in the maximum cell density when initial glutamine concentration was varied from 3.0 mM to 7.6 mM. In addition, Dalili et al. (1990) showed that the maximum cell density increased with increased initial glutamine concentrations, however, when the glutamine concentrations were above 2mM, the maximum cell concentration started to be unchanged.

Elevated levels of initial glucose supply were found to decrease productivity of secreted proteins in the culture of CHO cell lines (Sugiura, 1992, Takagi et al., 2001). In contrast, the cultures with lower initial glucose concentrations demonstrated improvement in productivity of secreted protein (Kurokawa et al., 1994). However, the perfusion culture of CHO cell line with a controlled level of glucose at <0.1 mM showed a slight decrease (15%) in immunoglobulin G productivity as compared to the high glucose culture (Takuma et al., 2007). It was found that specific productivity of secreted proteins increased with increased initial glutamine concentrations in the culture of hybridoma cell lines (Dalili et al., 1990, Schneider and Lavoix, 1990). However, in the culture of CHO cell line, an elevated initial glutamine concentration (at 5 mM) resulted in lower specific productivity, as compared to the control (Takagi et al., 2001), suggesting that the effect of initial glutamine concentration on productivity might be cell-line specific. Rajendra et al. (2011) showed that a controlled-concentration of glutamine at a low level achieved higher production of an IgG mAb in CHO and HEK-293E cell cultures (Rajendra et al., 2011). Kurokawa et al. (1994) also showed that maintaining glucose and glutamine concentrations at a low level (0.2 and 0.1 g/L, respectively) enhanced productivity of mAbs in the hybridoma cell cultures. In addition, by implementing a feeding strategy to control glucose and glutamine at a low level, productivity was increased (Khattak et al., 2010).

Generally, the initial concentration of glucose affects the specific consumption rate of glucose, and thus the specific production rate of lactate. It was also suggested that a Michaelis-

Menten correlation between the glucose consumption rate as well as the lactate production rate and the initial glucose concentration could be drawn (Cruz et al., 1999). Lowering glucose initial concentrations reduced glucose consumption rates (Takuma et al., 2007), and thus lactate production rates (Sugiura, 1992). Given that a significant increase in the specific oxygen consumption rate as well as a sharp decrease in the yield of lactate over glucose were observed at low initial glucose levels, a metabolic shift toward less lactate production could be induced (Miller et al., 1988a). However, Takagi et al. (2001) showed that there was no significant effect of initial glucose concentrations on glucose (and thus lactate) and glutamine (and thus ammonia) metabolism. Elevated initial glutamine concentrations were found to increase the glutamine consumption rate, and thus the production rate of ammonia (Takagi et al., 2001) as well as the consumption rate of glucose, and thus the production rate of lactate (Schneider and Lavoix, 1990). These metabolic activities were found to be reduced when lowering initial glutamine concentrations (Rajendra et al., 2011). However, there was a limit level of glutamine concentration where there was no significant increase in the rate of glutamine-associated metabolic activities with increased initial glutamine concentrations, as suggested by Cruz et al. (1999).

Glucose and glutamine initial concentrations were also found to affect product quality. Sugiura et al. (1992) showed that a high initial glucose concentration (at 3 g/L) reduced the bioactivity of the produced protein in the mono layer culture of CHO-B3 cell line. With the controlled glucose at a low level (<0.1 mM) in the continues culture of CHO cell line producing an IgG mAb, a slight increase in terminal galactosylation was observed, suggesting that glucose limitation could change galactosylation patterns (Takuma et al., 2007). Lowering initial glutamine concentrations was also found to enhance the galactosylation index (GI) and the sialylation index (SI), which are indicators for quality of the secreted product in the culture of CHO cell line (Aghamohseni et al., 2014).

2.5.2 Lactate and ammonia initial concentrations

In general, the impact of lactate on cell growth depends on its concentration, modes of culture and cell lines. The presence of 25 mM lactate at the beginning of the hybridoma cell culture increased cell density (Reuveny et al., 1986), and 44 mM of the lactate initial concentration did not affect cell growth in the continuous hybridoma cell culture (Miller et al., 1988b). However, lactate was found to negatively affect cell growth of other hybridoma cell lines (Kromenaker and Srienc, 1994), given that only half of cell density that was achieved in the control culture was achieved in the culture with 20 mM of lactate initial concentration (Duval et al., 1992). The inhibitory effect of lactate concentration was also seen in the culture of BHK cell line (Cruz et al., 2000) and CHO cell lines (Lao and Toth, 1997, Yang and Butler, 2000, Choi et al., 2007). Lao et al. (1997) also excluded possible effects of change in osmolarity due to sodium lactate additions in order to elevate initial lactate concentrations, and they suggested that cell growth reduction was caused by the presence of lactate, not by osmolarity, which is in agreement with a later study (Chen et al., 2009). Ammonia, in general, was found to have stronger inhibitory impact on cell growth than lactate, given that cell growth inhibition was seen at a lower concentration of ammonia compared to that of lactate. The inhibitory effect on cell growth was observed in the culture of hybridoma cell lines with ammonia concentrations at above 2 mM (Reuveny et al., 1986, Miller et al., 1988b, Newland et al., 1994). Cell growth inhibition was also observed in the culture of BHK cell line with an ammonia concentration at 3.5 mM (Cruz et al., 2000) while there was no significant effect of ammonia on cell growth in the culture of CHO cell line (Lao and Toth, 1997).

Given that lactate and ammonia are metabolic by-products, they have effects on metabolic activities, especially ones involving production of them. The presence of lactate appears to inhibit the production rate of lactate. Both the specific rate of glucose utilisation and

the production rate of lactate were found to be decreased by elevated initial lactate concentrations in the culture of hybridoma cell line (Kromenaker and Srienc, 1994), and CHO cell lines (Cruz et al., 2000, Choi et al., 2007). In addition to glucose consumption and lactate production, elevated initial concentrations of lactate also have inhibitory effects on glutamine consumption as well as ammonia production, and alanine production indicating the effect of lactate on glutaminolysis (Cruz et al., 2000). However, Miller et al. (1988) suggested that an inhibitory level of lactate could be higher than 44 mM for the continuous culture of hybridoma cell line, given no significant effect on nutrient consumption rates (glucose and glutamine) and the lactate production rate observed (Miller et al., 1988b). The effect of ammonia on metabolic activities is similar to that of lactate. The specific production rate of ammonia was reduced by elevated ammonia initial concentrations in the culture of hybridoma and CHO cell lines (Miller et al., 1988b, Lao and Toth, 1997, Yang and Butler, 2000). Miller et al (1988) also suggested that there was a shift in the glutaminolysis pathway in response to elevated initial concentrations of ammonia, given that glutamine and oxygen consumption were reduced while there was an increase in alanine production. Lao and Toth (1997) also suggested a shift in the glutaminolysis pathway given that glutamate and aspartate consumption rates were increased.

Lactate and ammonia initial concentrations also have effect on production and quality of desired therapeutic proteins. Generally, elevated initial concentrations of lactate were found to increase final secreted protein titre. This phenomenon was observed in the culture of hybridoma cells (Reuveny et al., 1986, Kromenaker and Srienc, 1994), and CHO cell lines (Lao and Toth, 1997, Choi et al., 2007). Choi et al. (2007) suggested that an elevated initial lactate concentration (at 40 mM) enhanced pyruvate generation (indicated by an observed higher level of lactate dehydrogenase (LDH) activity), and ultimately increased production of the EPO protein due to pyruvate being more available. This suggestion was later confirmed with experimental data showing that the culture of LDH and pyruvate dehydrogenases (PDHs)-

deficient cells achieved 70% increase in volumetric production of antibody (Zhou et al., 2011). However, Cruz et al. (2000) showed that elevated initial lactate concentrations caused a decrease in specific productivity (Cruz et al., 2000). Elevated initial ammonia concentrations were found to decrease (Reuveny et al., 1986, Cruz et al., 2000) as well as increase (Yang and Butler, 2000) production and productivity of secreted bio-proteins. In addition, it was found that quality of secreted therapeutic proteins was negatively affected by an elevated initial ammonia concentration (at 9 mM) in the culture of CHO cell lines (Borys et al., 1994, Yang and Butler, 2000). It was suggested that elevated levels of ammonia essentially affect the post-glycosylation process at Golgi apparatus rather than ER and cytosol compartments, as indicated by the low expression of sialylation and galactosylation-associated genes and the unchanged expression of cytosol and ER localised genes in the ammonia-treated cell culture (Chen and Harcum, 2006).

2.6 Strategies to enhance therapeutic protein production

High production of heterologous proteins is one of the most desirable characteristics of the mammalian cell cultures. Given the key limitations found in mammalian cell cultures for production of biopharmaceuticals (sub-section 2.3.4), enhancing the production is however not trivial. The control of cell proliferation is believed to be one of strategies to overcome the limitations, and thus achieve enhanced production of therapeutic proteins (Kumar et al., 2007). In addition, apoptosis has long been identified as the main cause of cell death in the cultures (Goswami et al., 1999, DiStefano et al., 1996, Browne and Al-Rubeai, 2011a, Singh et al., 1994). It is therefore extremely unwanted since it causes reduction in culture viability as well as final secreted protein titre. Also, the higher level of dead cells, the poorer product quality and the more complicated the downstream processes (Yoon et al., 2003b, Majid et al., 2007, Tey et al., 2000a). Therefore, suppression of apoptosis is also believed to be a potential strategy

for higher production of secreted proteins. This section reviews cell proliferation control as well as apoptosis suppression toward improvements in production of biopharmaceuticals. As shown in Figure 2.6.1, the review discusses the effect of those strategies on cellular activities, including growth, metabolism and death (apoptosis). In addition, the relationship among cell proliferation (cell cycle), apoptosis and metabolism is discussed here.

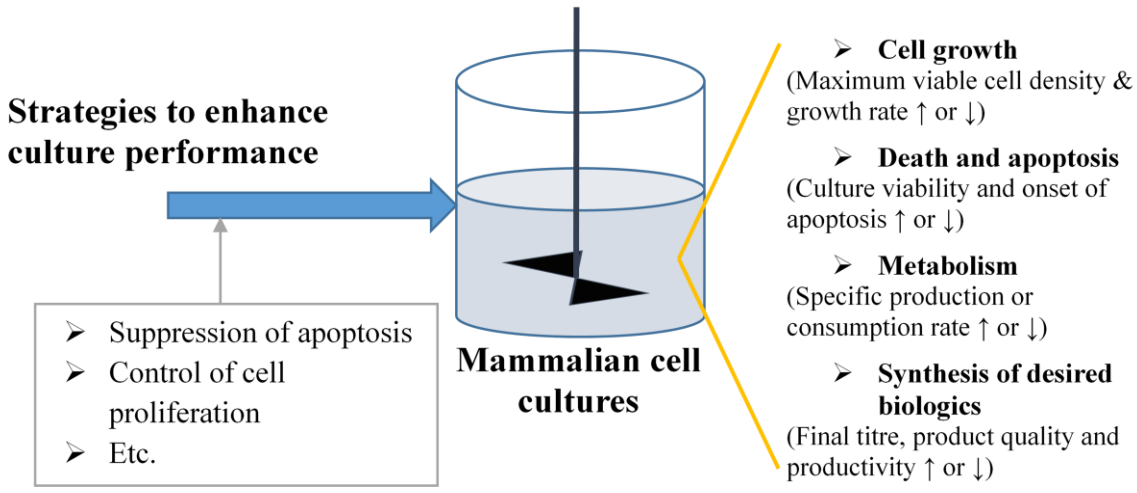


Figure 2.6.1 Literature review for the effect of cell proliferation control and suppression of apoptosis, which are accounted as strategies for enhancement of desired biologics production, on cellular activities in the mammalian cell cultures.

2.6.1 Control of cell proliferation

Control of cell cycle progression was found to have effects on secreted protein production/productivity. There are a number of cyclin-dependant kinase inhibitors (CdkIs) that play a regulatory role in G_1/G_0 cell cycle arrest, including p21 and p27 (Brugarolas et al., 1999). Cell lines metabolically engineered with these cell cycle regulator genes appear to increase productivity. The batch culture of a CHO cell line engineered with multi-genes, including *p21* with *p27*, demonstrated that there was a cell cycle arrest at G_1/G_0 phase and the culture achieved a significant increase in productivity (Fussenegger et al., 1998a). The cell cycle arrest at G_1/G_0

phase was also observed in the batch culture of a GS-NS0 cell line with inducible *p21* transfection, where IgG4 antibody productivity was at least 4 times higher than the control (Watanabe et al., 2001). In addition to ceasing cell proliferation at G_1/G_0 phase, *p21* overexpression appears to enable cells to better adapt themselves to a new environment during culture passages or transferring (Astley et al., 2007). The biogenesis of a new mitochondria associated with an increase in cell size was suggested as a possible mechanism when cell proliferation was inhibited by overexpression of *p21*. This also suggests that cell growth was possibly separated from cell cycle progression, which might underlie the observed increase in productivity (Bi et al., 2004). Similar to that of *p21*, the transfection of inducible *p27* in a CHO cell line producing a protein for the cold treatment appeared to cease cell cycle progression at G_1/G_0 phase, and thus enhanced productivity (Meents et al., 2002). Overall, the cessation of cell proliferation at G_1/G_0 phase by overexpressing these CdkIs (predominantly p21) appears to help boost secreted protein productivity as well as production. This approach becomes a fundamental platform for multi-genes engineering where other strategies for improvements in secreted protein production can be combined, such as the co-expressing transfection of *p21* and *bcl-2* (Astley and Al-Rubeai, 2008, Ibarra et al., 2003), which combines cell proliferation control with anti-apoptotic effects.

2.6.2 Suppression of apoptosis

Attempts have been made to prevent the mammalian cell cultures from apoptosis in order to prolong culture viability, and thus increase productivity and/or final titre. The metabolic engineering of Bcl-2, an anti-apoptotic protein as described in section 2.2.1, is one of predominant strategies for apoptosis suppression given that Bcl-2 molecules can suppress apoptosis at a very early stage (Dorai et al., 2010). *bcl-2* overexpression appears to rescue CHO and BHK cell lines from apoptosis caused by several lethal insults including viral infection,

glucose as well as serum deprivation, and ammonia at a high level (50 mM) (Mastrangelo et al., 2000b, Mastrangelo et al., 2000a, Figueroa et al., 2001). Furthermore, in addition to Bcl-2, Bcl-xL, which can also inhibit apoptosis, is a promising target for metabolic engineering toward suppression of apoptosis and improvement of mammalian cells cultures. The batch cultures of both BHK and CHO cell lines engineered with *bcl-xL* achieved inhibition of apoptosis, despite the cultures being under exposure to those lethal insults (Mastrangelo et al., 2000b, Mastrangelo et al., 2000a). The protective effect of *bcl-xL* transfection was also observed in the cultures of CHO and hybridoma cell lines with exposure to various lethal culture stresses (Charbonneau and Gauthier, 2000, Figueroa et al., 2004). Figueroa et al. (2004) also showed that the transfection of *aven*, another anti-apoptotic gene, could also limit the onset of apoptosis. Moreover, the cultures of mammalian cell lines, which were engineered with 1) caspase inhibitors (XIAP and CrmA) and 2) a heat shock protein (hps70), showed a similar result to those with the *bcl-2* and *bcl-xL* transfection (Lasunskaia et al., 2003, Sauerwald et al., 2003). To enhance the protection for mammalian cell cultures against apoptosis, multi-anti-apoptotic gene engineering was explored. The co-expressing transfection of *bcl-xL* and *aven* in the culture of CHO cell line showed prolonged culture viability, suggesting that *aven* could enhance the ability of *bcl-xL* to limit apoptosis (Figueroa et al., 2004).

2.6.3 Impact of apoptosis inhibition on productivity and final titre

Overall, mammalian cell cultures with anti-apoptotic gene(s), such as *bcl-2*, transfection share similar characteristics; inhibition of apoptosis, and consequently enhanced viable cell densities and prolonged culture viability. However, to the best of my knowledge, cultures with overexpression of anti-apoptotic gene(s) did not always achieve a significant increase in productivity as compared to those of wild type cells. The batch culture of GS-NS0 cells with *bcl-2* transfection, despite achieving a 20% and 100% increase in the maximum

viable cell density and cultivation time, respectively, did not achieve an increase in final mAb titre (Tey et al., 2000a). A similar result were observed in the culture of *bcl-2* transfected GS-CHO cell line. The amount of mAb produced from the transfected cell culture was equal to that from the control (wild-type), though a higher viable cell number was achieved (Tey et al., 2000b), suggesting a decrease in mAb productivity. Having argued that nutrient exhaustion during the final phases of the batch culture limits the mAb secretion and thus no increase in mAb productivity (Tey et al., 2000a, Simpson et al., 1999b), fed-batch and continuous cultures of a variety of cell lines were investigated. Despite achieving final mAb titre around 50% higher than that from the control culture, it appeared that productivity did not increase in the fed-batch culture of *bcl-2* transfected GS-NS0 cells, given a 60% rise in the maximum viable cell number (Tey et al., 2000a). The perfusion culture of GS-NS0 cells also showed a similar result; a higher cell density but lower mAb productivity as compared to the control culture (Tey and Al-Rubeai, 2004, Tey and Al-Rubeai, 2005). Similarly, the continuous culture of hybridoma cells with *bcl-2* overexpression achieved a higher viable cell number and longer culture viability than the control culture, though there was no increase in final mAb titre (Simpson et al., 1999b). One of possible reasons could be that cells utilise fed nutrients for biomass synthesis rather than mAb secretion (Tey and Al-Rubeai, 2004, Tey and Al-Rubeai, 2005).

Other strategies for inhibition of apoptosis attained a similar outcome to that with *bcl-2* overexpression. By adding a caspase activity inhibitor, Z-VAD-fmk, it showed that apoptosis induction was reduced, and thus culture viability and viable cell density were enhanced. However, there was no improvement in mAb productivity (McKenna and Cotter, 2000). No significant increase in recombinant factor VIII protein productivity was witnessed in the culture of BHK cells with co-overexpression of *aven* and *EIB-19K*, though apoptosis was found to be inhibited (Nivitchanyong et al., 2007). Recently, the culture of an EPO-producing CHO cell

line with overexpression of *bcl-xL* at 33°C and 37°C also showed no difference in EPO productivity compared to the control culture at both temperatures (Kim and Lee, 2009).

However, there were several studies showing increases in secreted protein/mAb productivity. In the *bcl-2* transfected hybridoma cell culture, there was a significant increase in mAb productivity together with prolonged culture viability and a higher number of viable cells (Itoh et al., 1995, Terada et al., 1997). DMSO, which is a reagent that can be toxic to cells, was added to the culture of a *bcl-xL* transfected CHO line cell producing EPO. It was suggested that EPO degradation was prevented from DMSO toxicity, and consequently an increase in EPO productivity were observed (Kim et al., 2011). Recently, co-transfection of *bcl-2* or *bcl-xL* and the cytokine IL-2 protein expressing maker in the cultures of CHO and HEK-293 cell lines was investigated. This study demonstrated that the culture of 10 wt% of cells with the transfection of the anti-apoptotic gene (and 90 wt% of cells with only protein expressing marker transfection) achieved in an improvement in specific productivity (Zustiak et al., 2014).

2.6.4 Apoptosis inhibition and cell cycle arrest

It was established that overexpression of the anti-apoptotic genes could also cease cell proliferation at G_1/G_0 cell cycle phase (Janumyan et al., 2003, Mazel et al., 1996). The culture of a *bcl-2* transfected hybridoma cell line showed a high percentage of cells at G_1/G_0 cell cycle phase, indicating G_1/G_0 cell cycle arrest (Simpson et al. 1999), while cell cycle arrest at G_2/M phase was seen in the culture of a *bcl-2* transfected GS-NS0 cell line (Tey and Al-Rubeai, 2005). When considering the fact that an improvement in protein/mAb productivity was attained in the culture with cell proliferation arrest at G_1/G_0 cell cycle phase (Ibarra et al., 2003), it seems contradictory to unchanged, and sometimes decreased, productivity achieved from the cultures of anti-apoptotic gene transfected cell lines, where cell cycle arrest at G_1/G_0 phase was also observed. The possible explanation could be that transfection of the anti-apoptotic genes

and cell cycle regulators might affect metabolic activities in a different manner. This can be seen in the case of *aven* and *E1B-19K* overexpression when compared to the parental cell, which there was a difference in metabolic profiles among them (Nivitchanyong et al., 2007). Therefore, different shifts in metabolic states could elucidate why cell cycle arrest at G_1/G_0 phase due to anti-apoptotic gene overexpression has a different effect on productivity to that with overexpression of cell cycle regulators. It was suggested that an optimal level of overexpression of anti-apoptotic gene(s) might hold the key to a beneficial compromise between apoptosis inhibition and an improvement of productivity (Zustiak et al., 2014).

2.6.5 Apoptosis inhibition and product quality

Apoptosis has a detrimental effect on quality of bio-therapeutic products. Generally, intracellular contents released from dead cells can degrade quality of bio-therapeutic products and complicate downstream processes (Tey et al., 2000a). Inferior product quality as a result of low culture viability was observed in the culture of a CHO cell line producing human interferon gamma (IFN-γ). The produced IFN-γ was found to have a lower degree of sialylation and a shorter glycan length, suggesting degradation being enhanced by several enzymes released from dead cells (Chee Furng Wong et al., 2005). The sialylation degree of IFN-γ, produced from the culture of a CHO cell line with anti-apoptotic gene (*Fadd* and *Faim*) overexpression or pro-apoptotic gene (*Alg-2* and *Requiem*) knockdown, was higher than that from the control culture, suggesting that apoptosis inhibition helps enhance product quality (Wong et al., 2006). Furthermore, it was suggested that lactate consumption, which was seen in the culture of a CHO cell line with anti-apoptotic gene transfection, helps reduce osmolality and balance culture pH, which is required for better product quality (Dorai et al., 2009).

2.6.6 Protein expression and unfolded protein response

The recombinant protein is synthesised on the ER surface and is processed (folding, oligomerisation and post-translational modifications) before leaving the ER (Kober et al., 2012). Therefore the protein expression could generate extra workload on the ER and ultimately lead to apoptosis through the activation of UPR and later the ER-stress associated apoptotic pathway (Figure 2.2.3-4). There are conditions that the ER cannot manage the protein folding properly, thus generating the ER stress, and eventually triggering the UPR. The UPR then activates relevant components in its various pathways, which in turn play regulatory roles in many signalling cascades including transcription and translation, metabolism as well as apoptosis (Figure 2.2.3), in order to alleviate the ER stress as discussed in Section 2.2.2.

It was recently shown that the expression of anti-CD20 antibody fragment in *Arabidopsis* seeds generated a certain level of the ER stress (Wang et al., 2015), which was in agreement with previous report suggesting that the UPR was found to be activated in response to the antibody expression (De Wilde et al., 2013). However, the effect of the UPR activation due to the antibody expression on cellular processes was not clearly observed in this system. It was also shown that an increase in IgG productivity in a batch culture of CHO cell line was associated with an increase in expression levels of majority of chaperones (Prashad and Mehra, 2015), which was in agreement with previous results (Smales et al., 2004). Following the high productivity period, components in the UPR pathways, including PERK, IRE1, ATF4, CHOP and XBP1, were up-regulated, suggesting the ER stress possibly due to the high IgG productivity (Prashad and Mehra, 2015). Previous results showed that the UPR can be regulated by metabolic stresses in addition to the ER stress; CHOP was found to be up-regulated in response to both glucose and glutamine limitation (Murphy et al., 2001, Lengwehasatit and Dickson, 2002). However, it was suggested that CHOP might not be always necessary for NS0

cells to activate apoptosis (Cudna and Dickson, 2006). Furthermore, Prashad and Mehra (2015) suggested, based on the expression profile of the UPR-related components, that each pathway in the UPR could potentially be activated by different cellular stresses arising from different sources, such as from the ER stress and/or the nutrient deprivation (glucose, amino acids, O_2), since the high productivity and the metabolic stress were interconnected in the batch culture.

The effect of the UPR on cellular processes was previously studied. As previously shown in Figure 2.2.3, the UPR can lead to the activation of ER-associated degradation (ERAD), which acts as a misfolded protein remover, allowing cells to avoid accumulation of undesirable proteins in the ER (Hussain et al., 2014). The UPR activation can promote lipid metabolism and ER membrane biogenesis through activation of XBP1(Sriburi et al., 2004) as well as ATF6 (Bommiasamy et al., 2009). Overexpression XBP1 in CHO cells showed an increased production of recombinant protein as a result of the expanded ER and golgi capacity (Tigges and Fussenegger, 2006) and this was in agreement with later studies showing expanded ER size being associated with the increased protein production (Hussain et al., 2014). In addition, given that the ER is where proteins are synthesised; believed to be the limiting step for the production of exogenous proteins, overexpression of UPR as well as chaperone-related components was introduced to mammalian cell cultures. This includes CHOP, ATF4 and GRP78 (or BIP). The effect of the overexpression of these components on production/productivity was variable depending on cell hosts and overexpressed components (Hussain et al., 2014). In addition to apoptosis, the UPR was reported to be associated with autophagy. Autophagy can be induced by the ER stress in order to alleviate the stress and restore ER functionality. It was reported that the UPR-related mediators (PERK, IRE1 and ATF6) can regulate the formation of autophagosome (a component of degradation unit structure) (Hussain et al., 2014).

2.6.7 Relationships between cell cycle as well as apoptosis, and metabolism

Apoptosis is subjected to metabolic stresses, including exhaustion of nutrients (glucose and amino acids) and toxic metabolite (lactate and ammonia) accumulation. It was revealed that apoptosis was triggered by starvation of glucose in the culture of SP2/0 hybridoma and wild type NS0 cell lines (Mercille and Massie, 1994a). It was suggested that a decrease in glucose metabolism due to glucose exhaustion causes a sudden decrease in intracellular ATP levels, and in turn dissipates mitochondria membrane potential and finally triggers the cytochrome c release, leading to induction of apoptosis (Moley and Mueckler, 2000). Furthermore, Mercille and Massie (1994) also showed that glutamine and cysteine exhaustion could result in induction of apoptosis (Mercille and Massie, 1994a). This result was in good agreement with the observation in the culture of a hybridoma cell line under exposure to deprivation of a single amino acid, where the majority of cells died via apoptosis (Simpson et al., 1998). They suggested that a mechanism to trigger apoptosis could be linked to defects in transcriptional and translational processes due to a decreased in intracellular ATP levels caused by the exhaustion of amino acid (Simpson et al., 1998). The up-regulated expression of activating transcription factor 5 (*atf5*) and transformation related protein 53 binding protein 2 (*trp53bp2*) genes could be associated with amino acid deprivation in the batch culture of GS-NS0 cells (Browne and Al-Rubeai, 2011b). Both *atf5* and *trp53bp2* were found to have regulatory roles in anti-apoptosis and pro-apoptosis pathways, respectively (Dluzen et al., 2011, Kobayashi et al., 2005). In addition to deprivation of glucose and amino acids, apoptosis induction was also observed in the culture of SP2/0 and NS0 cell lines with an oxygen-limited condition (Mercille and Massie, 1994b, Zhu et al., 2006). Serum deprivation was also found to trigger apoptosis in many studies (Zhu et al., 2006, Tey et al., 2000a, Singh et al., 1994).

It is worth discussing that autophagy, a cellular process whereby cells digest themselves to remove damage intracellular organelles and balance sources of cellular energy, was found to be induced by nutrient-starvation conditions, in addition to apoptosis (Glick et al., 2010). Two CHO cell lines producing mAbs underwent autophagy as well as apoptosis during the final stages of batch cultures where glutamine and glucose became exhausted (Hwang and Lee, 2008). In addition to suppressing apoptosis, overexpression of *bcl-xL* was found to repress *Beclin-1*, one of key mediators in the autophagic pathway, and thus inhibit autophagy (Kim et al., 2009). Furthermore, a higher degree of apoptosis was found when autophagy was inhibited and vice versa, suggesting that autophagy could be a survival mechanism that prevents cell from apoptosis (Han et al., 2011, Jardon et al., 2012). These recent findings suggest a possible link between apoptosis and autophagy. However, the role of autophagy remains inclusive (Munoz-Pinedo and Martin, 2014) given that autophagy was found not be a survival mechanism for cells that undergo glucose starvation-induced apoptosis (Ramírez-Peinado et al., 2013). Therefore, autophagy cannot be accounted as one of the main causes of cell death in the mammalian cell cultures.

Extremely elevated levels of lactate and ammonia appears to predominantly trigger necrosis, rather than apoptosis. It was found that ammonia at a lower concentration triggered both apoptosis and necrosis at a similar degree, while only necrosis was seen in the culture with an extreme level of ammonia (>50 mM) (Singh et al., 1994). Similarly, the cultures of SP2/0 hybridoma and NS0 cell lines with exposure to extreme levels of lactate (30 mM) and ammonia (3 mM) demonstrated that necrosis was the main cause of cell death in the cultures (Mercille and Massie, 1994a). Growth inhibition was also observed in cultures with the presence of ammonia and lactate. It appeared that the specific growth rate of a CHO cell line significantly decreased as the ammonia concentration rose (Kurano et al., 1990). Similarly, cell growth of a hybridoma cell line in the culture with an initial ammonia concentration at 4 mM exhibited a

50% decrease (Ozturk et al., 1992). Similarly, a negative effect of ammonia presence on the growth rate was seen in the culture of SP2/0 cells with an initial concentration of ammonia at 2 mM. In addition to growth inhibition, an increase in death rate was noticed (Newland et al., 1994), though cell death was not distinguished if it was due to apoptosis or necrosis. In the same way to ammonia, 55 mM of lactate accumulated appeared to halve hybridoma cell specific growth (Ozturk et al., 1992).

Given that apoptosis can be triggered by the deprivation of nutrients, the addition of key nutrients including glucose, amino acids, and proteins during the batch culture of GS-NS0 cells demonstrated that apoptosis can be delayed for at least 24 hours (DiStefano et al., 1996). The delay might be the result of shifts in metabolic pathways due to the nutrient addition (DiStefano et al., 1996). It was later confirmed that the delay of apoptosis due to the nutrient addition could be associated with a metabolic shift, which could relieve nutrient deprivation-induced apoptotic stresses (Zhou et al., 1997a). Zhou et al. (1997) also suggested that a transition from production to consumption of lactate and the onset of ammonia production might be indicators of the metabolic shift. The transition of lactate-associated metabolic activities was seen in the culture of a CHO cell line with transfection of multi-anti-apoptotic genes including *E1B-19K*, *XIAP*, *Aven*, and *bcl-2*. This suggests that overexpression of anti-apoptotic genes could enable a metabolic shift (Dorai et al., 2010, Dorai et al., 2009). A possible mechanism of *bcl-2* overexpression enabling a metabolic shift could be that *bcl-2* overexpression down-regulates the lactate dehydrogenase A (LDH-A) gene, and in turn slows down the corresponding LDH reaction whereby pyruvate is converted to lactate (Papas et al., 1999). The recent finding also confirmed that the amount of carbon from pyruvate entering TCA cycle during the lactate consumption phase was significantly more than that during the lactate production phase, suggesting a reduction in the LDH reaction activity (Templeton et al., 2014). However, *bcl-xL* overexpression did not have influence on the transition of lactate

production/consumption states (Ha et al., 2013). Furthermore, metabolic activities, including specific nutrient consumption/ metabolite production rates, could be influenced by certain accumulated levels of ammonia and lactate as regards cell growth inhibition and cell death (necrosis and apoptosis) (Newland et al., 1994, Ozturk et al., 1992).

The link between metabolism and control of cell cycle progression was also previously established. A slower rate of cell proliferation, compared to the control, together with a significant increase in cell population in G_1/G_0 phase was observed in the batch culture of a CHO cell line producing IFN-g using glutamine-free medium. This suggests that cell cycle arrest might be one of responsive mechanisms to the metabolic stress due to glutamine deprivation (Sanfeliu and Stephanopoulos, 1999). Increases in both mRNA and protein expressions of *p21* and *p27* were induced by histidine deprivation in the culture of HepG2 cells, suggesting that the exhaustion of histidine may cease cell cycle progression at G_1/G_0 phase (Leung-Pineda et al., 2004). Arrest of cell cycle progression was also seen in serum-starvation conditions, in a similar manner to that of essential amino acids (Sherr and Roberts, 1995). Arrest of cell cycle was believed to have a tight relation to apoptosis (Al-Rubeai and Singh, 1998, Kastan et al., 1995). It was established that *p21* activation, which facilitates cell cycle arrest at G_1/G_0 phase, was induced by an elevated endogenous *p53* expression as a result of exposure to apoptotic inducers (El-Deiry et al., 1994). The ultimate cell fate, between apoptosis or cell cycle arrest, is decided by the degree of cellular stresses as indicated by changes in activation levels of *p53* (Mason and Rathmell, 2011). There is a threshold level of cellular stresses that enables activated *p53* to initiate apoptosis, or otherwise cell cycle arrest (Kracikova et al., 2013). This might be a possible mechanism where metabolic stresses are linked with control of cell cycle and apoptosis.

2.7 Mathematical model development

2.7.1 An overview of mathematical model development

Table 2.7.1 Existing kinetics describing relations between substrates and rates of reactions.

Kinetic types	Mathematical expressions
Rate law	$r = k\,[A]^a[B]^b$
Michaelis–Menten kinetics	$r = k_E \cdot [E]_0 \frac{[S]}{[S] + K_m}$
Monod equation	$r_X = \mu_{X,max} \frac{[S]}{[S] + K_S} \cdot X$
Moser' formulation (Hill equation)[1]	$r_X = \mu_{X,max} \frac{[S]^n}{[S]^n + K_D{}^n} \cdot X$
Dual-limiting substrate kinetics[2]	$r_X = \mu_{X,max} \frac{[S_1]}{[S_1] + K_{S_1}} \cdot \frac{[S_2]}{[S_2] + K_{S_{21}}} \cdot X$
Substrate inhibition kinetics[3]	$r_X = \mu_{X,max} \frac{[S]}{\frac{[S]^2}{K_{i,s}} + [S] + K_S} \cdot X$

[1](Moser, 1958), [2](Megee Iii et al., 1972), [3](Andrews, 1968).

Where, "X" is the cell concentration (cell/L); "r" and "r_x" are the rate of reaction ($mol.L^{-1}.s^{-1}$) and the cell growth rate ($cell.L^{-1}.s^{-1}$), respectively; "[A]" and "[S]" are the concentration of species A and the limiting substrate concentration ($mol.L^{-1}$), respectively; "a" and "b" are the order of reaction with regards to A and B (assuming to be stoichiometric coefficients), respectively; "k" is the rate constant ($mol^{1-a-b}.L^{a+b-1}.s^{-1}$); "$k_E[E]_0$" is the maximum reaction rate (sometimes called V_{max}, $mol.L^{-1}.s^{-1}$); "K_m" is the Michaelis-menten constant ($mol.L^{-1}$); "K_s" is the limiting substrate concentration ($mol.L^{-1}$); "$K_{i,s}$" is the limiting substrate inhibition constant ($mol.L^{-1}$); n is the cooperative coefficient (depending on which biological context the equation is used).

There are a number of existing mathematical correlations that were previously introduced and became a basis for development of mathematical models for biological systems, such as Monod equation (Monod, 1949), Michaelis–Menten kinetics (Chen et al., 2010) and Hill equation, as shown in Table 2.7.1. These equations involve two types of variables: state and operational variables. The former stands for variables that describe states of the systems,

such as viable cell density, nutrient concentration, etc. The latter specifies conditions utilised in the systems such as temperature, feeding flowrate, initial nutrient concentration etc. According to both state and operational variables, mass balances can be constructed to complement kinetic correlations. For example, a mass balance of viable cell density represents an accumulation or a depletion rate of viable cell concentration, which depending on the specific rate of growth and death, as defined by kinetic equations (Augusto et al., 2008).

Given that both kinetic equations as well as mass balances require constants to represent physical reactions (i.e. rate constants, Monod and Michaelis constants), constructed mathematical models typically consist a number of parameters (Kent et al., 2013). Values of parameters can be given from existing models or previous studies, however, some need to be determined. Parameter estimation is the process whereby optimal values of parameters can be estimated through diminishing the difference between experimental and simulated data. To achieve experimental agreement, the constructed mathematical models should be validated with an independent set of experimental data under different conditions (Augusto et al., 2008).

2.7.2 Model classification

Given that cellular systems are highly non-linear and their behaviour is subject to a dynamic environment, it is therefore not trivial to construct a mathematical model that perfectly captures and predicts cellular responses under different circumstances. In addition, mathematical models have to be developed in a way that balances how much information must be included and model complexity. Several approaches for mathematical model development have been introduced in order to help handle complexity of cellular systems. Figure 2.7.1 illustrates model classification for cell cultures, which divides mathematical models into several types according to the approaches for model development.

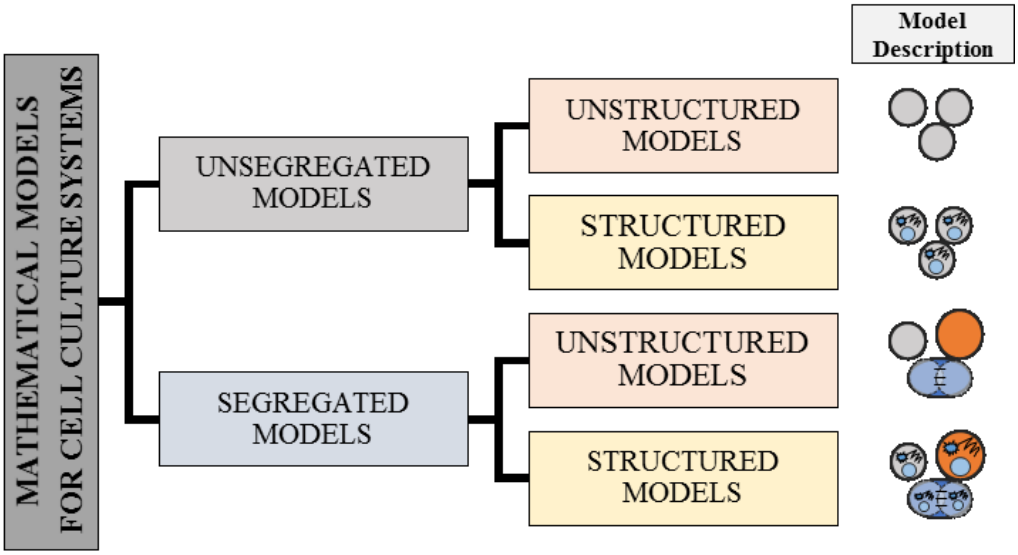


Figure 2.7.1 Model classification. Adapted from (Ramkrishna, 1979, Sidoli et al., 2004).

Mammalian cell cultures are often found to be non-homogenous; there are various cell populations in the cultures, such as cells in different stages of the cell cycle, sizes, metabolic conditions etc. There are two main modelling approaches to handle the heterogeneity in mammalian cell cultures: unsegregated and segregated. **Unsegregated models** assume that an average property and behaviour of cell populations represent the entire cell population. For example, biomass per unit volume is employed to represent the average behaviour of the entire system. **Segregated models** capture the heterogeneity in the cultures, offering opportunities to integrate cellular activities/properties specific to each cell population. Population Balance Models (PBMs) are examples of segregated models, and can be formulated based on a difference in DNA contents of each cell population in different stages of cell cycle (Liu et al., 2007, Hatzis et al., 1995). For example, production of IgG mAb in a hybridoma cell culture was found to be the highest one during G_1 and early S phase (Al-Rubeai and Emery, 1990) which can be mathematically linked to viable cell densities in G_1 and S phases for a higher degree of experimental agreement. However, this kind of model typically involves partial

differential equations, which are difficult to solve with highly sophisticated computational tools.

Mathematical models can be further divided into two subgroups: unstructured and structured, with regard to biological information included into the models (Figure 2.7.1). **Unstructured models** are frameworks that treat a single cell as "a black box", where only phenomenological changes of cell behaviour/properties in response to environmental conditions are considered. Monod kinetics, for example, does not include intracellular phenomena that underlie changes in growth of specific cell types. Unstructured models are relatively less complicated, and thus not computationally expensive; however, they sometimes fail to represent particular behaviour of cellular systems under various culture conditions. **Structured models** take into account intracellular structures and activities, and usually provide a better mechanistic representation than unstructured models. Given that more biological information is included, structured models often consist of complicated networks of ODEs, and may result in mathematical intractability.

In addition to the unsegregated/segregated and unstructured/structured ones, mathematical models can also be classified as **deterministic/stochastic** in accordance with whether likelihood of reactions occurring in the systems is considered. The models can also be divided as steady state or dynamic models. **State steady models** provide system information regardless of time, and thus require no mathematical term representing time dependence (time derivatives). Flux balance analysis (FBA), for instance, represents the direction and quantity of fluxes in biochemical pathways at a steady state (Knoop et al., 2013). Given that cellular systems are surrounded by a dynamic environment; FBA might not be able to capture transient shifts in cellular behaviour in response to environmental disturbances/signals. In contrast, **dynamic models** can capture behaviour with respect to time. Chemical kinetics or mass action law, for example, illustrate changes in reactions over time depending on concentrations of

reactants (Waage and Gulberg, 1986). However, compared to FBA, kinetics is more computationally intricate. Consequently, experimental validation required for kinetics can be relatively complicated.

As discussed above, each type of mathematical model has its own strong and weak points. **Hybrid models** are ones that combine two or more model types so that each included model type can complement the others' advantages and disadvantages. For example, a hybrid mathematical model for GS-NS0 cultures, which was the combination of a structured sub-model describing a detailed mechanism of antibody synthesis and an unstructured model describing cell growth and metabolism, can capture culture dynamics at different osmotic conditions with relatively less computational resources required (Ho et al., 2006). Dynamic FBA is also an example where the hybrid approach is utilised. Dynamic metabolic profiles were achieved through successively executing FBA in accordance with dynamic changes in extracellular metabolite concentration and cell density (Nolan and Lee, 2011, Yugi et al., 2005, Antoniewicz, 2013).

2.7.3 Computational tools for model analysis

Constructed mathematical models can be highly complicated, and may consist of a large number of parameters when considering a large number of biochemical reactions behind observed cellular activities as well as responses to environmental factors. Consequently, parameter estimation as well as experimental validation can be highly troublesome. Here, computational tools for model analysis are required in order to evaluate the constructed model characteristics, and thus help guide any further model modifications required prior to parameter estimation and experimental validation. In this way, model complexity as well as unnecessary experiments can be avoided.

Model identifiability

In addition to being capable of capturing cellular behaviour, the selected mathematical models should be identifiable. A model is considered as **unidentifiable** if they return the same simulated output in accordance with a given set of model input, no matter what the values of parameter are. On the contrary, the models are **identifiable** only if a relation between the simulated output and the given input can be reproduced from a limited number of values in a parameter range (Bellman and Åström, 1970, Walter and Lecourtier, 1981). They can be "globally" or "locally" identifiable depending how unique the values of parameter are (Cobelli et al., 1979). In addition, "structurally" identifiable models can be distinguished from "at-a-point" identifiable ones. The only difference is that "at-a-point" identifiability test can be performed only for models with given nominal values of parameters, and thus the model identifiability holds true only around the given nominal values. Structural ones analyse model identifiability regardless of values of parameters (Quaiser and Monnigmann, 2009).

Structural identifiability analysis

Structural identifiability analysis was firstly proposed by Bellman and Åström (1970) in an attempt to evaluate structural identifiability of model parameters. The analysis is performed based on a given set of model input without taking into account model uncertainty and measurement error (Bellman and Åström, 1970). Updated versions of structural identifiability analysis have been introduced so that it can study more complicated models, especially non-linear ODE systems (Chappell and Godfrey, 1992, Vajda et al., 1989). However, applications of structural identifiability analysis are limited to relatively small models, consisting less than 10 parameters (Sidoli et al., 2004). In addition, structural identification analysis can provide invalid information especially when mathematical models for noisy systems such as biological ones are concerned, resulting in a misleading conclusion

about the reliability of parameter estimates. Therefore, despite being structurally identifiable, models require further evaluation of their parameter reliability and accuracy. It is called "**practical identifiability analysis**", performed after parameters are estimated. The structural identifiability analysis can be considered as "a theoretical suggestion" and practical identifiability analysis is the validation of the suggestion (Miao et al., 2011).

Sensitivity analysis-based identifiability evaluation

Sensitivity analysis measures the variation of model output with respect to any change in model inputs including model parameters. If model output is found to be highly disturbed by small changes in a parameter value, this parameter is considered as a "significant" parameter. On the contrary, a large variation in an insignificant parameter value has little influence on model output (Kiparissides et al., 2009). Significant parameters are typically identifiable given their significant impact on the simulated model output while insignificant parameters are most probably unidentifiable. In this way, sensitivity analysis can indicate identifiability of model parameters. The sensitivity analysis can be performed prior to actual experiments, though it requires pre-estimates of model parameters. Unlike the structural identifiability analysis, the sensitivity approach is not concerned with model structure. Consequently, it can be applied to highly non-linear models. However, the sensitivity approach does not take into account uncertainties and measurement noises while practical identifiability analysis does (Miao et al., 2011).

Evaluation of model identifiability is performed based on sensitivities of parameters through several methods. The "correlation method" and the "orthogonal method" search for any possible dependent relations among parameters using the matrix of sensitivity coefficients representing the influence of each parameter on the simulated trajectories. If a parameter has a dependent correlation(s) to another, or other parameters, a change in simulated output caused

by a change in this parameter value can be compensated by changing other parameter values, and thus this parameter cannot be identifiable (Quaiser and Monnigmann, 2009, Yue et al., 2006, Rodriguez-Fernandez et al., 2006). Other methods called the "principle component analysis" (PCA) and the "eigenvalue method" utilise the sensitivity analysis to rank importance of parameters through calculating eigenvalues and their corresponding eigenvectors. The PCA employs the order of eigenvalues to justify discarding parameters while keeping any change in the simulated or observed output (due to discarding parameters) to a minimum (Degenring et al., 2004).

Global sensitivity analysis (GSA)

There are two main types of sensitivity analysis; local and global sensitivity analysis. Local sensitivity analysis (LSA) investigates each parameter sensitivity through varying a parameter estimate at a time while keeping the rest of parameter estimates unchanged. Global sensitivity analysis (GSA) provides sensitivity information of each parameter through simultaneously and randomly varying all parameter estimates (Kiparissides et al., 2009, Yue et al., 2006). Given that LSA does not take into account model uncertainties and depends on parameter nominal values, it might provide incomplete information of parameter sensitivities. GSA provides parameter sensitivities regardless of given nominal parameter values and variation ranges of parameter values. In addition, GSA takes into account model uncertainty given that it analyses parameter sensitivities through the simultaneous variation of all model parameters. It also provides the information about interactions or correlations between/among parameters (Kent et al., 2013, Kiparissides et al., 2009). Therefore, GSA becomes a superior choice for model analysis, though it requires relatively more computational resources.

GSA can be performed through two main approaches: 1) one that employs the model approximation to investigate significance of parameters, and 2) the other that measures

significance of parameters through estimating the total variance of model output. The variance-based approach is superior since it can provide information about interactions between/among parameters (Cho et al., 2003, Kiparissides et al., 2009). Sobol (2001) introduced variance-based GSA, so-called Sobol' method, which estimates sensitivity indices representing global parameter sensitivities. This method represents the output variability as a function of model parameters variability, through integrable and orthogonal summands of increasing dimensionality, called ANOVA decomposition (Sobol, 2001), as shown in Eq. 2.7.1. The output variability is defined as f(**X**) depending on a parameter vector **X**. This function is defined in the n-dimensional unit cube (In), where n is the number of model parameters of interest.

Eq. 2.7.1 ANOVA decomposition

$$f(X_1, \ldots, X_n) = f_0 + \sum_{i=1}^{n} f_i(X_i) + \sum_{1 \le i < j \le n} f_{ij}(X_i, X_j) + \ldots + f_{1,2,\ldots,n}(X_1, X_2, \ldots, X_n)$$

Constant — The first order — The higher orders

Where, f_0 is a constant and refers to the mean effect on output variability (the zeroth order term); $f_i(X_i)$ is the first order term that stands for the fractional contribution of single parameter (X_i) variation to output variability; $f_{ij}(X_i, X_j)$ is the second order term that accounts for the synergic effect of parameter X_i and parameter X_j on output variability; The higher order terms ($f_{1,2,\ldots,n}(X_1, X_2, \ldots, X_n)$) accounts for impact of cooperative interactions among two more parameters on output variability f(X).

As can be seen in Eq. 2.7.1, the first order effects, or so-called "main effects" can be distinguished from the higher order ones. It was suggested that the importance of parameters should not be ranked using only main effects. In addition, determining the higher order terms is essential to understand model parameter interactions and their impact on output variability (Chan et al., 1997).Therefore, the main effects and the "total sensitivity indices" (TSIs), which are the main effects combined with associated higher order effects, are recommended to be calculated in order to sort parameters into the right order of significance (Homma and Saltelli, 1996) as well as recognise the influence of interactions among model parameters (Kiparissides

et al., 2009). Sobol (2001) demonstrated a practical approach to estimate the terms in the ANOVA decomposition. To estimate terms in the ANOVA decomposition, Monte Carlo (MC) algorithm, which employs repeated random sampling in order to estimate the summands, is employed. In this way, uncertainties are also introduced to each parameters through (Quasi) MC random sequences. This makes it possible to practically estimate both the main effects and TSIs (Sobol, 2001).

In addition to the Sobol' method, there are other variance-based methods for GSA including updated versions of the Sobol' method. The extended Fourier amplitude sensitivity test (FAST) have been found to be on par with Sobol' method since it gives identical main effects and TSIs to those from Sobol' method (Chan et al., 1997, Kiparissides et al., 2009). Recently, the original Sobol' algorithm has been improved and it became more efficient for model evaluation (Sobol et al., 2007). One of the improvements is the method of high dimensional model representation (HDMR), which appears to be more computationally efficient. This method is fundamentally based on Sobol' algorithm, and thus the main effects and the TSIs can be obtained. Since this method requires much less space for repeated random sampling as compared to the original Sobol' method, the required computational time is reduced and the method can be applied to a wider range of applications (Ziehn and Tomlin, 2009).

2.7.4 Frameworks for predictive mathematical model development

A framework for development of mathematical models is a workflow, where steps for constructing, analysing and validating mathematical models are systemically organised to ensure that the resultant models are capable of capturing behaviour of systems of interest. Generally, the framework is comprised of model construction, model analysis (using GSA or LSA-based identifiability evaluation) and parameter estimation. Many mathematical models

for biological systems were introduced with their own frameworks which were based on such similar principles (Fang et al., 2009, Bucher et al., 2011, Nolan and Lee, 2011, Vargas et al., 2011).

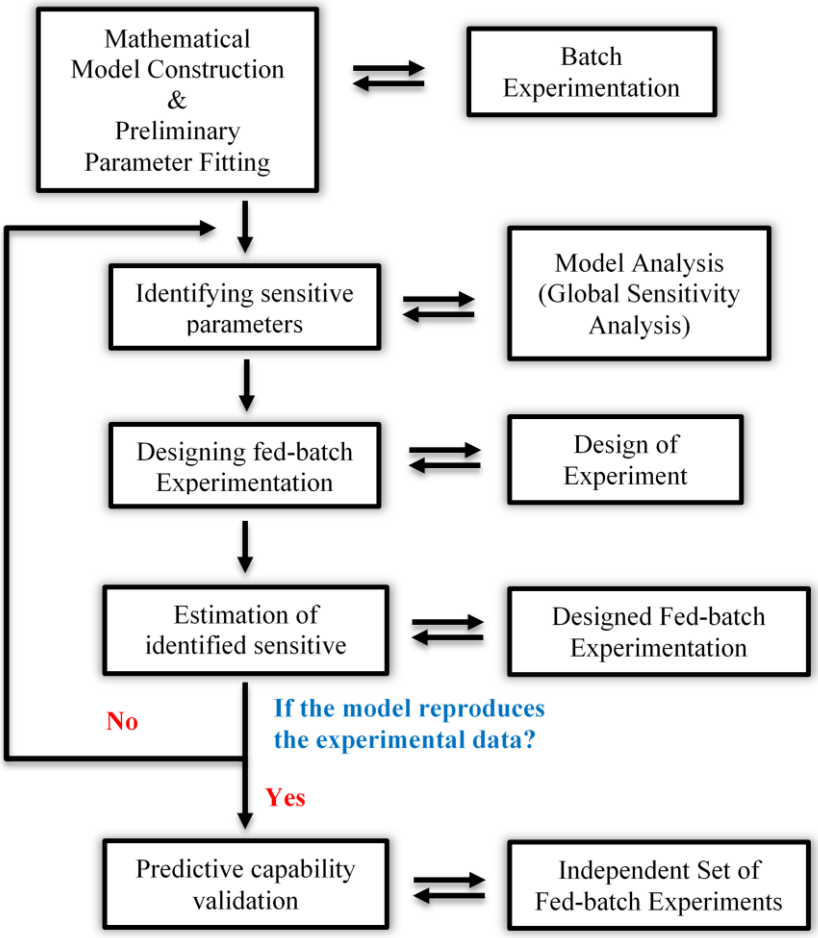


Figure 2.7.2 The framework for predictive mathematical model development proposed by (Kontoravdi et al., 2010).

However, the resulting models often lack predictability, especially when the models are applied for simulating situations other than one(s) used in experimental validation. For instance, the model developed based on a batch culture can fail to capture fed-batch and perfusion modes of cultures. Kontoravdi et al. (2010) introduced a systematic framework, where model analysis, design of experiment (DOE) and model validation are incorporated in a cooperative manner in order to achieve optimal estimates of sensitive and identifiable

parameters, as can be seen in Figure 2.7.2. DOE was performed to generate an optimal experimental condition in the fed-batch mode of cell cultures (optimal feeding interval, feeding concentration, etc.) in an attempt to validate the mathematical model constructed based on batch experiments. The mathematical model was then validated with experimental data from the designed experiment(s) and parameter values can be adjusted accordingly. The model with amended parameter estimates was tested with sets of experimental data including batch and fed-batch experiments. If satisfied, parameters were assumed to be well-fit, otherwise the whole process would be repeated until the simulated trajectories satisfactorily matched with the experimental data. The predictability of the model with the finalised parameter estimates from model validation was tested with data from independent set of experiments (Kontoravdi et al., 2010).

The finalised version of the mathematical model for the culture of a hybridoma cell line (CRL-1606), which was developed through the proposed framework, was able to capture an independent fed-batch culture profile (Kontoravdi et al., 2010). Ho et al. (2006) proposed the similar framework to Kontoravdi et al.'s to develop a mathematical model of mAb synthesis in the culture of a GS-NS0 cell line under different hyperosmotic conditions. GSA was performed to identify important parameters and to also guide identifiability of parameters. Modifications of the model developed based on a normal osmotic condition were performed in accordance with the GSA results (Ho et al., 2006). The predictive ability of the finalised version of the model was verified with an independent set of hyperosmotic experiments (Ho et al., 2012).

2.8 Mathematical models for cell growth, metabolism and death

Over the last few decades, mammalian cell cultures for industrial production of bio-therapeutics have allowed mathematical modelling to emerge as a powerful tool for *in silico*

studies of culture condition effects on culture performance. The models can provide the possible outcome of the cultures with regards to the variation of culture conditions, and thus help avoid trial-and-error experiments. To date, there are a number of mathematical models for bio-therapeutics production platforms, which are exploited as a basis for model development herein.

2.8.1 Unstructured models for cell growth and metabolism

Monod equation has been applied in order to represent the specific growth rate of mammalian cells under influence of limiting nutrients and metabolic by-products. The generic form can be written as shown in Eq. 2.8.1. The maintenance energy model was employed to describe utilisation rates of limiting substrates (Pirt, 1965, Pirt, 1982), which was formulated based on an assumption that substrates could be consumed for cell growth and cellular maintenance (Eq. 2.8.2). The generation rate of metabolic by-products was assumed to be proportional to the utilisation rate of substrates. The synthesis of antibodies was mathematically expressed by a simple linear correlation, where antibody synthesis can be dependent ($\alpha\mu$) and/or independent (β) from cell growth, as can be seen in Eq. 2.8.3.

Eq. 2.8.1 Monod equation for the specific growth rate

$$\mu = \mu_{max}\left[\frac{S_1}{S_1 + K_{S_1}}\right]\left[\frac{S_2}{S_2 + K_{S_2}}\right]\left[\frac{K_{P_1}}{P_1 + K_{P_1}}\right]\left[\frac{K_{P_2}}{P_2 + K_{P_2}}\right]$$

"Limiting" "Inhibiting"

Where, μ is the specific growth rate (s^{-1}); μ_{max} is the maximum specific growth rate (s^{-1}); S_1 and S_2 are the extracellular concentrations of limiting substrates ($mol.L^{-1}$); P_1 and P_2 are the extracellular concentrations of metabolic by-products ($mol.L^{-1}$); K is the substrate limitation or inhibition constant according to the subscripts ($mol.L^{-1}$).

Note that when substrate availability benefits the specific growth rate, the "limiting" term is used (the more available the substrate, the higher the term value), while the "inhibiting" term is used when substrate availability is detrimental to the specific growth rate (the more available the substrate, the lower the term value).

Eq. 2.8.2 The constant maintenance energy model

$$q_S = \frac{\mu}{Y_{X,S}} + m_S$$

Where, q_S is the specific substrate utilisation rate ($mol.cell^{-1}.s^{-1}$); $Y_{X,S}$ is the maximum yield of cell on substrate S ($cell.\ mol^{-1}$); m_S is the maintenance energy constant, subject to the substrate S ($mol.cell^{-1}.s^{-1}$).

Eq. 2.8.3 The correlation between the production rate of mAb and the specific growth rate

$$q_{mAb} = \alpha\mu + \beta$$

Where, q_{mAb} is the specific production rate of mAb ($mg.cell^{-1}.s^{-1}$); α is the growth-related constant ($mg.\ cell^{-1}$) and β the growth-independent constant ($mg.cell^{-1}.s^{-1}$).

These equations were widely used as a basis for development of cell growth and metabolism mathematical models for the mammalian cell cultures, as can be seen in Table 2.8.1. Model description may vary depending on (1) assumptions based on the observed phenomena and (2) characteristics of culture systems, including modes of culture, cell lines, and culture conditions. For example, with the culture of a hybridoma cell line, Bree et al. (1988) assumed that glutamine is the sole substrate that influenced growth kinetics as well as mAb production, while Miller et al. (1988) additionally took into account the impact of glucose on the specific growth rate. Models for glutamine consumption often neglect the maintenance energy term (m_S). de Tremblay et al. (1992) modified the growth-related constant in the mAb production equation in order to refine the effect of cell growth on the mAb production rate. Dalili, M., et al. (1990) found that both serum and glutamine affected cell growth, consequently the mathematical expression for cell growth was derived to take into account the impact of initial concentration of serum, and glutamine concentration. Frame, K. K. and Hu, W.-S. (1991) mathematically modelled the specific growth rate to be dependant only on glucose, given their experimental observation.

Table 2.8.1 Equations for the specific growth rate, the specific utilisation rate of substrates, the specific production rate of metabolic by-products, and the antibody synthesis rate. Adapted from (Pörtner and Schäfer, 1996).

Reference	Cell growth rate models	Substrate utilisation rate	By-product generation rate	Antibody synthesis rate
(Bree et al., 1988)	$\mu_X = \mu_{X,max} \cdot \left[\frac{Gln}{Gln + K_{X,Gln}}\right] \cdot \left[\frac{K_{X,Amm}}{Amm + K_{X,Amm}}\right] \cdot \left[\frac{K_{X,Lac}}{Lac + K_{X,Lac}}\right]$	$q_{Glc} = \frac{\mu_X}{Y_{X,Glc}} + m_s$ $q_{Gln} = \frac{\mu_X}{Y_{X,Gln}} + \frac{q_{mAb}}{Y_{X,Gln}} + \frac{q_{Amm}}{Y_{Amm,Gln(1)}}$	$q_{Amm} = Y_{Amm,Gln(2)} \cdot q_{Gln}$ $q_{Lac} = Y_{Lac,Glc} \cdot q_{Glc}$	$q_{mAb} = \alpha_{max} \frac{K_{p,Gln}}{Gln + K_{p,Gln}} \cdot \frac{X_V}{X_V + K_{p,X}}$
(Miller et al., 1988a)	$\mu_X = \mu_{X,max} \cdot \left[\frac{Glc}{Glc + K_{X,Glc}}\right] \cdot \left[\frac{Gln}{Gln + K_{X,Gln}}\right] \cdot \left[\frac{K_{X,Amm}}{Amm + K_{X,Amm}}\right] \cdot \left[\frac{K_{X,Lac}}{Lac + K_{X,Lac}}\right]$	-	-	-
(Pörtner and Schäfer, 1996)	$\mu_X = \mu_{X,max} \cdot \left[\frac{Gln}{Gln + K_{X,Gln}}\right]$	$q_{Gln} = \mu_{S,max} \cdot \left[\frac{Gln}{Gln + K_{S,Gln}}\right]$	$q_{Amm} = Y_{Amm,Gln} \cdot q_{Gln}$	*Constant* (4×10^{-10} mg cell^{-1} hr^{-1})
(de Tremblay et al., 1992)	$\mu_X = \mu_{X,max} \cdot \left[\frac{Glc}{Glc + K_{X,Glc}}\right] \cdot \left[\frac{Gln}{Gln + K_{X,Gln}}\right]$	$q_{Glc} = \frac{\mu_X}{Y_{X,Glc}} + m_s \cdot \left[\frac{Glc}{Glc + K_{S,Glc}}\right]$ $q_{Gln} = \frac{\mu_X}{Y_{X,Gln}}$	$q_{Amm} = Y_{Amm,Gln} \cdot q_{Gln}$ $q_{Lac} = Y_{Lac,Glc} \cdot q_{Glc}$	$q_{mAb} = \frac{\alpha}{\mu_X + K_{mAb}} \cdot \mu_X + \beta$

Table 2.8.1 (continue) Equations for the specific growth rate, the specific utilisation rate of substrates, the specific production rate of metabolic by-products, and the antibody synthesis rate. Adapted from (Pörtner and Schäfer, 1996).

Reference	Cell growth rate models	Substrate utilisation rate models	By-product generation rate models	Antibody synthesis rate models
(Frame and Hu, 1991)*	$\mu_X = \mu_{X,min} + \left[\frac{(\mu_{X,max} - \mu_{X,min})\,(Glc - Glc_{thres})}{(Glc - Glc_{thres}) + K_{X,Glc}}\right]$	$q_{Glc} = \frac{\mu_X - \mu_{X,min}}{Y_{X,Glc}}$ $q_{Gln} = \frac{\mu_X - \mu_{X,min}}{Y_{X,Gln}}$	-	-
(Dalili et al., 1990)	$\mu_X = \mu_{X,max} \cdot [Serum]_0 \left[\frac{Gln}{Gln + K_{X,Gln}}\right]$	$q_{Gln} = \frac{\mu_X}{Y_{X,Gln}} + K_{deg}$	-	$q_{mAb} = \beta \cdot [Serum]_0 \left[\frac{Gln}{Gln + K_{mAb}}\right]$
(Kurokawa et al., 1994)	$\mu_X = \mu_{X,max} \cdot \left[\frac{Glc}{Glc + K_{X,Glc}}\right] \cdot \left[\frac{K_{X,Lac}}{Lac + K_{X,Lac}}\right]$	$q_{Glc} = \frac{\mu_X}{Y_{X,Glc}} + m_s$	$q_{Lac} = Y_{Lac,Glc} \cdot q_{Glc}$	-

* The minimum specific growth rate or μ_{min} is the growth rate when the substrate level is at the minimum level, or the threshold substrate concentration (S_t), that cell can still grow.

There were attempts to incorporate relatively more detailed biological information into the simplified mathematical equations. Suzuki and Ollis (1989) proposed a mathematical model that aimed to capture cell growth in association with cell cycle progression, and associated production of antibody with culture progression through cell cycle phases. The total production of antibody was calculated based on the summation of the production of antibody of each cell cycle phase (Suzuki and Ollis, 1989). Unlike the model by Suzuki and Ollis (1989), Jang and Barford (2000) proposed an unstructured model that included production of mAb from cells arrested at G1 phase. The model was based on Monod-type equation (Eq. 2.8.1) accounting for the impact of limiting nutrients and metabolic by-products on the specific growth rate (Jang and Barford, 2000). Lam et al. (2008) adopted the same principle as Suzuki and Ollis (1989) to develop a mathematical model for the culture of a hybridoma cell line, which accounted for the influence of cell cycle progression on cell growth, death and mAb production. This model aimed to reproduce batch and fed-batch data toward feeding optimisation (Lam et al., 2008).

Kontoravdi et al. (2007) developed a model library for metabolism of 19 amino acids, which was based on the maintenance energy model (Eq. 2.8.3) as well as Monod-like expressions (Eq. 2.8.1) (Kontoravdi et al., 2007). Mathematical models for the culture for GS-NS0 cell line were constructed to capture the impact of intracellular ATP on the specific growth rate through Monod-type expressions (Kiparissides et al., 2011b). Recently, a mathematical model accounting for effects of culture temperature as well as temperature shifts on cell cycle progression and antibody production in the culture of a hybridoma cell line (CRL-1606) was proposed. The model was aimed to guide an optimal time point for the temperature shift to allow the cultures achieve the maximum antibody production. The model was formulated based on previous cell cycle models (where the specific growth rate depends on cell cycle time and

the production of mAb is subject to cell cycle phases) and Monod-type expressions (García Münzer et al., 2015).

2.8.2 Detailed cell growth and metabolism models

Unstructured mathematical models can be capable of reproducing observed phenomena. Nevertheless, sometimes they fail to capture particular circumstances where cells are dynamically adapting in response to environment changes, such as lag phases in the cultures(Fredrickson, 1976). Furthermore, advances in analytical techniques and measurements enable us to build up detailed insight into mechanisms of biochemical/cellular processes (cell growth, death and metabolism) as well as spatial properties of intracellular organelles/structures. Such detailed biological knowledge is essential to be incorporated into mathematical models in order to extend model predictive ability.

Structured models

Fredrickson (1976) proposed a formulation of a structured mathematical model, which was derived from the law of mass action together with mass balances of metabolic species (Fredrickson, 1976). Batt and Kompala (1989) adopted the model formulation by Fredrickson (1976) to build a structured mathematical model where metabolism was simplified by lumping similar metabolic species together as regards their biological relevance. Interactions among 4 intracellular and extracellular metabolic species was mathematically expressed by the combination of material balances, the law of mass action, and Monod-based expressions (Batt and Kompala, 1989).

Sanderson et al. (1999) developed a model that captured metabolic and transport activities throughout the entire cellular system that are applicable to the process of mAb synthesis. The reaction rates and specific growth rates were mathematically expressed using

Monod-type equations, while the rates of inflow/outflow of nutrients through cell membrane as a result of concentration differences (between intracellular and extracellular ones) were described using Michaelis-Menten kinetics. The model consists of around 90 ODEs, 109 algebraic equations (AEs) and around 390 parameters (Sanderson et al., 1999a). By manually adjusting parameter values to fit experimental data, 60 of these parameters were found to be significant (Sanderson et al., 1999c). Jang et al. (2000) also adopted the same approach to identify significant parameters, and then modified the model, which was developed based on the batch culture of a hybridoma cell line, to be able to reproduce experimental data from the batch culture of an insect cell line (Jang et al., 2000, Sanderson et al., 1999b). Bibila and Flickinger (1991) developed a structured, unsegregated mathematical model for the intracellular process of antibody synthesis, describing how molecules of antibody are synthesised; from transcription of heavy and light chains mRNAs, translation of the corresponding mRNAs and the process of antibody molecules being constructed (Bibila and Flickinger, 1991).

Hybrid models

Kontoravdi et al. (2005) combined a structured model for mAb synthesis, previously proposed by Bibila and Flickinger (1991), to an unstructured model describing cell growth and metabolism in the culture of hybridoma and NS0 cell lines. For the unstructured part, Monod-type mathematical expressions as well as the maintenance energy model were used to capture cell growth (subject to nutrient limitation and by-product inhibition), and nutrient utilisation as well as metabolic by-product generation, respectively. Like the original model, the mechanism of intracellular mAb synthesis was mathematically described using mass action kinetics (Kontoravdi et al., 2005). This model was later called a “hybrid model” where its model complexity is a compromise between unstructured and structured ones. Later, another hybrid model, which is based on the model by Kontoravdi et al., (2005), was constructed to capture

the effect of osmotic pressure on production of mAb in the culture of a NS0 cell line, and was modified to capture the culture under various osmotic conditions (Ho et al., 2006, Ho et al., 2012).

Dynamic metabolic flux analysis (dMFA)

The hybrid approach was also applied to MFA, so that it can provide changes in intracellular metabolic states under influence of a dynamic environment. It was suggested that metabolic shifts could be subject to the levels of glucose and glutamine (Zhou et al., 1997b, Sanfeliu et al., 1997). Zhou et al. (2006) proposed a dMFA describing intracellular metabolic activities (using a quasi-steady state assumption for intracellular metabolic activities), with links to Monod-type kinetics describing dynamic changes in extracellular conditions. The model can capture two different metabolic states: lactate consumption and production with regard to changes in specific glycolysis rates (Zhou et al., 2006). Another dynamic MFA was developed for the fed-batch culture of a CHO cell line. Kinetic expressions for dynamic change in extracellular conditions (i.e. concentration of glucose, lactate, amino acids, etc.,) were combined with quasi-steady state analysis for intracellular metabolic activities. The model was validated with various culture conditions, including temperature shifts, inoculum density, and concentration of nutrients (Nolan and Lee, 2011).

Population balance models (PBMs)

PBMs are mostly formulated based on detailed dynamics of cell cycle. The transition rate of cells, from one phase to the subsequent phase, is defined as a probabilistic function. This function is typically correlated with specific cellular characteristics that indicate when the phase transition could take place, such as cell size and DNA content. Liu et al. (2007) proposed a three-phase cell cycle (G_1, S, G_2/M) PBM to capture dynamics of cell cycle in the culture of a myeloma cell line. The probabilities that allow cells to move from G_1 to S phase and from

G_2/M to cell division was defined to depend on cell volume, while the probabilities of cell transition from S to G_2/M phase was correlated with DNA content. The model was also combined with the regulator model, which helps limit cell growth during the lag phase in the cultures, and took into account the limiting effect of lysine (Liu et al., 2007). A recent PBM describing four cell cycle phases (G_0, G_1, S, G_2/M) also employed the same transition probability functions to the model by Liu et al. (2007). However, these function applied more constraints such as cell shape factors, cell volume thresholds, etc., (Fadda et al., 2012).

2.8.3 Unstructured cell death kinetics

Cell death has a direct influence on culture viability and production as well as quality of the secreted bio-proteins. Kinetics of cell death is therefore undoubtedly required to be included in the mathematical models for mammalian cell cultures. It can be linked to limiting nutrient availability, cell growth as well as accumulation of toxic metabolic by-products, depending on assumptions as well as experimental observation. Table 2.8.1 summarises the existing mathematical expressions for cell death kinetics, most of which were constructed based on Monod-type expressions (Eq. 2.8.1).

As can be seen from the table, the specific death rates were correlated with the levels of nutrients: glucose (Frame and Hu, 1991) and glutamine (Dalili et al., 1990, Pörtner et al., 1996), given that these nutrients were assumed to be limiting. In addition, the death rates were assumed to be dependent on the concentrations of toxic metabolites, such as lactate and ammonia (Batt and Kompala, 1989). The specific death rate can be assumed to depend on the limiting substrates and the metabolites (Bree et al., 1988, de Tremblay et al., 1992), given that they were found to influence cell death in the cultures (Ozturk et al., 1992). The specific death rate may also be assumed to be an inverse function of the specific growth rate. Sanderson et al. (1999) employed the inhibition term of the Monod kinetics to describe the correlation between

the specific growth and death rates. Glacken et al. (1989) and Linardos et al. (1991) assumed the specific death rate to be inversely proportional to the exponential function of the specific growth rate, given that potential causes and detailed mechanisms for the onset of cell death was not still well-defined (Dodge et al., 1987).

Table 2.8.2 Models for the specific cell death rate. Adapted from (Pörtner et al., 1996).

Reference	Cell death rate models
(Frame and Hu, 1991)	$\mu_d = (\mu_{X,min} - D_{min}) - \mu_{d,max} \cdot \left[\frac{(Glc-Glc_{thres})}{(Glc-Glc_{thres}) + K_{d,Glc}}\right]$
(Dalili et al., 1990)	$\mu_d = k_{d,min} + (k_{d,max} - k_{d,min}) \cdot \left[\frac{K_{d,Gln}}{Gln + K_{d,Gln}}\right]$
(Pörtner et al., 1996)	$\mu_d = b_1 + \left[\frac{b_2}{Gln + b_3}\right]$
(Batt and Kompala, 1989)	$\mu_d = \mu_{d,max} \cdot \left[\frac{Amm}{Amm + K_{d,Amm}}\right] \cdot \left[\frac{Lac}{Lac + K_{d,Lac}}\right]$
(Bree et al., 1988)	$\mu_d = \mu_{d,max} \cdot \left[\frac{Amm}{Amm + K_{d,Amm}}\right] \cdot \left[\frac{Lac}{Lac + K_{d,Lac}}\right] \cdot \left[\frac{K_{d,Gln}}{Gln + K_{d,Gln}}\right]$
(de Tremblay et al., 1992)	$\mu_d = \frac{\mu_{d,max}}{\left(\mu_{X,max} - K_{d,Lac} \cdot Lac\right)\left(\mu_{X,max} - K_{d,Amm} \cdot Amm\right)} \cdot \left[\frac{K_{d,Gln}}{Gln + K_{d,Gln}}\right]$
(Jang and Barford, 2000)	$\mu_d = \left[\frac{\mu_{d,max}}{1 + \left(K_{d,Amm}/AMM\right)^n}\right]$
(Linardos et al., 1991).	$\mu_d = d_0 e^{d_1/\mu_X}$
(Glacken et al., 1989)	$\mu_d = C_1 e^{C_2 \cdot \mu_X}$
(Sanderson et al., 1999a)	$\mu_d = \mu_{d,max} \cdot \left[\frac{K_{d,\mu_X}}{\mu_X + K_{d,\mu_X}}\right]^2$

Later, Ho et al. (2006) adopted the specific death rate equation, proposed by de Tremblay et al. (1992), to account for kinetics of cell death in the culture of GS-NS0 cells. Since this culture does not suffer from ammonia accumulation and intracellular glutamine can be intracellularly house produced, the ammonia and glutamine terms in the original equation were omitted, and thus it was dependent only on lactate accumulation (Ho et al., 2006). Zhou

et al., (2006) and Liu et al., (2008) adopted the death rate equation, proposed by Sanderson et al. (1999), to describe kinetics of cell death in the myeloma cell cultures (Zhou et al., 2006, Liu et al., 2008). Jang and Barford (2000) related the specific cell death rate with ammonia concentrations through Hill functions (Table 2.7.1) (Jang and Barford, 2000). This expression was later applied to the mathematical models for the cultures of hybridoma and HEK-293 cells (Kontoravdi et al., 2005, Kontoravdi et al., 2007). The cell death kinetics in the mathematical model for the cultures of CHO cell lines was formulated based on the previously observed threshold levels of lactate and ammonia that CHO cells can tolerate. If the levels of lactate and ammonia were less than the threshold, the death rate would be reduced and vice versa (Kontoravdi et al., 2007).

2.9 Mathematical model description for apoptosis

Apoptosis becomes in the spotlight since the biochemical reaction network underlying apoptotic events as well as the kinetics of apoptosis was established (Vomastek and Franěk, 1993, Hengartner, 2000, Franěk et al., 1992). Furthermore, the onset of apoptosis is subject to various cellular processes, especially cell metabolism (Mason and Rathmell, 2011, Majors et al., 2007). Most importantly, apoptosis is found to be the main cause of the viability loss in the culture of mammalian cell lines (Goswami et al., 1999, DiStefano et al., 1996, Browne and Al-Rubeai, 2011a, Singh et al., 1994)). For these reasons, mathematical modelling is required for the study of apoptosis as well as its dynamic behaviour in response to various death stimuli in the mammalian cell cultures.

2.9.1 Mathematical models for apoptotic pathways

As above discussed, apoptosis is a physiological process that is triggered and executed in an organised manner (Saini and Walker, 1998). There are a number mathematical models

developed based on mechanistic understanding of biochemical reaction networks underlying the apoptotic pathways. These models aim to establish a core apoptotic cascade, whereby cell death fate is governed in accordance with death signals. Given that apoptosis induction was observed to be a fast process in a single cell level while the speed of apoptosis induction was much slower when a cell population level was concerned, Eissing et al. (2004) proposed a kinetics-based model describing interactions among apoptotic species in the receptor-induced apoptotic pathway: caspase-3, caspase-8, and inhibitors of apoptosis proteins (IAPs), with an additional effect of bifunctional apoptosis regulator (BAR). This regulatory cascade displays irreversible bistability, where there are two stable states existing in the system, and this characteristic might reflect how cell fate is governed and reconciles the fast apoptotic induction in the single cell level with the slow induction speed in the cell population level (Eissing et al., 2004).



(A) (B)

Where, Act is Activator, Ena is Enabler, InBax is Inactive Bax/Bak, acBax is Active Bax/Bak and MAC is Mitochondrial Apoptosis Channel.

Figure 2.9.1 Two models of the Bcl-2 family member interactions. The difference between (A) and (B) is the auto-activation of active bax. Adapted from (Cui et al., 2008).

Bistability, which can reflect as apoptotic switch-like responses, is often found arising from interactions among species forming feedback regulatory networks. Legewie et al. (2006) suggested that an implicit feedback loop could arise from the interaction network where active caspase-3 molecules enhance itself by neutralising the inhibitory effect of XIAP on caspase-9. The simulated results from the proposed kinetics-based model demonstrated that the positive

feedback generates bistability, and also irreversibility when considering together with another feedback loop where activation of capase-9 is enhanced by the feedback signal from activation of caspase-3. This model also suggests that how apoptotic responses to death signals; whether switch-like (all-or-none) or gradual; and reversible or irreversible, depends on to what extent apoptosis inhibitors (i.e. XIAP) become involved in the feedback loop (Legewie et al., 2006). Given that the mechanism of interactions among Bcl-2 family members underlying apoptosis induction at the upstream of the mitochondrial pathway was still elusive, Cui et al. (2008) proposed possible molecular mechanisms of the interactions, as shown in Figure 2.9.1. The simulated results suggested that two proposed positive feedback networks; 1) active Bax inhibiting Bcl-2; and 2) auto-activation of Bax, can bring about bistability indicating the apoptotic switch-like response. By performing stochastic simulations, this model can reproduce the experimental data where bimodal Bax-activation distribution of cell populations was observed (Cui et al., 2008).

Bagci et al. (2006) developed a mathematical model for the mitochondria-mediated apoptotic pathway, which cooperative binding (or Hill function) was included to describe the formation of apoptosome complex. They pointed out that bistability arose from the cooperativity in the apoptosome formation and it was found to be more robust to intrinsic noises than other earlier proposed models (Bagci et al., 2006). The concept of cooperative binding was applied to Bax-polymerisation, where Bax molecules cooperatively bind to each other to form an active, tetrameric compound of bax molecules (active Bax). A mathematical model was developed to capture Bax polymerisation in responses to lethal stimuli. It was pointed out that a bistable switch with irreversibility (survive or apoptosis) arose from the cooperative mechanism for Bax-polymerisation. By analysing the model both deterministically and stochastically, the model has high resistance to stochastic noises (Chen et al., 2007).

In addition to mathematical models that aim to establish a core module governing apoptotic switch-like responses, there are mathematical models that account for the entire picture of apoptotic pathways. Fussenegger et al. (2000) developed a mass action kinetics-based mathematical model where both the intrinsic (mitochondria-dependent) and the extrinsic (receptor-mediated) pathways were included (Fussenegger et al., 2000). Although the simulated results were comparable to experimental observation, it lacks of experimental validation. Furthermore, anti-apoptotic mechanisms were omitted in this model, and consequently the model always progresses toward the onset of apoptosis (Bagci et al., 2006). Bentele et al. (2004) developed a GSA-associated systematic framework for constructing a kinetics-based mathematical model for CD95-induced apoptosis where both apoptotic pathways were involved. The use of GSA helps simplify the complexity of resulting model and guides to create experimental design for parameter estimation (Bentele et al., 2004).

Hua et al. (2005) constructed a computational model that describes the death receptor mediated apoptosis, where the death signals are transduced from the interactions between Fas and Fas ligands to activate caspase-8, and in turn activate caspase-3 as well as the mitochondria-induced pathway. Two-third of parameter values were determined by manually adjusting the values until the model could reproduce the experimental data. The sensitivity study of lethal stimuli suggests that expected symmetric effects on apoptotic responses could not always be achieved, given the experimental data showing that Bcl-2 overexpression had inhibitory impact on activation of caspase-3 while Bcl-2 knockdown had insignificant impact on caspase-3 activation. In addition, the dominant pathway to initiate the caspase-3 activation could be both apoptotic pathways depending on expression levels of apoptotic molecules (Hua et al., 2005). Okazaki et al. (2008) scrutinised the switch between the two apoptotic pathways, as suggested by Hua et al., 2005, via computational simulations. They adopted the mathematical model originally developed by Hua et al., (2005), which was then refined by 1)

omitting parameters insensitive to activation of caspase-3 via the receptor-mediated apoptotic pathway and 2) applying kinetics consideration, including equilibrium and quasi-steady state assumptions. It was suggested that the transition from the receptor-dependent pathway to the mitochondrial pathway is subject to the activation rate of caspase-8 and the initial expression level of caspase-9 (Okazaki et al., 2008).

Zhang et al. (2009) proposed a kinetics-based mathematical model for the intrinsic pathway with a link to the death receptor pathway via activation of caspase-8. What makes this model differ from other ones describing both apoptotic pathways is that it generates apoptotic switch-like characteristics. The model was applied to study dynamics behaviour of apoptosis in various scenarios, including in mutants (overexpression and knockdown of XIAP) and the variable levels of p53-associated apoptotic proteins. It was suggested that cell cycle arrest and DNA repair are among the very first cellular processes that respond to the cellular stress due to DNA damage, and apoptosis is the ultimate destination in case cells could not manage to relieve the stress (Zhang et al., 2009).

Given the involvement of the UPR-associated pathways in apoptosis, mathematical models for ER-stress associated apoptosis were introduced. Tyson et al. (2011) developed a preliminary mathematical model to account for the oestrogen signalling network in breast cancer cells. The model included the UPR pathways in accordance with the ER stress with links to cell cycle progression, autophagy and apoptosis. The model, despite not experimentally validated, showed decision-making mechanisms where cells decide to survive or die, grow or arrest, and repair or bypass (Tyson et al., 2011). A mathematical model accounting for mechanistic activation of the three pathways of the UPR was firstly developed. The model was constructed using ODEs and consists of interconnected four modules. The module of receptor activation accounts IRE1, PERK and ATF6 activities. The module of translation attenuation represents translation and apoptosis control by PERK. There are two adaptive response

modules accounting for IRE1 and ATF6 branches in the pathways. The model consists of 82 parameters, most of them were arbitrarily assigned given no experiment conducted for parameter estimation. Bifurcation analysis showed that there were three states (low, intermediate and high) of behaviour arising from the pathways depending on the level and duration of the stress as well as the level of BIP. Oscillation responses, especially in translation, were observed in the intermediate state and were thought to be how cells adapt to the ER stress (control of apoptosis and translation process) (Erguler et al., 2013).

2.9.2 Mathematical models for apoptosis in mammalian cell cultures

Apoptosis can represent cell death in the mammalian cell cultures, given that the majority of dead cells is a result of apoptosis. There are several existing mathematical models for the cultures of mammalian cells manufacturing bio-pharmaceuticals that describe apoptosis with its link to other cellular processes. Meshram et al. (2012) proposed a population-based mathematical model that describes induction of apoptosis via both two pathways in the batch culture of a CHO cell line producing Anti-RhD mAb. They assumed that the receptor-mediated apoptotic pathway was induced by death signal transduction from cell-cell communication, while the mitochondrial pathway was assumed to be triggered by metabolic stresses. Apoptotic cell sub-populations were characterised by the difference in activation levels of caspase-8, 9 and 3. For example, the healthy cell population was defined by a low activation level of all caspases while the receptor-mediated apoptotic cell population was the group of cells with a higher activation level of caspase-8, but caspase-9 and -3. The transition rates between sub-populations in the direction that cells eventually underwent apoptosis were presumed to be linear (Meshram et al., 2012). MFA was combined with the apoptotic population-based model in order to account for interplay between apoptosis and metabolism (i.e. ammonia production, and cell growth) (Meshram et al., 2011). However, this apoptosis model was apparently

independent from the metabolic model since it was assumed that cell growth and the apoptotic triggers were the result of changes in levels of an unidentified substrates which was not included in the metabolic sub-model.

Naderi et al. (2011) studied dynamics of apoptotic cells though a combined mathematical modelling and experimental approach. Similar to the model presented by Meshram et al. (2012), a logistic model was applied to represent dynamics of cell populations, where non-growing cells were separated from growing cells. The logistic model and the MFA-associated dynamic equations, which describe intracellular metabolic fluxes and their links to kinetics of extracellular metabolites, were interlinked through the estimation of cell populations (growing and non-growing) and the impact of metabolite levels on the onset of apoptosis (glucose and ammonia). Parameter estimation was performed with batch experimental data where initial glucose and glutamine were varied and the model with the parameter estimates was validated with an independent fed-batch experiment (Naderi et al., 2011). Later, this model was modified to account for the inhibitory effect of a pH reducing unidentified compound since experimental observation pointed out the impact of reducing pH on cell growth and viability. (Naderi et al., 2014).

Chapter 3

Thesis Goal

3.1 Research gaps

As the literature review (Chapter 2) attests, there are several areas that have not been explored although they could be the key to better construct understanding of apoptosis in the mammalian cell cultures. The following are concluding remarks as well as research gaps extracted from the literature review:

- Apoptosis is the main cause of cell death in the mammalian cell cultures for bio-therapeutic proteins production. It has strong links to cell proliferation (cell cycle progression) and metabolism, nevertheless this links have not been clearly demonstrated.
- The control of cell cycle progression and the apoptosis suppression, despite being closely interlinked, show different effects on production and productivity of secreted bio-proteins. This could be because they affect metabolic activities in a different manner, and how they affect metabolic activities could be the key to establish how to balance apoptosis and cell proliferation to achieve higher production and productivity of secreted bio-proteins.
- Apoptosis induction involves significantly transcriptional processes, which are activated in accordance with metabolic stresses. In addition, there is a potential link between the expression of heterologous proteins and the increased ER stress that can induce apoptosis. However, understanding of apoptosis induction at the transcriptional and post-translational levels with its association with the metabolic stresses as well as the ER stress is still not clearly demonstrated.
- Culture temperature and medium contents are among those culture conditions that can significantly affect cell growth, death and metabolism. However, their effects on apoptosis have not been clearly elucidated.

- Apoptosis found to be delayed in fed-batch cultures. It is necessary to further study apoptosis and its mechanism in response to addition of nutrients, given that fed-batch cultures are widely utilised for industrial manufacture of bio-therapeutics and prolong culture viability via apoptosis suppression is one of potential strategies used to improve productivity and production of the cultures.
- Cell death has been superficially described in mathematical models for the mammalian cell cultures. Given that apoptosis represents cell death in the cultures, mathematical models for apoptosis in the mammalian cell cultures are recently presented (Meshram et al., 2012, Meshram et al., 2013, Naderi et al., 2011, Naderi et al., 2014). However, these models are based on the quasi-steady-state assumption, which dynamic change in concentrations of metabolic species is omitted and thus links to metabolism are not well described. These models also lack mechanistic representation of apoptosis; they are based on logistic equations and include no mechanism for inhibition of apoptosis which plays an important role in the control of apoptosis induction.
- Sensitivity analysis is extensively included in proposed frameworks for model development. It helps identify significant parameters, and thus allows managing unnecessary information included into mathematical models through discarding insignificant parameters.
- GSA employs simultaneous variations of parameter estimates, and thus provides parameter sensitivities regardless of given nominal parameter values and also accounts for model uncertainty. In addition, interactions among parameters can be evaluated using GSA. Therefore, GSA is a superior tool for model analysis which is essential for evaluation of model parameter significance and identifiability.

3.2 Thesis goal

Given the identified research gaps, further investigation of apoptosis is crucial to the improvement of mammalian cell cultures toward higher mAb production and productivity. Given that mAb production is subject to viability and metabolic states of the cultures, the onset of apoptosis and its links with relevant cellular processes, including cell cycle progression and metabolism, need to be investigated. The study of the effects of culturing conditions, including temperature and extracellular nutrient concentrations, on apoptosis is also essential for the improvement of mammalian cell cultures since the culturing conditions directly affect cell growth, death and metabolism. In order to construct a mechanistic insight into apoptosis; its links with cell growth and metabolism; and the effects of the culturing conditions on apoptosis, the study has to be performed in a systemic way where apoptosis is scrutinised as regards dynamic change in the culturing conditions, as well as cell proliferation and metabolic activities. To the best of my knowledge, such the systematic view of apoptosis has not been extensively conducted in any systems of mammalian cell cultures.

In this study, the combined experimental and computational approach is adopted to study apoptosis in the GS-NS0 cell cultures. The research aim of this thesis is to develop understanding of apoptosis, its association with other cellular processes, as well as its dynamic behaviour in response to potential apoptotic stimuli in the cultures. The strategy is to firstly investigate apoptosis kinetics in batch cultures. The insight into apoptosis gained from the batch experiments form the basis for fed-batch experimentation as well as mathematical model development. The observed phenomena in the fed-batch cultures can be used to validate observed results in the batch cultures as well as assumptions made based on the batch data. The model development utilises both batch and fed-batch data in order to enhance model reproducibility and practicability toward the fed-batch cultures. Model analysis is employed

for further improvements of the developed mathematical model. Overall, the goal is to utilise the herein established understating of apoptosis for the construction of a mathematical model for apoptosis in the GS-NS0 cell cultures which can reproduce what was observed in the batch and fed-batch cultures.

Chapter 4

Materials and Methods

4.1. Mammalian Cell cultures

4.1.1 Cell line

The NS0 mouse myeloma cell line, kindly provided by Lonza Biologics (Slough, UK), was used in this study. The cell line is transfected with the GS selectable marker and DNA vectors encoding a chimeric B72.3 IgG4 antibody. Therefore, the cell line can be grown in glutamine-free medium and produce the antibody. The antibody is designed to recognise the Tag-72 tumour marker in colorectal cancer.

4.1.2 Medium preparation

Table 4.1.1 Medium preparation.

Components	Final concentration	Amount (mL)
Advance DMEM (Invitrogen, 12491-023)	81% v/v	810
FBS (Invitrogen, 26400-044); Lot# 1082741	10% v/v	100
GS-supplement, 50X (Sigma-Aldrich, 58672C-100mL)	1X	20
MEM amino acid solution, 50X (Invitrogen, 11130-036)	1X	20
MEM non-essential amino acid solution, 100X (Sigma-Aldrich, M7145)	2X	20
MEM vitamin solution, 100x (Invitrogen, 11120-037)	1X	10
Penicillin-Streptomycin Solution, 10,000 I.U./mL (ATCC, 30-2300)	100 I.U./mL	10
4.5mM MSX (Sigma-Aldrich, M5379)	25µM	10
	Total	**1000**

The medium used for maintaining the cell line is based on glutamine-free Advance DMEM. The medium was also supplemented by adding dialysed Fetal Bovine Serum (dFBS), amino acids and vitamins (the formulation of the added amino acids and vitamins is as the DMEM medium). Penicillin-Streptomycin was used as an antibiotic in the medium and L-

methionine sulfoximine (MSX) was added to the medium so that cells without GS-overexpression are selectively removed. Table 4.1.1 describes the amount as well as the sources of each component required to compose a 1 litre of the medium.

The medium pH was measured, using S20 SevenEasy™ pH meter (Mettler-Toledo) and adjusted to pH 7.1 – 7.2 by adding drops of 1M NaOH. The adjusted pH medium was then filter-sterilised. A sample from the sterile filtered medium was taken and checked for the final pH level. Typically, the final pH was around 7.3 to 7.4. The medium was then stored at 4°C for up to 2 weeks.

4.1.3 Cryopreservation and cell expansion

The cell line was cryopreserved in a cryovial with the medium containing 10% by volume of dimethyl sulfoxide (DMSO). For cell expansion, a cryovial containing cryopreserved cells was thawed in a water bath (37°C) for 1 minute. Then, the thawed cells were transferred to 10 mL of pre-warmed fresh medium (37°C) in a 15 mL sterile falcon tube. The suspension was then centrifuged using Rotina 46R centrifuge (Hettich Zentrifugen) for 5 minutes at 800 rpm to remove the cryopreservation medium containing DMSO that can be toxic to cells (Galvao et al., 2014). The cell pellet was then re-suspended with 25 mL of pre-warmed medium (37°C) and transferred to a 125 mL Erlenmeyer flask (Corning, 431143). The routine subcultures were conducted every 2.8-2.9 days with 2×10^5 cells/mL inoculation cell density for 5 to 6 times prior to the experiments.

4.1.4 Culture conditions

The cell culture was performed in triplicate (n=3) on NU-5500E (Triple Red) humidified incubator under a sterile condition at 37°C and 5% CO_2. In the incubator, the cell culture was conducted on an orbital shaker (Stuart, SSL1) with the shaking speed at 125 rpm.

The conditions were verified and calibrated with independent measurements of temperature and CO_2 level before starting the culture. A 125 mL flask consisting of 25 mL of the sterile medium was treated as a negative control to confirm the sterile condition.

4.1.5 Experiments

Batch culture

The cell line was maintained in the 1 litre Erlenmeyer flask (Corning, 431146) with 250 mL working volume under the culture condition as previously described. The duration of the culture was 7 days without changing any environmental conditions neither adding nutrients during the culture period. Samples were regularly harvested for further analysis; it can be once a day or twice a day depending on analytical techniques to be performed. This is discussed in the following sections.

Culture temperature and conditioned medium studies

These experiments employed the same culturing condition as the batch experiment, except that 1) for the culture temperature study, the culture temperature was shifted during the culture progression; 2) for the medium shift study, the amount of fresh medium was varied at the beginning of the culture. The details of these experiments are discussed in Chapter 6.

Fed-batch culture

The fed-batch experiments were conducted under the same culturing conditions as the batch experiment. However, there were feeding streams of glucose and amino acids during the culture progression. The characteristics of the feeding strategies is discussed in Chapter 6.

4.1.6 Sample collection

Given that there are analytical techniques that require only cells while others require cell-free spent medium, cells have to be separated from the spent medium using centrifugation. Separated cells can be divided into two groups: The first group is for the live cells analysis, including apoptotic cell quantification. The other group can be stored under appropriate conditions for later analysis, such as cell cycle analysis and gene expression measurements. More specifically, the separated supernatant samples can be stored at -20°C for later metabolite and mAb quantification. Prior to centrifugation, a part of the sample was used for measurements of cell density and viability.

4.2. Cell analysis

4.2.1 Cell density and viability

Cell density and viability were determined with the use of the haemocytometer. More specifically, 25 μL of fresh samples were mixed with 25 μL of 0.1% erythrosine B stain (ATCC, 30-2404). Then, the resulting blend was placed on the haemocytometer (Marienfeld-Superior, 0630030) with a cover glass. The counts of viable and dead cells were performed under the light microscope (Leica, DM IL LED), where the dead cells are stained red while the viable cells remain unstained (white). The estimation of both viable and dead cell density was performed through the following equations.

Eq. 4.2.1 Cell density estimation

$$\text{Cell density } \left(\frac{\text{cell}}{\text{mL}}\right) = \frac{\text{Average live or dead cells per a square}}{\text{volume of a square (0.0001 mL)}} \times \text{Dilution factor (2)}$$

Eq. 4.2.2 Viability estimation

$$\text{Viability } (\%) = \frac{\text{Viable cells}}{\text{Viable cells + Dead cells (Total cells)}} \times 100$$

The following is an example of how cell density and viability are estimated. Assume that viable/dead cell counts were obtained under microscope as shown in Figure 4.2.1.

28/3		32/5
	21/2	
25/4		24/6

Figure 4.2.1 Cell count example (viable/dead).

- ✓ The total viable cell count; 28 + 32 + 21 + 25 + 24 = 130 cells.
- ✓ The average viable cell count; 130/5 = 26 cells.
- ✓ The total dead cell count; 3 + 2 + 5 + 4 + 6 = 20 cells.
- ✓ The average dead cell count; 20/5 = 4 cells.
- ✓ The total number of cell counts; 130 + 20 = 150 cells.
- ✓ Therefore, the percent of cell viability = 130/150 × 100 = 86.67% (Eq. 4.2.1).
- ✓ The viable cell density = $^{26}/_{0.0001} \times 2$=520,000 cells/mL (Eq. 4.2.2).
- ✓ The dead cell density = $^{4}/_{0.0001} \times 2$=80,000 cells/mL (Eq. 4.2.2).

4.2.2 Apoptotic cell quantification

There are morphological and physiological changes that can be accounted as “apoptotic characteristics”; namely activation of apoptotic proteins, mitochondrial elements, changes in plasma membrane, cell shrinkage, chromatin condensation as well as DNA fragmentation (Ormerod, 1999). These distinct apoptotic characteristics generate corresponding analytical

techniques that can indicate the occurrence of apoptosis. However, each technique has both advantages and disadvantages. The light microscopic technique, for example, identifies apoptotic cells by their specific morphological changes, such as cell blebbing, as well as cell shrinkage. It has proved to be the most reliable measurement for apoptosis, however, it is not suitable for kinetic and statistic studies that request accurate quantitation given its subjective nature (Vermes et al., 1995). DNA fragmentation can be observed in both necrosis and apoptosis, and therefore techniques measuring DNA fragmentation (such as TUNEL assay as well as gel electrophoresis) can provide false-positive apoptotic events. In addition, they are more qualitative than quantitative, therefore not suitable for quantitative studies (Milner et al., 1996, Ormerod, 1999, Vermes et al., 1995).

In this study, we employ a flow cytometry based technique that measures the externalisation of phosphatidyl serine (PS), which is one of key morphological changes occurring during the progression of apoptosis. This event was found to be a downstream feature of early caspase activation, and occurs as early as chromatin condensation and earlier than DNA fragmentation. In addition, it lasts until the final stage of apoptosis (Cotter and Martin, 1996, van Engeland et al., 1998). This technique provides quantification of apoptotic cells.

The dual staining assay consists of Annexin-V-FITC (Biolegend, 640906), which is specifically binding to PS, and 20 μg/mL Propidium Iodine (PI, Sigma-Aldrich, P4170) in the binding buffer. Apoptotic cells can be categorized into 1) early stage apoptotic (ESA) cells and 2) late stage apoptotic (LSA) cells or secondary necrotic cells. The latter are characterized by the rupture of the cell membrane, one of the final morphological changes occurring during final stages of apoptosis (Ormerod, 2000). Therefore, LSA cells are PI positive. In contrast, viable cells and ESA cells are PI negative, given that their cell membranes are still intact. Annexin V binds to PS, which is a phospholipid cell membrane component that normally faces toward

cytoplasm. When undergoing apoptosis, PS is externalized. Thus, both ESA and LSA cells are Annexin V positive, while viable cells are Annexin V negative (Browne and Al-Rubeai, 2011a). In this way, ESA cells (Annexin-V positive, PI negative) can be distinguished from LSA cells (both positive) and Viable cells (both negative).

The separated, fresh cell pellets, isolated from each culture replicate as previously described, were immediately re-suspended in the binding buffer (Biolegend, 422201). The amount of the binding buffer used depended on how many cells (in total) in the pellets in order to make 1×10^6 cell/mL cell suspension; for example, add 0.6 mL for 6×10^5 cells. Then, take 100 µL from the cell suspension for each microtube as indicated in Table 4.2.1. They were then differently stained in order to create controls for the compensation together with the sample.

Table 4.2.1 ESA cell analysis.

Microtube	Sample	Staining
Control 1	100 µL	No staining
Control 2	100 µL	5 µL of Annexin V-FITC solution
Control 3	100 µL	3.5 µL of the PI Solution
Sample	100 µL	5 µL of Annexin V-FITC + 3.5 µL of the PI Solution

The stained samples and controls were incubated for at least 15 minutes but not over 30 minutes, in the dark and at room temperature. They were then re-suspended with another 300 µl of the binding buffer, just before the flow cytometry analysis. The data collection was performed using LSRFortessa cell analyzer (BD Biosciences). At least 3×10^4 events were recorded and all data were then processed and analysed in FlowJo 7.6.5 (Tree Star Inc). The gates to discriminate population were created in accordance with the controls and as suggested from previous studies (van Engeland et al., 1998, Vermes et al., 1995). Appendix A.1 shows

the fluorescent laser configuration set for recording the events and how the gates were created to distinguish the apoptotic populations.

4.2.3 Cell cycle analysis

Cell cycle analysis is basically the measurement of DNA content by using PI staining. PI is a highly fluorescent agent when binding to nucleic acids and it binds to DNA/RNA molecules by intercalating between the bases inside these molecules (Suzuki et al., 1997). Thus the DNA content in samples can be proportionally measured using a fluorescence measurement. To remove any unwanted RNA contamination in samples, the samples were treated with Ribonuclease A which was added in the PI staining solution.

The separated cell pellet from spent medium, as previously described, was re-suspended in cold methanol (Sigma-Aldrich, 179337) in order to fix the cells. The suspension was maintained at -20°C for 1 week before analysis. By fixing the cells, their cell membranes are permeable, and therefore PI can diffuse into cells. The fixed samples were then centrifuged to remove the fixing agent. The remaining cell pellets were washed with PBS (Invitrogen, 10010-015) and then were stained with 1 mL of 50 µg/mL PI (Sigma-Aldrich, P4170) and 100 µg/mL of Ribonuclease A (Sigma-Aldrich, R4875) in PBS. The stained samples were incubated at room temperature in the dark for 30 minutes prior to flow cytometer analysis. At least 10,000 events were recorded on LSRFortessa. All data were then processed and analysed in FlowJo 7.6.5 (Tree Star Inc). The gates to distinguish G_1/G_0, S, G_2/M were applied in accordance with the previous study (Watson et al., 1987). Appendix A.2 describes the data acquisition as well as the data analysis performed in Flowjo.

4.2.4 The profiling of cyclins and Ki-67 proliferation marker

These analytical techniques were conducted in collaboration with D. G. García Münzer (PhD candidate) and A. Gauthier (Master student).

Fixation and permeabilization

The following sample preparation procedure was used for both Ki-67 staining and cycling profiling. The cell pellets (around 1×10^6 cells) isolated from the harvested samples were fixed and permeabilised by drop-wise adding 1 mL of pure and cold methanol for cyclin D1 and B1 analysis, or 1 mL of 75% cold ethanol (VWR, 20821) for cyclin E1 analysis. Then, the fixed samples were kept at -20°C for up to 48 hours prior to analysis.

To start analysing the samples, the fixing agent was then removed by centrifugation (at the same condition to that for cell culture). The fixed cell pellets were gently washed with 1 mL of the washing solution. The washing solution is the PBS (Invitrogen, 10010-015) based solution containing 1% (w/v) bovine serum albumin (BSA) (Sigma-Aldrich, A9418) and 0.01% (w/v) sodium azide (Sigma Aldrich, S2002). Then, the washing solution was removed by centrifugation at the same condition. The remaining cell pellets were re-suspended with 50 µL of the saponin based washing solution prior to the staining. The suspension was then stained with either Ki-67 marker or anti-cyclins.

Cyclin profiling

The measurement of cyclins employs the principle of immunocytochemistry, where a primary antibody with a fluorescent tag is used to specifically bind to a protein or an antigen of interest. This allows us to track down cyclin activities along with the progression of cell cycle. In addition, the threshold expression of cyclins in each phase of the cell cycle can be determined. Here, various antibodies were used as specific markers for the corresponding

cyclins: mouse IgG1 anti-human cyclin B1 FITC-labelled (BD Biosciences, 554108), rabbit polyclonal IgG FITC-labelled anti-cyclin E1 (Bioss USA, bs-0573R-FITC) and mouse IgG2a anti-human cyclin D1 FITC-labelled (Invitrogen, AHF0088). Given that false positive results might arise from non-specific binding or unexpected protein-protein interactions, an isotype control antibodies which are corresponding to the cyclin antibody markers were included into the assay: mouse IgG1 FITC-labelled isotype control (BD, 554108) for the anti-cyclin B1, rabbit polyclonal IgG FITC-labelled anti-mouse isotype control (Bioss USA, bs-0296R-FITC) for the anti-cyclin E1 and mouse IgG2a FITC-labelled isotype control (Invitrogen, MG2a01) for the anti-cyclin D1. This was treated as a negative control of the assay, indicating the background signal.

The antibodies as well as the isotope antibodies were mixed with the suspension, obtained as above described, as per manufacturer's instruction. For example, 10 µL of mAb anti-cyclin D1 FITC conjugate and 20 µL of mouse IgG2 FITC conjugate (Invitrogen, #MG2A01) were added to the samples for cyclin D1 analysis. The incubation was performed for 30 minutes at room temperature in the dark.

Ki-67 proliferation marker

Given that Ki-67 protein is present during proliferative states of cycle cell (G_1, S, G_2 and M) and absent in G_0 phase where cells are in a quiescent state (Gerdes et al., 1984), the expression of Ki-67 can be used to distinguish the resting cells (at G_0 phase) from the proliferative cells.

The suspension, obtained from the sample preparation step, was stained by adding 20 µL of a PE Mouse Anti-Human Ki-67 or the isotype (BD, 556087). Then, the stained samples were incubated for 30 minutes at room temperature in the dark.

Cell cycle analysis integration

DNA can be also stained in both Ki-67 stained samples and anti-cyclin stained samples in order to gain the cell cycle prolife together with the Ki-67 expression and the profile of cyclins, respectively. The Ki-67 stained samples and anti-cyclin stained samples were washed with the washing solution, followed by removing the solution through the centrifugation. Then, DNA was stained using the PI solution. The procedure for cell cycle anlysis is described in Sub-section 4.2.3. However, FxCycle violet stain (Invitrogen, F10347) could be used for staining DNA in case there were more than two staining in a sample (ex. Ki-67, cyclins and DNA were all stained). The procedure is the same as the PI, except the flow cytometer set up for data acquisition. Appendix A.3 shows the flow cytometer configuration and the quantification of cyclins using Flowjo.

4.2.5 Gene expression measurements

The separated cell pellet from supernatant can be stored at -80°C for up to 6 months until the analysis can be performed. The frozen cell pellet was thawed at room temperature. Total RNA was extracted from the cell pellet using RNeasy® Mini kit (Qiagen, 74104). The steps in the RNA extraction were described as per the manufacturer's instruction. The thawed cell pellet was firstly lysed and then was homogenized using a QIAshredder spin column (Qiagen, 79654). The flow-through was collected and then mixed with 70% ethanol (VWR, 10107EP) in nuclease-free water (Invitrogen, AM9937). The mix was transferred to RNeasy spin column (provided in the kit) where RNA molecules were retained inside the column. RNA molecules were eluted by up to 50 µL of nuclease-free water. The total RNA concentration was measured using a biophotometer (Eppendorf AG, Germany). The ratio of 260 nm absorbance over 280 nm absorbance being greater than 1.9 confirms the purity of the extracted RNA samples. 1 µg of the total RNA was immediately taken for complementary Deoxyribonucleic

acid (cDNA) synthesis using Reverse Transcription System (Promega Ltd, A3500). The reagents and conditions in the cDNA synthesis were as per the manufacturer's instruction. The 1 µg of RNA was mixed with the master mix consisting of 1) Reverse transcriptase enzyme, 2) Random primers, 3) Ribonuclease inhibitor, 4) Nucleotides, and 5) the buffer. The reverse transcription reaction was carried out using GS1 thermo cycle (G-Storm, UK) with the temperature profile as follows; incubate at the room temperature for 10 minutes, then incubate at 42°C for 40 minutes and finally incubate at 4°C for 4 minutes. The cDNA can be indefinitely stored at -20°C for later real-time polymerase chain reaction (PCR). The real-time PCR was carried on using StepOnePlus™ Real-Time PCR machine (Applied Biosystems, USA). cDNA samples were mixed with 1) SYBR buffer provided in the SensiFAST™ Hi-ROX SYBR kit (Bioline, BIO-92005) and 2) primers specific to genes of interest. All sequences of the primers used in this study are shown in Table 4.2.2.

Table 4.2.2 Primer sequences used in this study.

Genes	Forward Sequences	Reverse Sequences
atf5[1]	GGGTCATTTTAGCTCTGTGAGAGAA	ATTTGTGCCCATAACCCCTAGA
trp53bp2	TTGCTGATAACGAACGGATGTT	ACACTTGGATCTTGGGATCTCG
bcl-2	GGGAGAACAGGGTATGATAACCG	TAGCCCCTCTGTGACAGCTTA
bax	TGAAGACAGGGGCCTTTTTG	AATTCGCCGGAGACACTCG
p21	CCTGGTGATGTCCGACCTG	CCATGAGCGCATCGCAATC
casp8	CAACTTCCTAGACTGCAACCG	TCCAACTCGCTCACTTCTTCT
casp3[2]	CCTCAGAGAGACATTCATGGGCC	GCTGCTCCTTTTGCTATGATCTTCC
gapdh	AGGTCGGTGTGAACGGATTTG	GGGGTCGTTGATGGCAACA

[1]from (Sheng et al., 2010), [2]from (Francini et al., 2009), The rest are from PrimerBank (Wang et al., 2012).

The two-step temperature cycling condition was employed to proceed the real-time PCR. The mix was incubated at 95°C for 2 minutes to activate polymerase enzymes. Then, the mix was under the two-step thermal cycle: the 1st step is at 95°C for 5 seconds (denaturation), and then cooling down to the 2nd step at 60°C for 20 seconds (annealing and elongation). 40

cycles of the two-step thermal cycle were performed to amplify the genes of interest. Data were recorded at the end of each thermal cycle. The analysis of the collected data was conducted using StepOne Software v2.1 (Applied Biosystems, USA). The gene expression was estimated using the $\Delta\Delta C_T$ approach, where the expression of the genes of interest is normalised to the expression of the housekeeping gene, *gapdh*, and the expression of the same genes of interest of the sample at the beginning of the culture (time = 0 hour). Appendix A.4 describes the estimation of gene expressions using the $\Delta\Delta C_T$ approach.

Given that this method measures and calculates gene expressions based on the housekeeping gene expression, the estimated expression might not represent actual change in expression of genes of interest in case the housekeeping gene expression is also affected as regards the different conditions or factors in the cultures (i.e. culturing time, temperature, growth factors, etc.). In this study, *gapdh* is selected as a reference expression based on the previous study by Browne and Al-Rubeai (2011b) using *gapdh* as a reference expression. However, the estimated expression could take in the change in *gapdh* expression as regards the culturing time as well as experimental conditions (i.e. feeding strategies and medium contents) and might not represent actual change in expression of genes of interest. It is recommended that at least two housekeeping genes should be included into the measurement and estimation of gene expression in order to cross-check between estimates of gene expression obtained from different housekeeping genes.

It is worth noting that the makers for apoptosis and cell cycle (Table 4.2.2) were selected based on previous studies that has established the role of each marker in the apoptotic (Hengartner, 2000, Majors et al., 2007) and cell cycle (Gartel and Tyner, 2002b) pathways. In addition, previous data reporting the expression of makers related to apoptosis and cell cycle in the similar cell culture system to this study were predominantly considered. A significant change in *trp53bp2* and *atf5* expressions was reported during the culture of GS-NS0 cells

(Browne and Al-Rubeai, 2011b). In addition, the role of these genes in apoptotic pathways and their links to metabolic stresses were established in various cell culture systems. As can be seen from Figure 2.2.2, these genes basically sense cellular stresses and involve in regulating apoptotic pathways, especially through the p53-mediated pathway. Given these reasons, *trp53bp2* and *atf5* were selected as apoptosis makers in this study.

Given that apoptosis can be induced through three different pathways as discussed in Section 2.2, there are a number of apoptotic species that can be chosen as apoptotic markers. In this study, the number of apoptotic markers that can be applied was limited, therefore, the markers were selected based on their relevance to apoptosis pathways, especially the death receptor and mitochondrial pathways. *bcl-2* (the anti-apoptotic factor) and *bax* (the pro-apoptotic factor) were reported to involve both upstream as well as downstream signalling apoptosis pathways, as discussed in Section 2.2. These include the apoptosis induction through external (receptor) and internal (mitochondria) pathways and also the ER-stress meditate pathway. In addition, the activity of them can partly represent the activity of the Bcl-2 family proteins, especially in the category of all domain (BH-1 to 4) proteins (anti-apoptotic) and without BH4 proteins (pro-apoptotic). Therefore, *bax* and *bcl-2* were among those selected as apoptosis markers in this study. The executors of apoptosis were ones of potential choices for the apoptosis markers given their roles in apoptotic pathways (Figure 2.2.1). *casp3* was chosen since caspase-3 is an important final executor of all apoptosis pathways. Given that caspase-8 is the executor in the external pathway and is the bridge between the external and internal pathways (Figure 2.2.1), *casp8* was selected as a marker in this study. In addition to apoptosis, cell cycle progression was observed. *p21* stands out as the excellent marker for cell cycle progression given its role and its link with p53-mediated apoptosis pathway.

The death receptor and mitochondrial pathways were predominantly investigated in this study given the list of selected markers. Although some of them involve the ER-stress mediated

pathway; including *atf5* (a direct target of eIF2), *bcl-2*, *bax* and *casp3*, but it might be not possible to draw any conclusion about the activity of the ER-stress apoptotic pathway. *casp-12*, *atf6*, *CHOP*, *PERK* and *IRE1* could be excellent markers for the future study of this pathway. Another limitation is that only the mRNA level of these selected markers was measured and it might not represent the protein level of the markers. In this way, the activities of apoptotic protein species might be misestimated. Despite apoptotic gene expression being essential in apoptosis induction (as discussed in Section 2.2.1), apoptosis can also be executed by the interaction of the pre-existing store of apoptotic proteins in response to lethal signals. Given that the signal transduction in apoptotic pathways involves protein-protein interactions; such as ligand-receptor interactions in the death receptor pathway, and direct proteolytic processing of downstream caspases. The execution of apoptosis could happen only relying on the pre-existing store of apoptotic proteins and might not involve the *de novo* synthesis of protein. Therefore, in order to cross-check the observed apoptosis activation based on the mRNA level of the markers, the measurement of protein expression needs to be included for the future study of apoptosis.

4.3. Extracellular metabolite quantification

4.3.1 Nutrient and metabolite quantification

The spent medium or supernatant collected and stored at -20°C as described earlier, was thawed at room temperature. 1.5 mL of the supernatant was taken for the measurement of glucose, glutamate, ammonia and lactate. The measurement was performed using a BioProfile 400 Analyzer (Nova Biomedical Ltd.). The accuracy of the measurement was calibrated with five levels of quality controls.

4.3.2 Amino acid quantification

250 µL of the thawed supernatant was collected for amino acid analysis. 10 kDa filter columns (Millipore, MRCPRT010) were used to filter out macromolecules, which were larger than 10,000 Da, with at least 95% recovery. All flow-through was collected for the pre-column derivatization, whereby amino acids were converted into their derivatives. The derivatization reaction conducted in this work involves 2 consecutive steps: 1) o-Phthalaldehyde (OPA) derivatization where OPA stably reacts with primary amino acids (18 amino acids) resulting to their derivatives; and 2) 9-fluorenylmethyl chloroformate (FMOC) derivatization that converts the remaining amino acids (4 amino acids) into their derivatives. Table 4.3.1 shows the automated procedure for the pre-column derivatization using an automatic sampler (1329B autosampler, Agilent Technologies, UK) as per the manufacturer's technical notes.

Table 4.3.1 The procedure for the pre-column derivatization.

Step No.	Action	Volume taken
1	Draw	2.5 µL from 0.4M borate buffer (Agilent, 5061-3339)
2	Draw	1.5 µL from Sample vials
3	Mix	4.0 µL in air (washport) default speed 5 times
4	Wait	0.2 min
5	Draw	0.5 µL from 10 mg/mL OPA solution vial (Agilent, 5061-3335)
6	Mix	4.5 µL in air (washport) default speed 10 times
7	Draw	0.4 µL from 2.5 mg/mL FMOC (Sigma-Aldrich, 23186) in acetonitrile (ACN, Sigma; 34998) vial
8	Mix	4.9 µL in air (washport) default speed 10 times
9	Draw	32 µL from injection diluent vial
10	Mix	20 µL in air (washport) default speed 8 times (8X)

* Injection diluent was made from the solution consisting of 1 mL of mobile phase A (which is described later) and 4 µL of phosphoric acid solution, H_3PO_4 (Sigma-Aldrich, 79607-500ML).

These derivatives have different hydrophobicity with each other. Therefore, each derivative can be separated using the reversed-phase chromatographic technique, where the more hydrophilic the molecules, the faster the molecules are eluted from the column. The amino acid derivatives were injected through the 4.6 × 100 mm rapid resolution high throughput reversed-phase column with 1.8 μm particle size (Agilent Technologies, 959964-902). The chromatography was conducted using an HPLC Agilent 1260 Infinity system (Agilent Technologies).

Table 4.3.2 The composition of mobile phases (1 L).

Mobile phase A (ionic solution)	**Mobile phase B (organic solvent)**
1.4 g of anhydrous Na_2HPO_4 3.8 g of $Na_2B_4O_7 \cdot 10H_2O$ 32 mg of NaN dH_2O making up to 1 liter	450 mL of acetonitrile (ACN) 450 mL of methanol 100 mL of d H_2O

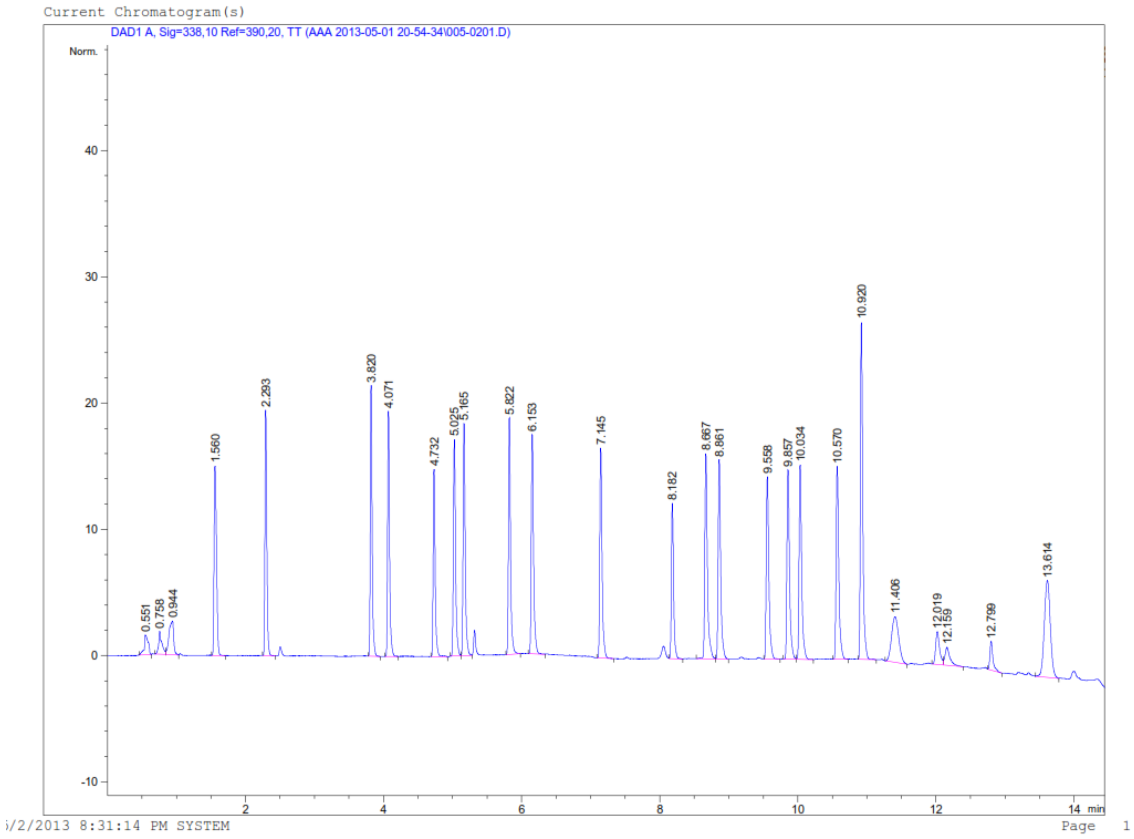
Table 4.3.3 The fraction of mobile phase B in the total flowrate of the eluting mobile phase.

Time (min)	**%B**
0.0	2
0.4	2
13.4	57
13.5	100
15.7	100
15.8	2
16	end

*The total flowrate (mobile phase A+B) was 1.5 mL/min.

The eluting mobile phase, which was used to carry the derivatized amino acids through the column, consisted of two aqueous solutions. One is relatively “polar” (mobile phase A), while the other is relatively “non-polar” (mobile phase B), as shown in Table 4.3.2. Given the

difference in hydrophobicity of the derivatives, the gradient flowrate of mobile phase B was used to elute each derivative at a different time, as shown in Table 4.3.3.



*Note that 1.560 is aspartate, 2.293 is glutamate, 3.82 is asparagine, 4.07 is serine, 4.732 is histidine, 5.023 is glycine, 5.165 is threonine, 5.822 is arginine, 6.153 is alanine, 7.145 is tyrosine, 8.182 is cysteine, 8.667 is valine, 8.861 is methionine, 9.558 is tryptophan, 9.857 is phenylalanine, 10.034 is isoleucine, 10.570 is leucine, 10.920 is lysine and 13.614 is proline.

Figure 4.3.1 The chromatogram of the standard of 19 amino acids.

Given that these derivatives are highly fluorescent (Woodward et al., 2007), each eluted derivative is detected using a diode array detector (DAD, Agilent Technologies). Signals from eluted derivatives were collected using two fluorescence wavelengths: 1) 338nm for OPA derivatives and 2) 262 nm for FMOC derivatives. The plot between the fluorescence intensity and the eluted time is called “chromatogram”. In the chromatogram, there are a number of peaks, each of which specifically represents each derivative, and implicitly each amino acid. The identification of each peak and its corresponding amino acid was previously performed as per the manufacturer’s technical note (Woodward et al., 2007). Figure 4.3.1 illustrates a

chromatogram of known concentration (0.12 mM) of 19 amino acids. Glutamine can also be identified by adding the glutamine standard with the standard solution of amino acids. The peak indicating glutamine presence is at around 4.580, locating just before the peak of histidine in the chromatogram.

The chromatogram was analysed using OpenLAB Chromatography Data System C.01.04 (Agilent Technologies) to estimate the area under each peak. The concentration of amino acids was estimated by comparing to the calibration curves, where the concentration of each amino acid was plotted against the area under the peak corresponding to the amino acid (Henderson Jr and Brooks, 2010). Appendix A.5 shows the calibration curves that were used to estimate the concentration of extracellular amino acids in unknown samples.

4.3.3 cB72.3 mAb quantification

The thawed supernatant was filtered through a 13 mm syringe filter with 0.22 μm PTFE membrane (VWR, 28145-491). The chromatography was carried on using an HPLC Agilent 1260 Infinity system (Agilent Technologies). 50 μL of the filtered supernatant was injected into the affinity column, Bio-Monolith Protein A (Agilent Technologies, 5069-3639). Mobile phase A; PBS buffer with pH 7.4, was used to carry the injected sample and to allow mAb molecules to attach onto the protein A molecules inside the column. Then, mobile phase B; 0.5 M acetic acid with pH 2.6, was introduced to the column to elute the mAb. The flowrate of both mobile phases used was 1.5 mL/min. The eluted mAb was detected using the fluorescent detector (Diode Array Detector, Agilent Technologies) at the collection fluorescence wavelength of 280 nm. The chromatogram obtained from the detector was then processed using OpenLAB Chromatography Data System C.01.04 (Agilent Technologies). A series of the mAb standard dilutions enables us to create the calibration curve, which was used to estimate the concentration of mAb in unknown samples, as shown in Appendix A.6.

4.3.4 cB72.3 mAb quality assessment

This section describes two analytical techniques: protein gel electrophoresis and enzyme-linked immunosorbent assay (ELISA), used in this study in order to assess to a certain extent the quality of the produced mAb as well as cross-check the mAb quantification by the HPLC technique.

Protein gel electrophoresis was conducted in collaboration with D. G. García Münzer (PhD candidate) and Sarantos Kyriakopoulos (PhD candidate). Each supernatant sample and each dilution of cB72.3 mAb standard (kindly provided by Lonza Biologics (Slough, UK)) were mixed with the non-reducing Sample Buffer (Thermo Scientific, BN2003). The mixing ratio between the sample buffer and each sample (as well as each dilution of the mAb standard) was 1:3. The samples and the standards with the sample buffer, and the 10-180 kDa protein ladder (Thermo Scientific, 26616) were then loaded on the native precast protein gel (Thermo Scientific, BN1004BOX) in the NativePAGE™ running buffer (Thermo Scientific, BN2007). The electrophoresis was performed at 115 V for 50 minutes.

The sandwich ELISA was performed on a 96-well plate (Greiner Bioone, 655 101). The wells in the plate were firstly coated with $F(ab')_2$ Fragment Goat Anti-Human IgG Fc (Jackson Immunoresearch Labs Inc., 109-006-098) in the coating buffer (0.05 M sodium carbonate pH 9.6). The coating buffer consisted of sodium carbonate (Na_2CO_3, Sigma-Aldrich, 451614) and sodium bicarbonate ($NaHCO_3$, Sigma-Aldrich, S6297) and deionised water. The coated plate was incubated overnight at 4°C on a level surface. Then the wells were emptied and washed 6 times with the washing buffer (comprised of PBS and 0.05% by volume Tween 20 (Sigma-Aldrich, P2287)). The wells were blocked with the blocking buffer consisting of the coating buffer with 0.5% w/v Casein Hammerstein (Sigma-Aldrich, C3400) and the plate was incubated at room temperature for 1 hour. The wells were emptied and washed 6 times before

plating out a series of dilutions of mAb standard, unknown samples as well as negative controls. The plate was incubated at room temperature for 1 hour. The wells were again emptied and washed 6 times before plating out anti-human IgG kappa peroxidase conjugate targeting human κ light chains (Sigma-Aldrich, A7164) and incubating the plate at room temperature for 1 hour. During this incubation, the peroxidase substrate solution, 3,3′,5,5′-Tetramethylbenzidine (TMB, Sigma-Aldrich, T3405) in the 0.05 M phosphate citrate buffer pH 5.0 with 2 μL of hydrogen peroxide (H_2O_2, Sigma-Aldrich, H1009) was prepared without light exposure. The phosphate citrate buffer consisted of 0.2 M Sodium phosphate dibasic solution (Na_2HPO_4, Sigma-Aldrich, 71640) and 0.1 M citric acid (Sigma-Aldrich, 251275). After the conjugate incubation, the wells were again emptied and washed 6 times before plating out the substrate solution in the dark. The plate was then incubated in the dark at room temperature on an orbital plate shaker for 30 minutes. The peroxidase reaction was stopped by adding 2.5 M sulphuric acid (H_2SO_4, Sigma-Aldrich, 320501) to the wells. The absorbance obtained from the reaction was read using the plate reader at 450 nm.

4.4. Data analysis

4.4.1 The estimation of cell culture descriptive parameters

Culture parameters were estimated at different phases of the culture: early and exponential phases, stationary phase and death phase. The numerical method, the trapezoid rule, was employed to estimate the integral of viable cells (IVC), as shown in the following equation (Balcarcel and Stephanopoulos, 2001).

Eq. 4.4.1 The estimation of IVC

$$\text{IVC (cell.mL}^{-1}\text{.hr)} = \sum_{i=1}^{k} \frac{1}{2}(n_{v,t_{i-1}} + n_{v,t_i})(t_{i-1} + t_i)$$

Where n_{v,t_i} stands for the viable cell density at time t = i.

The specific cell growth rate was estimated using the net number of viable cells over the cultivation time as shown in the following equation (Balcarcel and Stephanopoulos, 2001).

Eq. 4.4.2 The estimation of specific growth rate

$$\text{Specific growth rate (day}^{-1}) = \frac{\ln (n_{v,t_2} - n_{v,t_1})}{t_2 - t_1}$$

The specific consumption/production rates of extracellular metabolites were estimated using the graphical method. The plots between the concentration of each metabolite (y-axis) and IVC (x-axis) were performed. Linear correlations between the y axis and the x axis were generated, and the slopes obtained from the linear trendlines represent the specific consumption/production rates ($\mu mol.10^{-6} cell.\ day^{-1}$). The yield of lactate over glucose (mol/mol) was also obtained by the graphical method. Appendix A.7 shows an example of the estimation of the specific consumption/production rates and the lactate over glucose yield.

4.4.2 Statistical Analysis

The one-way analysis of variance (ANOVA)

The one-way analysis of variance (ANOVA) can identify any difference among the means of more than two groups under a single factor or treatment. To obtain reliable results from the ANOVA, several assumptions are required to be satisfied; 1) the distribution population of each group follows the Normal Distribution (with mean and variance), 2) errors in each group; defined as deviations of actual observed values from the group mean, are independent with each other, and 3) the variance of data in each group should be equal to each other. The ANOVA is basically based on the F-test statistic, however it does not specify exactly which groups different from one another (Seltman, 2012). To estimate the F-statistic, Mean

Squares (MS) are required to be determined. MS can be calculated from Degrees of Freedom (DF) and Sum of Squares (SS, the sum of squares between groups and the sum of squares between samples within the groups) as shown in Eq. 4.4.3. The F-statistic can be calculated as Eq. 4.4.4. Appendix A.8 shows an example of F-statistic calculation.

Eq. 4.4.3 Mean Squares

$$MS_{\text{between groups}} = \frac{SS_{\text{between groups}}}{DF_{\text{between groups}}} = \frac{\sum_{j=1}^{k} n_j(\hat{Y}_j - \hat{Y})^2}{k-1}$$

$$MS_{\text{within groups}} = \frac{SS_{\text{within groups}}}{DF_{\text{within groups}}} = \frac{\sum_{j=1}^{k} (n_j-1)(SD_j)^2}{N-k}$$

Where k is the number of groups, n is the number of samples within the groups, N is the number of total sample size, $\hat{Y}_j$ is the sample mean of the j group and $\hat{Y}$ is the overall mean. The $MS_{\text{within groups}}$ is also calculated from sample standard deviations (SD) given that it is actually the weighted average of sample variances.

Eq. 4.4.4 F-statistic

$$F = \frac{MS_{\text{between groups}}}{MS_{\text{within groups}}}$$

The null and alternative hypotheses need to be set in the ANOVA. The null hypothesis is that there is no difference among the means of the groups of interest while the alternative is the opposite; at least two group means are different. *p*-value is defined as the probability of obtaining a value being equal to or more extreme than the actual experimental observation under the null hypothesis (the shaded area in Figure 4.4.1). Given that *p*-value is probability, its value is between 0 and 1. It indicates how possible it is that the observed difference arises from chance. On one hand, if the value is near 0, the observed difference is less likely to be

occur due to chance; on the other hand, if the value is near 1, the observed difference could be contributed by chance (Dahiru, 2008). The hypotheses testing (subject to the null hypothesis being true) requires us to specify a significant level (or alpha which is normally set at 0.05) and the corresponding critical F value (the F-critical value representing where the null hypothesis is rejected if the observed F-statistic is larger), and to calculate the observed F-statistic (as above shown) and *p*-value (corresponding to the observed F value). In order to be able to compare between the observed F-statistic (calculated as Eq. 4.4.4) and the F-critical, the F-critical has to be determined using the cumulative F-distribution function as shown in Eq. 4.4.5 which requires DF (both $DF_{between\ groups}$ and $DF_{within\ groups}$) and cumulative probability (F(x)). The F-distribution with 3 and 10 degrees of freedom ($DF_{between\ groups}$ and $DF_{within\ groups}$, respectively) can be created using the F-distribution function (Eq. 4.4.6) as can be seen from Figure 4.4.1. If the significant level is set at 0.05; or 0.95 cumulative probability (F(x) = 0.95), F-critical is equal to 3.71 (Eq. 4.4.5). If the observed F-statistic is larger than the critical one (thus *p*-value is less than alpha), the null is rejected, and vice versa (Dahiru, 2008, Seltman, 2012).

Eq. 4.4.5 the cumulative F-distribution function

$$F_{n,m}(x) = 2n^{\frac{(n-2)}{2}} \left(\frac{x}{m}\right)^{\frac{n}{2}} \frac{2F_1\left(\frac{1}{2}(n+m), \frac{1}{2}n;\ 1+\frac{1}{2}n;\ -n\frac{x}{m}\right)}{B\left(\frac{1}{2}n, \frac{1}{2}m\right)}$$

$2F_1(a, b; c; z)$ is a hypergeometric function and $B(a,b)$ is the beta function as shown below:

$$2F_1(a, b; c; z) = \sum_{n=0}^{\infty} \frac{(a)_n (b)_n}{(c)_c} \frac{z^n}{n!};\ |z|<1$$

$$B(a,b) = \frac{(a-1)!(b-1)!}{(p+q-1)!}$$

Eq. 4.4.6 the F-distribution function

$$f_{n,m}(x) = \frac{m^{\frac{m}{2}}\, n^{\frac{n}{2}}\, x^{\frac{n}{2}-1}}{(m+nx)^{\frac{(n+m)}{2}}\, B(\frac{1}{2}n, \frac{1}{2}m)}$$

Where n is $DF_{between\ groups}$; m is $DF_{within\ groups}$; x is the corresponding F-statistic. These equations are adapted from (Weisstein, 2016).

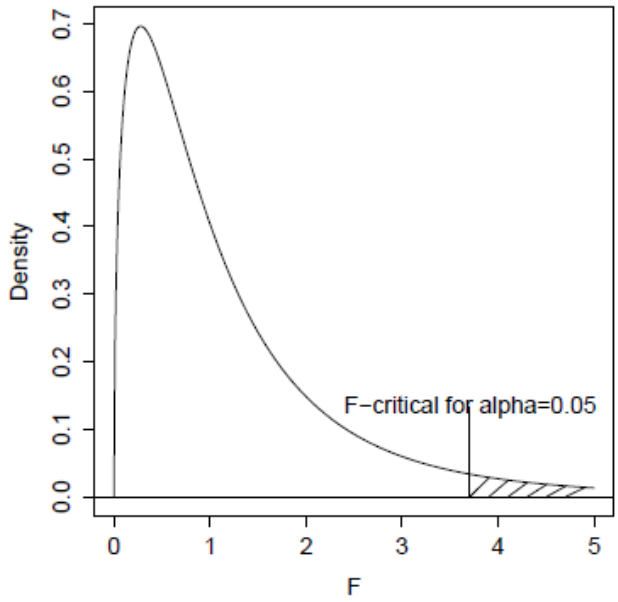


Figure 4.4.1 The F-distribution with 3 and 10 degrees of freedom. The vertical line at around F=3.71 indicates the F-critical value at α = 0.05. The shaded area is *p*-value indicating the likelihood of getting an F-statistic being equal to or larger than the observed F-statistic. In this case, the observed F-statistic is equal to the F-critical, therefore, *p*-value = 0.05 which is equal to α. If the observed F-statistic is larger than the F-critical, then *p*-value is less than α and the null hypothesis is rejected. Adapted from (Seltman, 2012).

It is worth noting that to identify whether the observed difference is significant could not be completely concluded based on the hypothesis testing as well as the obtained *p*-value. Getting *p*-value < alpha means that it is much more likely to see the difference however there

are chances that the indifference could also happen (i.e. 1 in 20 comparisons if *p*-value = 0.05). In addition, using alpha = 0.05, despite common, is not the definite line to judge whether the observed difference is significant or not. However, what can be claimed is that there is a stronger likelihood against the null hypotheses (no difference observed) as the *p*-value becomes less (Dahiru, 2008).

Following the ANOVA, if any difference among groups is found, further data analysis is performed in order to exactly specify which groups different to one another. This is based on multiple pairwise comparison. There are a number of methods that has been introduced for this purpose in order to avoid any errors (i.e. type I errors) arising from the multiple comparison. Tukey's test and Student–Newman–Keuls (SNK) method are among those that has been applied with the ANOVA extensively. It was reported that the SNK method is more powerful than the Tukey one (so it is more likely to reveal any difference than the Tukey) since it is less conservative. The SNK controls the type I errors among tests of means of all groups while the Tukey controls the errors for all comparison simultaneously. Given its nature, The SNK might suffer from the errors and could generate unreliable results. However, the results from both methods are comparable (Seltman, 2012, Abdi and Williams, 2010, SigmaStat, 2006a).

In this study, the one-way ANOVA was applied for analysis of experimental data. It was conducted using SigmaStat 3.5 (Systat Software, Inc, Germany). The alpha value of 0.05 was assigned as the significant level. The SNK method was employed for any multiple pairwise comparison following the ANOVA. All data shown represent their mean values with the standard deviation from the triplicate experiments (n = 3).

Determination of the correlation coefficient (CC)

There are a number of methods of determining correlation coefficient (CC) providing information about to what extent two variables are associated or correlated. In this study, Pearson product-moment CC (r_p) and Spearman's rank CC (r_s) were applied to indicate the strength of the potential correlation between two variables. The former is the parametric test based on an assumption that errors (differences between the observed data and the corresponding data on the regression line) are normally distributed with constant variance, while the latter is the non-parametric one that does not require the normality of the errors and provides the correlation measure based on data ranking (SigmaStat, 2006b). In other words, the former is a measure of correlation based on determining the linear regression (linear relationship) while the latter rather seeks for a monotonic relationship that is not necessary to be linearly correlated.

Both methods provide 1) the CC and 2) *p*-value. The CC is mathematically calculated based on how a pair of variables are linearly associated (normalised covariance). The value can be varied from -1 to 1. If the CC is close to -1, an inversely proportional correlation could be concluded. In contrast, if the CC is close to 1, a proportional correlation could be claimed. However, if the CC is close to 0, there might be no relationship between the two variables. As above discussed, the *p*-value here stands for the probability of being wrong in rejecting the null hypothesis; there is no correlation between the two variables (SigmaStat, 2006b). Therefore, to interpret the CC needs to consider the *p*-value. In this study, alpha=0.05 was used as the significant level where the two variables are more like to be correlated. The determination of the CC was performed in SigmaStat 3.5 (Systat Software, Inc, Germany).

Chapter 5

A Map of the Dynamic Interplay between Cell Cycle and Apoptosis, and Metabolism

5.1 Background

Metabolic stresses, including nutrient deprivation and toxic metabolite accumulation, can hinder mammalian cell cultures in their viability and productivity. They essentially influence cell cycle progression as well as facilitate apoptosis induction, causing a deterioration in the final titre as well as quality of manufactured therapeutic proteins. Therefore, understanding of relationships between control of cell cycle and apoptosis, and the metabolic stresses is critical for the improvement of the mammalian cell culture toward higher bio-therapeutic production.

Chapter 5 presents an experiment that aims to establish the effect of metabolic stresses, especially nutrient deprivation, on the induction of apoptosis and cell cycle progression in the GS-NS0 cell culture. Flow cytometry as well as real-time PCR were exploited to measure shifts in cell cycle profiles as well as apoptotic gene expressions in response to metabolic stresses. A complete map of the induction of apoptosis as well as the cell cycle progression as regards culture phases can be achieved from the results.

5.1.1 Introduction

Mammalian cell cultures are widely utilised for industrial production of biologics of importance, such as mAbs. The total sale of mAbs was valued at 18.5 billion dollars in 2010 and it was speculated that the global demand for mAbs would be continuously increasing within the next future years (Buss et al., 2012, Elvin et al., 2013). This draws attention to improvement in mammalian cell culture systems toward a higher quantity as well as a better quality of mAbs produced. However, given limitations of mammalian cell cultures as listed in the sub-section 2.3.4; including relatively slow growth and production rate of desired products

as well as being sensitive to environmental conditions, increasing mAb production is one of greatest challenges facing the biotechnology and bioprocess community nowadays.

There are a number of strategies for the improvement of mammalian cell cultures toward mAb production enhancement. One of them is the suppression of apoptosis. Apoptosis, or programmed cell death, was previously identified as the main cause of cell death occurring in the mammalian cell cultures (Goswami et al., 1999, DiStefano et al., 1996, Browne and Al-Rubeai, 2011a, Singh et al., 1994). The onset of apoptosis can be delayed through overexpression of anti-apoptotic genes, including *bcl-2* and *bcl-xL*. The effect of apoptosis suppression on mAb production as well as productivity was reported to be variable, depending on cell line and culturing systems. The hybridoma cell cultures with *bcl-2* overexpression showed an increase in mAb productivity (Itoh et al., 1995, Terada et al., 1997) while the GS-NS0 cell cultures with *bcl-2* overexpression showed no improvement in mAb productivity (Tey et al., 2000a, Tey et al., 2004, Tey et al., 2005). However, a higher viable cell number and longer culture viability were typically obtained in the cultures with the overexpression of anti-apoptotic genes (Simpson et al., 1999b). The control of cell proliferation was also established as a strategy to increase mAb production and productivity. Cell proliferation can be regulated through overexpression of cyclin-dependant kinase inhibitors, including p21 and p27, which facilitate cell cycle arrest resulting in a slowdown in cell cycle progression or cell proliferation (Brugarolas et al., 1999). This strategy generally enables cultures to achieve higher production and productivity (Fussenegger et al., 1998b, Watanabe et al., 2002), suggesting a positive effect of cell cycle arrest on cellular mAb synthesis.

As earlier reviewed in Chapter 2, the established findings/data are, however, contradictory and variable among cell lines. As above mentioned, the control of cell proliferation in the mammalian cell cultures often results in an increase in productivity (Fussenegger et al., 1998b, Watanabe et al., 2002); however, this is not always the case when

cell proliferation arrest is a result of apoptosis suppression (Ibarra et al., 2003, Tey et al., 2000a, Tey and Al-Rubeai, 2004). It was found that overexpression of anti-apoptotic genes, especially *bcl-2* resulted in cell proliferation arrest (Simpson et al., 1999b) as similar to that of cell cycle regulator overexpression. Despite the similar effect on cell proliferation, the different effects on productivity were achieved (Ibarra et al., 2003, Tey et al., 2000a, Tey and Al-Rubeai, 2004). This could be because the apoptosis suppression and the cell proliferation control might affect differently metabolic activities underlying the difference in productivity (Nivitchanyong et al., 2007). Thus, a balanced degree of apoptosis suppression (Zustiak et al., 2014) and cell proliferation arrest is potentially the key to allow the cultures to achieve higher production/productivity. In order to establish the key, it is necessary to construct systematic understanding of interplay between apoptosis and cell cycle and its relations to metabolism including production/productivity in the mammalian cell cultures.

A relationship between metabolic stresses, and induction of apoptosis as well as control of cell proliferation was previously investigated (Mercille and Massie, 1994a, Simpson et al., 1998, Dorai et al., 2009, Newland et al., 1994). The onset of apoptosis was found to be subject to availability of nutrients, including glucose and amino acids (DiStefano et al., 1996, Zhou et al., 1997a). The apoptotic responses to metabolic stresses were reported to be at the transcriptional level (Browne and Al-Rubeai, 2011b). In addition to apoptotic responses, metabolic shifts, which can be considered as a survival mechanism in response to metabolic stresses, was found to be subject to availability of nutrients (Dorai et al., 2009, Dorai et al., 2010). Apoptosis and cell cycle progression were also found to be intimately correlated through interactions between p53 and p21, key transcription factors that play regulatory roles in apoptosis and cell cycle arrest, respectively (El-Deiry et al., 1994, Mason and Rathmell, 2011).

To the best of my knowledge, a complete picture of the relationship between apoptosis, and metabolism as well as cell cycle; where kinetics of apoptosis and its association with cell

cycle progression with respect to dynamic metabolic changes, has not been constructed. The backbone of the relationship is at the transcriptional level, where changes in apoptosis and cell cycle associated gene expressions take place in response to the metabolic stresses and underlie the control of cell proliferation and apoptosis. Therefore, the effect of metabolic stresses on apoptosis and cell cycle needs to be investigated at a transcriptional level, so that understanding of the relationship can be elucidated.

5.1.2 Objectives

This chapter aims to establish cell cycle and apoptosis associated cellular responses, at the transcriptional level, to the metabolic stresses as a result of extracellular nutrient deprivation as well as toxic metabolic by-product accumulation. The scientific objectives were set as the following:

- Design and conduct an experiment of GS-NS0 cell culture with analytical techniques that would enable to elucidate cellular dynamic responses at the transcriptional level, especially apoptosis and cell cycle, to metabolic stresses.
- Identify relevant metabolic stresses occurring in the culture of GS-NS0, and establish relevant links between the metabolic stresses, and the induction of apoptosis and cell cycle arrest for future model development.

5.2 Methodology

A batch culture of GS-NS0 cell line was conducted in triplicate, with the medium composition, and on the incubator under the culturing condition as previously discussed in Chapter 4. The culture lasted for 6 days (139 hours) without nutritional additions and culturing condition shifts. Sample were collected twice a day and were prepared for immediate or later analysis, as previously discussed in Chapter 4.

The analytical techniques that were performed are as follows – cell density and viability estimation (haemocytometer), apoptotic cell quantification and cell cycle analysis (flow cytometer), gene expression quantification (real-time PCR), measurements of nutrients and metabolite levels (BioProfile 400 and HPLC), and mAb quantification (HPLC). The procedure was as per manufacturer's instruction if not described in Chapter 4.

5.3 Results

5.3.1 Cell growth and metabolic profiles

The batch culture of GS-NS0 cells was carried out to study the impact of nutrient deprivation and toxic by-products accumulation on cell proliferation (Figure 5.3.1-A&B). Figure 5.3.1-A.2 shows the plot of viable cell concentration on the base 10 logarithmic scale Y-axis, allowing to identify culture phases. The boundary between early-exponential and exponential phases was located at around 24 hours of the culture while the boundary between exponential and stationary phases was defined at around 50 hours of the culture. The death phase starting at around 80 hours was identified by the late stage apoptotic cell fraction and viability as can be seen from Figure 5.3.1-B. This was in agreement with the significant difference in specific growth rate among the phases (Table 5.3.1).

During the first 24 hours of culture, a significantly lower cell growth rate was observed compared to the exponential growth phase (p=0.003). Cell viability remained constant and high (approx. 90%) during the early exponential phase (Figure 5.3.1-B). During this phase, no significant change in the glucose and glutamate concentrations was observed, while lactate concentration significantly increased (Figure 5.3.1-C & D). The lactate to glucose yield in both early and exponential phases proved to be statistically significant (p=0.007) different to the stationary phase (Table 5.3.1). Following the early exponential phase, cell concentration started

to increase rapidly at the exponential phase. Simultaneously, lactate concentration constantly increased with a non-statistically significant different yield on glucose when compared to the early exponential phase (p=0.739). The cell density peaked soon after glutamate was completely exhausted (approximately 50 hours of the culture).

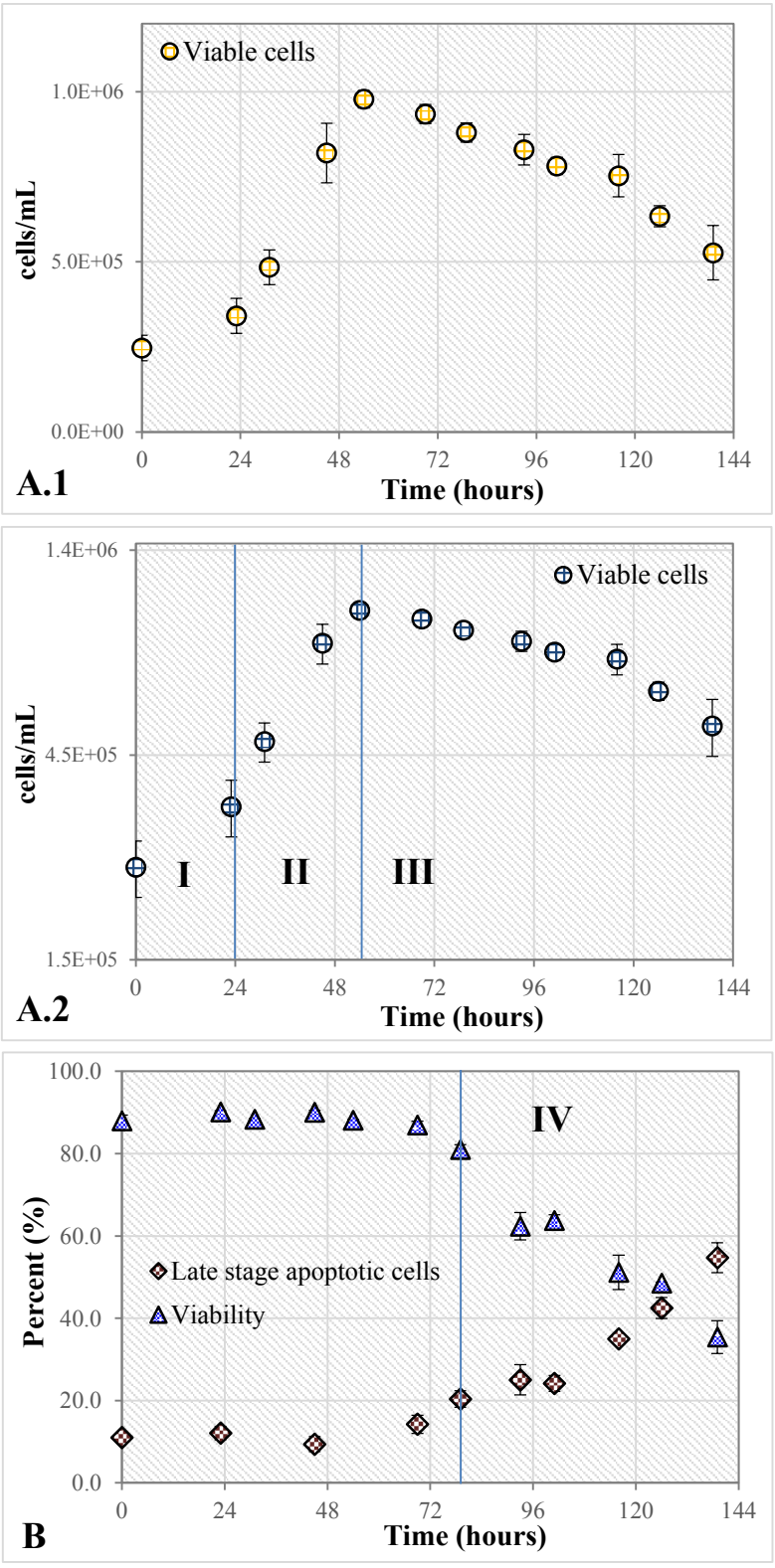
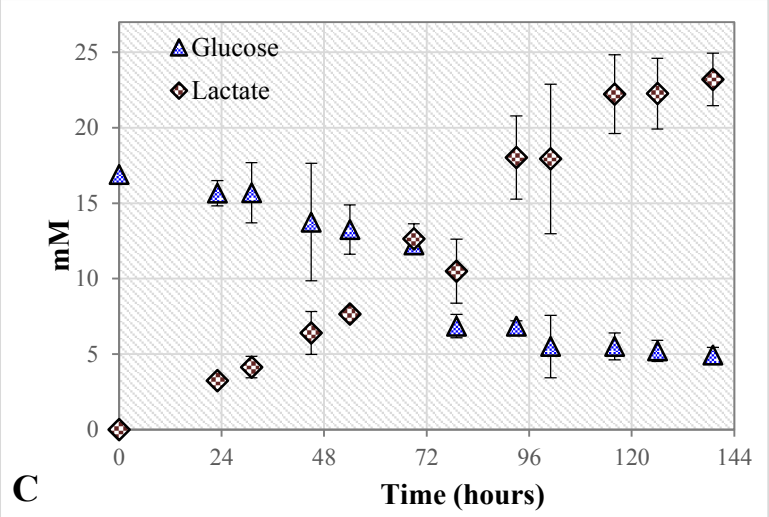
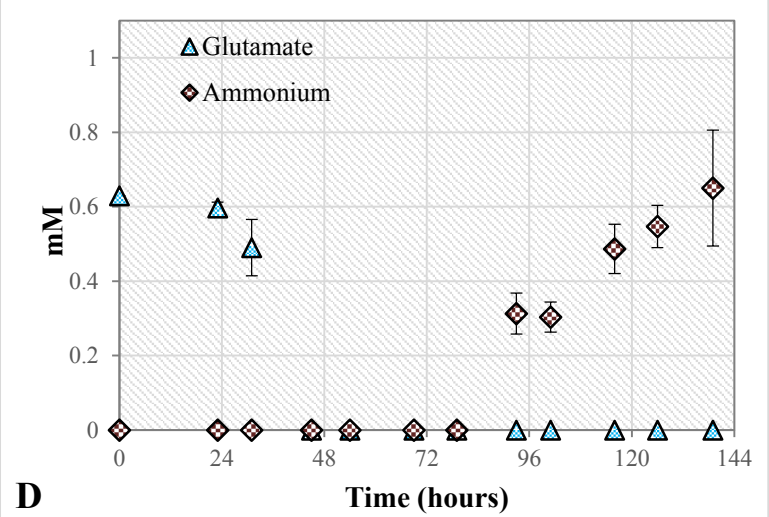


Figure 5.3.1 Cell growth, dead and extracellular nutrient level profiles of the batch culture of GS-NS0: (A) viable cell concentration; (A.1) on linear scale Y-axis and (A.2) on base 10 logarithmic scale Y-axis; (B) Late stage apoptotic (LSA) cell fraction and viability; (C) glutamate and ammonium; (D) glucose and lactate and (E) Extracellular c72.3 mAb titer. I indicates early-exponential phase, II indicates exponential phase, III indicates stationary phase and IV indicate death phase. The normal vertical lines indicate each culture phase boundary (n=3, error bar = SD).





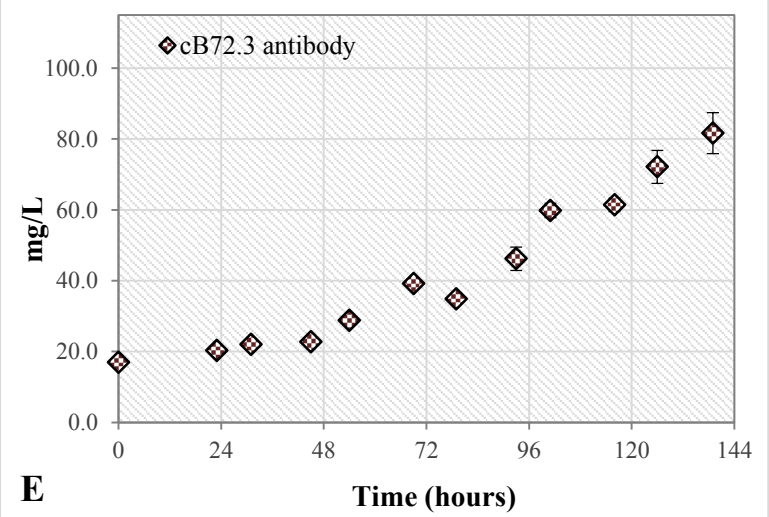
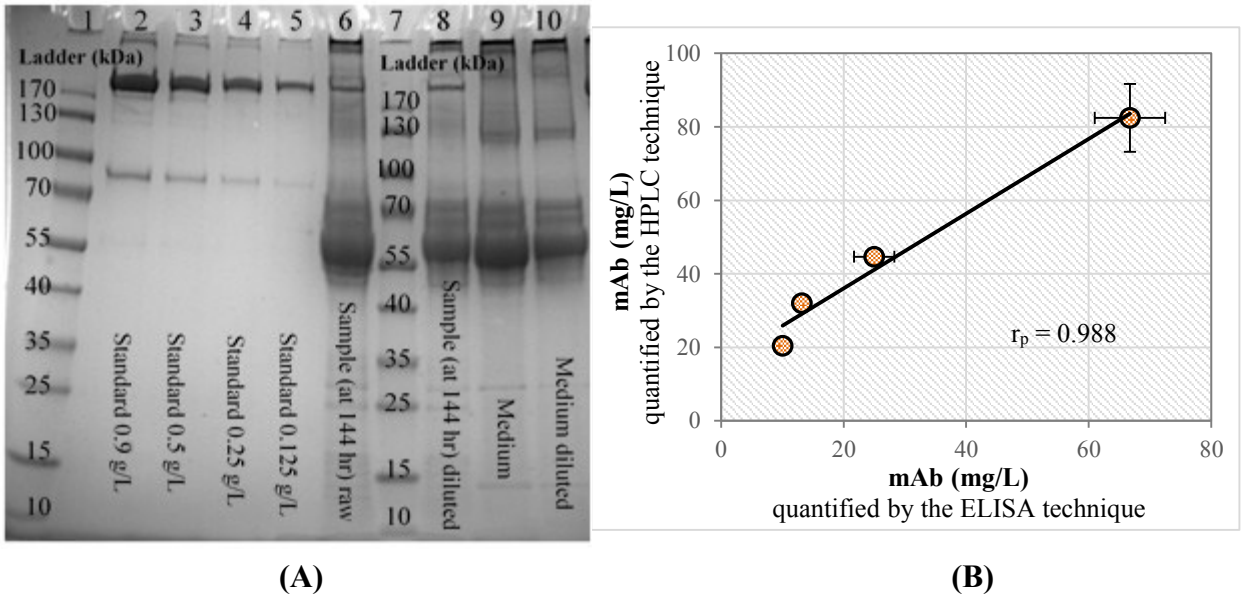


Figure 5.3.1 (Continued) Cell growth, dead and extracellular nutrient level profiles of the batch culture of GS-NS0: (A) viable cell concentration; (A.1) on linear scale Y-axis and (A.2) on base 10 logarithmic scale Y-axis; (B) Late stage apoptotic (LSA) cell fraction and viability; (C) glutamate and ammonium; (D) glucose and lactate and (E) Extracellular c72.3 mAb titer. I indicates early-exponential phase, II indicates exponential phase, III indicates stationary phase and IV indicate death phase. The normal vertical lines indicate each culture phase boundary (n=3, error bar = SD).

The culture then entered the stationary phase (between 50 and 80 hours of the culture), where the cell density started to decrease without a significant change in viability (Figure 5.3.1-B). In this phase a steeper decrease in the glucose concentration (Figure 5.3.1-C) – statistically

significant highest specific glucose consumption rate (p<0.001, Table 5.3.1) – was observed with a simultaneous increase in the mAb titre (Figure 5.3.1-E). In addition, ammonia was detected and started to increase at the end of this phase (80 hours of the culture). The LSA cell fraction (Figure 5.3.1-B) started to increase soon after the end of the stationary phase (after 80 hours of the culture), which corresponds with the drop in viability. In the death phase (between 80 and 140 hours of the culture), the LSA fraction constantly increased, as well as the mAb titre – statistically significant highest antibody specific production rate (p=0.0019, Table 5.3.1). Glucose concentration appeared to remain constant until the end of the culture, whereas lactate and ammonia showed a statistically significant increase between 80 hours to 120 hours (p<0.05), both concentrations remain statistically constant thereafter (from 120 hours of the culture).



(A) **(B)**

Figure 5.3.2 The assessment of produced mAb quality: (A) protein gel electrophoresis and (B) the comparison between mAb quantified by the HPLC technique and the ELISA technique. r_p represents the Pearson correlation coefficient.

The produced mAb was compared to the standard mAb through conducting the native PAGE. As can be seen in Figure 5.3.2-A, column 2 to 5, all dilutions of cB72.3 mAb standard

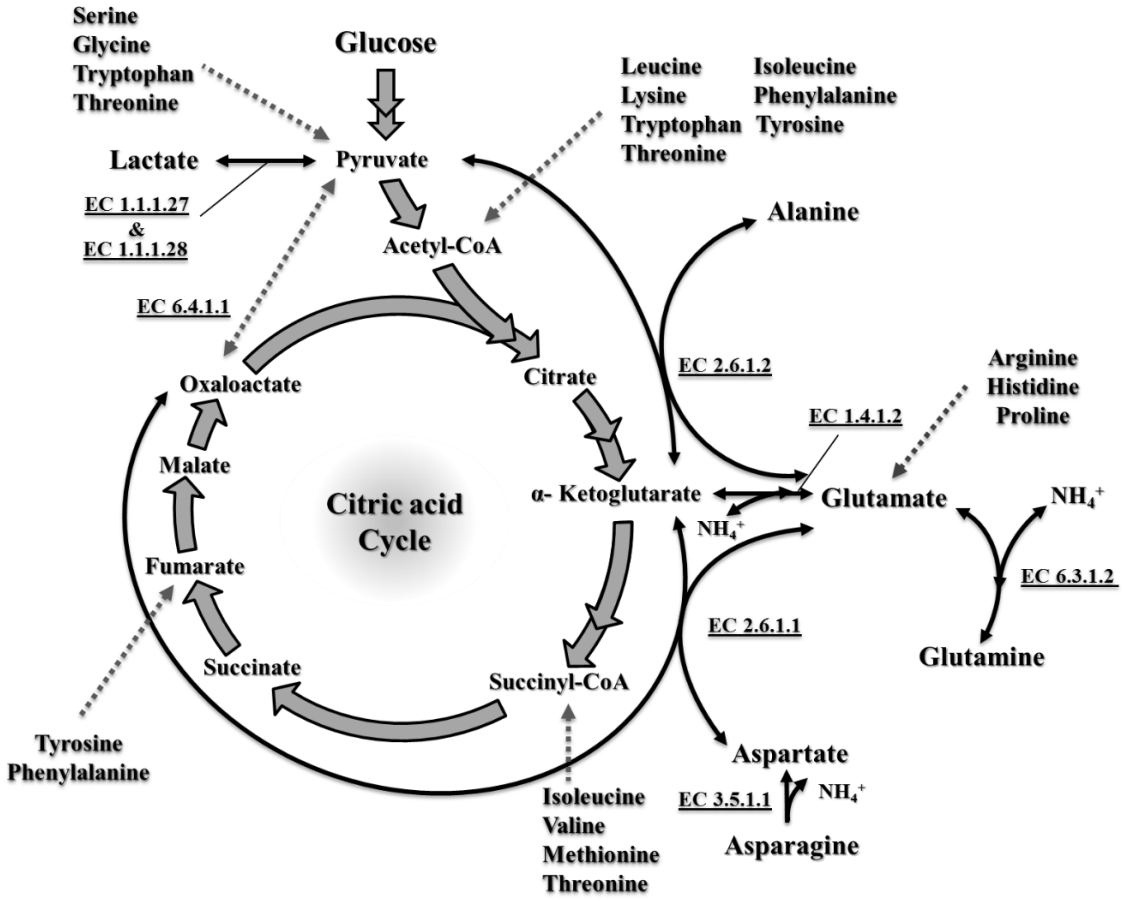
showed two bands different in size. One was around 170 kDa while the other was around 80 kDa, reflecting two different forms of the mAb; the 170 kDa form represented a complete IgG molecules (Y-shape) while the 80 kDa accounted for molecules containing both heavy and light chains but failing to assembly to the complete form of mAb as previously reported (Colcher et al., 1989, Mead et al., 2012). The supernatant sample, which was harvested from the culture at 144 hours, showed the 170 kDa band (Figure 5.3.2-A, column 6 and 8) indicating that the produced mAb had the same size and form as the mAb standard. However, the 80 kDa was not clearly visualised in the both raw and diluted samples. The amount of produced mAb was measured and cross-checked using the HPLC and ELISA techniques. Figure 5.3.2-B shows the comparison between two measurements obtained from the HPLC (Y-axis) and the ELISA (X-axis) techniques. The measurements were in the same order of magnitude and showed a positive linear correlation ($r_p = 0.988$). However, the ELISA measurement appeared to be lower than that of HPLC. This could be due to ELISA involving errors arising from 1) high dilutions given its relatively higher sensitivity and 2) human error. The difference in binding specificity between the two methods cannot be completely excluded given that the protein A in the HPLC technique can also bind to other classes of antibodies while the capture antibody in the ELISA can only bind to the IgG class of antibodies.

5.3.2 Amino acid profiles

Extracellular amino acids were measured over the duration of the culture. Alanine, an amino acid that can be converted into intermediates in the Citric Acid cycle (TCA, Figure 5.3.3), showed a different trend compared to other key amino acids such as glutamate, aspartate, asparagine and arginine (Figure 5.3.4-A, B&C). Alanine concentration increased 60% from the beginning up to 50 hours of culture (Figure 5.3.4-C), whereas other amino acids concentrations showed a statistical significant decrease ($p<0.001$, Figure 5.3.4-A&B). The

glutamate and aspartate levels (Figure 5.3.4-A) rapidly decreased from the beginning of the culture and became limited at around 50 hours of the culture – when the culture entered the stationary phase. After these two amino acids were exhausted, a switch in the alanine concentration profile (started to decrease) was observed. Arginine showed a similar trend to asparagine (Figure 5.3.4-B), both decreased over the entire culture and were exhausted at the end of the culture. After glutamate and aspartate were exhausted, the asparagine consumption showed a statistical significant increase during the stationary phase and decreased again in the death phase ($p<0.001$, Table 5.3.1). However, the arginine consumption showed a statistical significant decrease after the exponential phase ($p=0.05$).

Leucine, lysine, isoleucine, and valine concentrations (Figure 5.3.4-D&E) decreased gradually over the culture, but were not exhausted. Serine (Figure 5.3.4-C) and proline (Figure 5.3.4-F) showed a similar trend, both concentrations decreased steadily before levelling off at around 80 hours of the culture. Other amino acids such as histidine ($p=0.695$), threonine ($p=0.757$), phenylalanine ($p=0.158$), and glycine ($p=0.111$) showed no significant change during the culture (Figure 5.3.4-F, I&J). A summary of the relevant amino acid reactions involved in the TCA is presented (Figure 5.3.3). At the early and exponential phases, the observed yield of lactate over glucose was greater than 2.00 mol/mol. Aerobic glycolysis occurs in most cancer cells with a high glucose-lactate yield (Filipp et al., 2012), though lactate can also be converted back to pyruvate via the lactate dehydrogenase reaction (EC 1.1.1.27 & EC1.1.1.28). This inefficient pathway to generate ATP is known as the Warburg effect (Vander Heiden et al., 2009, Warburg et al., 1927) and could be a remaining signature as the GS-NS0 cell line, which is derived from myeloma cells (Barnes et al., 2000a).



Reaction Name	Number (EC)	Reaction
Asparaginase	3.5.1.1	L-asparagine + H_2O ↔ L-aspartate + NH_3
Aspartate transaminase	2.6.1.1	L-aspartate + α-ketoglutarate ↔ oxaloacetate + L-glutamate
Alanine transaminase	2.6.1.2	L-alanine + α-ketoglutarate ↔ pyruvate + L-glutamate
Glutamate dehydrogenase	1.4.1.2	L-glutamate + H_2O + NAD^+ ↔ α-ketoglutarate + NH_3 + NADH + H^+
Glutamine synthetase (GS)	6.3.1.2	ATP + L-glutamate + NH_3 ↔ ADP + phosphate + L-glutamine
Pyruvate carboxylase	6.4.1.1	ATP + pyruvate + HCO_3^- ↔ ADP + phosphate + oxaloacetate
L-lactate dehydrogenase	1.1.1.27	L-lactate + NAD^+ ↔ pyruvate + NADH + H^+
D-lactate dehydrogenase	1.1.1.28	D-lactate + NAD^+ ↔ pyruvate + NADH + H^+

Figure 5.3.3 A metabolic network of relevant amino acids and reactions involved in the TCA. Modified from (Nelson and Cox 2004; Sellick et al. 2011).

The decrease in both aspartate and asparagine levels implies the activation of the asparaginase reaction (EC 3.5.1.1) and the aspartate transaminase reaction (EC 2.6.1.1). In addition, at both early and exponential phases the alanine transaminase reaction (EC 2.6.1.2) appeared to be favouring the backward reaction as supported by the increasing alanine levels (Figure 5.3.4-C). The backward reaction (EC 2.6.1.2) is also supported by the glutamate consumption. However, glutamate consumption during the early and exponential phases could

also be attributed to the glutamate dehydrogenase (EC 1.4.1.2) and the glutamine synthetase (GS) (EC 6.3.1.2). The later reaction is supported by the absence of ammonium (below detection), indicating that the ammonia produced is being consumed. In addition, glutamine - which is absent in the initial media composition - appears to be produced as indicated by the relative specific glutamine rate in the early and exponential phases (Table 5.3.1). An extracellular mass balance around the glutamate consumption rate and the alanine/glutamine production rates (Table 5.3.1) for the early and exponential was performed. The mass balance revealed that approximately 67% for the early-exponential and 50% for exponential phase of the glutamate was consumed towards these reactions (EC 2.6.1.2, EC 6.3.1.2). Presumably the rest of the glutamate was used for the production of the intermediate α-ketoglutarate (EC 1.4.1.2) as it is a key reaction of the TCA (Altamirano et al., 2013). A reaction network for the early and exponential phases is proposed (Figure 5.3.5-A) summarizing the key reactions and their possible directions.

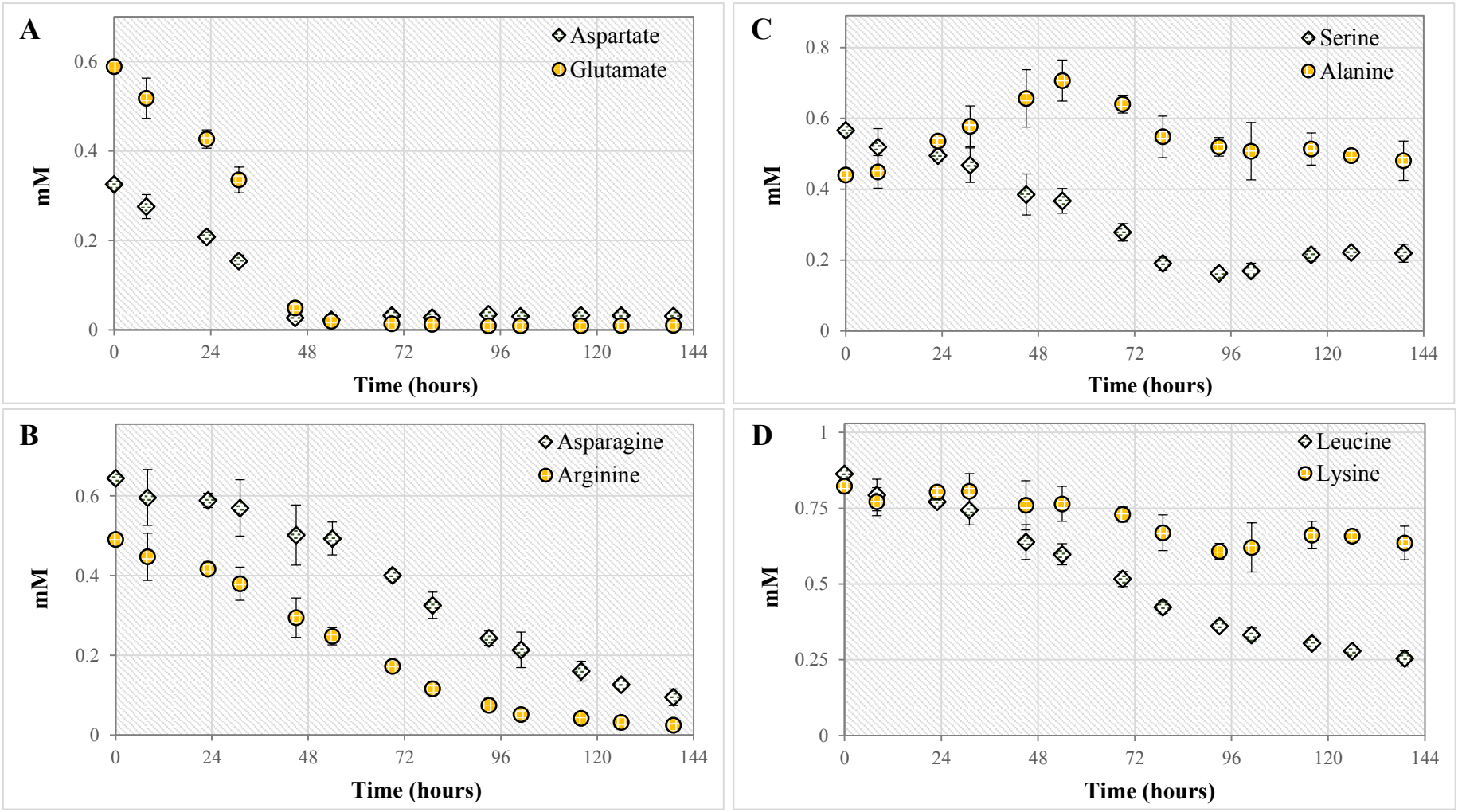


Figure 5.3.4 Extracellular amino acid concentrations in the batch culture of GS-NS0: A) aspartate and glutamate; B) asparagine and arginine; C) serine and alanine; D) leucine and lysine E) valine and isoleucine; F) cysteine and proline; G) tryptophan and histidine; H) methionine and tyrosine; I) threonine and phenylalanine; and J) glycine. (n=3, error bar = SD).

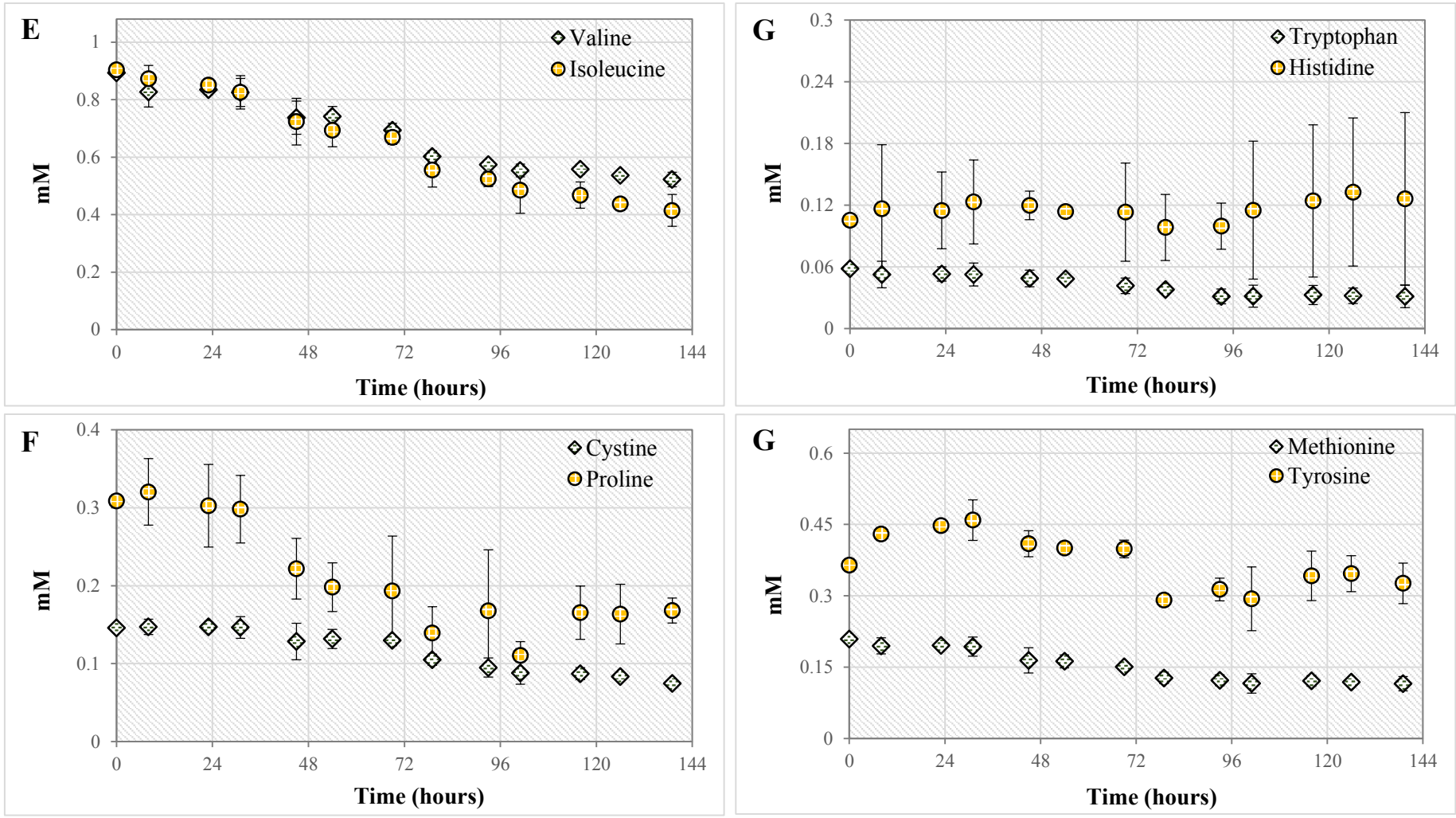


Figure 5.3.4 (Continued) Extracellular amino acid concentrations in the batch culture of GS-NS0: A) aspartate and glutamate; B) asparagine and arginine; C) serine and alanine; D) leucine and lysine E) valine and isoleucine; F) cystine and proline; G) tryptophan and histidine; H) methionine and tyrosine; I) threonine and phenylalanine; and J) glycine. (n=3, error bar = SD).

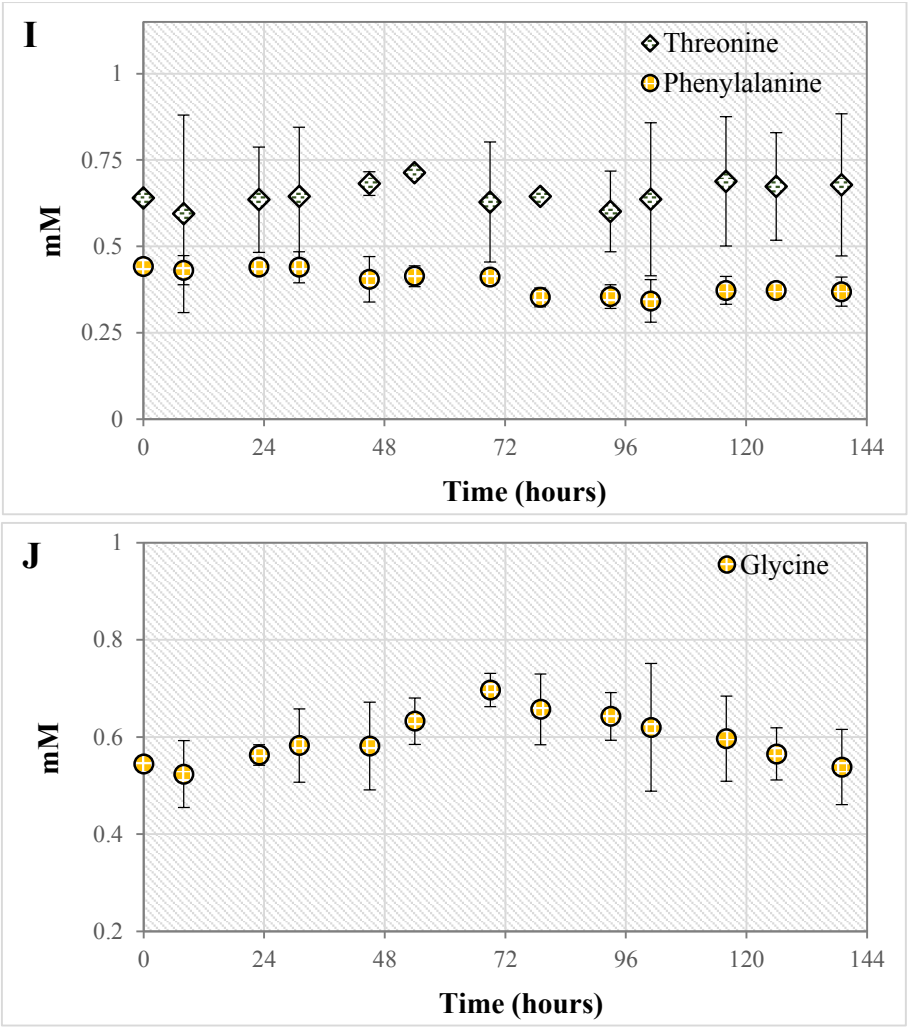
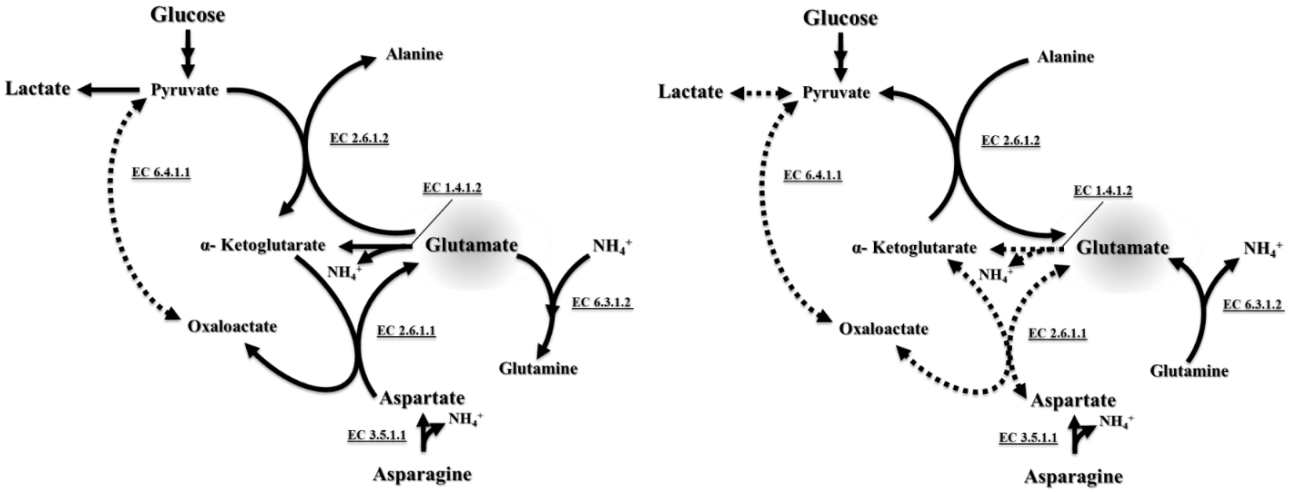


Figure 5.3.4 (Continued) Extracellular amino acid concentrations in the batch culture of GS-NS0: A) aspartate and glutamate; B) asparagine and arginine; C) serine and alanine; D) leucine and lysine E) valine and isoleucine; F) cysteine and proline; G) tryptophan and histidine; H) methionine and tyrosine; I) threonine and phenylalanine; and J) glycine. (n=3, error bar = SD).

During the stationary phase, the significant decrease of asparagine indicates that the asparaginase reaction (EC 3.5.1.1) remains in the forward direction in order to provide aspartate (which was extracellularly depleted). However, the reaction direction of the aspartate transaminase (EC 2.6.1.1) is not clear as it was not detected extracellularly. Plausibly the reaction direction might be shifting in order to keep a balance of extra ammonium production

due to sudden glutamine consumption (Altamirano et al., 2013). The relative specific glutamine rate (Table 5.3.1) in this phase suggests that glutamine is uptaken (and potentially consumed in the GS reaction). In addition, the decrease in the alanine level suggests that the forward reaction of alanine transaminase (EC 2.6.1.2) is taking place producing glutamate. Despite a net glutamate production balance from glutamine and alanine (Table 5.3.1), glutamate was not detected extracellularly. This suggests that glutamate was consumed and converted to either aspartate (EC 2.6.1.1) or α-ketoglutarate (EC 1.4.1.2). Furthermore, the yield of lactate over glucose decreased (Table 5.3.1) suggesting that there is a change in the net lactate dehydrogenase rate. A reaction network for the stationary phase is proposed (Figure 5.3.5-B).



(A) Early- and Exponential phase (B) Stationary phase

Figure 5.3.5 Cell culture dependent metabolic networks: A) early and exponential phases; and B) stationary phase. Notation: solid arrows show the supported direction by the results, dashed arrows show the proposed direction.

At the death phase, mAb productivity increased and it appeared to be the highest statistically significant productive phase of the culture (Table 5.3.1). However, this could be a result of a high lysis rate. Although most of the amino acid profiles appeared to level off at the death phase, the consumption of asparagine was still significant. In addition, ammonium was

detected at the beginning of the death phase and increased thereafter. In contrast, the change in glutamine concentration was not significant. The yield of lactate on glucose, increased during this phase although the glucose consumption rate was at its minimum. Overall, the metabolic reaction network appeared to remain unchanged compared to the stationary phase.

Table 5.3.1 Calculated specific consumption/production rates and yields.

Analysis	Culture Phase			
	Early-exponential phase (0 - 24 h)	Exponential phase (24 - 50 h)	Stationary phase (50 - 80 h)	Death phase (80 - 140 h)
Specific Growth rate (day^{-1})	0.34 ± 0.32	0.96 ± 0.14	-0.05 ± 0.05	-0.24 ± 0.09
Metabolites, Amino acids ($\mu mol.10^{-6}$ cell. day^{-1})				
Glucose	-2.64 ± 0.31	-2.73 ± 0.22	-5.41 ± 0.13	-1.21 ± 0.33
Lactate	11.47 ± 0.26	5.95 ± 0.38	6.36 ± 1.56	4.39 ± 2.22
Ammonium	--	--	0.20 ± 0.03	0.27 ± 0.07
Glutamate	-0.58 ± 0.02	-0.49 ± 0.02	-0.01 ± 2E-3	--
Aspartate	-0.42 ± 0.05	-0.22 ± 0.01	0.01 ± 2E-3	--
Asparagine	-0.12 ± 0.12	-0.12 ± 0.04	-0.17 ± 0.01	-0.11 ± 0.01
Alanine	0.25 ± 0.11	0.18 ± 0.01	-0.12 ± 0.01	-0.02 ± 0.01
Arginine	-0.26 ± 0.06	-0.19 ± 0.04	-0.12 ± 0.02	-0.03 ± 0.01
Valine	-0.21 ± 0.07	-0.12 ± 0.04	-0.12 ± 0.03	-0.03 ± 0.02
Isoleucine	-0.17 ± 0.10	-0.20 ± 0.05	-0.13 ± 0.05	-0.07± 0.02
Leucine	-0.33 ± 0.09	-0.21 ± 0.03	-0.17 ± 0.02	-0.08 ± 0.01
Lysine	-0.07 ± 0.18	-0.06 ± 0.10	-0.11 ± 0.01	0.03 ± 0.04
Glutamine	0.05 ± 0.01	0.05 ± 0.01	-0.02 ±1E-3	--
cB72.3 mAb ($\mu g.10^{-6}$ cell. day^{-1})	11.95 ± 2.78	8.72 ± 1.02	10.61 ± 1.00	23.36 ± 1.89
Yield (mol/mol) Lactate over Glucose	2.68 ± 0.12	2.00 ± 0.78	0.72 ± 0.25	1.98 ± 1.55

5.3.3 Cell cycle and apoptosis

Cell cycle distribution was tracked over the culture (Figure 5.3.6-A). The culture started with a high fraction of cells in the G_1/G_0 phase (approximately 60%), which rapidly exited this

state to join the proliferating population. Concomitantly, an increase in G_2/M phase cell fraction – from 20% to 35% – was observed during the first 24 hours of the culture. This was followed by a decrease in the G_2/M fraction (back to ~20%) with the corresponding increase in G_1/G_0 fraction (above 50%); both in agreement with the growth phases (early and exponential). Next, a decrease (to around 43%) in the G_1/G_0 population during the stationary phase of the culture (starting at around 60 hours) with a minor increase in the S and G_2/M populations (to approximately 28%) was observed. These changes took place simultaneously with the sudden increase in the ESA cell fraction (Figure 5.3.6-B). After 24 hours of increase in the ESA fraction (at 80 hours of the culture) a continuous decrease in viable cell numbers and viability was observed (Figure 5.3.1-A&B). In the death phase of the culture, there was an accumulation of the G_1/G_0 population (back to ~60%), which remained constant after 120 hours. The observed G_1/G_0 population increase was accompanied by a decrease in the S and G_2/M populations. During this period, the fraction of ESA cells was about 3 times higher than at the beginning of the culture and stayed at this level until the end of culture.

5.3.4 Pro-apoptotic and anti-apoptotic gene expressions

Pro-apoptotic and anti-apoptotic genes showed different expression levels between the growth phases (early and exponential) and the death phase. Three of the pro-apoptotic gene expressions *casp3, casp8* and *trp53bp2* showed a similar trend (Figure 5.3.7-A&B). *casp8* and *trp53bp2* were suppressed during the early and exponential phases showing a statistically significant decrease between 0 and 50 hours of the culture ($p<0.001$ and $p=0.007$, respectively). Although there was no significant decrease in *casp3* expression between 0 and 50 hours ($p=0.376$), both *casp8* and *casp3* (Figure 5.3.7-B), reached a two-fold increase (compared to at 50 hours) in their expressions by the end of the culture, which was triggered after extracellular glutamate and/or aspartate were exhausted. Similarly, *trp53bp2* also doubled its expression

(Figure 5.3.7-A), but the triggering effect appeared to be delayed 24 hours after the up-regulation of *casp8* and *casp3*. Additionally, the up-regulation of *casp8* and *casp3* took place simultaneously with the increase in the ESA and LSA cell fractions (i.e. in the stationary phase). Conversely, *bax* (Figure 5.3.7-A), one of the pro-apoptotic genes in the mitochondrial pathway, showed a different trend as compared to the others. Its expressions significantly increased (p<0.001) between 0 and 50 hours and significantly decreased between 50 and 96 hours (p<0.001).

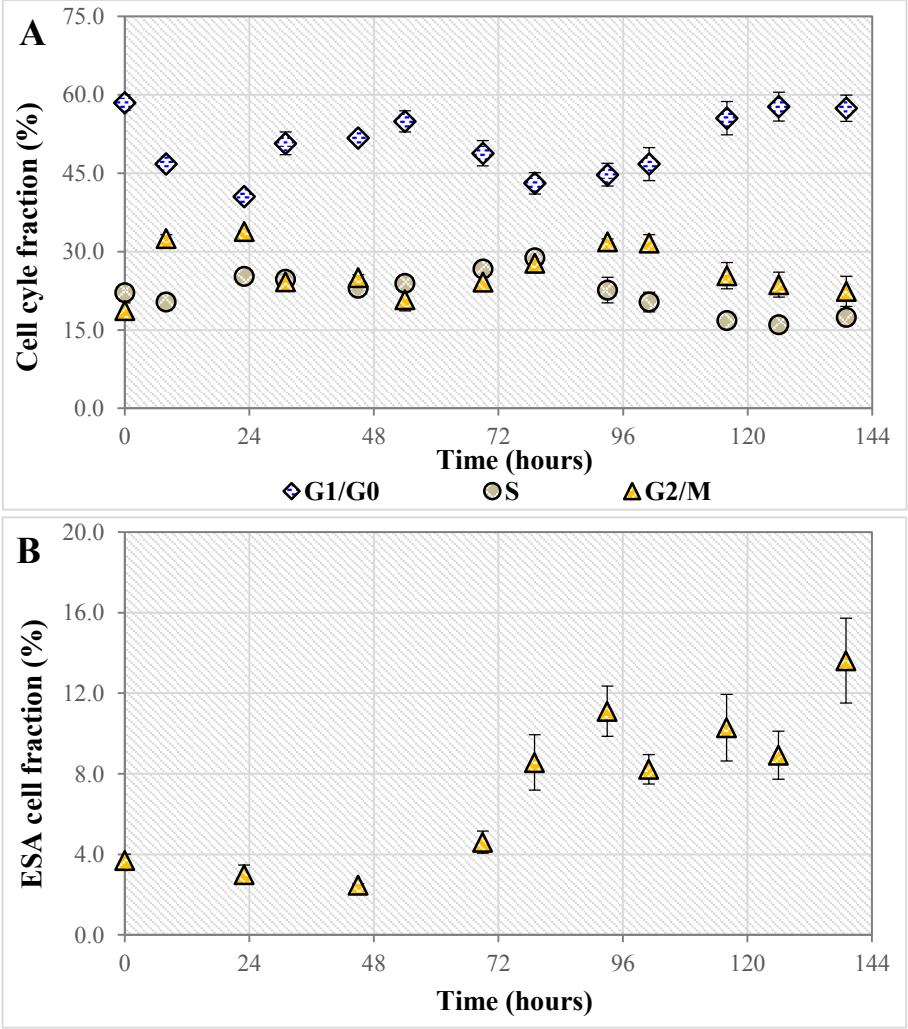


Figure 5.3.6 Cell cycle distribution and early stage apoptotic cell fraction in the batch culture of GS-NS0 cells: A) cell cycle distribution; and B) early stage apoptotic cells. (n=3, error bar = SD).

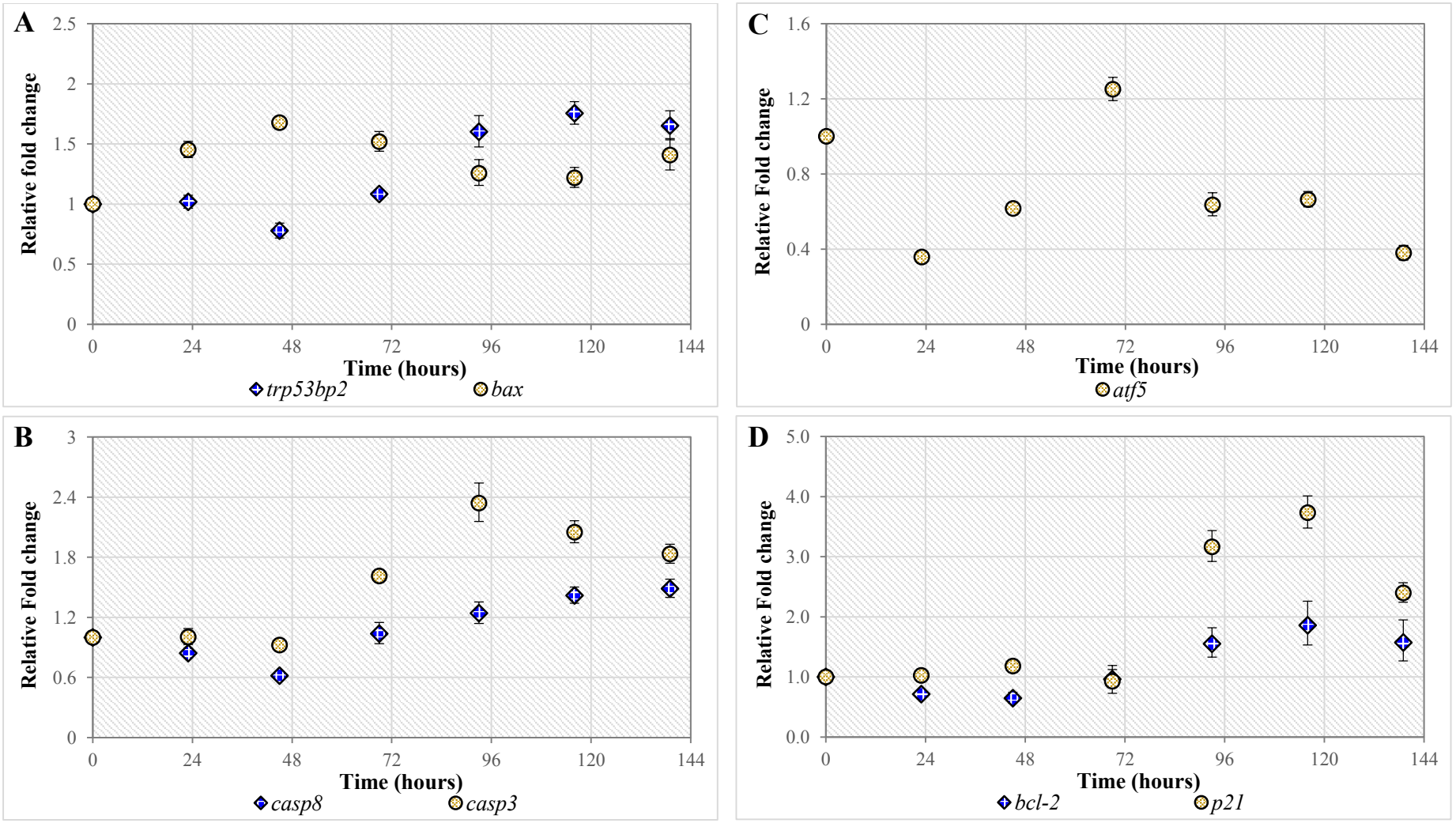
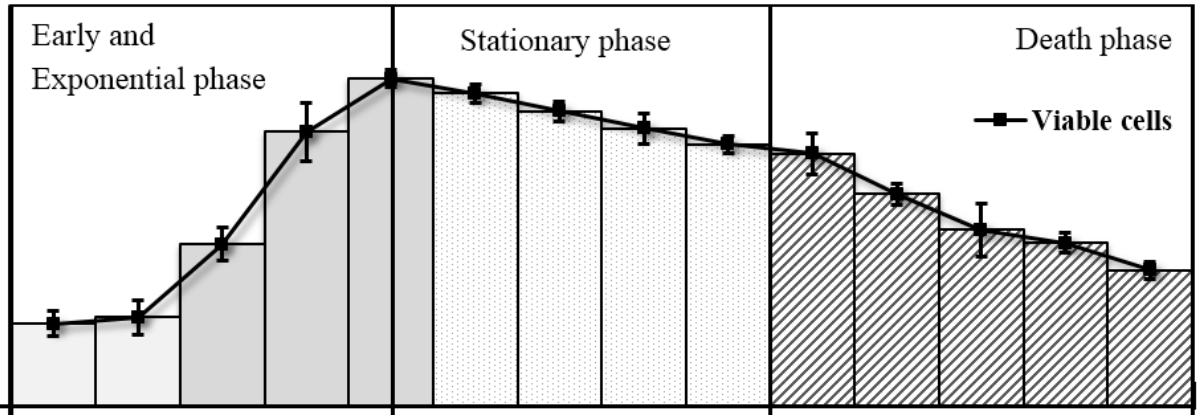


Figure 5.3.7 Relative expressions of key apoptotic and cell cycle-related genes: A) *trp53bp2* and *bax*; B) *casp3* and *casp8*; C) *atf5*; D) *bcl-2* and *p21*. Notation: relative gene expression quantification normalized to *gapdh* (housekeeping gene) and with respect to the time at 0 hour. (n=3, error bar = SD).



	Early and Exponential phase	Stationary phase	Death phase
Cell cycle & Apoptosis	**Cell proliferation** • An increase in G_2/M cell fraction • A drop in G_1/G_0 cell fraction • Both of them returning to the starting values after 24 hours **Apoptosis** • A slight drop in ESA cell fraction	**Cell Density Peak** **Cell proliferation** • A increase in G_2/M cell fraction • A drop in G_1/G_0 cell fraction **A drop in viability at the end of the phase** **Apoptosis** • A surge in ESA cell fraction	**Cell Cycle arrest** • A decrease in G_2/M cell fraction • A increase in G_1/G_0 cell fraction **Apoptosis** • ESA cell fraction remaining a high level
Extracellular Metabolites	**Extracellular Metabolites** • A drop in **glutamate** and **aspartate** levels • A gradual drop in **amino acid**[1] and **glucose** levels • A gradual rise in **alanine** level • No **NH_4^+** generation • A gradual rise in **lactate** level **cB72.3 mAb** • A slight increase in mAb level	**Glutamate and Aspartate limited** **Extracellular Metabolites** • A continuous drop in amino acid[1] and **glucose** levels • A drop in **alanine level** • **NH_4^+** generation • A continuous rise in **lactate** level **cB72.3 MAb** • A surge in mAb level	**Extracellular Metabolites** • A continuous drop in amino acids[2] • Amino acids[3], **glucose** and **lactate** levels being roughly constant • **NH_4^+** generation • **Arginine** becoming exhausted • **Asparagine** being limited at very end of the culture • **Lactate** levelling off **cB72.3 MAb** • A constant increase in mAb level
Gene Expressions	**Gene Expressions** • Most of observed genes being down-regulated	**Gene Expressions** • *atf5* peaks • A sudden rise in *casp8* and *casp3* levels • *bcl-2, p21* and *trp53bp2* rising after *casp8* and *casp3*	**Gene Expressions** • A decrease in *atf5* level • The remaining genes remaining a high expression levels

[1]Serine, Arginine, Asparagine, Leucine, Proline, Cystine, Isoleucine, Valine, Methionine, Tryptophan.
[2]Asparagine, Leucine, Cystine, Isoleucine, Valine.
[3]Proline, Arginine, Serine, Tryptophan, Methionine.
Other amino acids remained roughly constant; Histidine, Threonine, Tyrosine, Phenylalanine, Glycine.

Figure 5.3.8 Map of events occurring in each phase of the GS-NS0 culture.

The *atf5* anti-apoptotic gene (Figure 5.3.7-C) showed a different expression compared to the other genes. The *atf5* expression levels decreased during the growth phases (early and

exponential) to its minimum (24 hours), and soon after it started rising during the exponential phase (p<0.001). The rise resulted in the *atf5* peak expression (80 hours), back to the starting level (at time 0 hour), being 3 times higher when compared to the early and exponential phases. After peaking, the *atf5* gene expression decreased (halved) and remain fairly constant until the end of the culture.

The cell cycle regulatory gene *p21* and anti-apoptotic gene *bcl-2* (Figure 5.3.7-D), showed similar expression patterns to the pro-apoptotic genes. There was an increase in *p21* expression at the end of the stationary phase (80 hours), concurrently with the rise of the ESA and LSA cell populations. The significant increase and peak of *p21* expression (p<0.001) was followed by a significant rise in the percentage of cells at the G_1/G_0 phase. The *bcl-2* expression also increased at the end of the culture. However, the *bcl-2* expression showed an insignificant decrease (p=0.322) during the exponential phase as compared to at 0 hour, and began to rise during the stationary phase (p=0.025, after 80 hours). A map of events summarizing the main findings on the gene expression, metabolic profiling, cell cycle and apoptosis level is shown in Figure 5.3.8.

5.4 Discussion

5.4.1 Extracellular metabolite levels and its effect on cellular activities

Glutamate and aspartate were identified as key limiting nutrients, as cell proliferation ceased immediately after these amino acids were exhausted. Consequently, the drop in cell viability and concomitant increase in ESA and LSA cell fractions were identified to be associated with the glutamate and aspartate levels rather than with glucose. After the depletion of glutamate and aspartate a constant increase in the LSA cell fraction (and concurrent viability

drop) was observed with a high and constant ESA fraction. The observed profiles for the ESA and LSA appeared to support that ESA is a fast dynamic process (Riccardi and Nicoletti, 2006).

The extracellular dynamic profiles of amino acids provide an indication of the intracellular amino acid levels (Sellick et al., 2011). Therefore, it is possible to make inferences on the metabolism based on the extracellular measurements. The shifts in the extracellular amino acid levels during the early and exponential phases indicate the activation of TCA cycle, thus providing intermediates, some of which are required for biosynthesis (Nelson and Cox, 2004). The proposed reaction networks summarise the key observations for each phase. During the early and exponential phases the extracellular glutamate appeared to be preferentially diverted towards alanine and glutamine. Alanine production can be seen as a path to produce key TCA intermediates such as α-ketoglutarate (Nelson and Cox, 2004). In addition, the GS reaction pathway produces glutamine necessary for biological function of the GS-NS0 cells (Barnes et al., 2000a), which is supported by the detection of extracellular glutamine. Other consumption patterns, such as the elevated consumption of asparagine in the early exponential phase, appeared to be linked to the passage history. Given that the cells are passed every 3 days prior to starting the batch culture, the cells experience a short period of glutamate and aspartate exhaustion (between 50 hours and 72 hours), which appeared to trigger an increase asparagine uptake (as observed in the stationary phase). The asparagine increased uptake suggests the conversion first to aspartate and further to glutamate. Glutamate metabolism includes the glutamate dehydrogenase (as observed in the early and exponential phases) or via transaminases (aspartate transaminase or alanine transaminase), which have a closed loop structure and is used by cells as an internal mechanism to adjust to culture conditions (Altamirano et al., 2013).

It is worth discussing about possible involvement of leucine in cell growth, metabolism and protein synthesis given its observed monotonically-decreasing profile and previous studies

suggesting its effects. The mammalian target of rapamycin (mTOR)-associated signalling pathway was found to be subject to hormones (i.e. insulin) as well as amino acids, especially leucine. This pathway is involved mainly in protein synthesis (translation) which is linked to cell growth, apoptosis, metabolism (Proud, 2004, Edros et al., 2014). Leucine availability was found to promote mitochondrial metabolism through; in addition to its oxidative decarboxylation, binding to glutamate dehydrogenase, and thus facilitating the reaction where glutamate is converted to α-ketoglutarate (EC 1.4.1.2) (Xu et al., 2001, Proud, 2004, Yang et al., 2010). This is in agreement with our observed data and suggested directions of metabolic reactions (Figure 5.3.5). In addition, leucine availability was reported to have a positive effect on growth-related protein synthesis through the activity of the mTOR Complex 1 (mTORC1) (Proud, 2004, Dodd and Tee, 2012), which was found to be a nutrient-sensitive factor in the mTOR pathway (Kim et al., 2002). This effect of leucine was observed in insulin-secreting β cells (Proud, 2004, Yang et al., 2010) as well as muscle cells (Lynch, 2001). In the mammalian cell culture systems, it was found that the activity of the mTORC1 pathway was promoted by nutritional feeding (glucose and amino acids). Given the involvement of the mTORC1 signalling pathways in growth, metabolism and protein synthesis, its activation could underlie the observed increased growth and recombinant protein productivity in the fed-batch cultures (Edros et al., 2014, Dadehbeigi and Dickson, 2015).

At the stationary phase, it could be hypothesized that the exhaustion of glutamate and aspartate triggers certain metabolic changes. Previous reports support metabolic changes in order to provide alternative sources for intracellular energy and biosynthetic precursors (Young, 2013, Sellick et al., 2011), as well as the adaptation to the nutrient availability (Vander Heiden et al., 2009). The change in the alanine reaction direction is most likely due to the use of glutamate as main source for intermediate generation in the TCA cycle, as well as the biological relevance of glutamine. Alanine biosynthesis is reported to provide a bridge between

the glycolytic and glutaminolytic metabolism (Filipp et al., 2012). In addition, glutamate can also be generated from several amino acids (Nelson and Cox, 2004). Arginine is a plausible candidate for the glutamate's supply as its level constantly decreased during the culture, particularly after glutamate is depleted (Dempsey et al., 2003, Nelson and Cox, 2004). The continuous consumption of asparagine in the stationary phase suggests its conversion to provide aspartate intracellularly, as aspartate is exhausted extracellularly. It can be inferred that glucose was converted into pyruvate and not diverted to lactate due to the decreased calculated yield, compared to the early and exponential phases. However, in order to validate the decrease in the lactate dehydrogenase activity a specific assay is required. As a result of the changes both in the glucose metabolism and the alanine transaminase reaction, there is possibly an increase in the pyruvate level. Herein, we hypothesized that the increased pyruvate levels are partially diverted towards the production of oxaloacetate via pyruvate carboxylase reaction, which serves as an intermediate for both biosynthesis and energy production. In order to fully quantify and validate the metabolic fluxes and active pathways both intracellular metabolic measurements, as well as carbon-labelled experiments are required.

At the death phase, the highest mAb productivity was observed despite key substrates having been depleted. Although a possible reason for the increased mAb productivity would be the conversion of other available amino acids for biosynthesis; it is also possible that this is an effect of cell lysis, as viability decreased sharply. The sharp viability decrease could be enhanced by the lactate inhibitory levels reached in the late stages of culture (Hassell et al., 1991, Lao and Toth, 1997, Ozturk et al., 1992). It can be inferred that glutamate is still being produced by 1) aspartate transaminase and possibly from 2) GS reaction given the steep and significant ammonia increase.

5.4.2 The genetic control of cell cycle and apoptosis linked to metabolic stresses

During the early and exponential phases, cell proliferation is supported by the observed viable cell density, changes in the cell cycle, and gene expression. Constant changes in the cell cycle together with the down-regulated cell cycle regulatory gene *p21*, and anti-apoptotic gene *bcl-2,* allow us to infer a highly proliferative state (Simpson et al., 1999a, Watanabe et al., 2002). In addition, during this period the effects of metabolic stresses (toxic byproduct and nutrient deficiency) are negligible. This is reflected in the invariant levels of ESA/LSA cell fractions and the significant decrease in the pro-apoptotic genes (*casp8*, *trp53bp2* and *casp3*) expression levels. Similarly, the anti-apoptotic gene *atf5*, responsible for sensing an endoplasmic reticulum (ER) metabolic stress induced by amino acid deprivation (Watatani et al., 2007, Zhou et al., 2008), was down-regulated during the early exponential phase and started increasing during the exponential phase. Consequently, the *bcl-2* anti-apoptotic mechanism was not activated and the expression level of *bcl-2* significantly decreased in this period. At the end of the exponential phase (when glutamate and aspartate were exhausted) the cell density peaked while the cells accumulated at the G_1/G_0 phase. However, given the unchanged *p21* expression it can be concluded that the cells were not arrested.

The expression of *casp3, casp8* and *trp53bp2*, whose target proteins are caspase3, caspase8 and 53BP2, respectively, plays a role in facilitating apoptosis (Hengartner, 2000, Kobayashi et al., 2005). After glutamate and aspartate were exhausted, there was a significant increase in the ESA cell fraction and pro-apoptotic gene expression, mainly *casp8* and *casp3*. Thus, glutamate/aspartate deprivation is linked with the onset of apoptosis at the genetic level. This is in agreement with previous studies that showed that apoptosis can be triggered by single amino acid deprivation (Simpson et al., 1998, Tintó et al., 2002). Similarly, ASPP2 encoded

by *trp53bp2* is believed to stimulate the transactivation of p53, which ultimately triggers apoptosis via the mitochondrial pathway (Kobayashi et al., 2005, Patel et al., 2008, Samuels-Lev et al., 2001). In contrast, p53 activation also can regulate metabolic defensive adaptations to lethal signals (Hu et al., 2010, Maddocks et al., 2013). The increase in *trp53bp2* expression, 24 hours later than the surge in *casp8* and *casp3* expression and the ESA cell fraction increase, suggests that apoptosis initiated via the death receptor pathway followed by activation of the mitochondrial pathway at a later time. Caspase-8 is an upstream protein in the death receptor pathway that activates caspase-3, which is the final executor of both apoptosis pathways (Stennicke et al., 1998). The observed delay to up-regulate *trp53bp2* can be attributed to two possible causes: 1) there is a lag from the moment that the extracellular glutamate is exhausted until it is internally exhausted, and/or 2) the cell was able to synthesize glutamate from other sources delaying the *trp53bp2* up-regulation. The latter is supported from the availability of extracellular glutamine synthesized in the early and exponential phases and depleted at the stationary phase. The peak of *atf5* expression was observed at the end of the stationary phase, after glutamine became exhausted, and it transactivates the anti-apoptotic gene *bcl-2* as previously reported (Dluzen et al., 2011). These changes took place simultaneously with the increase both in the G_1/G_0 cell fraction and the ESA fraction. The observed increase in the G_1/G_0 cell fraction appeared to be a defensive mechanism to apoptosis (Moore et al., 1997, Sanfeliu and Stephanopoulos, 1999) driven by the simultaneous increase of the cell cycle regulator *p21*. It has been reported that *p21* expression leads to cell cycle arrest in the G_1/G_0 cell fraction (Bissonnette and Hunting, 1998). The *bcl-2* gene is known to play a role in the control of cell cycle progression, while the *p21* has a suppressive effect on the onset of apoptosis (Gartel and Tyner, 2002a, Hockenbery et al., 1990, Niculescu et al., 1998). At the start of the death phase, both ESA and LSA cell fractions remained high, suggesting that cell death (apoptosis) is dominant.

It is worth discussing about the expression profile of *bax*. The role of *bax* has been found to be associated with pro-apoptotic and anti-apoptotic molecules. There was an inversely proportional correlation between *bax* and *bcl-2* (Paul-Samojedny et al., 2005), suggesting that the Bcl-2 associated survival mechanism involves supressing *bax* expression. In contrast, *bax* was found to be one of transcriptional targets of *p53* (Toshiyuki and Reed, 1995), suggesting its pro-apoptotic effect. Given these facts, the observed *bax* expression profile could be therefore influenced by both pro-apoptotic and anti-apoptotic molecules. The increase in its expression could be the result of pro-apoptotic signals being dominant, while the decrease in its expression could be driven by anti-apoptotic signals.

The observed batch culture profiles at the gene transcription, cell cycle distribution and apoptosis extent are summarized in a map. The map can serve as a tool for developing feeding strategies of key amino acids in the fed-batch systems maintaining a balance between cell proliferation, arrest at G_1/G_0 phase and the induction of apoptosis. Such feeding strategies will allow the culture to achieve longer culture times, while keeping a high viability and mAb production. For instance, the addition of key amino acids can prolong the cultivation duration (Kiparissides et al., 2014). Further, the selected feeding profile could be constraint or bounded to partially achieve a control between cell proliferation arrest at G_1/G_0 phase and the induction of apoptosis as herein observed.

5.5 Conclusions

This chapter aims to identify metabolic stresses in the batch culture of GS-NS0 cells and investigate cell cycle and apoptosis-related dynamic responses to the identified metabolic stresses. Metabolism, cell cycle and apoptosis were extensively investigated. In addition, relationships among them were previously reported. However, kinetics of apoptosis and its

association with cell cycle as respect to dynamic metabolic changes have not been clearly elucidated. Our work shows that apoptosis and cell cycle are intimately related at the genetic level and also linked to the extracellular conditions. A map of events occurring in each phase of the GS-NS0 culture based on the experimental observation was presented. The *atf5* gene showed a prompt response to extracellular glutamate/aspartate deprivation, while *casp8* and *casp3* genes up-regulation indicates cell death via apoptosis in response to the metabolic stresses. Furthermore, the up-regulation of *p21* during the end of stationary phase and death phase and a high G_1/G_0 cell fraction implies that cell cycle arrest is the mechanism to delay apoptosis when cells are lethally insulted. The gene markers provide relevant information to detect unfavourable conditions that reduce cell viability. Furthermore, the metabolic shift occurring in the culture as regards the glutamate/aspartate deprivation was proposed. This involves redirecting metabolic fluxes in relevant metabolic reactions in an attempt to relieve the metabolic stresses. All this information can be potentially use to formulate feeding strategies beyond improving product quality and productivity, which could partially control key cell cycle events such a cell proliferation and apoptosis.

Chapter 6

The Impact of Temperature, Medium Composition and Nutrient Addition, on Apoptosis

6.1 Background

Temperature levels, medium composition as well as additional nutrients are culturing conditions that can directly influence a cell culture performance. They are preferentially optimised so as to enable the cultures to achieve higher production of therapeutic proteins. However, this task is challenging given that detailed understanding of their effects on cell growth, viability as well as productivity have not been well established.

In this chapter, a set of experiments aiming to investigate the impact of these culturing conditions is presented. The effects of 1) temperature shifts, 2) the variation of medium contents (using conditioned medium), and 3) different nutrient feeding strategies predominantly on induction of apoptosis in the culture of GS-NS0 cells, were studied. The expression of apoptotic genes under the influence of these parameters was monitored using real-time PCR techniques. Based on the observed results, optimal culturing conditions for the GS-NS0 cell culture can be elucidated.

6.1.1 Introduction

As previously discussed, high-yielding mammalian cell culture systems are greatly desirable for production of bio-therapeutics. There are a number of culturing conditions that can directly affect culture performances including cell growth, death and metabolism (product synthesis). It is, therefore, essential to understand the effect of the culturing conditions on cellular processes so that an optimal culturing condition where synthesis of bio-therapeutics is highly facilitated can be identified.

Culturing temperature stands out from other culturing conditions given that it can be measurable and manipulated during the cultivation. 37°C, which is the physiological temperature level where cellular systems can perform their normal activities, is believed to be

an optimal level for the mammalian cell cultures. Given that temperature does not only affect yield of desired products but also other cellular processes such as cell growth and death, culturing at 37°C might not be the optimal one that enables the cultures to achieve the highest yield of desired products. Medium composition, which specifies initial supply of nutrients; including glucose and amino acids, and metabolites; including lactate and ammonium, is also one of important culturing conditions that can designate the fate of the culture. The addition of nutrients during the cultivation, including glucose and amino acids, is also considered as an important culturing condition given that fed-batch cultures are widely utilised in large-scale production of biologics. Given the relationship between extracellular nutrient concentrations and the cellular processes, to identify an optimal supply of nutrients and metabolites as well as nutrient feeding strategy requires mechanistic understanding of cellular responses with respect to medium composition and nutrient addition.

The impact of temperature shifts, medium composition as well as addition of nutrients, including glucose and amino acids, on cellular activities: cell growth, metabolism and death, has been extensively studied. However, variable effects of these culturing parameters were observed from various cultures. For example, the shift to hypothermic temperature, which is the condition where culturing temperature is lower than the physiological one, during the exponential phase of cell cultures enhanced final antibody or protein of interest titre and/or productivity (Furukawa and Ohsuye, 1999, Kaufmann et al., 1999, Fox et al., 2004, Hendrick et al., 2001, Rodriguez et al., 2005, Oguchi et al., 2006, Bollati-Fogolín et al., 2005), while other cultures with the similar temperature shift did not (Barnabé and Butler, 1994, Weidemann et al., 1994, Marchant et al., 2008). A high initial glutamine concentration was found to enhance the productivity in the culture of a cell line (Dalili et al., 1990, Schneider and Lavoix, 1990), while the culture of another cell line with the high glutamine concentration did not achieve the productivity improvement (Takagi et al., 2001).

Adding complexity to the problem, relevant cellular activities affected by the culturing conditions are essentially interlinked, making the determination of an optimal state of these conditions highly difficult. On the one hand, the presence of growth factors as well as an elevated level of nutrients and metabolic by-products, for example, can promote cell proliferation and metabolic activities (Miller et al., 1988a, Reuveny et al., 1986). On the other hand, the absence of these factors can cause growth arrest as well as induction of apoptosis (Fussenegger and Bailey, 1998, Mercille and Massie, 1994a, Simpson et al., 1998, Singh et al., 1994). Hypothermia generally causes growth arrest and thus prolonged culture viability, nevertheless, the effect of hypothermia on the final titre and productivity appears to be variable (Swiderek and Al-Rubeai, 2007, Barnabé and Butler, 1994, Yoon et al., 2006). Feeding nutrients during the culture progression was found to delay the onset of apoptosis (DiStefano et al., 1996, Xu et al., 2014) and improve the production of therapeutic proteins. However, excessive amount of added nutrients can cause an excessive level of toxic metabolite accumulation (Xie and Wang, 1994), thereby causing induction of cell death and deterioration in both production and quality of secreted proteins.

As the discussion above attests, a systematic view of the culturing condition effects, which takes into account their cell line-specific characteristics as well as the interrelation among affected cellular processes, is the key to establish optimal conditions. To the best of my knowledge, apoptosis-associated responses to these culturing conditions as well as links to cell proliferation and metabolic activities have not been clearly elucidated for the GS-NS0 cell cultures. These stresses the necessity of expanding the understanding of the effect of these culturing conditions predominantly on apoptosis induction. In this way, strategies to control the degree of apoptosis while enhancing protein production/productivity in the GS-NS0 cell cultures can be ultimately devised.

6.1.2 Objectives

This chapter aims to investigate the effect of temperature shifts, medium contents and nutrient additions on apoptosis in the culture of GS-NS0. The following are the scientific objectives proposed for the study:

- Design and conduct GS-NS0 culture experiments that would enable to assess the effect of temperature shifts on apoptosis.
- Design and conduct GS-NS0 culture experiments that would enable to elucidate apoptosis responses at a transcriptional level to the variation in medium contents.
- Design and conduct GS-NS0 culture experiments that would enable to elucidate apoptosis responses at a transcriptional level to the different nutrient additions.
- Identify key relations between these culturing conditions and apoptosis induction for further model development.

6.2 Methodology

6.2.1 Temperature fluctuations

The impact of temperature fluctuations was studied in the batch cultures of GS-NS0 cell line. The cultures were performed in triplicate using the same medium composition and incubation condition as described in Chapter 4. In this experiment, cells were inoculated at 2.5 $\times 10^5$ cells/mL and the temperature shifts were implemented to the cultures. The cultures were maintained at 37°C for the first 30 hours of the culture, then the temperature was shifted to either 35°C or 39°C. The level of temperature shifts (±2°C from 37°C) was adopted based on the fact that cell could experience excessive stresses (due to extreme temperature difference) to the extent that cells could not manage to adapt themselves for the new temperature condition

(Sureshkumar and Mutharasan, 1991). The cultures were maintained for 5 days (120 hours). The batch culture at 37°C, as described previously in Chapter 4 and discussed in Chapter 5, was used as a control culture, to which the cultures exposed to temperature fluctuations were compared.

The analysis performed in this experiment includes cell density and viability determination (haemocytometer), apoptotic cell and cell cycle analysis (flow cytometer), cyclin D1 profiling (flow cytometer), measurements of nutrient and metabolite levels (BioProfile 400), and mAb quantification (HPLC). The procedure of the performed analysis is described in Chapter 4, otherwise it is as per manufacturer's instruction. Samples were harvested twice a day for the analysis, except for apoptotic cell quantification and cyclin D1 profiling that samples were collected daily.

This experiment was conducted in collaboration with D. G. García Münzer (PhD candidate) and A. Gauthier (MSc student).

6.2.2 Medium composition

The effect of the medium composition was investigated in the batch cultures of GS-NS0 cell line. The cultures were performed in triplicate, and under the same incubation condition as described in Chapter 4; though the inoculation cell density, the medium contents, the size of cultivation flask as well as the sampling time point were different. In this experiment, cells, isolated from the mid-exponential phase of the sub-culture (using the centrifugation with the condition as described in Chapter 4), were seeded at 5×10^5 cells/mL in 250 mL Erlenmeyer flask (Corning, 431144) with 50 mL working volume. The different medium blends used for growing cells include 1) 100% fresh medium + 0% spent medium (100%FM), 2) 50% fresh medium + 50% spent medium (50%FM), and 3) 0% fresh medium + 100% spent medium

(0%FM). The spent medium was isolated from the culture at the late stationary phase (day 4 and 5 of the sub-cultures).

Samples were collected every 6 hours until 24 hours of culture in order to reveal short-term responses induced by the medium content change. The analysis involved measuring cell density and viability (haemocytometer), apoptotic cell and cell cycle fractions (flow cytometer), the expression of cyclins (flow cytometer), gene expression (Real-time PCR), nutrient and metabolite levels (BioProfile 400), and mAb titre (HPLC). The procedure for the analysis is described in Chapter 4.

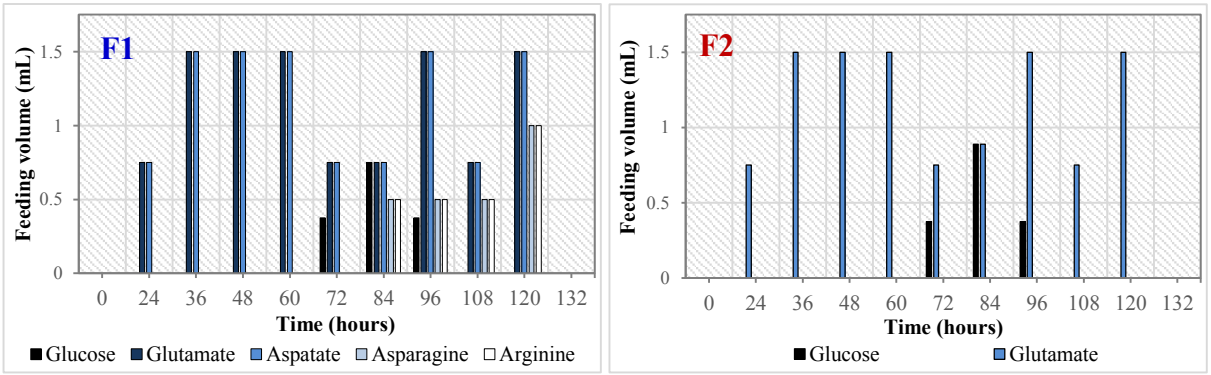
This experiment was conducted in collaboration with D. G. García Münzer (PhD candidate).

6.2.3 Nutrient additions

This experiment includes fed-batch cultures of GS-NS0 cell line, aiming to evaluate the effect of nutrient additions during the culture progression. The cultures employed the same incubation condition as well as medium composition, as described in Chapter 4. There were two feeding strategies implemented in this experiment: F1 and F2, as shown in Figure 6.2.1. They were devised based on the understanding established in Chapter 5, suggesting limiting substrates in the culture of GS-NS0 cell line as well as and the time point that these substrates should be fed. The difference between F1 and F2 is the number of substrates that were fed into the culture. F2 assumes that glutamate and glucose are only limiting substrates (Figure 6.2.1-B) while F1 takes into account the limiting effect of aspartate, asparagine and arginine in addition to glucose and glutamate (Figure 6.2.1-A).

The feeding volume was determined based on the facts that 1) the net culture volume change due to the nutrient additions and sampling should not be larger than ± 30% of the culture

volume (Trummer et al., 2006) in order to avoid the dilution effect (Kyparissidis, 2012), 2) any increases in nutrient concentration in the culture should not be over the concentration of these nutrients in the fresh medium in order to avoid possible cytotoxicity caused by excessive amount of nutrients (Sellick et al., 2011). The concentration of feeding nutrient stock solutions (Figure 6.2.1) were made up by dissolving glucose (Sigma-Aldrich, G7021-1KG), glutamate (Sigma-Aldrich, G8415-100G), aspartate (Sigma-Aldrich, A7219-100G), asparagine (Sigma-Aldrich, A4159-25G) and arginine (Sigma-Aldrich, A8094-25G) in sterile de-ionised water (< 18.2 mΩ cm).



(A) (B)

Figure 6.2.1 Two different schemes of nutrient additions in the fed-batch cultures: (A) F1 (glucose, glutamate, aspartate, asparagine and arginine); and (B) F2 (glucose and glutamate). The concentration of each feeding nutrient stock solution is as follows: 200 g/L (1.1 M) of glucose; 7.5 g/L (50mM) of glutamate; 5 g/L (37.5 mM) of aspartate; 10 g/L of (76 mM) asparagine; and 10 g/L (57.5 mM) arginine.

Samples were harvested twice a day after the nutrient feeding. The analytical assays performed in this experiment is as follows: cell density and viability determination (haemocytometer), apoptotic cell and cell cycle analysis (flow cytometer), gene expression (real-time PCR), measurements of nutrient and metabolite levels (BioProfile 400 and HPLC), and mAb quantification (HPLC). The procedure for these assays is described in Chapter 4.

6.3 Results & Discussion

6.3.1 Temperature fluctuations

Cell proliferation and apoptosis

In this study, the culture temperature was shifted to either 35°C or 39°C, though the temperature could be shifted to higher than 39°C or lower than 35°C as can be seen from previous studies (Masterton and Smales, 2014). The reason why these temperature shift levels were selected specifically for this study is that our cultures with the temperature shift to less than 35°C or higher than 39°C experienced no growth and a sudden drop in cell viability, and thus the cultures could not be maintained. Therefore, ±2°C from 37°C could be the working temperature range for our culture system. It is worth noting that the difference in how lower (or higher) the culture temperature is shifted to in a cell culture might induce different responses. In addition, despite applying the same level of hypothermic (and also hyperthermic) temperature, different effects might also be observed from different cell culture systems (i.e. different cell lines, different medium used, etc.) (Masterton and Smales, 2014, Marchant et al., 2008).

The maximum cell concentration was affected by the temperature shifts in the culture of GS-NS0 cells. As can be seen from Figure 6.3.1-A, the culture with the temperature shift to 35°C achieved a lower maximum cell concentration while the culture with the temperature shift to 39°C demonstrated a comparable cell density profile, compared to the control culture or the culture at 37°C. More specifically, cell growth became slower after 30 hours of the culture (where the temperature shift to 35°C was introduced), given that cell density did not changes significantly. In addition, compared to the control culture, the culture with temperature shift to 39°C demonstrated a faster cell density drop after 96 hours of the culture.

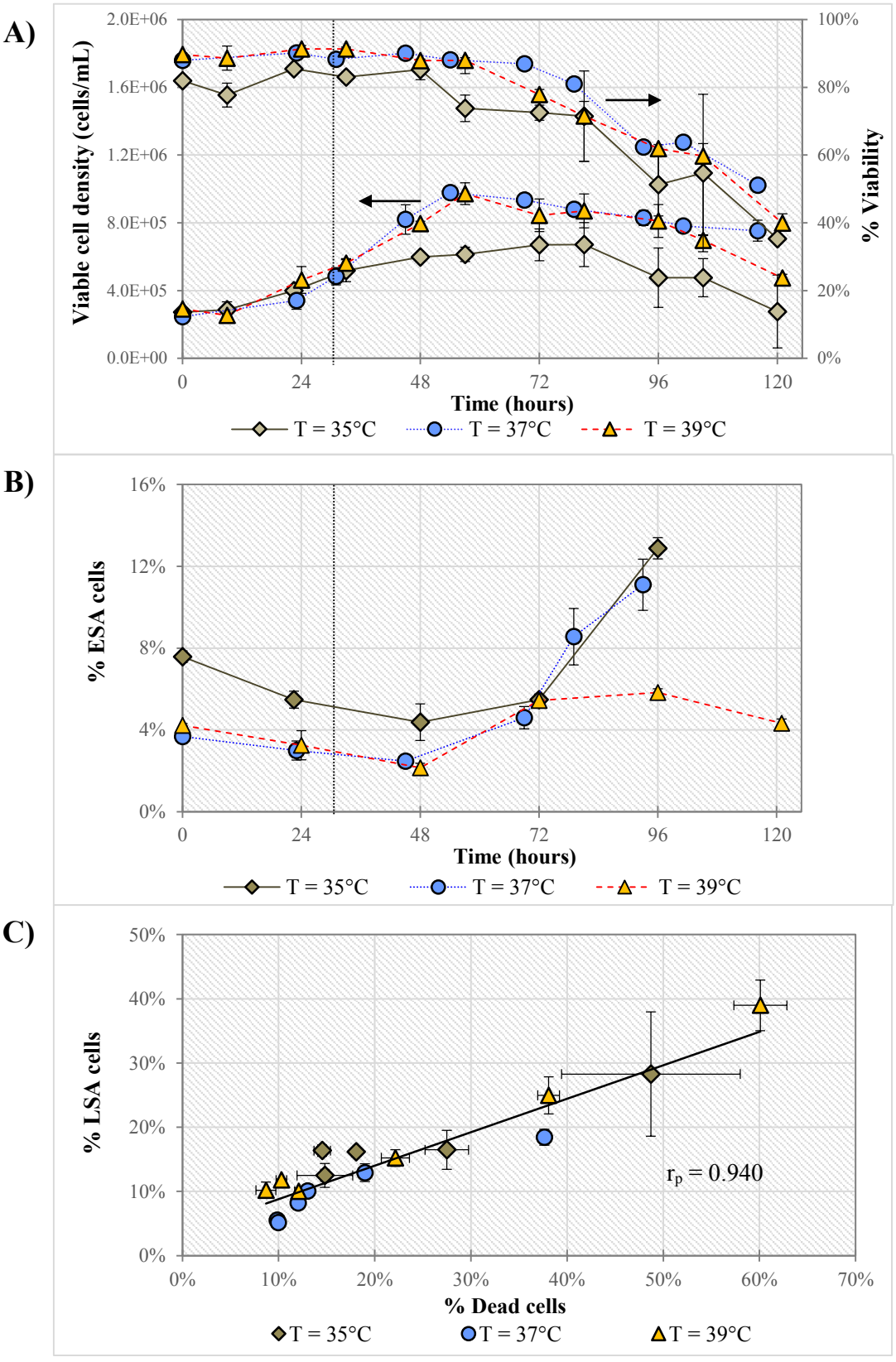


Figure 6.3.1 The profiles of A) cell density and viability; B) % ESA; and C) % LSA VS. % dead cells, in the temperature shift experiment. The vertical dot line represents the temperature shift. The arrows indicate the corresponding axes to the data (n=3, error bar = SD). r_p represents the Pearson correlation coefficient.

Generally, the cultures exposed to the temperature fluctuations showed a similar pattern of culture viability to the control culture. However, a sudden culture viability drop in the cultures exposed to temperature fluctuations was observed at around 60 hours, earlier than the control culture (Figure 6.3.1-A). ESA cells appeared to be affected by the temperature shifts in a similar manner to cell density. After 30 hours until 72 hours of the culture, there was no significant change in % ESA cells in the culture with the temperature shift to 35°C, while the culture with temperature shift to 39°C as well as the control culture demonstrated a sudden rise in % ESA cells (Figure 6.3.1-B) as a result of glutamate became exhausted (Figure 6.3.2-A). The unchanged level of ESA cells in the culture with temperature shift to 35°C suggests the effect of hypothermic condition that helped delay the onset of apoptosis. After 72 hours, % ESA cells in the culture with the temperature shift to 35°C, however, was suddenly increased and became comparable to % ESA cells in the control culture. In the meantime, the culture with the temperature shift to 39°C did not change until the end of culture, despite the observed viability drop. Figure 6.3.1-C confirms that there was no significant error in the cell viability determination technique or the cell count given the strong linear correlation between % LSA cells obtained from flow cytometry and % dead cells ($r_p = 0.940$) obtained from the cell viability determination technique.

The observed effects of the temperature shift to 35°C are in good agreement with previous data. A lower maximum cell density (Kaufmann et al., 1999, Hendrick et al., 2001, Fox et al., 2004, Bollati-Fogolín et al., 2005, Oguchi et al., 2006) as well as the delay in apoptosis induction (Furukawa and Ohsuye, 1998, Shi et al., 2005, Moore et al., 1997, Marchant et al., 2008) have been reported from the culture of various cell lines with the temperature shifts to hypothermic conditions. In addition, the observed result showing no prolongation of culture viability is also in agreement with previous data (Furukawa and Ohsuye, 1999, Rodriguez et al., 2005). Nevertheless, it is contrary to other previous studies reporting that culture viability

is prolonged in the culture under mild hypothermic conditions (Swiderek and Al-Rubeai, 2007, Yoon et al., 2006). The observed phenomena in the culture with the temperature shift to 39°C are in agreement to the previous data (Sureshkumar and Mutharasan, 1991) showing a comparable level of the maximum cell density between the temperature shifted culture and the control culture. However, Barnabé and Butler (1994) showed that the temperature shift to a hyperthermic condition decreased the maximum cell density. The sudden viability drop despite lowering %ESA cells, observed in the culture with the temperature shift to 39°C, could be because apoptosis is a highly dynamic process (Riccardi and Nicoletti, 2006), and the increase in temperature could increase the transition rate between ESA and LSA. This observed viability drop is confirmed by previous data showing fast cell death in hyperthermic cultures (Barnabé and Butler, 1994, Furukawa and Ohsuye, 1998). Another explanation is that ESA could be inhibited by activation of heat shock proteins (HSPs) in response to the hyperthermic condition while the observed drop in viability could be contributed by other types of cell death. Many of HSPs, including HSP70, HSP90 and HSP27, were found to have anti-apoptotic roles, where apoptosis can be blocked at either upstream, mitochondrial or downstream pathways of apoptosis (Lanneau et al., 2008), as previously discussed in Chapter 2. The activity of cold shock proteins (CSPs) in response to hypothermia might underlie the observed lower viable cell concentration as well as delay in apoptosis in the hypothermic culture. As discussed in Chapter 2, CIRP and RBM3, ones of CSPs, can inhibit apoptosis in response to hypothermia (Kita et al., 2002, Sakurai et al., 2006). In addition, CIRP was found to partly contribute to cell cycle arrest (Kumar et al., 2007).These CHPs could partly contribute to the observed effect of hypothermia in the culture.

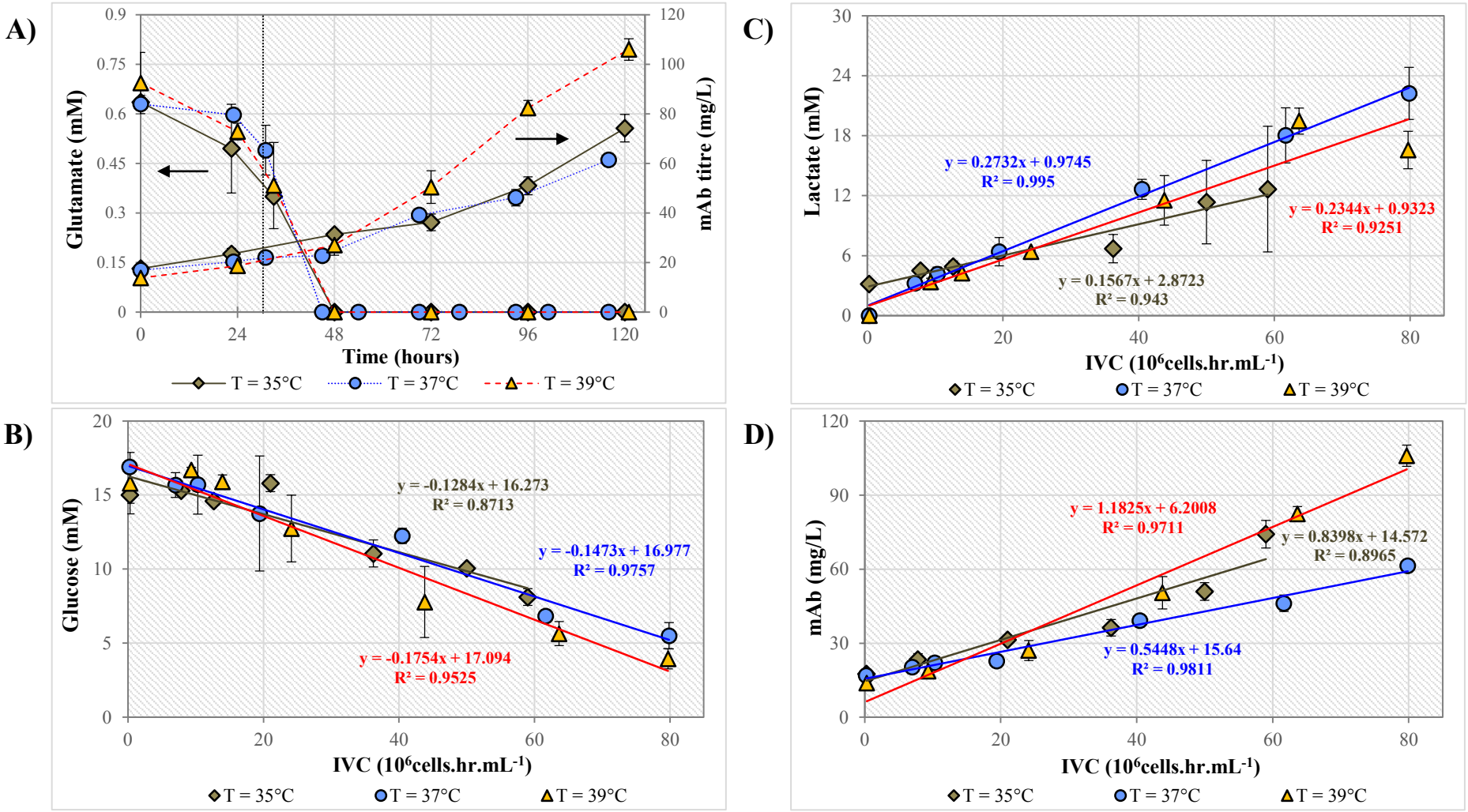


Figure 6.3.2 The metabolic and mAb profiles and in the batch cultures with the temperature shifts: A) glutamate and mAb concentrations; B) specific glucose consumption rates; C) specific lactate generation rates; and D) specific mAb productivity. The vertical dot line represents the temperature shift. The arrows indicate the corresponding axes to the data (n=3, error bar = SD).

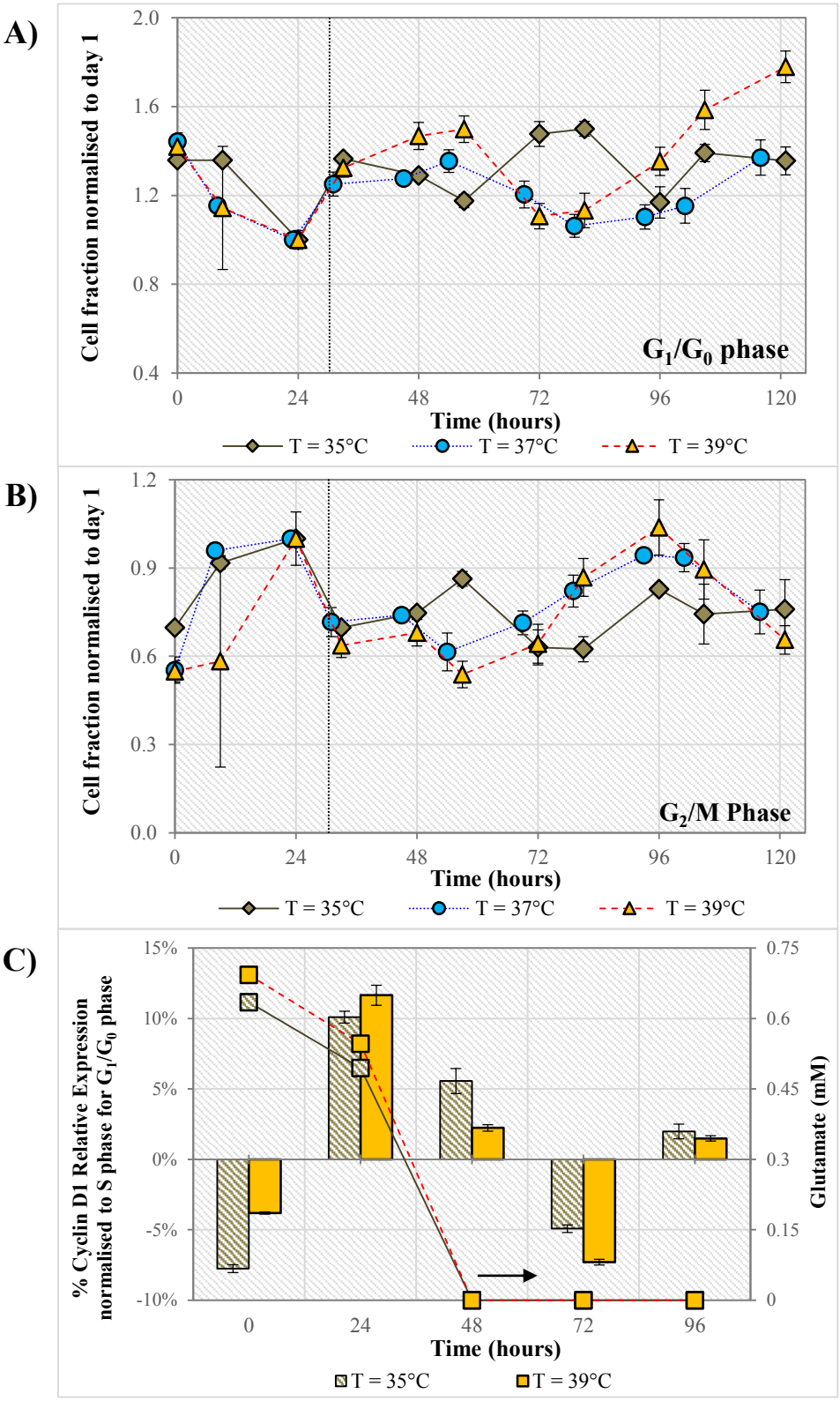


Figure 6.3.3 The cell cycle analysis: A) cell fraction in G_1/G_0 lumped phase; B) cell fraction in G_2/M lumped phase; and C) cyclin D1 profile with glutamate concentration. The vertical dot line represents the temperature shift. The arrows indicate the corresponding axes to the data (n=3, error bar = SD).

Metabolic activities and mAb production

As shown in Figure 6.3.2-A, the profile of glutamate level was similar among the cultures. Glutamate was completely consumed at around 48 hours of the cultures. Despite the lowest maximum cell density in the biphasic and hypothermic culture, the culture showed the lowest rate of specific lactate generation as well as the comparable specific glucose consumption rate to that of the control culture (Figure 6.3.2-B&C). The yield of lactate over glucose in the culture with the temperature shift to 35°C appeared to be the lowest one (~1.2 mol/mol) as compared to that of the other cultures (Appendix B1). These results are in agreement with the previous report, showing reduction in lactate production (Weidemann et al., 1994, Barnabé and Butler, 1994, Moore et al., 1997) as well as reduction in the yield of lactate on glucose (Sureshkumar and Mutharasan, 1991). However, several studied demonstrated that hypothermia in general reduced metabolic activities, including glutamine and glucose consumption (Reuveny et al., 1986, Barnabé and Butler, 1994, Weidemann et al., 1994, Swiderek and Al-Rubeai, 2007, Marchant et al., 2008), which is contrary to our observation. The specific glucose rate in the culture with the temperature shift to 39°C appeared to be the highest one among the cultures, as shown in Figure 6.3.2-B. The observed result is in good agreement with previous data (Barnabé and Butler, 1994, Trummer et al., 2006). However, these previous studies showed that there was an increase in lactate production rates under hyperthermic conditions, which is contrary to our observed result where the specific lactate generation rate did not change significantly, compared to the control culture (Figure 6.3.2-C).

For the first 48 hours, the trend of mAb titre among the cultures did not significantly vary with each other (Figure 6.3.2-A). However, after 72 hours, it appeared that the mAb titre in the culture with the temperature shift to 39°C was significantly higher than those of the other cultures. Figure 6.3.2-D illustrates the specific mAb productivity among the cultures. It appeared that the cultures with the temperature shift to 35°C and 39°C achieved around 1.5 times

and 2.2 times, respectively, higher mAb productivity than that of the culture at 37°C. The observed increase in mAb productivity in the biphasic hypothermic culture could be because the reduced activity in global mRNA translation and metabolism, and the enhanced mRNA stability (could be due to the CSP activation (Kumar et al., 2007), as a result of the reduced temperature, occurred simultaneously. This provided more chance, as compared to the normal cultures, for the recombinant mRNAs to undergo translation and post-translational protein processing, leading to enhanced productivity (Masterton and Smales, 2014, Marchant et al., 2008). The observed increased mAb productivity in the hyperthermic culture could be linked to the activation of HSPs due to the increased temperature given that they act as chaperones helping facilitate the process of the recombinant protein folding and prevent possible aggregation as well as misfolding arising from denatured proteins (Sonna et al., 2002).

Cell cycle progression and links to apoptosis

Cell cycle profiles were similar among the observed cultures (Figure 6.3.3). There was no clear evidence of immediate cell cycle responses to the temperature shifts, given that most changes were observed long after the temperature shifts. There was a temporary and sudden increase in G_2/M cell fraction during 48 to 60 hours (Figure 6.3.3-B), before the temporary increase in G_1/G_0 cell fraction after 72 hours in the culture with the temperature shift to 35°C (Figure 6.3.3-A). This might indicate cell cycle arrest at G_2/M lumped phase due to the effect of hypothermic temperature shift. This suggestion is supported by the previous studies demonstrating that there were an increase in cell fraction in G_2/M lumped phase (Shi et al., 2005) and an increase in *Cdc2* (G_2/M regulator) expression (Swiderek and Al-Rubeai, 2007) under hypothermic conditions. It appeared that the increase in G_1/G_0 cell fraction in the cultures exposed to temperature fluctuations and the control culture was followed by the increases in ESA cell fraction. In the culture with temperature shift to 39°C and the control culture, the increases in G_1/G_0 cell fraction were seen during 24 to 48 hours (Figure 6.3.3-A), followed by

the increases in ESA cell fraction with the drop in G_1/G_0 cell fraction after 48 hours of the cultures (Figure 6.3.1-B). In the culture with temperature shift to 35 °C, the increase in ESA cell fraction was observed at 72 hours, after the increase in G_1/G_0 cell fraction (Figure 6.3.3-A). These observed results agree with the previous data showing that cells progress to apoptosis via the late G_1 cell cycle phase (Fussenegger and Bailey, 1998), suggesting the link between G_1/G_0 cell cycle arrest and the induction of apoptosis (El-Deiry et al., 1994).

The observed cyclin D1 expression for the G_1/G_0 lumped phase in the cultures exposed to temperature fluctuations did not significantly vary with each other (Figure 6.3.3-C). This observed result is not in agreement with the previous study demonstrating that hyperthermia caused an increase in cyclin D1 expression (Han et al., 2002). However, it supports the correlation between substrate availability and the cyclin D1 expression as previously suggested (García Münzer, 2014), given that the similar correlation between cyclin D1 expression and glutamate level was observed. At the beginning of the culture, the cycling D1 expression was at a low level due to the nutrient exhausted condition cells experienced in the sub-culture prior to the temperature shift experiment. As can be seen in Figure 6.3.3-C, the cyclin D1 increased with the abundant glutamate availability and decreased with the glutamate exhaustion. This suggests that the cyclin D1 expression in the cultures exposed to temperature fluctuations is predominantly affected by the nutrient availability, though there is no clear evidence of no impact of hyperthermia and hypothermia on the cyclin D1 expression.

6.3.2 Medium composition

Cell proliferation and apoptosis

There was a difference in the cell growth profile among the cultures. At the end of the cultures (24 hours), the culture with medium blends containing fractions of fresh medium (i.e. 50%FM and 100%FM) achieved significantly higher viable cell concentrations than the culture

using only conditioned medium (Figure 6.3.4-A). The highest viable cell density was achieved in the culture with 50%FM blend, however, it was not statistically significant different to the culture with 100%FM blend. There was also a difference in culture viability between the culture with 0%FM blend and the other cultures at 24 hours. All cultures started at the high cell viability (>94%) as shown in Figure 6.3.4-A. The culture with 0%FM blend showed around 10% drop in viability, while the other cultures maintained the initial viability. There was a significant increase in ESA cell fraction in the culture with 0%FM blend after 24 hours as compared to the ESA cell fraction at the time 0 hour (Figure 6.3.4-B). This was corresponding to the drop in viability. In addition, the culture with 0%FM blend demonstrated a significantly higher ESA cell fraction than those of the other two cultures (50%FM and 100%FM). There was no significant difference in ESA cell fraction between these two cultures. There was also no significant difference in Ki-67 positive cell fraction among all the cultures, although, after 6 hours, a slight drop in Ki-67 positive cell fraction was observed in the culture with 0%FM blend.

Metabolic activities and mAb production

Differences in glucose and lactate concentration profiles were observed among the cultures with different medium blends. More specifically, after 24 hours, there was a significant decrease in glucose concentration as well as a corresponding increase in lactate concentration in the cultures with medium blends containing fractions of fresh medium, compared to the beginning of the cultures (Figure 6.3.5-A). The increase in lactate concentration in the culture with 100%FM blend was found to be steeper than that in the 50%FM blend. This could be because the presence of lactate at the beginning of the culture inhibits the production of lactate, as previously reported (Cruz et al., 2000, Choi et al., 2007). There was no clear evidence of glucose consumption in the culture with 0%FM blend, given that there was no significant decrease in glucose concentration after 24 hours. In contrast, lactate concentration was found

to decrease after 24 hours of the 0%FM blend culture. It was previously reported that the metabolic shift to lactate consumption is subject to the level of limiting substrates, especially glucose and glutamine (Zhou et al., 1997b, Sanfeliu et al., 1997, Zhou et al., 2006) as well as conditions of slow cell growth and low glycolysis flux (Zagari et al., 2013, Li et al., 2012). Our result suggests that the observed lactate consumption could be induced by the absence of limiting substrate(s), most likely glutamate, as well as the high initial concentration of lactate resulting in the reduction in lactate production as well as cell growth (Cruz et al., 2000, Choi et al., 2007, Chen et al., 2009).

There was a sudden decrease in glutamate concentration in the cultures with medium blends containing fractions of fresh medium where glutamate was present, as can be seen in Figure 6.3.5-B. After 24 hours, the produced mAb concentration in the cultures with 100%FM was the lowest one as compared to the other cultures (Figure 6.3.5-C&D), despite achieving a high level of viable cell density. In addition, there was no significant difference in the profile of mAb titre between the culture with 50%FM and 0%FM blends. It could be inferred from these results that the increase in the mAb production is associated with spent medium, given that medium used in these two cultures contained a fraction of conditioned medium containing metabolites released from cells such as lactate and ammonia. Previous studies showed that elevated levels of lactate at the beginning of the culture enhanced the final secreted protein titre (Reuveny et al., 1986, Kromenaker and Srienc, 1994, Lao and Toth, 1997) through the metabolic shift that favours the process of the protein synthesis (Choi et al., 2007, Zhou et al., 2011). However, it cannot be firmly concluded that the observed increase in the mAb production was due to the presence of lactate, given that condition medium also consists of other known and unknown factors. In addition, cell lysis might partly contribute to the increase in the mAb titre, especially in the culture with 0%FM blend. Therefore, further experimentation is required to identify factors in conditioned medium that enhance the mAb production.

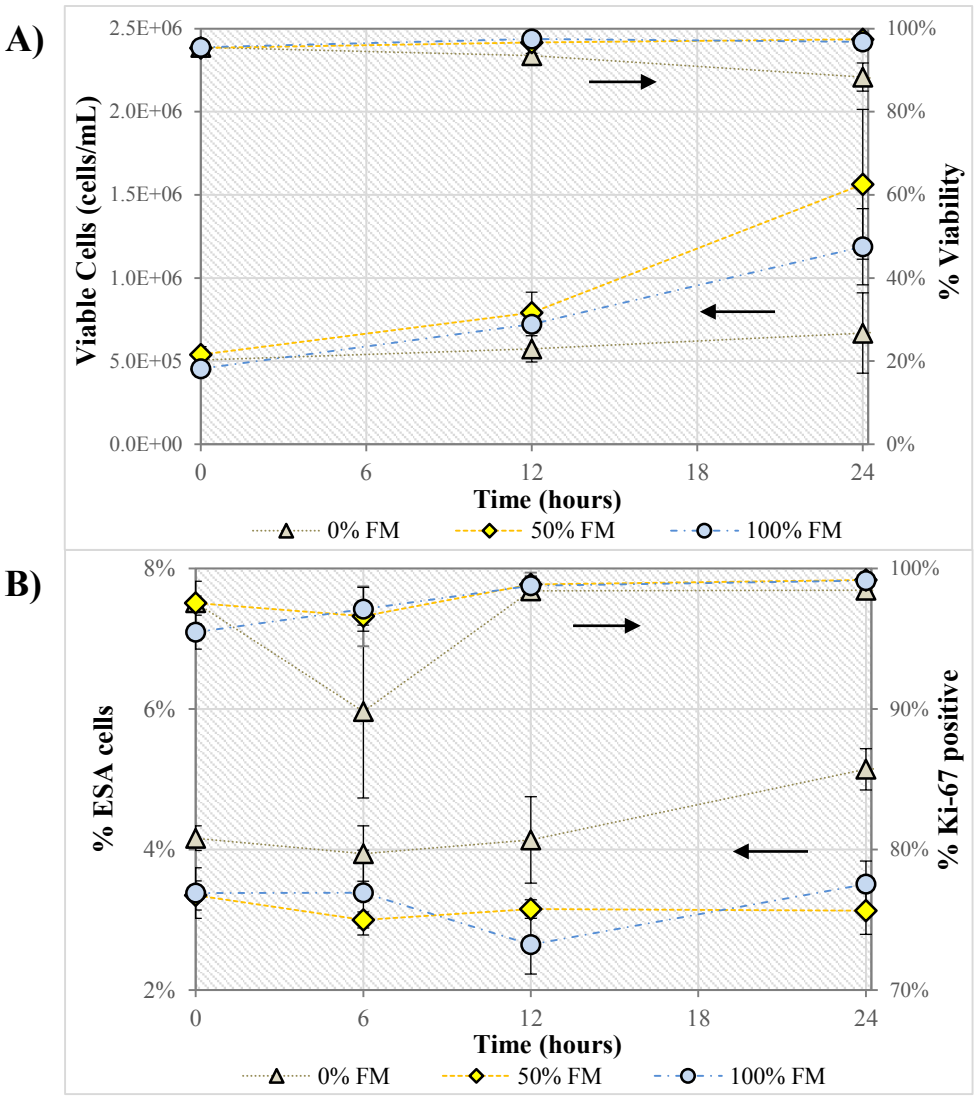


Figure 6.3.4 Cell proliferation profiles in the medium blend experiment: A) viable cell density and viability; and B) apoptotic & Ki-67 positive (proliferative) cell fraction. FM is fresh medium and the arrows indicate the corresponding axes to the data (n=3, error bar = SD).

Apoptosis-related gene expressions

The expression profiles of apoptosis-related genes varied among the cultures with difference medium compositions, as can be seen in Figure 6.3.6. After 24 hours, the cultures with medium containing fractions of fresh medium (50%FM and 100%FM) showed a significant decrease in the expression of *atf5* (Figure 6.3.6-A). However, the 100%FM culture showed a temporary increase in the *atf5* expression, significantly higher than that of the 50%FM

culture, before decreasing to its minimum at 24 hours. In the meantime, it appeared that there was a significant increase in the expression of *atf5* in the culture with 0%FM medium blend. The observed changes in *atf5* expression are in agreement with previous reports. The immediate increase in *atf5* expression (i.e. in the culture with only conditioned medium) could be a result of the limitation of amino acids (Watatani et al., 2007) as well as endoplasmic reticulum (ER) stress (Izumi et al., 2012). Nevertheless, the temporary rise (and later decrease) in the *atf5* expression in the culture with 100%FM medium blend might be due to the absence of unidentified factors present in spent medium, causing the culture to experience adaptation.

After 24 hours, the culture with 100%FM blend demonstrated a significant decrease in the *bcl-2* expression (Figure 6.3.6-B). A similar trend of *bcl-2* expression was also observed in the 50%FM culture, though the *bcl-2* expression started to decrease after 12 hours of the culture. The culture with 0%FM medium blend did not show a significant change in the *bcl-2* expression, though the *bcl-2* expression became the highest one among the cultures after 24 hours. Given that *bcl-2* is one of transcriptional targets of *atf5* (Dluzen et al., 2011), the observed high and maintained level of *bcl-2* expression could be induced by the increase in *atf5* expression level. However, the possibility that the *bcl-2* expression can be governed by the activation of other apoptosis-related factors, such as p53 (Miyashita et al., 1994) and nuclear factor kappa B (Catz and Johnson, 2001), cannot be completely excluded. The expression profile of cyclin-dependent kinase inhibitor gene *p21*, however, did not show a significant difference among the time points in all cultures (Figure 6.3.6-C), suggesting that immediate responses to the variation in medium contents is not growth arrest-associated. Nevertheless, there was a drop and an increase in *p21* expression at 12 hours and 6 hours in the culture with 100%FM and 0%FM medium blends, respectively.

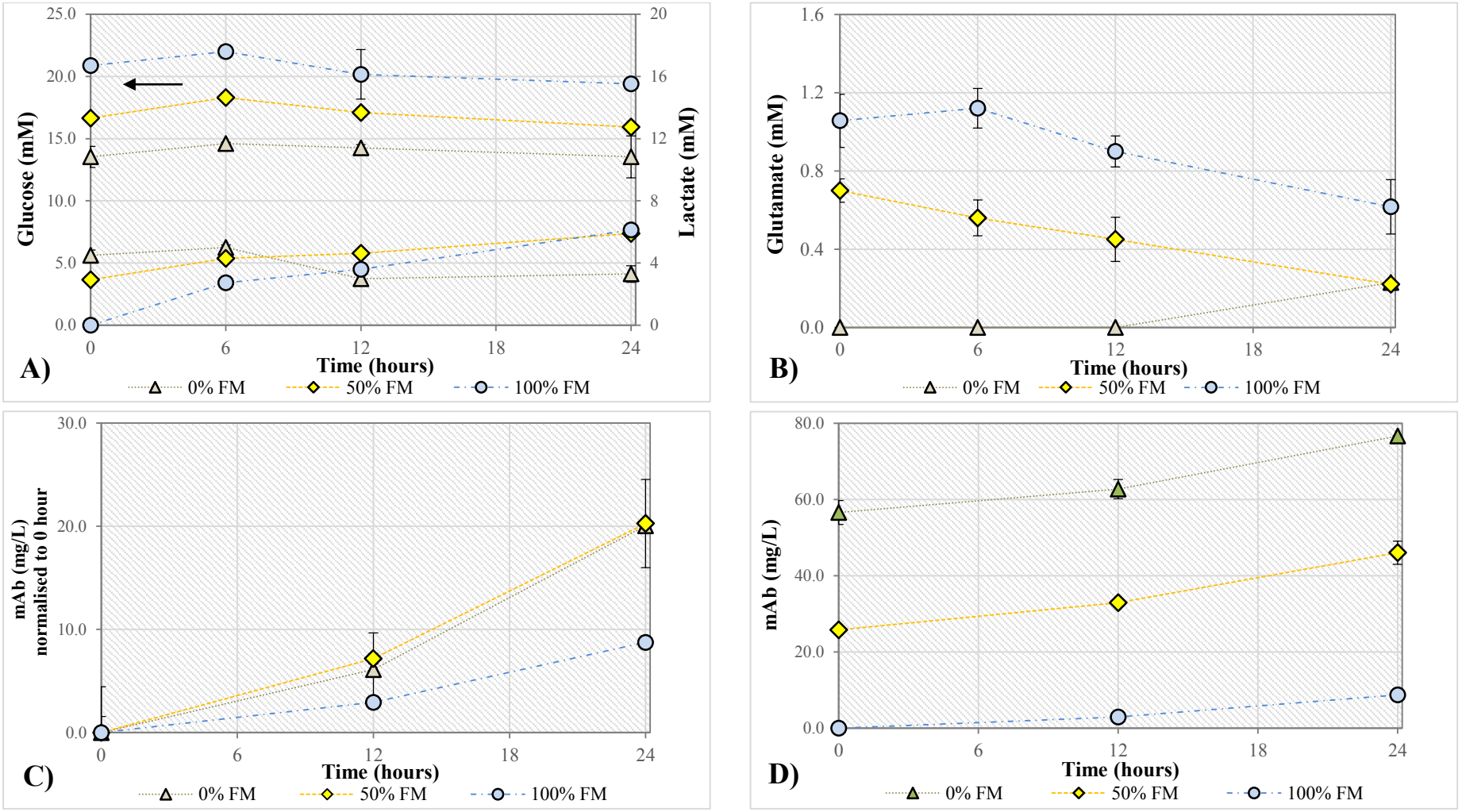


Figure 6.3.5 Nutrient, metabolite and mAb concentration profiles in the medium blend experiment: A) glucose and lactate; B) glutamate; C) normalised mAb; and D) measured mAb. The normalised mAb represents "measured mAb at a given time – measured mAb at t = 0 hour". FM is fresh medium and the arrows indicate the corresponding axes to the data (n=3, error bar = SD).

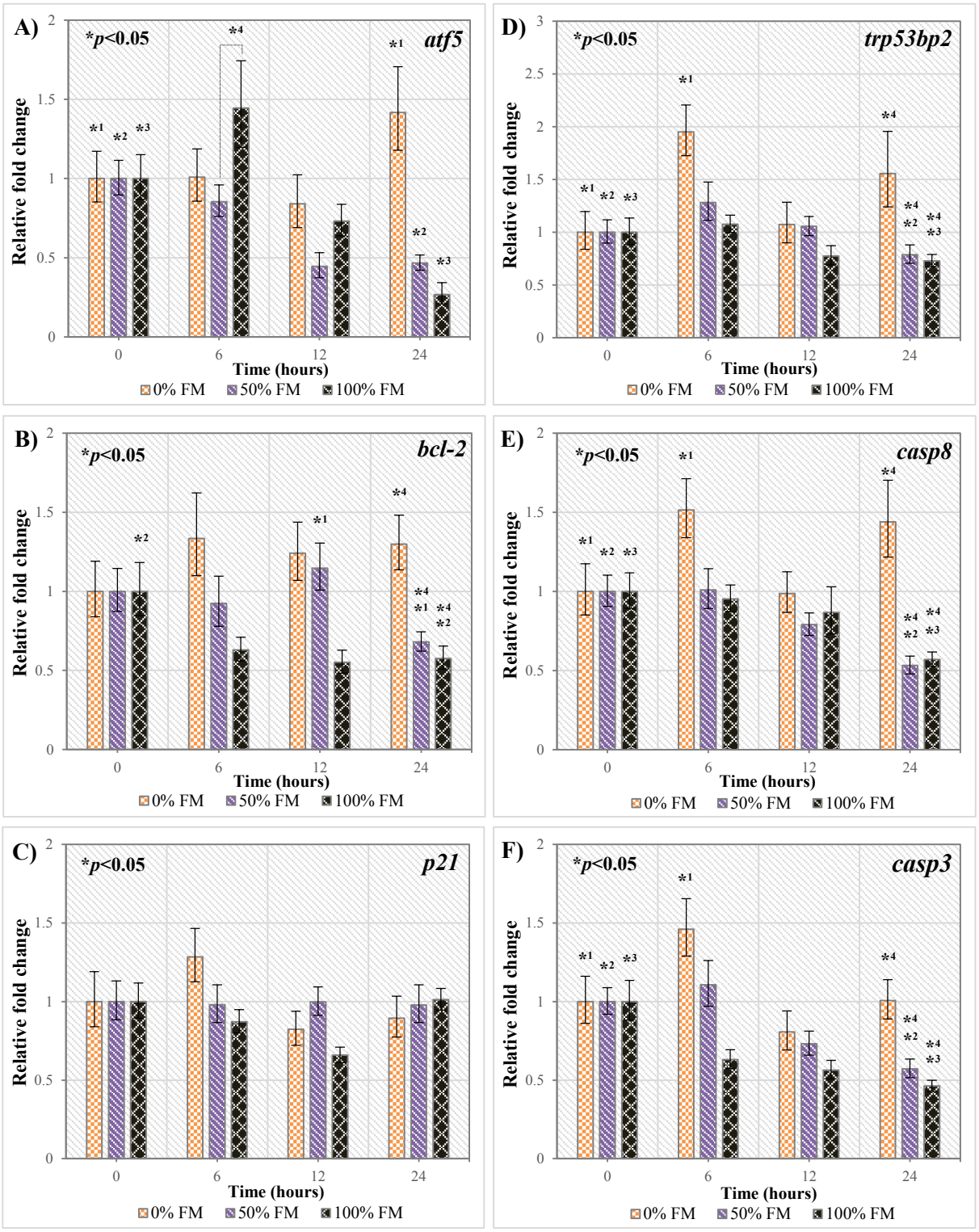


Figure 6.3.6 The expressions of genes related to apoptosis and cell cycle in in the medium blend experiment: A) *atf5*; B) *bcl-2*; C) *p21*; D) *trp53bp2*; E) *casp8*; and F) *casp3*. The relative fold change represents the gene expression normalised to 0 hr and the housekeeping gene, *gapdh* (see Appendix A). "*" indicates $p<0.05$ and the corresponding p-values are showed in Appendix B.3, (n=3, error bar = SD).

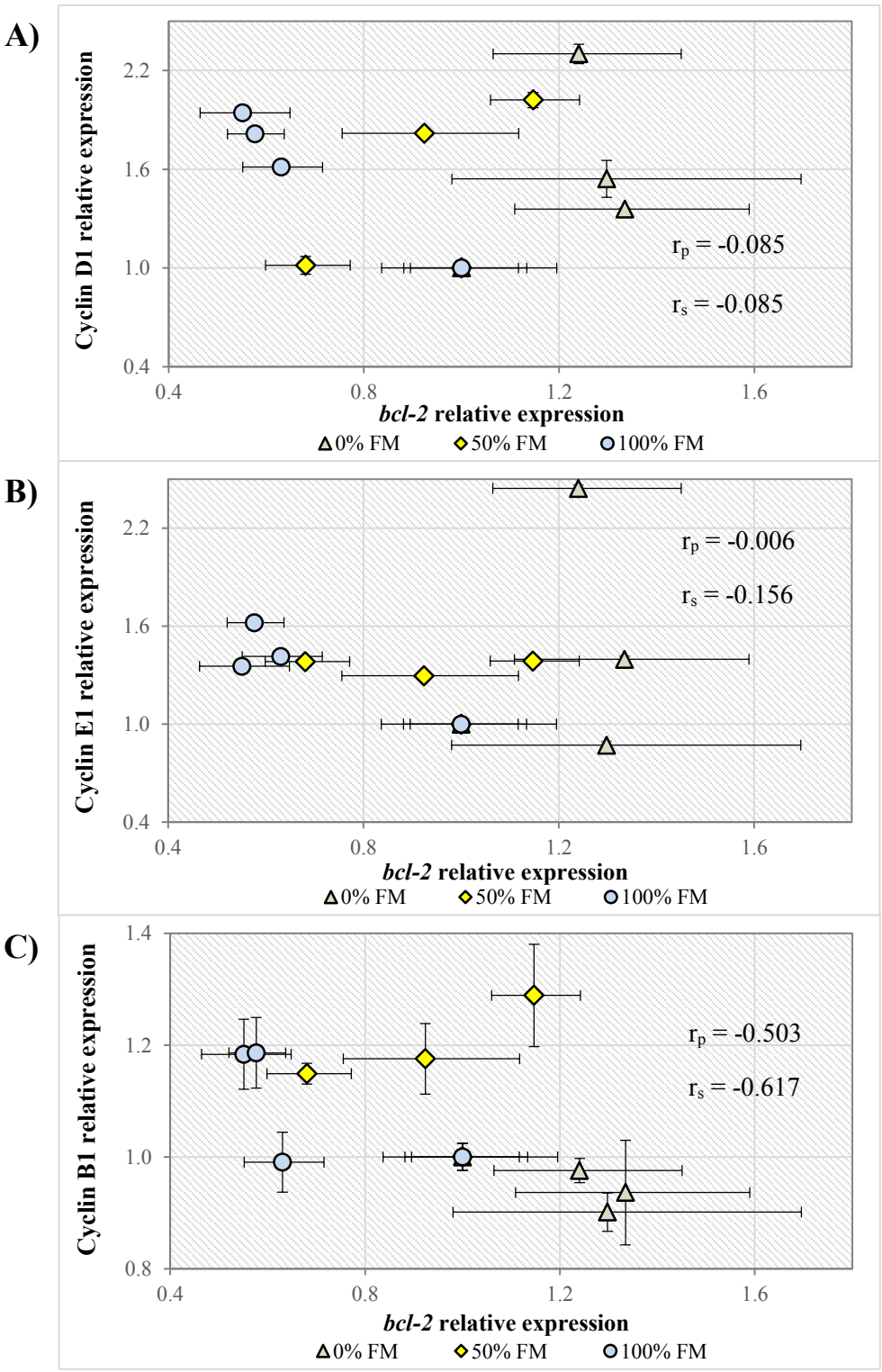


Figure 6.3.7 Scatter plots between *bcl-2* and cyclins in the medium shift experiment: A) *bcl-2* and cyclin D1 expressions; B) *bcl-2* and cyclin E1 expressions; and C) *bcl-2* and cyclin B1 expressions. FM is fresh medium and the dash dot lines represent the basal expressions. All relative expressions were normalised to time 0 hour (n=3, error bar = SD). r_p and r_s represent the Pearson and Spearman, respectively, correlation coefficients.

The expression profiles of *trp53bp2*, *casp8* and *casp3* showed a similar pattern among the cultures as can be seen in Figure 6.3.6-D, E & F, respectively. After 24 hours, there was a significant decrease in the expression of these genes in the culture with fractions of fresh medium. In contrast, in the 0%FM culture, there was a significant increase in the expression of these genes from the beginning to 6 hours of the culture. From 6 hours to 12 hours, the expression of these genes decreased, before rising and becoming the highest ones at 24 hours as compared to those in the other cultures. Given that these genes are apoptosis markers, these results agree with the observed profile of ESA cell fraction and viability. The results also suggest that the limitation of nutrients as well as the presence of metabolites introduce stresses to cells, given the observed increase in the expression of these apoptotic makers. The temporal drop in the expression of these apoptotic makers could be affected by a survival mechanism in response to the stresses as indicated by the elevated expression level of *atf5* and *bcl-2* (Dluzen et al., 2011, Izumi et al., 2012, Persengiev et al., 2002). However, given the increase in these apoptotic maker expressions after 12 hours, it can be inferred that the culture progresses toward apoptosis.

The link between cell cycle and apoptosis

The link between cell cycle progression and the onset of apoptosis could be established, given the previously reported roles of the apoptosis-related genes. p21 has been reported to regulate cell cycle progression (Gartel and Tyner, 2002b) through the suppression of cyclin-dependent kinases (CDKs) as well as cyclin-CDK complexes, which are required for the cell cycle transition from G_1 to S phase (Fussenegger and Bailey, 1998, Cazzalini et al., 2010) as well as from G_2 to M phase (Niculescu et al., 1998). The pro-apoptotic gene, *trp53bp2* encodes 53BP2 (p53-binding protein 2), which specifically interacts with p53 to trigger apoptosis via the intrinsic pathway (Samuels-Lev et al., 2001, Kobayashi et al., 2005). It has been reported that p53 controls the G_2/M cell cycle checkpoint through p21 activation-associated mechanisms

(Bunz et al., 1998, Agarwal et al., 1995), one of which involves the deactivation of cyclin B complexes (Innocente et al., 1999). Furthermore, a correlation between the expression of Bcl-2 (protein) and cyclin D1 has been reported (Lin et al., 2001a, Hong et al., 2008), given that Bcl-2 was found to arrest cell proliferation in response to apoptotic stimuli (Simpson et al., 1999b, Janumyan et al., 2003). The overexpression of *bcl-2* was also found to cause G_2/M cell cycle arrest. It was suggested that its role involves the deactivation of cyclin-CDK complexes for the G_2/M checkpoint (Crescenzi et al., 2002).

The prolife of cyclins (D1, E1 and B1) was measured as a part of the collaboration work with D.G. García Münzer (PhD candidate). Cyclin D1 and E1 have regulatory roles in the cell cycle progression through G_1-phase (Coqueret, 2002, Mazumder et al., 2004), while cyclin B1 facilitates the cell cycle progression though G_2-phase (Kawamoto et al., 1997). Therefore, the plots between the relative expression of apoptosis-related genes and cyclins can reveal any possible correlations among them. As previously suggested, a moderate positive correlation can be indicated by the correlation coefficient being between 0.4 to 0.59 (hence, -0.4 to -0.59 for a moderate negative correlation) while the correlation coefficient being between 0.0 to 0.19 indicates a very week positive correlation (and between 0 to -0.19 for a negative one) (Evans, 1996). As shown in Figure 6.3.7-C, a moderate negative correlation between the *bcl-2* expression and the cyclin B1 expression could be drawn given the r_p and r_s. However, the suggested correlation might be only a monotonic negative relationship rather than a linear one given the *p*-value equal to 0.096 obtained by the Pearson method while the *p*-value equal to 0.031 obtained by the Spearman method. The correlation found here is in agreement with the previous studies (Crescenzi et al., 2002, Furukawa et al., 2000). Although Bcl-2 were found to cause the inhibition of G_1 to S phase transition (Mazel et al., 1996), there were very week correlations observed from the plots between the expression of *bcl-2* and cyclin D1, and between the expression of *bcl-2* and E1 as can be seen from the r_p and r_s (Figure 6.3.7-A&B).

The plots between the relative expression of *p21* and all cyclins demonstrates a correlation where the expression of *p21* is inversely proportional to the expression of cyclins (Appendix B1). However, the cyclin D1 and E1 expressions in the culture with 0%FM blend at 6 hours do not follow this correlation. Given that there was the corresponding drop in %Ki-67 cell fraction (and thus cell proliferation arrest), it can be inferred that the *p21* expression partly underlie the cell proliferation arrest (Bi et al., 2004) and the observed imbalances of cyclin D1 and E1 expression. The relationship between the relative expression of *trp53bp2* and all cyclins could not be clearly drown from the plots (Appendix B1). This might be because *trp53bp2* is the factor that is predominantly responsible for the induction of apoptosis as a result of p53 activation (Samuels-Lev et al., 2001). In addition, the association of p53 with the control of cell cycle progresses through intricate pathways; for example, through the transactivation of p21 (Li et al., 1994) and the interaction with Bcl-2 (Naumovski and Cleary, 1996), making it difficult to draw any direct relations between them.

The herein proposed relations between the expression of relevant genes and cyclins are subject to the experimental conditions presented in this study. In order to validate the proposed relations, further experimentation is needed. In addition, the cultures in this study employed medium containing a fraction of serum which consists of a number of unknown factors, therefore complicating the analysis. However, the observed results point out the importance of the link between cell cycle and apoptosis.

6.3.3 Nutrient additions

Cell proliferation and apoptosis

There was a significant difference in the profiles of viable cell density in the cultures with different nutrient feeding schemes as can be seen in Figure 6.3.8-A. The maximum viable cell concentrations in the fed-batch cultures were higher than that in the batch culture. The F1

fed-batch culture achieved the maximum viable cell density of 16×10^5 cells/mL at 96 hours, while the F2 fed-batch culture achieved the maximum viable cell density of around 14×10^5 cells/mL at around 72 hours. After 24 hours, it appeared that the F2 fed-batch culture showed a faster growth rate (0.72 day^{-1}), as compared to the other cultures (around 0.35 day^{-1} for the other cultures). The decrease in viable cell concentration in the F1 fed-batch culture occurred after 96 hours, while the F2 fed-batch and the batch cultures experienced the decrease in viable cell concentration at earlier time points: 72 hours and 54 hours, respectively. All the cultures showed a similar pattern of culture viability, though that in the F2 fed-batch culture started to decrease before the other cultures (Figure 6.3.8-B). In contrast, the F1 fed-batch culture demonstrated the highest viability as compared to the other cultures at the same time point. The observed profile of ESA cell fraction was corresponding to the viability profile (Figure 6.3.8-C). The %ESA cells in the F2 fed-batch culture started to increase after 36 hours, earlier than the increase in %ESA cells observed in the other cultures. The %ESA cells in the F1 fed-batch culture and the batch culture started to rise at around 70 hours; however, the %ESA cells in the F1 fed-batch culture remained the lowest one due to the gradual increase in %ESA cells. The observed results suggest that the induction of apoptosis might be delayed in the F1 fed-batch culture, which is in agreement with the previous study (DiStefano et al., 1996, Zhou et al., 1997a). However, the F2 fed-batch culture did not follow the reported data, given the higher %ESA and the earlier drop in culture viability.

Metabolic activities and mAb production

There was a difference in the concentration profiles of glucose and lactate among the cultures. For the first 60 hours, all cultures showed a similar decrease in glucose concentration (Figure 6.3.9-A). During this period, the specific glucose utilisation rates were comparable among the fed-batch cultures (2.2 and 2.3 $\mu mol.10^{-6}cell.day^{-1}$ in the F1 and F2 cultures, respectively); however, they were lower than the batch culture (3.2 $\mu mol.10^{-6}cell.day^{-1}$). It

appeared that during 72 and 84 hours (after the 1st glucose feeding) the F2 fed-batch culture showed a higher glucose consumption (2.2 $\mu mol.10^{-6}cell.day^{-1}$) than the F1 culture (0.5 $\mu mol.10^{-6}cell.day^{-1}$), resulting in the lower glucose concentration observed at 84 hours. After 84 hours, the glucose concentration profiles of the fed-batch cultures were comparable. The batch culture after 72 hours showed the lowest concentration of glucose as a result of no glucose addition. An increase in lactate concentration was observed in all cultures, which was corresponding to the decrease in glucose concentration (Figure 6.3.9-B). However, the observed specific lactate production rates in the fed-batch cultures were significantly lower than that in the batch culture (1.3, 1.9, and 5.7 $\mu mol.10^{-6}cell.day^{-1}$ for the F1, F2 and batch cultures, respectively). While the lactate production continued until the final stages of the batch culture, the F1 and F2 fed-batch cultures showed decreases in lactate concentration after 60 hours and 84 hours, respectively. In addition, a similarity between the concentration profile of produced lactate and consumed serine was observed in all cultures (Figure 6.3.9-C).

After 36 hours, glutamate and aspartate were exhausted in the F2 culture, earlier than the other cultures, as shown in Figure 6.3.9-D&E. The observed specific glutamate consumption rate during the first 36 hours in the F2 culture was the highest one among the cultures (0.45, 0.75, and 0.6 $\mu mol.10^{-6}cell.day^{-1}$ for the F1, F2 and batch cultures, respectively), nevertheless the observed specific aspartate consumption rate was comparable to that in the batch culture. Up to 72 hours, It appeared that there was no significant difference in the specific consumption rates of asparagine (0.16 and 0.17 $\mu mol.10^{-6}cell.day^{-1}$) as well as arginine (0.25 and 0.25 $\mu mol.10^{-6}cell.day^{-1}$) among the fed-batch cultures (F1 and F2, respectively), though they were higher than those in the batch culture (0.13 and 0.18 $\mu mol.10^{-6}cell.day^{-1}$ for asparagine and arginine specific consumption rates, respectively). This indicates that nutrient additions (glucose and glutamate) could enhance the consumption rates of limiting amino acids. There was a difference in the profile of alanine concentration among the cultures, as can be

seen in Figure 6.3.9-F. The F1 fed-batch culture demonstrated a continuous increase in alanine concentration until the end of the culture. The level of alanine in the F2 culture also continuously increased, though it stayed unchanged between 60 and 84 hours of the culture. The concentration profile of glutamine, however, did not vary among the cultures (Appendix B1).

The concentration profiles of other amino acids, mostly essential ones, showed a similar pattern among the cultures. These amino acids include lysine, valine, isoleucine, tryptophan, leucine, cystine, phenylalanine, threonine, and methionine. Their profiles shared a common pattern as similar to the concentration profile of leucine shown in Figure 6.3.9-G. The fed-batch cultures showed steeper decreases in these amino acid levels than the batch, causing these amino acid levels becoming lower than those in the batch culture during final stages of the cultures. In addition, some of these amino acids, such as leucine and methionine, became exhausted especially in the F1 culture after 120 hours (Figure 6.3.9-G). The fed-batch cultures showed higher production of mAb, as compared to the batch culture (Figure 6.3.9-H). The F1 and F2 cultures seemed to achieve the similar final mAb titre at 120 hour. However, given the viable cell concentration profiles, the specific productivity of the F2 culture (13.8 $\mu g.10^{-6}cell.day^{-1}$) was higher than that of the F1 culture (11.6 $\mu g.10^{-6}cell.day^{-1}$), despite similar to that of the batch culture (13.7 $\mu g.10^{-6}cell.day^{-1}$). In addition, the mAb titre during the exponential and stationary phases in the F2 culture was the highest compared to the other cultures.

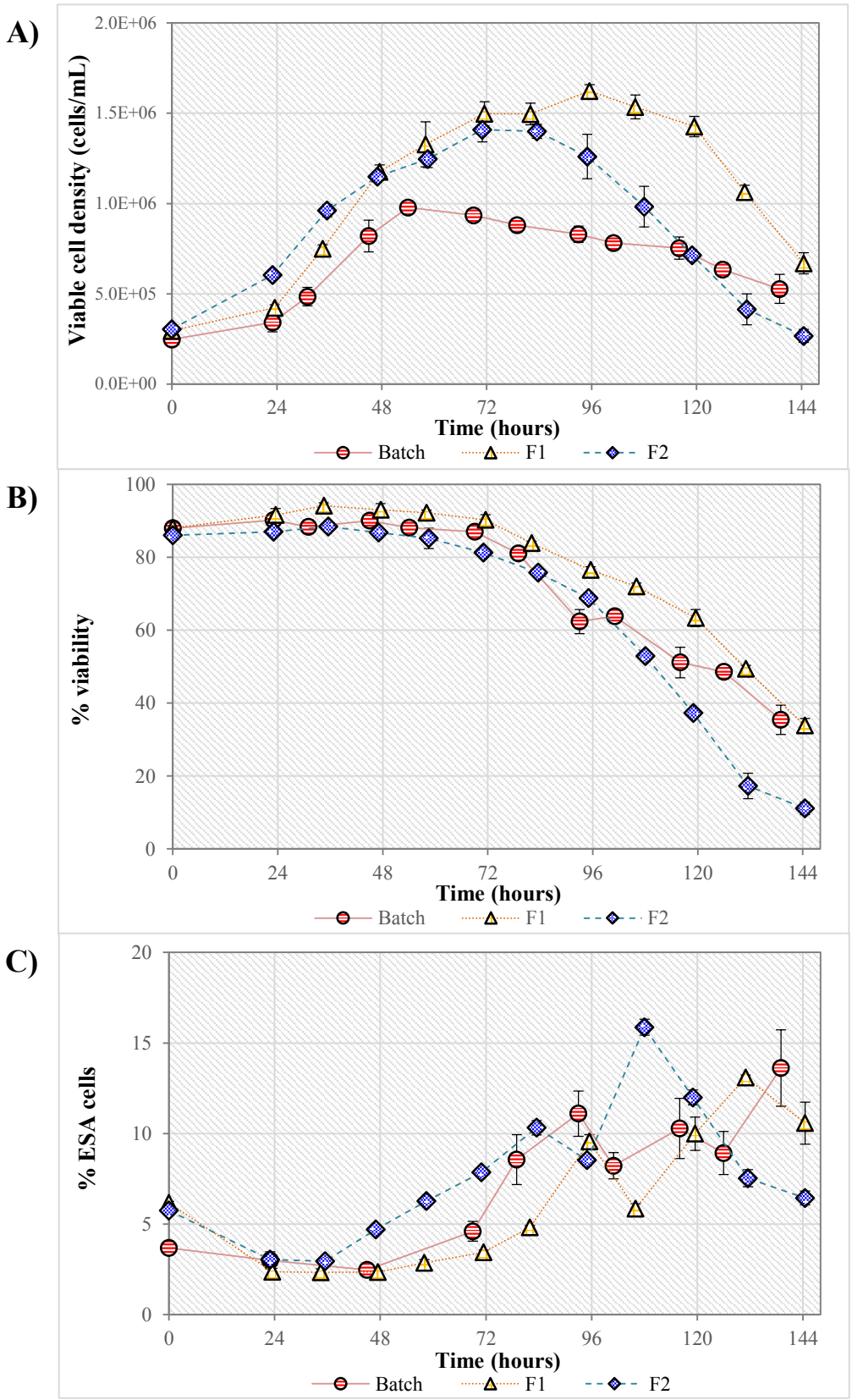


Figure 6.3.8 Cell growth and ESA cell profiles in the batch & fed-batch cultures: A) viable cell concentration; B) viability; and C) %ESA cells. F1 and F2 represent the feeding strategies as described in section 6.2.3. (n=3, error bar = SD).

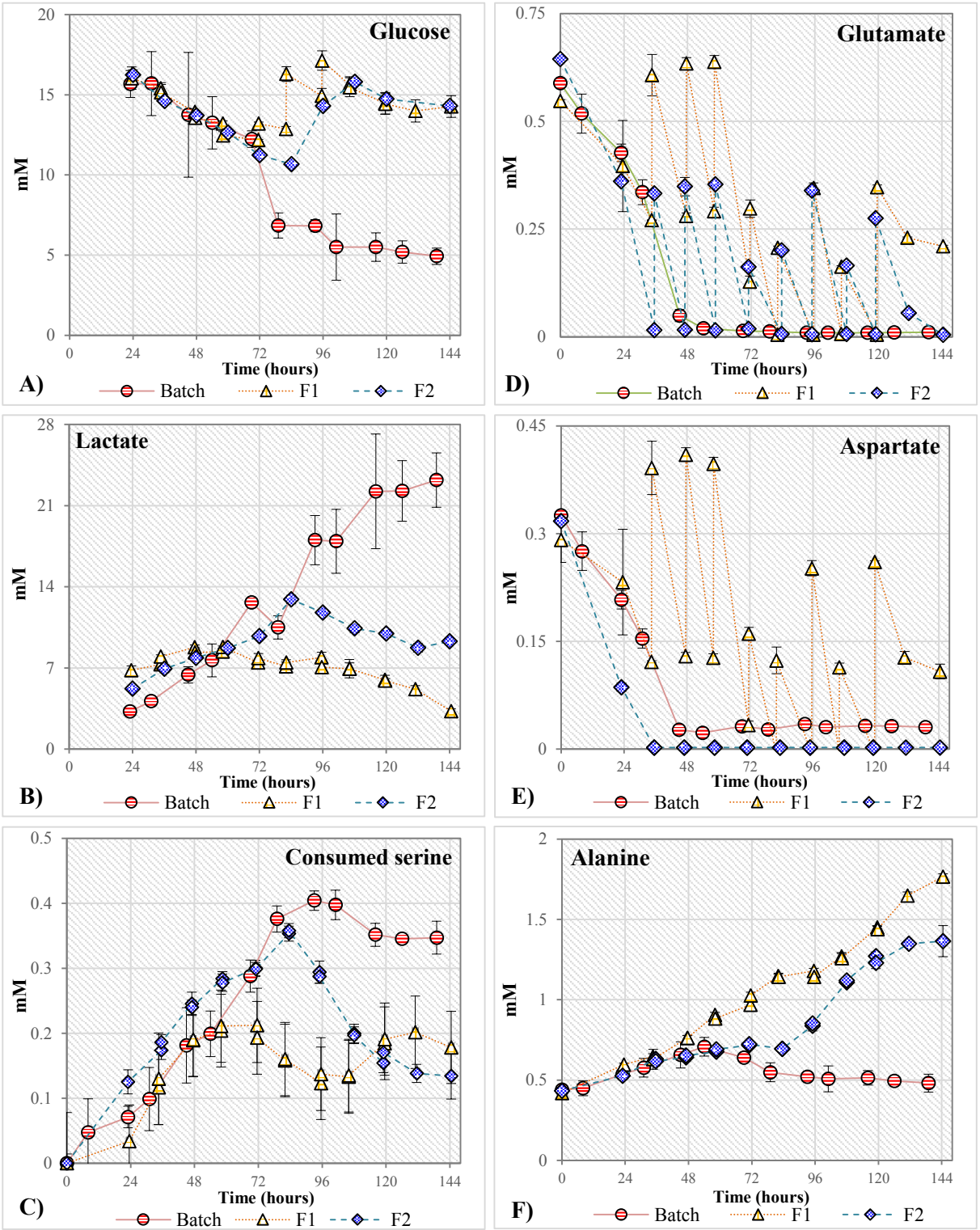


Figure 6.3.9 The concentration profiles of A) glucose; B) lactate; C) consumed serine; D) glutamate; E) aspartate; F) alanine; G) leucine; and H) mAb in the batch & fed-batch cultures. F1 and F2 represent the feeding strategies as described in section 6.2.3. (n=3, error bar = SD).

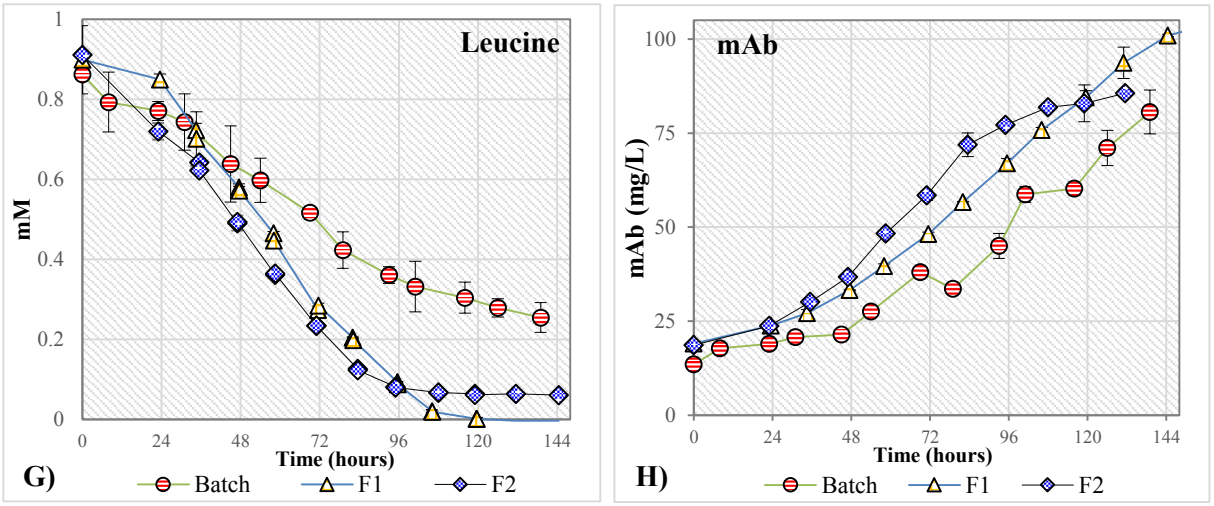


Figure 6.3.9 (continued) The concentration profiles of A) glucose; B) lactate; C) consumed serine; D) glutamate; E) aspartate; F) alanine; G) leucine; and H) mAb in the batch & fed-batch cultures. F1 and F2 represent the feeding strategies as described in section 6.2.3. (n=3, error bar = SD).

As previously discussed in Chapter 5, the mTOR-associated pathway plays regulatory roles in cell growth, metabolism as well as protein synthesis and it is subject to nutrient levels, especially amino acids (i.e. leucine) (Dodd and Tee, 2012). The observed higher viable cell concentrations, enhanced amino acid metabolism as well as increased mAb production in the fed-batch cultures (compared to the batch culture) could be partly contributed by the activation of the mTOR pathway. This is in agreement with the previous report suggesting that the activation of mTORC1 due to feeding of nutrients (glucose and amino acids) to the culture of CHO cells might underlie the observed increased growth, metabolism and recombinant protein synthesis (Dadehbeigi and Dickson, 2015).

The observed decreases in glucose concentration and the corresponding increases in lactate concentration suggests lactate production phase in the cultures (Zagari et al., 2013, Young, 2013). In addition, the observed decreases in lactate concentration in the fed-batch cultures support previous studies showing lactate consumption phase in the fed-batch cultures

(Zhou et al., 1997a, Ma et al., 2009). It was suggested that the metabolic shift to lactate consumption was triggered by nutrient depletion (Zhou et al., 1997a), cessation of exponential growth as well as conditions of low glycolysis flux (Zagari et al., 2013, Li et al., 2012). However, this does not always hold true, given that there was no evidence of lactate consumption in the batch culture which experienced nutrient deprivation and cessation of cell growth. The observed lactate consumption at a different time point between the F1 and F2 fed-batch cultures suggests that lactate consumption might be subject to the level of metabolites as well as nutrients, which is in agreement with the previous report demonstrating that the metabolic shift to lactate consumption depends on medium composition (Zagari et al., 2013). This could provide the condition that favours lactate consumption, such as a low glycolysis flux as indicated by the observed lower specific glucose consumption in the fed-batch cultures. The observed similarity between the concentration profiles of consumed serine and lactate suggests the association of serine in lactate metabolism. Given that serine can be converted to pyruvate (Duarte et al., 2014), as well as intermediates in TCA cycle (Hoshino, 1987), it may play a critical role in supporting the metabolic shift to lactate consumption.

The observed higher specific glutamate utilisation rate, higher growth rate, higher ESA cell fraction as well as earlier drop in culture viability in the F2 culture follow the previous study suggesting that the higher substrate utilisation rate can cause the culture to earlier reach the point of commitment to apoptosis as a result of substrate exhaustion (Pavlostathis et al., 2006). Given that the metabolic shift to alanine consumption is subject to glutamate exhaustion as discussed in Chapter 5, the difference in alanine concentration profile between the F1 and the F2 cultures confirms that the F2 culture experienced glutamate deprivation as a result of its fast growth rate nature, though glutamate was supplied during the culture. The similar final mAb titre between the fed-batch cultures could link to the limitation of amino acids required for the mAb synthesis, given a number of amino acids became exhausted at final stages of the

cultures (Carrillo-Cocom et al., 2014). However, the possibility that the increase in mAb titre from the lysed or broken cells due to cell death cannot be completely excluded.

Cell cycle profile

The cell cycle profile varied among the cultures, as shown in Figure 6.3.10. There was a steeper increase in relative change in G_1/G_0 phase cell fraction in the F2 fed-batch culture during 36 to 48 hours as compared to the other cultures (Figure 6.3.10-A). The relative change in G_1/G_0 phase cell fraction in the F2 culture remained the highest one between 48 to 120 hours, while the F1 and batch cultures demonstrated a similar level of relative change in G_1/G_0 phase cell fraction until 96 hours. After 96 hours, there was an increase in cell fraction in G_1/G_0 phase in the F2 and batch cultures. In the meantime, the cell fraction in G_1/G_0 phase in the F1 culture did not significantly change. The relative change in S phase cell fraction in the F1 culture was significantly higher than the other cultures after 24 hours (Figure 6.3.10-B). Between 54 and 108 hours, there were increases in relative change in G_2/M phase cell fraction in all cultures (Figure 6.3.10-C). The steepest increase was in the batch culture, while the increase in the F1 culture started after 72 hours and the F2 fed-batch culture showed a gradual one.

Given the relation between cyclin D expression and substrate availability in the temperature shift study, the observed high relative change in G_1/G_0 phase cell fraction in the F2 culture could be linked to the glutamate limitation. The observed highest level of relative change in G_1/G_0 phase cell fraction in the F2 culture also suggests that the F2 culture experienced stronger metabolic stresses related to nutrient availability than other cultures. The gene expression results (see later) support this suggestion. It appeared that the feeding scheme F1 enables more cells to stay in S phase of cell cycle. However, given the observed lowest mAb productivity in the F1 culture, it can be inferred that the mAb synthesis is not S phase dependent (Banik et al., 1996), which are not in agreement with previous reports (Chong et al., 2008, Al-

Rubeai and Emery, 1990). On the other hand, the mAb synthesis might be dependent on other cell cycle phases (Robinson and Memmert, 1991, Kubbies and Stockinger, 1990, Turner et al., 1985, Buell and Fahey, 1969), given the highest mAb titre along the culture progression and the highest mAb productivity in the F2 and batch cultures, respectively.

Apoptosis-related gene expressions

The F2 fed-batch culture showed the steepest increase in the expression of *atf5* since the 24 hours of the culture (Figure 6.3.11-A). Unlike that of the F2 culture, the *atf5* expression significantly dropped between 0 and 24 hours before starting to rise to its peak at 72 hours in the batch culture. The *atf5* expression in the F1 culture, however, showed a significant change after 72 hours of the culture and reached its peak at 120 hours. The observed up-regulated level of *atf5* expression indicates amino acid deprivation as well as ER associated metabolic stresses (Watatani et al., 2007, Izumi et al., 2012) as previously discussed. It can be inferred that the batch and F2 cultures experienced the metabolic stresses earlier than the other culture (F1) given the significant increase in *atf5* expression from 24 hours. The F1 culture might suffer from the stresses from 72 hours as indicated by the increase in *atf5* expression. All cultures demonstrated a similar trend of *bcl-2* and *p21* expression as can be seen in Figure 6.3.11-B&C. The *bcl-2* expression significantly decreased from the beginning of the fed-batch cultures, before rising after 72 hours and 96 hours of the F1 and the F2 cultures, respectively. The steepest one was observed in the F2 culture reaching the *bcl-2* expression peak at 96 hours, while the F1 culture showed a gradual increase in *bcl-2* expression until the final stages of the culture. The batch culture, however, showed a significant increase in *bcl-2* expression after 72 hours without a significant decrease in *bcl-2* expression during the first 72 hours of the culture. After 96 hours, there was a significant drop in *bcl-2* expression in the F2 culture. The F2 and batch cultures showed a significant increase in the *p21* expression after 72 hours of the cultures, while the increase in the *p21* expression took place in the F1 culture after 96 hours (Figure 6.3.11-C).

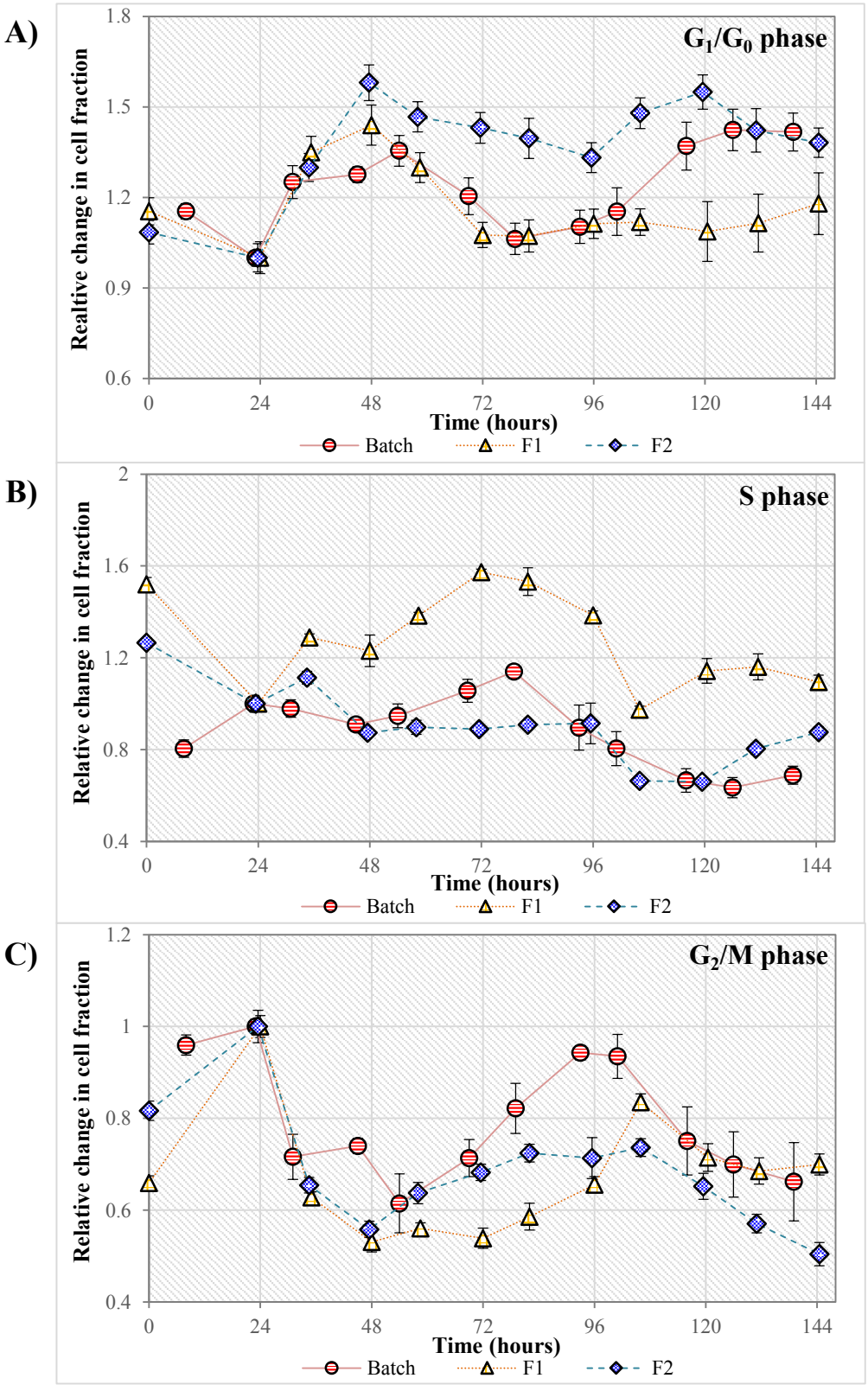


Figure 6.3.10 Cell cycle profiles in in the batch & fed-batch cultures: A) G_1/G_0 lumped; B) S; and C) G_2/M lumped phases. The relative change in cell fraction was the cell fractions that were normalised to the time 24 hours of cultures. F1 and F2 represent the feeding strategies as described in section 6.2.3. (n=3, error bar = SD).

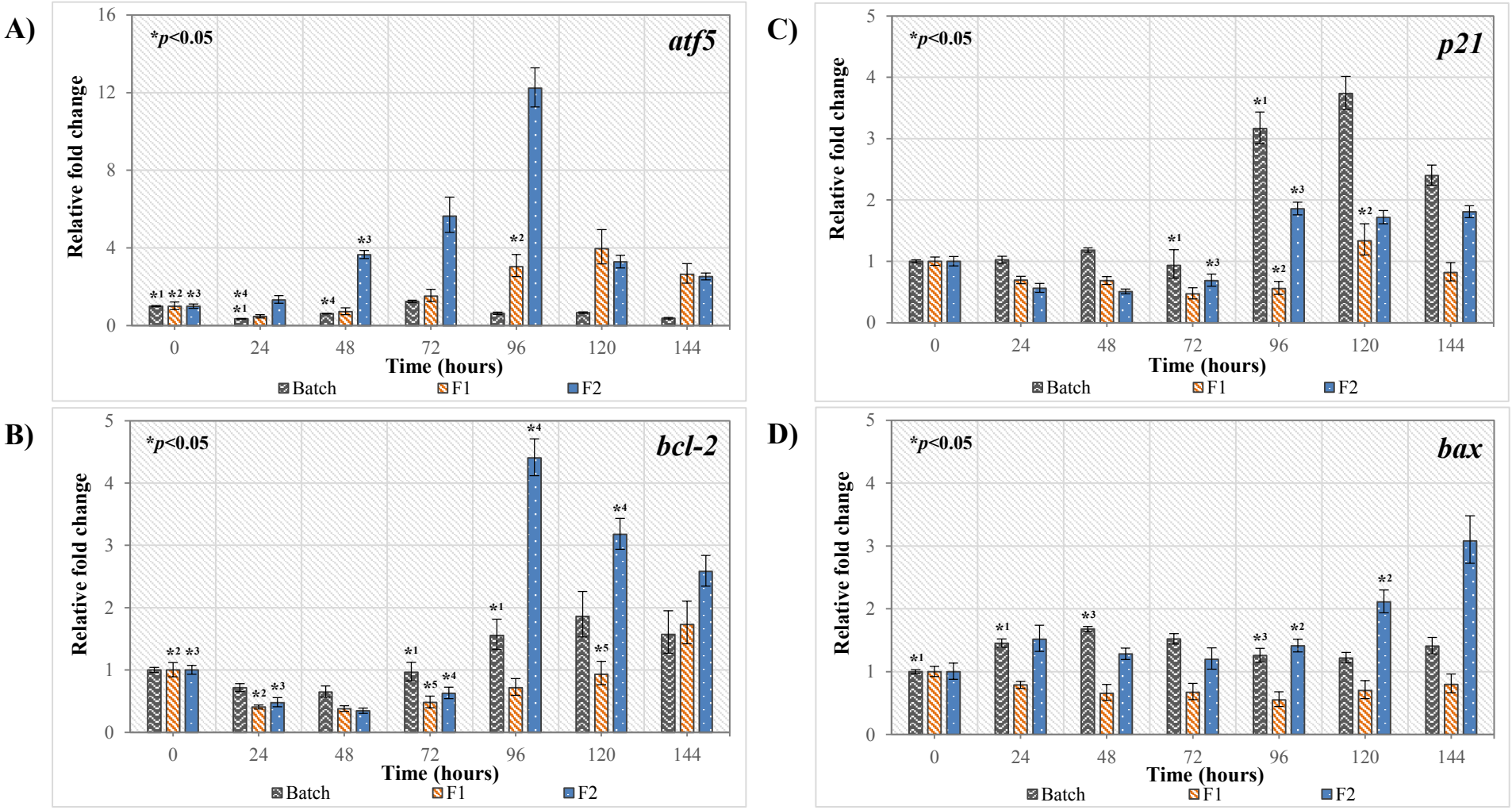


Figure 6.3.11 The expression profiles of apoptosis-associated genes in the batch & fed-batch cultures: A) *atf5*; B) *bcl-2*; C) *p21*; D) *bax*; E) *trp53bp2*; F) *casp8*; and G) *casp3*. The gene expressions were normalised to time 0 hour and a housekeeping gene (*gapdh*). F1 and F2 represent the feeding strategies as described in section 6.2.3. "*" indicates p<0.05 and the corresponding *p*-values are showed in Appendix B.3, (n=3, error bar = SD).

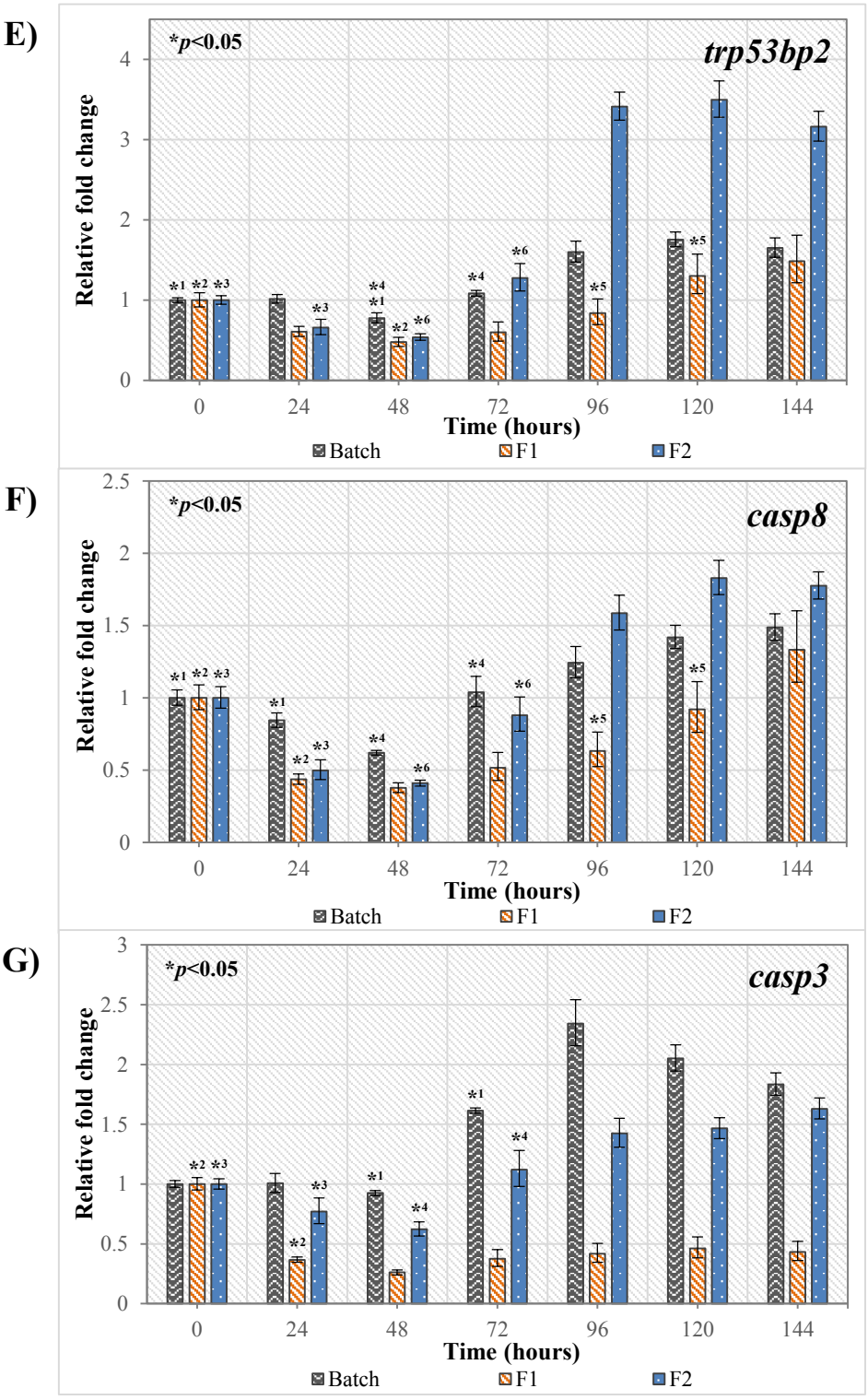


Figure 6.3.11 (continued) The expression profiles of apoptosis-associated genes in the batch & fed-batch cultures: A) *atf5*; B) *bcl-2*; C) *p21*; D) *bax*; E) *trp53bp2*; F) *casp8*; and G) *casp3*. The gene expressions were normalised to time 0 hour and a housekeeping gene (*gapdh*). F1 and F2 represent the feeding strategies as described in section 6.2.3. "*" indicates $p<0.05$ and the corresponding *p*-values are showed in Appendix B.3, (n=3, error bar = SD).

The expression profiles of pro-apoptotic genes, including *bax*, *trp53bp2*, *casp8* and *casp3*, in the F1 culture did vary from the other cultures (Figure 6.3.11-D, E, F&G). While the batch culture showed both increase and decrease in the expression of *bax* as discussed in Chapter 5, the fed-batch cultures showed no significant change in the *bax* expression during the first 72 hours (Figure 6.3.11-D). After 96 hours, there was a significant increase in the *bax* expression in the F2 culture. Contrary to the F2 and batch cultures, the F1 culture maintained insignificant change in *bax* expression until the end of the culture. Generally, the expression of *trp53bp2*, *casp8* and *casp3* did significantly decrease by the 48 hours of the batch and fed-batch cultures, except that there was no significant change in the expression of *casp3* between 0 and 48 hours in the batch culture. The expression of *trp53bp2* started to rise after 48 hours in the batch and F2 cultures (Figure 6.3.11-E). Like that of *trp53bp2*, the increase in *casp8* (Figure 6.3.11-F) and *casp3* (Figure 6.3.11-G) expressions in the batch and F2 cultures also occurred after 48 hours of the cultures. The F2 culture showed a steeper increase in *trp53bp2* and *casp8* expressions, while the batch culture showed a steeper increase in *casp3* expression. Contrary to the F2 and batch cultures, a significant increase in *trp53bp2* and *casp8* expressions in the F1 culture occurred after 96 hours of the culture (Figure 6.3.11-E&F). In addition, unlike that of the batch and F2 cultures, there was no significant change in *caps3* expression after 24 hours of the F1 culture (Figure 6.3.11-G).

The observed expression profiles of *bcl-2* and *p21* during the exponential phase could indicate a proliferative state, as discussed in Chapter 5. The impact of metabolic stresses, as indicated by the increase in *atf5* expression, became dominant after the proliferative state. As discussed in Chapter 5, the elevated levels of *bcl-2* and *p21* as well as the increase in relative change in G_1/G_0 phase cell fraction during the death phase suggest the occurrence of cell cycle arrest at G_1/G_0 phase as an anti-apoptotic mechanism in response to the metabolic stresses (Moore et al., 1997, Sanfeliu and Stephanopoulos, 1999). The ultimate cell fates, between

apoptosis and cell cycle arrest, are governed by the level of metabolic stresses (Mason and Rathmell, 2011, Kracikova et al., 2013). However, it can be inferred from the observed results of cell cycle analysis and gene expressions that cell cycle arrest at G_1/G_0 phase might not occur in the F1 culture.

Both batch and F2 cultures appeared to undergo apoptosis via both intrinsic and extrinsic pathways given the elevated expression of *caps8*, *trp53bp2* and *casp3* as well as the profiles of %ESA cells and culture viability (Stennicke et al., 1998, Kobayashi et al., 2005). Nevertheless, cell death in the F1 culture appeared to involve apoptosis in a different manner. The observed delay in the increase in %ESA, the drop in culture viability and the elevated pro-apoptotic gene expressions levels in the F1 culture indicate that the F1 feeding strategy helps delay the onset of apoptosis, though the degree of ESA at the final stages of the F1 culture is comparable to that in the other cultures. Contrary to the high level of %ESA cells and the drop in viability, the *casp3* expression, believed to be the final executor of apoptosis pathways (Hengartner, 2000, Majors et al., 2007), was down-regulated until the final stages of the F1 culture. This suggests the possibility that, in addition to apoptosis, there was apoptosis-like cell death occurring in the culture. This type of apoptosis is independent of caspase-3 activation while it can induce morphological (especially, PS externalisation) as well as physiological (DNA fragmentation) apoptotic characteristic-like changes (Cummings et al., 2004, Meng et al., 2000). Therefore, it can be inferred that the F1 feeding scheme might enable the culture to experience other cellular stresses that favour caspase-3 independent apoptosis over the caspase-mediated apoptosis (Carmody and Cotter, 2000).

It is worth mentioning that the effect of the feeding schemes (F1 and F2) on cell growth, metabolism and apoptosis cannot be directly compared, given that there was a difference in the profile of growth rates as well as glutamate consumption. The variation from a culture to

another culture can contribute to the nature of biological heterogeneity and errors. For example, serum, one of medium composition, has a number of known and unknown growth factors as well as proteins. Its content can be varied from batch to batch, and the slight variation in a growth factor level can result in a different profile of cell growth as well as metabolism (Vander Heiden et al., 2001). Further experimentation is required in order to confirm those hypotheses and to be able to make a fair comparison between the nutrient feeding strategies.

6.4 Conclusions

This chapter aims to investigate the effect of culturing conditions, including temperature, medium composition and addition of nutrients including glucose and amino acids, on apoptosis in the culture of GS-NS0 cells. The novelty of this chapter is the systematic investigation of apoptosis in order to establish apoptosis-related responses to the variation in culturing conditions. The temperature shift experiment demonstrated that the shift to hypothermia caused a slower growth, a reduction in metabolic activities, a delay in the induction of apoptosis, as well as no significant change in mAb productivity as compared to the control culture. The opposite effect was observed in the culture with the shift to hyperthermia, except that there was no significant increase in cell growth.

The medium shift experiment revealed the effect of medium composition on the induction of apoptosis. The culture with 0% FM showed a decrease in cell growth as well as viability in a period of 24 hours. A higher degree of apoptosis was also seen at the transcriptional level as well as morphological changes (% ESA). In addition, the metabolic shift to lactate consumption was observed, which could be attributed by glutamate deprivation as well as the elevated initial lactate concentration. The cultures with medium containing fractions of FM showed a similar cell growth, viability as well as apoptosis-related gene

expression. The expression of apoptosis-related genes was correlated with the cyclin expressions, supporting the previous established link between apoptosis and cell cycle arrest.

The fed-batch experiment suggests the effect of nutrient addition on apoptosis. Compared to the batch culture, the fed-batch cultures achieved a higher cell density as well as final mAb titre. However, there was no significant improvement in mAb productivity. The metabolic shift to lactate consumption was observed in the fed-batch cultures, though glutamate was sufficiently available, suggesting that there might be other causes of the metabolic shift than what was hypothesised based on the medium shift experiment. Given the observed %ESA cells as well as pro-apoptotic gene expressions, the F1 feeding scheme appeared to delay apoptosis while the F2 culture showed no delay in the apoptosis onset. The apparent apoptosis in the F1 culture might be associated with the apoptosis pathway dependently from the activation of caspase-3. The observed high cell growth as well as fast glutamate consumption could be the reason why apoptosis in the F2 culture was not delayed.

Chapter 7

An Experimentally-Validated Mathematical Model of Apoptosis

7.1 Background

Chapter 7 presents an experimentally-validated mathematical model capturing the induction of apoptosis in the culture of GS-NS0 cells. This includes mathematical expressions of cell growth and metabolism with their links to the transcriptional regulation of apoptosis. GSA was applied to the constructed mathematical model to reveal relationships between model output and parameters, and evaluate the significance of model parameters. Based on the mathematical model, an optimal culture condition where higher final titre mAb is achieved can be computationally simulated, and thus trial-and-error experiments can be avoided.

7.1.1 Introduction

Given that cellular processes are essentially interlinked, it is not trivial to construct understanding of their dynamic behaviour in response to environmental changes. Mathematical modelling has been utilised to cope with such the complexity in biological systems. This approach involves formulating a system of mathematical equations that relates culture conditions, such as temperature and nutrient levels, with cellular responses, including cell growth, nutrient utilisation, protein synthesis and cell death. Thus, dynamic behaviour of cellular systems as respect to culture conditions can be quantitatively predicted, providing valuable information for process control, development and optimisation. Furthermore, the number of possible trial and error experiments can be reduced.

Mathematical models can be classified according to biological information included into the mathematical models. Segregated models take into account heterogeneity occurring in the cell cultures while unsegregated ones assume properties in the cultures to be homogenous. In addition, mathematical models can be structured or unstructured depending on how much mechanistic understanding, both extracellularly and intracellularly, is included into the

constructed models. Given that cellular activities are highly non-linear, segregated and structured models tend to be mathematically complicated. Thus, it might not be possible to experimentally validate these models, and to achieve an insight into the model dynamic behaviour. Unsegregated and unstructured models are mathematically friendly and can be experimentally validated, however they lack mechanistic representation of cellular activities, making it difficult to gain detailed insight into cellular responses. Hybrid models are ones that combine detailed models (such as structured models) with simple models (such as unstructured models) so that a good balance between the mathematical complexity of resulting model and mechanistic biological information included into the model can be achieved. The hybrid approach, therefore, enables to mathematically model complex systems, like cellular ones, while the resulting models remain computationally inexpensive.

A large number of mathematical models has been proposed with an attempt to capture dynamic behaviour of the mammalian cell cultures for production of bio-pharmaceuticals. Monod kinetics and its variants, which are classified as unstructured models, are widely used to describe cell growth (Eq. 2.8.1). These equations link cell growth (viable cell concentrations) with nutrient availability (extracellular nutrient levels), including glucose and amino acids (Pörtner and Schäfer, 1996). Cell metabolism; including nutrient utilisation, metabolite production and desired protein synthesis, is usually mathematically described using a linear equation, such as the constant maintenance energy model (Eq. 2.8.2), which assumes that the metabolic activities depends on both growth and non-growth associated activities. In addition, there are structured models for cell growth and metabolism, where mechanistic understating of cell growth and metabolism is incorporated into the models. Population balance models, for example, were constructed to describe cell growth in association with cell cycle progression (Liu et al., 2007, Fadda et al., 2012). In addition, the mechanistic assembly of mAbs was

mathematically modelled to capture kinetics of synthesis of mAbs (Bibila and Flickinger, 1991).

Although there are a large number of mathematical models constructed for mammalian cell cultures; cell death, which is also one of the most important cellular events in the cultures, has been superficially described in these proposed models (Pörtner and Schäfer, 1996). The mathematical equations describing cell death were based on empirical correlations which lack mechanistic representation as well as links between cell death and other cellular processes. Given that production and quality of bio-therapeutic proteins depend greatly on the occurrence of cell death (Yoon et al., 2003b, Majid et al., 2007, Tey et al., 2000a) representing the significance of it in the cultures, it is necessary to include detailed mechanism of cell death into mathematical models.

Over the last two decades, apoptosis has emerged as the major cause of viability loss in the mammalian cell cultures for production of bio-pharmaceuticals (Goswami et al., 1999, DiStefano et al., 1996, Browne and Al-Rubeai, 2011a, Singh et al., 1994). Given that apoptosis is an orderly physiological process (Hengartner, 2000), its established mechanistic understanding can be expressed as mathematical equations and can be linked to other relevant cellular processes including cell growth and metabolism. There are a couple of existing mathematical models for the cultures of mammalian cells that capture apoptosis. However, these models did not fully take into account dynamic behaviour in response to changes in culture conditions, links to other cellular activities as well as mechanistic regulation of apoptosis (Naderi et al., 2014, Meshram et al., 2012). In addition, mathematical models for apoptosis should incorporate the transcriptional regulation of apoptosis, which is a crucial part in apoptosis pathways and provides links to other cellular processes (Dudgeon et al., 2009, Yu and Zhang, 2005).

As the discussion above attests, mathematical description of apoptosis in the mammalian cell culture models needs to be further improved. Apoptosis has to be mathematically expressed in a way that represents its kinetics, relevant mechanisms as well as dynamic behaviour as respect to apoptotic stimuli. However, the increased degree of model complexity as a result of detailed mechanisms of apoptosis being extensively included has to be taken into consideration. Model analysis is therefore required for the mathematical model development framework to assure model identifiability as well as avoid unnecessary model complexity (Kent et al., 2013, Kiparissides et al., 2009, Ho et al., 2006, Saltelli et al., 2000).

7.1.2 Objectives

The aim of this chapter is to develop a first-principles mathematical model for the GS-NS0 cell culture that captures apoptosis as well as its links to metabolic stresses as suggested in Chapter 5 and Chapter 6. The following are herein scientific objectives:

- Propose a framework that would allow formulating mathematical model description and evaluating the resultant model structure.
- Construct mathematical expressions that would allow capturing kinetics of cellular activities, including cell growth, metabolism as well as apoptosis, and their interrelationships with each other, based on the previously observed experimental data.
- Perform model analysis that would allow evaluating the validation of the constructed mathematical model, and identifying any further model modifications.

7.2 Methodology

7.2.1 The proposed model development framework

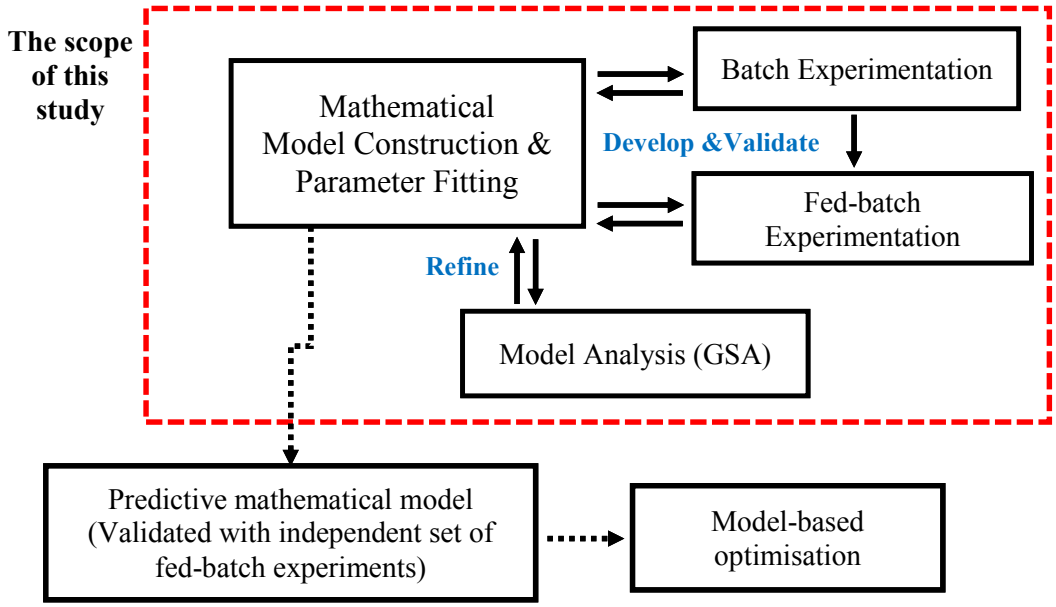


Figure 7.2.1 The proposed framework for the development of a mathematical model for the culture of GS-NS0 cells in this study.

A framework for the mathematical model development in this study was proposed as shown in Figure 7.2.1. The framework aims to integrate the observed phenomena in the GS-NS0 cell cultures, as previously discussed in Chapter 5 and Chapter 6, as well as the computational tool for model analysis into the process of mathematical model development. The model was initially constructed based on the observed results from the batch culture. In the meantime, the validation of the constructed model was evaluated using the experimental data from batch and fed-batch cultures. This step involved modifying and refining the model structure, as well as fitting parameter values so that the model could reproduce the experimental data. The constructed model with a set of preliminary parameter values (not optimised), that showed a reasonable fit for the experimental data, was analysed using global sensitivity analysis (GSA). The result from GSA determined whether the constructed model was required

to be further refined in order to remove unnecessary model complexity as well as to improve model identifiability. The refined model can be further validated with independent sets of experimental data to increase model predictability. The ultimate goal of the constructed model is to be applied with a model-based optimisation algorithm which can generate optimal culturing conditions where mAb titre can be maximised.

Previous mathematical models for the mammalian cell cultures were adopted as a basis for developing mathematical description in this study. However, given the observed phenomena which are specific to the cultures of GS-NS0 cells, they need to be improved, refined, and modified in order to be able to capture the observed experimental data. Parameter values in the constructed model were initially set as given from literature and then manually changed if needed. For example, literature parameters might be adjusted in case the structure of mathematical expressions was changed or modified. If there is no published parameter value; especially in mathematical expressions that has not been introduced before, these parameter values were preliminarily assigned based on the values of other parameters that are biologically relevant and their estimates can be assigned from literature.

7.2.2 Model construction

The mathematical model was herein formulated along the line of the hybrid approach (Ho et al., 2006, Kontoravdi et al., 2010) in order to be able to incorporate the observed phenomena in the GS-NS0 cultures (batch and fed-batch) while keeping the resulting model computationally traceable. The constructed model was the combination of three sub-models with different model types. The first sub-model was an unstructured model capturing cell proliferation with links to cell death and metabolism. The second one was also an unstructured model capturing cellular metabolism, including glucose and amino acid utilisation, metabolite production and mAb synthesis. The final one is a structured model represents transcriptional

and translational regulation of apoptosis with its links to growth and death kinetics as well as metabolic activities. All sub-models were constructed based on the general assumption that the cultures are homogenous, and thus there is no temporal and spatial variation in, for example, metabolite concentration and temperature throughout the culture systems.

Cell growth sub-model

The overall material balance over the cultures (both batch and fed-batch) provides a simple correlation among the volume of the culture, inlet and outlet streams shown as follows:

Eq. 7.2.1 Overall mass balance

$$\frac{dV}{dt} = F_{in} - F_{out}$$

Where, V is the total volume of the system (Litre, L), F_{in} is the total flowrate of feeding streams (L/hr) and F_{out} is the total flowrate of outlet streams (L/hr).

Given that there were up to 5 substrates added into the cultures (the fed-batch cultures), the following equation describes the summation of all feeding streams.

Eq. 7.2.2 The total flowrate of feeding streams

$$F_{in} = F_{in,\,glc} + F_{in,\,glu} + F_{in,\,asp} + F_{in,\,asn} + F_{in,\,arg}$$

Where, $F_{in,\,glc}$, $F_{in,\,glu}$, $F_{in,\,asp}$, $F_{in,\,asn}$ and $F_{in,\,arg}$ are the flowrates of fed glucose, glutamate, aspartate, asparagine and arginine, respectively (L/hr).

The following equations involve mass balances on cell populations. As can be seen in Figure 7.2.2, the flow of cell population started at the viable cell population where they were either proliferating, or dying via two major routes: apoptosis (Hengartner, 2000, Browne and Al-Rubeai, 2011a), and other cell death pathways such as necrosis and autophagy (Hwang and Lee, 2008, Singh et al., 1994). Apoptotic cells entered early stage apoptosis (ESA) before

eventually becoming late stage apoptotic (LSA) cells or dead cells. Cell death via other pathways than apoptosis, however, are characterised as a sub-set of the dead cells, given that they shared the same morphological markers, such as loss of plasma membrane integrity (Ormerod, 2000). Therefore, there is no net outflow or inflow between them (Figure 7.2.2).

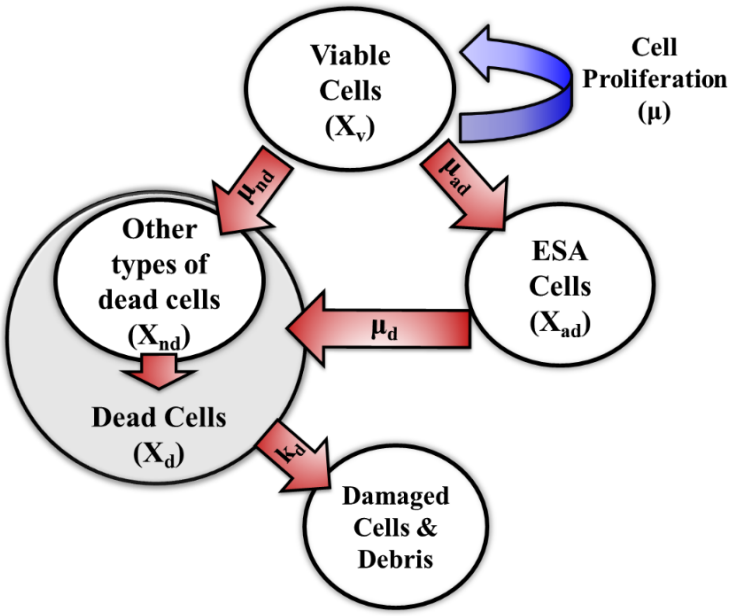


Figure 7.2.2 The flowchart of cell population kinetics in the culture of GS-NS0 cells. It was herein postulated based on the experimental observation and used as a basis for the construction of cell growth mathematical sub-model.

Eq. 7.2.3 Viable cell balance

$$\frac{d(VX_v)}{dt} = \mu VX_v - \mu_{ad} VX_v - \mu_{nd} VX_v$$

Eq. 7.2.4 Early stage apoptotic cell balance

$$\frac{d(VX_{ad})}{dt} = \mu_{ad} VX_v - \mu_d VX_{ad}$$

Eq. 7.2.5 Cell death via other pathways than apoptosis

$$\frac{d(VX_{nd})}{dt} = \mu_{nd} VX_v$$

Eq. 7.2.6 Dead cell balance

$$\frac{d(VX_d)}{dt} = \mu_{nd} VX_v + \mu_d VX_{ad} - k_d VX_d$$

Where, X_v is the viable cell concentration (cells/mL), X_{ad} is the ESA cell concentration (cells/mL), X_{nd} is the concentration of dead cells from other pathways than apoptosis (cells/mL), X_d represents dead cell concentration (cells/mL), μ_{ad} is the specific rate of early stage apoptotic death (hr^{-1}) and μ_{nd} is the specific rate of cell death via other pathways than apoptosis (hr^{-1}), and k_d is the degradation rate (hr^{-1}).

The total number of cells can be formulated as follows.

Eq. 7.2.7 The total number of cells

$$X_t = X_v + X_{ad} + X_d$$

Where, X_t is the total cell concentration (cells/mL).

Herein, based on the experimental data in Chapter 5&6, the specific growth rate was assumed to be dependent on the extracellular levels of limiting nutrients: glucose and glutamate. Given the observed viable cell concentration with respect to glutamate deprivation as well as the glucose uptake rate (Chapter 5), the specific growth rate was formulated to be the summation of the glucose-associated and the glutamate-associated cell growth rates. The mathematical expression for the glucose-associated specific growth rate was constructed based on the adapted version of Monod kinetics, which took into account the limiting effect of viable cell concentration (Contois, 1959). Hill equation was adopted for the glutamate-associated specific growth rate (Moser, 1958, Hill, 1913).

Eq. 7.2.8 The specific growth rate

$$\mu = \mu_{max,\,glc} \frac{Glc}{Glc + K_{glc} \cdot 10^{-6} \cdot X_V} + \mu_{max,\,glu} \frac{Glu^2}{Glu^2 + K_{glu}{}^2}$$

Where, Glc and Glu are the extracellular concentration of glucose and glutamate, respectively (mM); $\mu_{max,\,glc}$ and $\mu_{max,\,glu}$ are the glucose and glutamate-associated maximum specific growth

rates, respectively (hr^{-1}); K_{glc} and K_{glu} are glucose and glutamate limiting constants for the cell growth, respectively (mM).

As described in Chapter 4, phosphatidyl serine (PS) externalisation, one of morphological changes during apoptosis, was used to determine ESA cell fractions. This ESA marker was found to be one of the downstream targets of caspase activation and occurs as early as the caspase activation (van Engeland et al., 1998, Riccardi and Nicoletti, 2006). Given that caspase-3 is the final executor of the apoptotic pathways (Hengartner, 2000, Majors et al., 2007) and the onset of apoptosis is subject to its activation, the death rate of ESA was assumed to be dependent on the concentration of caspase-3 molecule. The following equation describes the ESA death rate using Monod-like kinetics, which is herein developed along the line of Monod-like kinetics.

Eq. 7.2.9 The specific death rate of ESA

$$\mu_{ad} = \mu_{max,\,ad} \frac{Casp3}{Casp3 + K_{casp3}}$$

Where, $\mu_{max,\,ad}$ is the maximum specific rate of early stage apoptotic death rate (hr^{-1}), Casp3 stands for the concentration of active caspase-3 molecule (mM), and K_{casp3} is the Monod constant for ESA (mM).

It was previously reported that the activation of caspases triggered both apoptotic physiological as well as morphological events, such as the lysis of plasma membrane and DNA degradation, during LSA (Widlak, 2000, Collins et al., 1997). The specific rate of LSA was, therefore, assumed to be proportional to that of ESA. It was also assumed to be dependent on ESA and LSA cell fractions given that apoptotic signals could be transmitted from apoptotic cells to surrounding cells (Jäger and Fearnhead, 2012, Pérez-Garijo et al., 2013). The

mathematical expression for the LSA specific death rate was herein constructed based on Monod-type expression.

Eq. 7.2.10 The specific death rate of LSA

$$\mu_d = \mu_{max,\,d} \frac{\mu_{ad} X_{ad}}{X_{ad} + X_d}$$

Where, $\mu_{max,\,d}$ is the maximum specific rate of LSA or dead cells (hr^{-1}).

Cell death via other pathways than apoptosis was not well investigated in this study. It can potentially be necrosis (Singh et al., 1994, Mercille and Massie, 1994a) or autophagy (Hwang and Lee, 2008, Glick et al., 2010, Jardon et al., 2012) as previously reported. Herein, the specific rate of cell death via other pathways than apoptosis was therefore assumed to be dependent on the concentration of lactate since it is only a factor that can be linked to the cause of cell death via other pathways than apoptosis (Mercille and Massie, 1994a). This rate was herein constructed based on Monod-like kinetics as described in the following equation.

Eq. 7.2.11 The specific death rate for cell death via other pathways than apoptosis

$$\mu_{nd} = \mu_{max,\,nd} \frac{Lac}{Lac + K_{Lac}}$$

Where, $\mu_{max,\,nd}$ is the maximum specific rate of cell death via other pathways than apoptosis (hr^{-1}), Lac is the extracellular lactate concentration (mM), and K_{lac} is the Monod constant for lactate limitation effect (mM).

The cell growth sub-model consists of 14 variables in total (7 of which are differential variables) and 10 parameters.

The cell metabolism sub-model

Dynamic changes in extracellular concentrations of nutrients (glucose and amino acids) as well as metabolites (lactate) were mathematically expressed based on mass balances as well as metabolic reactions among these molecules. The consumption/production rates were represented using the constant maintenance energy equation (Eq. 2.8.2), despite being modified to take into account the proposed interrelationships among substrates and metabolites, as shown in Figure 7.2.3. The interrelationships were described using Monod-like terms (limiting and inhibiting as shown in Eq. 2.8.1) which were adapted along the lines of models that were demonstrated in previous studies (Jang and Barford, 2000, Ho et al., 2006, Kontoravdi et al., 2007, Kiparissides et al., 2010).

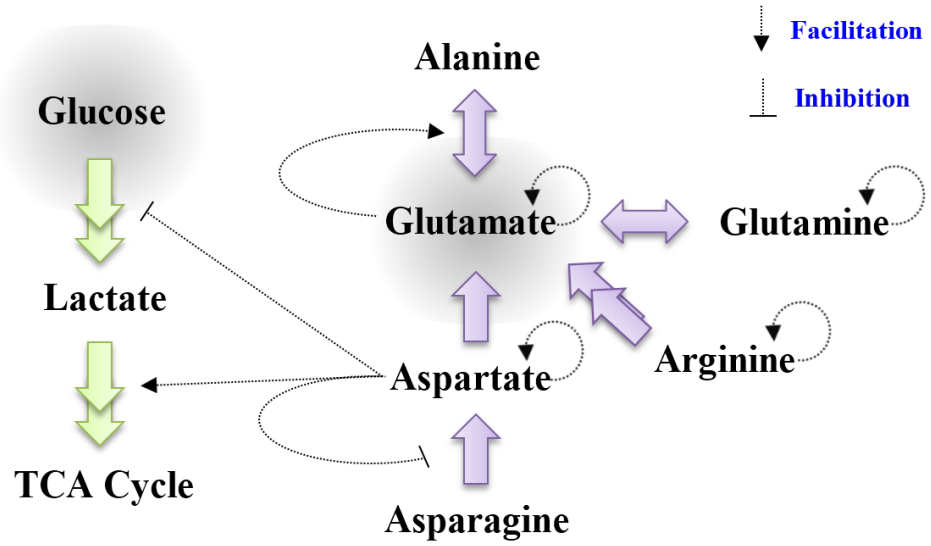


Figure 7.2.3 The network of enzymatic reactions among nutrients, metabolites and amino acids. This network was herein postulated based on the experimental observation and used as a basis for the construction of the unstructured sub-model for glucose and amino acid metabolism in the GS-NS0 cultures.

The following equations describe dynamic changes in extracellular glucose and lactate concentrations. The equations were constructed based on the proposed network of glucose and

lactate metabolism (Figure 7.2.3), where the production of lactate was assumed to be dependent of the flux of glucose utilisation, and to simultaneously coincide with lactate consumption. The lactate metabolism was also assumed to be governed by the aspartate concentration given the observed phenomena as shown in Chapter 5&6 (a rapid increase in glucose consumption in the batch culture and the lactate consumption in the fed-batch cultures). The highlighted term/equation is the modification herein developed using Monod-type expression in order to take into account the effect of the concentration of a substrate on another substrate utilisation/production rate(s) as well as reaction(s) as proposed in Figure 7.2.3 where the model was constructed based on.

Eq. 7.2.11 Glucose balance

$$\frac{d(VGlc)}{dt} = F_{in,\,glc}Glc_{in} - F_{out}Glc - Q_{glc}VX_v$$

Eq. 7.2.12 Glucose kinetics

$$Q_{glc} = \frac{\mu}{Y_{x,\,glc}} + m_{glc}\frac{Km_{glc,\,asp}^{\,2}}{Asp^2 + Km_{glc,\,asp}^{\,2}}$$

Eq. 7.2.13 Lactate balance

$$\frac{d(VLac)}{dt} = (Q_{lac,\,pro} - Q_{lac,\,con})VX_v - F_{out}Lac$$

Eq. 7.2.14 Lactate kinetics

$$Q_{lac,\,pro} = Q_{glc}Y_{lac,\,glc}$$

$$Q_{lac,\,con} = k_{lac,\,con}\frac{Asp}{Asp + Km_{lac,\,asp}}$$

Where, Glc_{in} is the concentration of fed glucose (mM); Q_{glc} is the specific glucose utilisation rate (mmol cells^{-1} hr^{-1}); $Y_{x, glc}$ is the yield of cells over glucose (cells/mmol); m_{glc} is the glucose associated maintenance energy constant (mmol.cells^{-1}.hr^{-1}); $Km_{glc, asp}$ and $Km_{lac, asp}$ are the Monod constants for aspartate-associated glucose and lactate limiting effects, respectively (mM); $Q_{lac, pro}$ and $Q_{lac, con}$ are the specific lactate production and consumption rates, respectively (mmol cells^{-1} hr^{-1}); $Y_{lac, glc}$ is the yield of lactate over glucose (mmol/mmol); and $k_{lac, con}$ is the specific lactate consumption constant (mmol.cells^{-1}.hr^{-1}).

The mass balance of glutamate involves enzymatic reactions that produce glutamate from the conversion of other amino acids, and that convert glutamate into other amino acids, as proposed in Figure 7.2.3. The consumption rate of amino acids was mathematically expressed using the constant maintenance energy equation with similar modifications to that for glucose metabolism. The production rates of alanine as well as glutamine, and the consumption rate of alanine were assumed to be governed by the availability of glutamate, as suggested in Chapter 5. The consumption rate of asparagine was assumed to be dependent on aspartate concentration, given the enzymatic relation between them. In addition, the availability of glutamate was assumed to positively affect its consumption rate, given previous reports (Takagi et al., 2001). This was also applied to aspartate, arginine and glutamine consumption rates (Figure 7.2.3).

Eq. 7.2.15 Glutamate balance

$$\frac{d(VGlu)}{dt} = F_{in, glu}Glu_{in} - F_{out}Glu - Q_{glu}VX_v + (f_{glu, ala}Q_{ala, con} - Q_{ala, pro} + f_{glu, gln}Q_{gln, con} - Q_{gln, pro} + f_{glu, asp}Q_{asp} + f_{glu, arg}Q_{arg})VX_v$$

Eq. 7.2.16 Glutamate kinetics

$$Q_{glu} = \left(\frac{\mu}{Y_{x,\,glu}} + m_{glu}\right)\frac{Glu^{0.5}}{Glu^{0.5} + Km_{glu,\,glu}^{0.5}}$$

Where, Glu_{in} is the concentration of fed glutamate (mM); Q_{glu}, Q_{asp}, Q_{arg}, $Q_{ala,\,con}$, and $Q_{gln,\,con}$ are the specific glutamate, aspartate, arginine, alanine and glutamine utilisation rates, respectively (mmol $cells^{-1}$ hr^{-1}); $Q_{ala,\,pro}$ and $Q_{gln,\,pro}$ are the specific alanine and glutamine production rates, respectively (mmol $cells^{-1}$ hr^{-1}); $f_{glu,\,asp}$, $f_{glu,\,arg}$, $f_{glu,\,ala}$, and $f_{glu,\,gln}$ are the yield of glutamate over aspartate, arginine, alanine and glutamine, respectively (mmol/mmol); $Y_{x,\,glu}$ is the yield of cells over glutamate (cells/mmol); m_{glu} is the glutamate-associated maintenance energy constant ($mmol.cells^{-1}.hr^{-1}$); $Km_{glu,\,glu}$ is the Monod constant for glutamate-associated glutamate limiting effect (mM).

Eq. 7.2.17 Aspartate balance

$$\frac{d(VAsp)}{dt} = F_{in,\,asp}Asp_{in} - F_{out}Asp + (f_{asp,\,asn}Q_{asn} - Q_{asp})VX_v$$

Eq. 7.2.18 Aspartate kinetics

$$Q_{asp} = \left(\frac{\mu}{Y_{x,\,asp}} + m_{asp}\right)\frac{Asp}{Asp + Km_{asp,\,asp}}$$

Where, Asp is the extracellular concentration of aspartate (mM); Asp_{in} is the concentration of fed aspartate (mM); Q_{asn} is the specific asparagine utilisation rates (mmol $cells^{-1}$ hr^{-1}); $f_{asp,\,asn}$ are the yield of aspartate over asparagine (mmol/mmol); $Y_{x,\,asp}$ is the yield of cells over aspartate (cells/mmol); m_{asp} is the aspartate-associated maintenance energy constant ($mmol.cells^{-1}.hr^{-1}$); $Km_{asp,\,asp}$ is the Monod constant for aspartate-associated aspartate limiting effect (mM).

Eq. 7.2.19 Asparagine balance

$$\frac{d(VAsn)}{dt} = F_{in,\,asn}Asn_{in} - F_{out}Asn - Q_{asn}VX_v$$

Eq. 7.2.20 Asparagine kinetics

$$Q_{asn} = \left(\frac{\mu}{Y_{x,\,asn}} + m_{asn}\right)\frac{Km_{asn,\,asp}}{Asp + Km_{asn,\,asp}}$$

Where, Asn is the extracellular concentration of asparagine (mM); Asn_{in} is the concentration of fed asparagine (mM); $Y_{x,\,asn}$ is the yield of cells over asparagine (cells/mmol); m_{asn} is the asparagine-associated maintenance energy constant ($mmol.cells^{-1}.hr^{-1}$); $Km_{asn,\,asp}$ is the Monod constant for asparagine-associated aspartate limiting effect (mM).

Eq. 7.2.21 Arginine balance

$$\frac{d(VArg)}{dt} = F_{in,\,arg}Arg_{in} - F_{out}Arg - Q_{arg}VX_v$$

Eq. 7.2.22 Arginine kinetics

$$Q_{arg} = \frac{\mu}{Y_{x,\,arg}} \cdot \frac{Arg}{Arg + Km_{arg,\,arg}} + m_{arg}$$

Where, Arg is the extracellular concentration of arginine (mM); Arg_{in} is the concentration of fed arginine (mM); Q_{arg} is the specific arginine utilisation rates ($mmol\ cells^{-1}\ hr^{-1}$); $Y_{x,\,arg}$ is the yield of cells over arginine (cells/mmol); m_{arg} is the arginine-associated maintenance energy constant ($mmol.cells^{-1}.hr^{-1}$); $Km_{arg,\,arg}$ is the Monod constant for arginine-associated arginine limiting effect (mM).

Eq. 7.2.23 Alanine balance

$$\frac{d(VAla)}{dt} = (Q_{ala,\,pro} - Q_{ala,\,con})VX_v - F_{out}Ala$$

Eq. 7.2.24 Alanine kinetics

$$Q_{ala,\,pro} = Q_{glu}Y_{ala,\,glu}$$

$$Q_{ala,\,con} = \frac{\mu}{Y_{x,\,ala}} \cdot \frac{Km_{ala,\,glu}}{Glu + Km_{ala,\,glu}} + m_{ala}$$

Where, Ala is the extracellular concentration of alanine (mM); $Y_{ala,\,glu}$ is the yield of alanine over glutamate (mmol/mmol); $Y_{x,\,ala}$ is the yield of cells over alanine (cells/mmol); m_{ala} is the alanine-associated maintenance energy constant ($mmol.cells^{-1}.hr^{-1}$); $Km_{ala,\,glu}$ is the Monod constant for alanine-associated glutamate limiting effect (mM).

Eq. 7.2.25 Glutamine balance

$$\frac{d(VGln)}{dt} = (Q_{gln,\,pro} - Q_{gln,\,con})VX_v - F_{out}Gln$$

Eq. 7.2.26 Glutamine kinetics

$$Q_{gln,\,pro} = Q_{glu}Y_{gln,\,glu}$$

$$Q_{gln,\,con} = \frac{\mu}{Y_{x,\,gln}} \cdot \frac{Gln^2}{Gln^2 + Km_{gln,\,glu}} + m_{gln}$$

Where, Gln is the extracellular concentration of glutamine (mM); $Y_{gln,\,glu}$ is the yield of glutamine over glutamate (mmol/mmol); $Y_{x,\,gln}$ is the yield of cells over alanine (cells/mmol); m_{ala} is the alanine associated maintenance energy constant ($mmol.cells^{-1}.hr^{-1}$); $Km_{ala,\,glu}$ is the Monod constant for alanine-associated glutamate limiting effect (mM).

Leucine plays an important role in the translation initiation of protein synthesis (Norton and Layman, 2006) through the mTOR signalling pathway (as previously discussed in Chapter 5). The activation of this pathway due to nutrient addition was suggested to underlie the observed increased productivity in a fed-batch culture of CHO cells (Dadehbeigi and Dickson, 2015). In addition, it was reported that the produced mAb contained a high content of leucine (González-Leal et al., 2011). Therefore, leucine must be included in the mAb synthesis kinetics in order to represent its effect on mAb production. However, our results showed that the production of mAb continued though leucine became exhausted in the fed-batch cultures, suggesting the mAb synthesis could be subject to other amino acids in addition to leucine. Asparagine was found to have a positive effect on the production of mAb in the GS-CHO cell culture (Xu et al., 2014). In addition, our data showed that there was a linear correlation between asparagine level and mAb produced in the batch culture. The following equations describe leucine utilisation and the synthesis of mAb which was assumed to be dependent on leucine and asparagine concentrations.

Eq. 7.2.26 Leucine balance

$$\frac{d(VLeu)}{dt} = - F_{out}Leu - Q_{leu}VX_v$$

Eq. 7.2.27 Leucine kinetics

$$Q_{leu} = \frac{\mu}{Y_{x,\,leu}} \cdot \frac{Leu}{Leu + Km_{leu,\,leu}} + m_{leu}$$

Where, Leu is the extracellular concentration of leucine (mM); Q_{leu} is the specific leucine utilisation rates (mmol cells^{-1} hr^{-1}); $Y_{x,\,leu}$ is the yield of cells over leucine (cells/mmol); m_{leu} is the leucine associated maintenance energy constant (mmol.cells^{-1}.hr^{-1}); $Km_{arg,\,arg}$ is the Monod constant for leucine -associated leucine limiting effect (mM).

Eq. 7.2.28 mAb balance

$$\frac{d(VAb)}{dt} = - F_{out}Ab + Q_{ab}VX_v$$

Eq. 7.2.29 mAb kinetics

$$Q_{ab} = \alpha_{ab}\left(\frac{Leu}{Leu + Km_{ab,\,aa}} + \frac{Asn}{Asn + Km_{ab,\,aa}}\right)$$

Where, Ab is the extracellular concentration of mAb (mg/L); Q_{ab} is the specific mAb prediction rate ($mg.cells^{-1}.hr^{-1}$); α_{ab} is the constant for the mAb synthesis rate ($mg\ cells^{-1}\ hr^{-1}$); $Km_{ab,\,aa}$ is the Monod constant for amino acid limiting effect on mAb synthesis (mM).

The cell metabolism sub-model consists of 19 variables in total (10 of which are differential variables) and 36 parameters (not including parameters for fed nutrient concentrations, i.e Glu_{in}, Glc_{in}, etc.).

The apoptosis sub-model

The apoptosis sub-model was aimed to describe dynamics of apoptotic events at the transcriptional level, with their links to metabolic stresses. The model also included the apoptosis regulatory network of protein-protein interactions given the relation between transcription and translation processes. These events were mathematically expressed using the combination of mass action kinetics, Monod-type as well as Hill equations, along the line of the previous mathematical models describing the genetic control of biodegradation with the links to kinetics of growth and metabolism in a microbial system (Koutinas et al., 2010, Koutinas et al., 2011). The highlighted term is the modification herein developed using Monod-type expression in order to take into account the effect of the mRNA level of an apoptotic species on the transcription rate of relevant apoptotic species as the proposed interactions among them (Figure 7.2.4) where this sub-model was constructed based on.

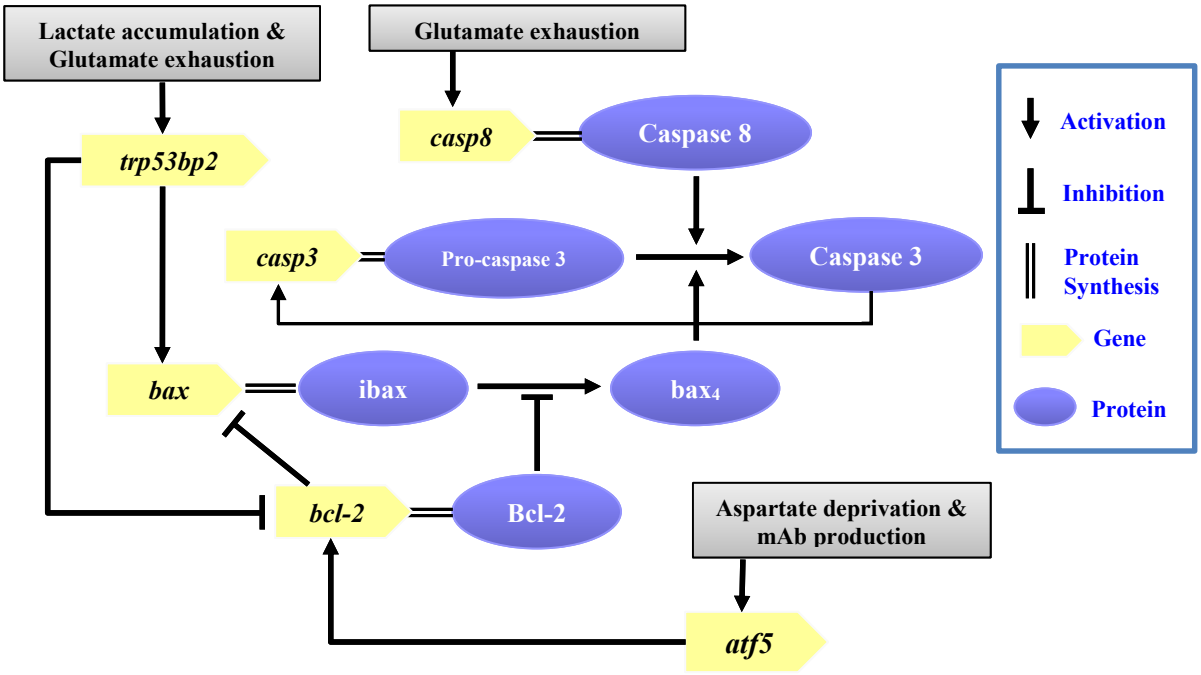


Figure 7.2.4 The transcriptional and translational regulatory network of apoptosis with links to metabolic stresses in the cultures of GS-NS0. This was herein proposed in accordance with previous reports as well as the herein experimental observation. This was used as a basis for the construction of the apoptosis structured sub-model.

The regulatory network of apoptosis as well as links to metabolic stresses were proposed based on previous studies and our experimental results, as can be seen in Figure 7.2.4. The expression of *atf5* was assumed to be dependent on the aspartate deprivation as well as the ER stress as a result of the synthesis of mAb, given its reported role in the survival mechanism in response to these metabolic stresses (Watatani et al., 2007, Zhou et al., 2008, Browne and Al-Rubeai, 2011b). The expression of *trp53bp2* and *casp8* was assumed to be subject to glutamate deprivation as well as lactate accumulation given the observed data in Chapter 5&6 and the previous study (Browne and Al-Rubeai, 2011b). The following equations represent the expression of *atf5*, *trp53bp2* and *casp8*, which was correlated with the concentrations of aspartate, glutamate and mAb.

Eq. 7.2.30 The transcription of *atf5*

$$\frac{d(mRNA_{atf5})}{dt} = \beta_{mRNA_{atf5}}\left(\frac{Km_{asp,\ atf5}}{Asp + Km_{asp,\ atf5}}\right)\left(\frac{Km_{ab,\ atf5}{}^{2}}{Ab^{2} + Km_{ab,\ atf5}{}^{2}}\right) - \alpha_{mRNA_{atf5}} mRNA_{atf5}{}^{0.5}$$

Where, $mRNA_{atf5}$ is the relative fold change of *atf5* expression (-); $\beta_{mRNA_{atf5}}$ is the maximal fold change of *atf5* expression (hr^{-1}); $Km_{asp,\ atf5}$ and $Km_{ab,\ atf5}$ are the Monod constants for *atf5* associated aspartate (mM) and mAb (mg/L) limiting effect, respectively; $\alpha_{mRNA_{atf5}}$ is the mRNA degradation rate of *atf5* (hr^{-1}).

Eq. 7.2.31 The transcription of *trp53bp2*

$$\frac{d(mRNA_{trp53bp2})}{dt} = \beta_{mRNA_{trp53bp2}}\left(\frac{Km_{glu,\ trp53bp2}}{Glu + Km_{glu,\ trp53bp2}}\right)\left(\frac{Lac^{2}}{Lac^{2} + Km_{lac,\ trp53bp2}{}^{2}}\right) - \alpha_{mRNA_{trp53bp2}} mRNA_{trp53bp2}$$

Where, $mRNA_{trp53bp2}$ is the relative fold change of *trp53bp2* expression (-); $\beta_{mRNA_{trp53bp2}}$ is the maximal fold change of *trp53bp2* expression (hr^{-1}); $Km_{glu,\ trp53bp2}$ and $Km_{lac,\ trp53bp2}$ are the Monod constants for *trp53bp2* associated glutamate and lactate limiting effect, respectively (mM); $\alpha_{mRNA_{trp53bp2}}$ is the mRNA degradation rate of *trp53bp2* (hr^{-1}).

Eq. 7.2.32 The transcription of *casp8*

$$\frac{d(mRNA_{casp8})}{dt} = \beta_{mRNA_{casp8}}\left(\frac{Km_{glu,\ casp8}{}^{0.5}}{Glu^{0.5} + Km_{glu,\ casp8}{}^{0.5}}\right) - \alpha_{mRNA_{casp8}} mRNA_{casp8}$$

Where, $mRNA_{casp8}$ is the relative fold change of *casp8* expression (-); $\beta_{mRNA_{casp8}}$ is the maximal fold change of *casp8* expression (hr^{-1}); $Km_{glu,\ casp8}$ is the Monod constants for *casp8* associated glutamate limiting effect, respectively; $\alpha_{mRNA_{casp8}}$ is the mRNA degradation rate of *casp8* (hr^{-1}).

The transcription of *bcl-2* was assumed to be dependent on the expression of *atf5* as well as *trp53bp2* since it was previously demonstrated that the expression of *bcl-2* was linked to the expression level of *atf5* (Dluzen et al., 2011), and *p53* (Haldar et al., 1994, Miyashita et

al., 1994) that was associated with the expression of *trp53bp2* (Naumovski and Cleary, 1996, Samuels-Lev et al., 2001, Kobayashi et al., 2005), respectively. The mathematical equation for the expression of *bax* was constructed based on previous studies showed that there was an inversely proportional correlation between *bax* and *bcl-2* (Paul-Samojedny et al., 2005). In addition, the equation includes the effect of *trp53bp2* expression on the *bax* expression given that *bax* is one of transcriptional targets of *p53* (Toshiyuki and Reed, 1995).

Eq. 7.2.33 The transcription of *bcl-2*

$$\frac{d(mRNA_{bcl2})}{dt} = \beta_{mRNA_{bcl2}} \left(\frac{mRNA_{trp53bp2}{}^{2}}{mRNA_{trp53bp2}{}^{2} + Km_{trp53bp2,\,bcl2} + mRNA_{atf5} / Km_{atf5,\,bcl2}} \right) - \alpha_{mRNA_{bcl2}} mRNA_{bcl2}$$

Where, $mRNA_{bcl2}$ is the relative fold change of *bcl-2* expression (-); $\beta_{mRNA_{bcl2}}$ is the maximal fold change of *bcl-2* expression (hr^{-1}); $Km_{trp53bp2,\,bcl\text{-}2}$ and $Km_{atf5,\,bcl\text{-}2}$ are the Monod constants for *trp53bp2* and *atf5* limiting effects, respectively, on *bcl-2* expression (-); $\alpha_{mRNA_{bcl2}}$ is the mRNA degradation rate of *bcl-2* (hr^{-1}).

Eq. 7.2.34 The transcription of *bax*

$$\frac{d(mRNA_{bax})}{dt} = \beta_{mRNA_{bax}} \left(\frac{Km_{bcl2,\,bax}}{mRNA_{bcl2} + Km_{bcl2,\,bax}} \right) \left(\frac{mRNA_{trp53bp2}{}^{2}}{mRNA_{trp53bp2}{}^{2} + Km_{trp53bp2,\,bax}{}^{2}} \right) - \alpha_{mRNA_{bax}} mRNA_{bax}$$

Where, $mRNA_{bax}$ is the relative fold change of *bax* expression (-); $\beta_{mRNA_{bax}}$ is the maximal fold change of *bax* expression (hr^{-1}); $Km_{bcl\text{-}2,\,bax}$ and $Km_{trp53bp2,\,bax}$ are the Monod constants for *bcl-2* and *trp53bp2* limiting effects, respectively, on *bax* expression (-); $\alpha_{mRNA_{bax}}$ is the mRNA degradation rate of *bax* (hr^{-1}).

Procaspase-3 is the catalytically inactive form of caspase-3 (Duan et al., 1996). However, once activated, the activation of caspase 3 was found to be auto-processing (Colussi

et al., 1998). Therefore, the expression of *casp3* was assumed to be proportional to the concentration of caspase 3 as shown in the following equation.

Eq. 7.2.35 The transcription of *casp3*

$$\frac{d(mRNA_{casp3})}{dt} = \beta_{mRNA_{casp3}} \left(\frac{Casp3^2}{Casp3^2 + Km_{casp3,\,iC3}{}^2} \right) - \alpha_{mRNA_{casp3}} mRNA_{casp3}{}^2$$

Where, $mRNA_{casp3}$ is the relative fold change of *casp3* expression (-); $\beta_{mRNA_{casp3}}$ is the maximal fold change of *casp3* expression (hr^{-1}); $Km_{casp3,\,iC3}$ is the Monod constant for caspase 3 limiting effect, respectively, on *casp3* expression (mM) ; $\alpha_{mRNA_{casp3}}$ is the mRNA degradation rate of *casp3* (hr^{-1}).

In addition to the transcription of apoptotic genes, cells require interactions among proteins involved in the apoptotic pathways to initiate or govern apoptosis (Sax and El-Deiry, 2003), and thus this should be also included in the apoptosis sub-model. The model should be constructed based on the reactions among apoptotic proteins and the connection between the mRNA levels of the apoptotic species of interest and the corresponding protein levels. As shown in Figure 7.2.4, the translation rates of procaspases-3, caspase-8, inactive Bax and Bcl-2, given the initial concentration of these proteins found in cells, were assumed to be dependent on the mRNA levels of *casp3*, *casp8*, *bax* and *bcl2*, respectively. The mathematical expression for the balances of these proteins accounts for the translation and protein-protein interactions among apoptotic proteins. The translation was mathematically expressed using Monod-type kinetics along the line of the mathematical models for microbial biodegradation by Koutinas et al. (2010), while the equations for protein-protein interactions were based on mass-action kinetics.

There are previous reports showing a positive correlation between the mRNA and the corresponding protein levels (Ghazalpour et al., 2011, Schwanhausser et al., 2011). However,

this is not always the case given that no/a very weak correlation between the mRNA and its corresponding protein levels was found in many cases, suggesting that the positive correlation is protein and pathways specific. For example, the mAb productivity did not increase as its mRNA levels were found increased due to hypothermia in GS-NS0 and GS-CHO cell cultures (Marchant et al., 2008). In a study of apoptosis in breast cancer brain metastases, Bcl-2 protein and *bcl-2* mRNA levels were found to have a positive correlation while there was no correlation found between Bax protein and *bax* mRNA expressions (Stark et al., 2006). It was also suggested, based on the observed result showing a weak correlation between the mRNA and its protein levels in human monocytes, that mRNAs can provide lots of information but may not be able to predict their corresponding protein expressions (Guo et al., 2008). This could be because mRNAs are not directly converted into proteins. During the process of protein synthesis, there are places where several factors can affect the process. This includes translation initiation (ribosomic binding site, presence of internal ribosome entry site, IRES), regulatory proteins as well as small RNAs (repressing its own translation), translational efficiency (as regards ribosomal density and ribosome occupancy), and protein half-life affecting post-translational protein levels (Maier et al., 2009). Given the above discussion indicating the inconsistent correlation between the mRNA and the corresponding protein levels, the assumption made for the apoptosis sub-model construction could not be truly valid, which is one of weakest points in the apoptosis sub-model. The proteins included in the model will need to be quantified to validate the assumption as well as confirm model estimation capability.

The activation of caspase-3 was assumed to be dependent on the concentration of caspase-8 and the active form of Bax (tetrameric complex); while the translation was assumed to be proportional to the expression of $mRNA_{casp3}$.

Eq. 7.2.36 Procaspase-3 balance

$$\frac{d(ViCasp3)}{dt} = \left(\beta_{iC3} \left(\frac{mRNA_{casp3}}{Kb_{iC3}+mRNA_{casp3}} \right) - k_{C3} Bax_4 iCasp3 - k_{C8} Casp8 iCasp3 \right) V - F_{out} iCasp3$$

Eq. 7.2.37 Caspase-3 activation

$$\frac{d(VCasp3)}{dt} = (k_{C3} Bax_4 iCasp3 + k_{C8} Casp8 iCasp3) V - F_{out} Casp3$$

Where, iCasp3, Casp3, bax_4 and Casp8 are the concentration of procaspases-3, Caspase-3, active bax and caspase-8, respectively (mM); β_{iC3} is the maximal procaspase-3 translation rate based on the expression of *casp3* ($mmol.hr^{-1}$); k_{C3} and k_{C8} are the rate constants for active bax and caspase-8, respectively, associated caspase-3 activation ($L.mmol^{-1}.hr^{-1}$); Kb_{iC3} is the Monod constant for $mRNA_{casp3}$ limiting effect on the translation of procaspase-3 (-).

Like that of procaspases-3, the mass balance of inactive Bax accounts for the translation and the relevant protein-protein interactions in apoptotic pathways (Eq. 7.2.38). It was previously proposed that the tetrameric form of Bax molecules is the active form that is required to activate the apoptosis pathway (Chen et al., 2007). The herein mathematical expression of Bax activation, therefore, was constructed using mass-action kinetics considering Bax-polymerisation, as shown in Eq. 7.2.39.

Eq. 7.2.38 Inactive Bax balance

$$\frac{d(ViBax)}{dt} = \left(\beta_{ibax} \left(\frac{mRNA_{bax}}{Kb_{ibax}+mRNA_{bax}} \right) - k_{bax} iBax^4 \right) V - F_{out} iBax$$

Eq. 7.2.39 Bax activation

$$\frac{d(VBax_4)}{dt} = (k_{bax} iBax^4 - k_{_bax} Bax_4 Bcl2) V - F_{out} Bax_4$$

Where, iBax and Bcl2 are the concentration of inactive Bax and Bcl-2, respectively (mM); β_{ibax} is the maximal inactive Bax translation rate based on the expression of *bax* ($mmol.hr^{-1}$); k_{bax} and $k_{_bax}$ are the rate constants for the Bax tetramerization ($L^3.mmol^{-3}.hr^{-1}$) and the inhibitive binding of Bcl-2 to active Bax ($L.mmol^{-1}.hr^{-1}$), respectively; Kb_{ibax} is the Monod constant for $mRNA_{bax}$ limiting effect on the translation of inactive Bax (-).

Mass balances of Bcl-2 and caspase-8 were proposed as the following equations (Eq. 7.2.40-41), which were constructed to account for the translation and apoptotic protein-protein interactions.

Eq. 7.2.40 Bcl-2 balance

$$\frac{d(Vbcl2)}{dt} = \left(\beta_{bcl2} \left(\frac{mRNA_{bcl2}}{Kb_{bcl2}+mRNA_{bcl2}} \right) - k_{_bax} bax_4 bcl2 \right) V - F_{out} bcl2$$

Where, β_{bcl2} is the maximal Bcl-2 translation rate based on the expression of *bcl2* ($mmol.hr^{-1}$); Kb_{bcl2} is the Monod constant for $mRNA_{bcl2}$ limiting effect on the translation of Bcl-2 (-).

Eq. 7.2.41 Caspase-8 balance

$$\frac{d(VCasp8)}{dt} = \beta_{C8} \left(\frac{mRNA_{casp8}}{Kb_{C8}+mRNA_{casp8}} \right) V - F_{out} Casp8$$

Where, β_{casp8} is the maximal caspase-8 translation rate based on the expression of *casp8* expression ($mmol.hr^{-1}$); Kb_{C8} is the Monod constant for $mRNA_{casp8}$ limiting effect on the translation of caspase-8 (-).

The apoptosis sub-model is basically the system of ODEs, which consists of 12 variables and all of which are differential variables. There are 34 parameters in this sub-model.

It is worth discussing about the validity of the presented model as well as its potential applications in the mammalian cell culture systems. The herein constructed mathematical

model was based on the batch and fed-batch cultures of GS-NS0 cells. In addition, the proposed mathematical equations were constructed preliminarily based upon existing biological knowledge; including cell growth kinetics, metabolism and apoptotic pathways, and were further modified along the line of what was experimentally observed in the cultures. Therefore, the validity of this model is most likely limited to the GS-NS0 cell cultures in either batch or fed-batch modes. However, given that the model was structured to a certain extent based on the generalised biological knowledge, it can be further modified either structurally or with regards to change in parameter values in order to be able to capture the behaviour of other mammalian cell culture systems, such as GS-CHO cells.

However, the presented model is still in the beginning steps toward the predictive mathematical model development. Its applications are therefore limited to only the system behaviour that the model was developed based on. The model can be potentially used for the study of effects of apoptosis induction/suppression on growth, metabolism, death and recombinant/exogenous protein synthesis in the GS-NS0 cell cultures given the model description. With the aid of the mathematical model simulations, the effect of overexpression/knockdown apoptotic genes (only ones included in the model) on cell viability and mAb synthesis, for example, could be evaluated. Thus, this helps us to narrow down the choice of apoptotic gene engineering toward higher mAb synthesis and longer culture viability, and plan the screening procedure and corresponding experiments before the experiments are actually conducted. This would ultimately help shorten the timeline for the process development stage for the improvement of the mammalian cell culture systems (Ho et al., 2013), given possible trial and error could be avoided.

7.2.3 Parameter values

The values of model parameters assigned herein were aimed to 1) provide a reasonable reproduction of the experimental data from batch and fed-batch cultures, 2) be preliminarily used for the model analysis to evaluate model characteristics as well as parameters significance (and thus model identifiability). Therefore, the parameter estimates shown here are not the finalised ones which are not yet be globally optimised.

Parameters in the proposed mathematical models can be roughly divided into two groups. The first one is the group of parameters that their values can be preliminarily estimated from literature. These values were treated as initial guesses, providing the information about the order of magnitude of these parameters. They were further manually adjusted in order to reproduce the experimental data. The second group is ones that their values could not be estimated from literature since they have not been introduced in any studies before. The values of these parameters were left at dummy values (such as 1, 0.1, 0.01 etc.) with a similar order of magnitude to the values of biological relevant variables or parameters. These values were then further adjusted manually and computationally (parameter estimator in the model builder software). The following tables shows the values and the sources of parameters used herein.

Table 7.2.1 The preliminary values of model parameters and their references.

	No	Parameters (unit)	Values used herein	Reference values
Cell growth sub-model	1	$\mu_{max,\ glc}$ (hr^{-1})	2.80E-02	[5.80E-03, 1.25E-01]; μ_{max} [1-5]
	2	K_{glc} (mM)	3.90E+01	[7.50E-01, 4.61E+01]; K_{glc} [1-5]
	3	$\mu_{max,\ glu}$ (hr^{-1})	1.70E-02	[5.80E-03, 1.25E-01]; μ_{max} [1-5]
	4	K_{glu} (mM)	1.00E-01	[3.00E-03, 4.27E-00]; K_{gln} [1-5]
	5	$\mu_{max,\ ad}$ (hr^{-1})	3.83E-02	[1.00E-02, 6.00E-02]; $\mu_{max,\ d}$ or $k_{d,\ max}$ [1-5]
	6	K_{casp3} (mM)	1.01E+00	1.76E+00; $K_{d,\ amm}$ [1,3]
	7	$\mu_{max,\ nd}$ (hr^{-1})	1.13E-02	[1.00E-02, 6.00E-02]; $\mu_{max,\ d}$ or $k_{d,\ max}$ [1-5]
	8	K_{lac} (mM)	1.03E+02	[4.50E+01, 1.77E+02]; $K_{I,\ lac}$ [1,3,5]
	9	$\mu_{max,\ d}$ (hr^{-1})	1.57E+01	[1.00E-02, 6.00E-02]; $\mu_{max,\ d}$ or $k_{d,\ max}$ [1-5]
	10	k_d (hr^{-1})	6.26E-05	[1.89E-05, 2.60E-03]; $K_{d,\ 1}$ or k_{lysis} [2, 3, 5]

Metabolism sub-model	11	$Y_{x,\,glc}$ (cells/mmol)	4.00E+05	[4.91E+4 to 1.21E+6]; 1/ $K_{glc,max}$ or $Y_{x,\,glc}$ [2,3]
	12	m_{glc} (mmol.cells^{-1}.hr^{-1})	5.14E-07	[3.16E-08, 4.1E-08]; m_{glc} [2]
	13	$Km_{glc,\,asp}$(mM)	1.00E-02	[1.00E-02, 1.00E-01]; $K_{amino\ acid}$ [5]
	14	$Y_{lac,\,glc}$ (mmol/mmol)	2.50E+00	[0.97E+00, 2.00E+00]; $Y_{lac,\,glc}$ [2-5]
	15	$k_{lac,\,con}$ (mmol.cells^{-1}.hr^{-1})	1.50E-07	Assumed to be similar to m_{glc}
	16	$Km_{lac,\,asp}$(mM)	1.00E-02	[1.00E-02, 1.00E-01]; $K_{amino\ acid}$ [5]
	17	$Y_{x,\,glu}$ (cells/mmol)	6.05E+06	[5.5E+05, 1.21E+6]; $Y_{x,\,glu}$ [3]
	18	m_{glu}(mmol.cells^{-1}.hr^{-1})	8.87E-09	[-4.5E-08, 5.91E-08]; m_{lac} [2]
	19	$Km_{glu,\,glu}$(mM)	1.00E-01	[1.00E-02, 1.00E-01]; $K_{amino\ acid}$ [5]
	20	$f_{glu,\,ala}$ (mmol/mmol)	5.00E-01	[1.00E-04, 1.00E-00]; $Y_{amino\ acid,\,amino\ acid}$ [5], but adjusted to 0.5 for all yields
	21	$f_{glu,\,gln}$ (mmol/mmol)	5.00E-01	
	22	$f_{glu,\,asp}$ (mmol/mmol)	5.00E-01	
	23	$f_{glu,\,arg}$ (mmol/mmol)	5.00E-01	
	24	$Y_{x,\,asp}$ (cells/mmol)	1.40E+06	Assumed to be similar to $Y_{x,\,glu}$
	25	m_{asp}(mmol.cells^{-1}.hr^{-1})	8.00E-10	Assumed to be similar to m_{glu}
	26	$Km_{asp,\,asp}$ (mM)	2.00E-02	[1.00E-02, 1.00E-01]; $K_{amino\ acid}$ [5]
	27	$f_{asp,\,asn}$ (mmol/mmol)	5.00E-01	[1.00E-04, 1.00E-00]; $Y_{amino\ acid,\,amino\ acid}$ [5], but adjusted to 0.5 for all yields
	28	$Y_{x,\,asn}$ (cells/mmol)	1.50E+06	Assumed to be similar to $Y_{x,\,glu}$
	29	m_{asn}(mmol.cells^{-1}.hr^{-1})	1.00E-09	Assumed to be similar to m_{glu}
	30	$Km_{asn,\,asp}$ (mM)	9.00E-02	[1.00E-02, 1.00E-01]; $K_{amino\ acid}$ [5]
	31	$Y_{x,\,arg}$ (cells/mmol)	2.50E+06	Assumed to be similar to $Y_{x,\,glu}$
	32	m_{arg}(mmol.cells^{-1}.hr^{-1})	1.00E-09	Assumed to be similar to m_{glu}
	33	$Km_{arg,\,arg}$(mM)	5.00E-02	[1.00E-02, 1.00E-01]; $K_{amino\ acid}$ [5]
	34	$Y_{x,\,ala}$ (cells/mmol)	3.00E+06	Assumed to be similar to $Y_{x,\,glu}$
	35	m_{ala}(mmol.cells^{-1}.hr^{-1})	3.50E-09	Assumed to be similar to m_{glu}
	36	$Km_{ala,\,glu}$ (mM)	9.00E-02	[1.00E-02, 1.00E-01]; $K_{amino\ acid}$ [5]
	37	$Y_{ala,\,glu}$ (mmol/mmol)	1.60E+00	[1.43E+00, 1.00 E+01]; $Y_{gln,\,glu}$ [5]
	38	$Y_{x,\,gln}$ (cells/mmol)	7.00E+05	Assumed to be similar to $Y_{x,\,glu}$
	39	m_{gln}(mmol.cells^{-1}.hr^{-1})	2.00E-09	Assumed to be similar to m_{glu}
	40	$Km_{gln,\,gln}$(mM)	7.00E-02	[1.00E-02, 1.00E-01]; $K_{amino\ acid}$ [5]
	41	$Y_{gln,\,glu}$ (mmol/mmol)	2.50E+00	1.43E+00 to 1.00 E+01; $Y_{gln,\,glu}$ [5]
	42	$Y_{x,\,leu}$ (cells/mmol)	2.00E+06	Assumed to be similar to $Y_{x,\,glu}$
	43	m_{leu}(mmol.cells^{-1}.hr^{-1})	1.00E-09	Assumed to be similar to m_{glu}
	44	$Km_{leu,\,leu}$(mM)	5.00E-02	[1.00E-02, 1.00E-01]; $K_{amino\ acid}$ [5]
	45	α_{ab} (mg cells^{-1} hr^{-1})	3.96E-07	[4.02E-11, 8.10E-11]; [3,4]
	46	$Km_{mab,\,aa}$ (mM)	1.00E-01	[1.00E-02, 1.00E-01]; $K_{amino\ acid}$ [5]
Apoptosis sub-model	47	β_{iC3} (mmol.hr^{-1})	9.08E-03	n/a: adjusted from a dummy value of 1.0E-03
	48	Kb_{iC3} (-)	2.00E-03	Assumed to be within the order of magnitude of *casp3* expression; [0, 1.0E+01]
	49	k_{C3} (L.mmol^{-1}.hr^{-1})	3.58E+00	n/a: adjusted from a dummy value of 1.0E-02
	50	β_{iC8} (mmol.hr^{-1})	1.02E-03	n/a: adjusted from a dummy value of 1.0E-03
	51	Kb_{iC8} (-)	1.45E-01	Assumed to be within the order of magnitude of *casp8* expression; [0, 1.0E+01]
	52	k_{C8} (L.mmol^{-1}.hr^{-1})	1.12E-02	n/a: adjusted from a dummy value of 1.0E-02
	53	β_{ibax} (mmol.hr^{-1})	2.97E-03	n/a: adjusted from a dummy value of 1.0E-03

	54	$k_{_bax}$ ($L.mmol^{-1}.hr^{-1}$)	2.96E+00	0.00E+00 [6]
	55	k_{bax} ($L^3.mmol^{-3}.hr^{-1}$)	1.82E+00	2.00E+00 [6]
	56	Kb_{ibax} (-)	8.47E-01	Assumed to be within the order of magnitude of *bax* expression; [0, 1.0E+01]
	57	β_{bcl2} ($mmol.hr^{-1}$)	2.38E-04	n/a: adjusted from a dummy value of 1.0E-03
	58	Kb_{bcl2} (-)	1.30E+01	Assumed to be within the order of magnitude of *bcl2* expression; [0, 1.0E+01]
	59	$\beta_{mRNA_{casp3}}$ (hr^{-1})	6.36E-02	n/a: adjusted from a dummy value of 1.0E-02
	60	$Km_{casp3,\ iC3}$ (mM)	1.41E-01	Assumed to be within the order of magnitude of caspase-3 concentration; 0.2 mM initial concentration [6]
	61	$\alpha_{mRNA_{casp3}}$ (hr^{-1})	1.25E-02	n/a: adjusted from a dummy value of 1.0E-02
	62	$\beta_{mRNA_{bax}}$ (hr^{-1})	1.11E-01	n/a: adjusted from a dummy value of 1.0E-02
	63	$Km_{trp53bp2,\ bax}$ (-)	6.27E-01	Assumed to be within the order of magnitude of *gene* expressions; [0, 1.0E+01]
	64	$Km_{bcl\text{-}2,\ bax}$ (-)	7.00E-01	
	65	$\alpha_{mRNA_{bax}}$ (hr^{-1})	1.81E-02	n/a: adjusted from a dummy value of 1.0E-02
	66	$\beta_{mRNA_{bcl2}}$ (hr^{-1})	6.83E-01	n/a: adjusted from a dummy value of 1.0E-02
	67	$Km_{trp53bp2,\ bcl\text{-}2}$ (-)	2.10E+00	Assumed to be within the order of magnitude of *gene* expressions; [0, 1.0E+01]
	68	$Km_{atf5,\ bcl\text{-}2}$ (-)	6.98E+00	
	69	$\alpha_{mRNA_{bcl2}}$ (hr^{-1})	1.97E-01	n/a: adjusted from a dummy value of 1.0E-02
	70	$\beta_{mRNA_{trp53bp2}}$ (hr^{-1})	4.68E-02	n/a: adjusted from a dummy value of 1.0E-02
	71	$Km_{lac,\ trp53bp2}$ (mM)	1.73E+00	Assumed to be within the order of magnitude of lactate [0, 3.0E+01] and glutamate levels [0, 1.0E+00]
	72	$Km_{glu,\ trp53bp2}$ (mM)	1.00E-01	
	73	$\alpha_{mRNA_{trp53bp2}}$ (hr^{-1})	2.01E-02	n/a: adjusted from a dummy value of 1.0E-02
	74	$\beta_{mRNA_{atf5}}$ (hr^{-1})	3.82E-01	n/a: adjusted from a dummy value of 1.0E-02
	75	$Km_{asp,\ atf5}$ (mM)	2.29E-02	Assumed to be within the order of magnitude of aspartate [0, 1.0E+00] and mAb levels [0, 1.0E+02]
	76	$Km_{ab,\ atf5}$ (mg/L)	2.77E+01	
	77	$\alpha_{mRNA_{atf5}}$ (hr^{-1})	5.42E-02	n/a: adjusted from a dummy value of 1.0E-02
	78	$\beta_{mRNA_{casp8}}$ (hr^{-1})	9.46E-02	n/a: adjusted from a dummy value of 1.0E-02
	79	$Km_{glu,\ casp8}$ (mM)	1.21E-01	Assumed to be within the order of magnitude of *casp8* expression; [0, 1.0E+01]
	80	$\alpha_{mRNA_{casp8}}$ (hr^{-1})	5.13E-02	n/a: adjusted from a dummy value of 1.0E-02

[1](Kontoravdi et al., 2010)&(Kiparissides et al., 2011a), [2](Ho et al., 2006), [3](Kiparissides et al., 2015), [4](Teixeira et al., 2005), [5](Kontoravdi et al., 2007), [6](Chen et al., 2007)& (Hua et al., 2005).

The initial conditions for differential variables (such as concentrations of viable cells, glucose, amino acids, etc.) were defined according to the experimental data obtained from Chapter 5&6. However, the initial conditions for apoptotic proteins, including procaspases-3, caspase-8, inactive Bax and Bcl-2 were assigned using the previously reported values (Chen et al., 2007, Hua et al., 2005).

7.2.4 Model analysis

All simulations and parameter fitting were performed on an Intel® Core™ i7 870 (2.93-3.07 GHz) personal computer with 8.00 GB of RAM memory. The proposed mathematical model was implemented in the advanced process model builder gPROMS version 4.0.0 (64bit) (gPROMS, 2014).

As discussed earlier, the validity of model parameters could not be fully claimed since the parameter values were non-optimised. Global sensitivity analysis (GSA) can provide sensitivity of each parameter through simultaneously and randomly varying all parameter values within a limited and pre-specified range using the Quasi-Monte Carlo method-based Sobol random number sequences. The randomness inherent in GSA enables to explore the sensitivity of values around the parameter nominal values (through randomly sampling values around the parameter nominal values within the range); in other words, to take into account uncertainty surrounding the parameter values (Kent et al., 2013, Kiparissides et al., 2009). Therefore, given the preliminary set of parameters used in the presented model, GSA was herein adopted as a computational tool for model analysis to identify sensitive or significant parameters.

The global parameter sensitivities were quantified using Sobol' method. This method allows acquiring the first order sensitivity indices as well as the total sensitivity indices (TSIs). Herein, the parameter significance was evaluated using the TSIs (Homma and Saltelli, 1996), while the interactions among model parameters were pinpointed by comparing the TSIs with the main effects of model parameters (Kiparissides et al., 2009).

The Sobol' sensitivity indices were estimated using GUI-HDMR software (Ziehn and Tomlin, 2009). The inputs for the software were 1) the Sobol' quasi-random sequences and 2) the variation of model variables with respect to the Sobol' quasi-random sequences. These

inputs were generated through the cooperation between Matlab (MATLAB, 2014) and gPROMS. A Sobol' sequence, which is a sequence of random numbers in the unit hypercube (0-1), was firstly generated in Matlab. Each random number in the sequence was treated as a percentage change of a model parameter. The parameter values were then varied from their nominal values in accordance with the random numbers in the sequence; nevertheless, they could only be changed within the pre-specified range/space that parameter values could be deviated from their nominal values. Matlab then sent the varied parameter values to gPROMS in order to acquire the effects of the parameter variation on model variables. Finally, gPROMS simulated the mathematical model with the variation of parameter values and sent the output back to Matlab, where all information was stored. This process was repeated with a newly generated Sobol's sequence. The iteration continued as the number of Sobol's sequences were pre-specified.

In this study, ±25% deviation from the nominal values of parameters was set for the range/space of parameter variation. 100,000 Sobol's sequences were employed in order to 1) allow exploring any possible scenarios of simultaneous variation of all model parameters, and 2) assure the convergence of the sensitivity results, as suggested previously (Benedetti et al., 2011). The sensitivity indices were collected at 0, 24, 48, 60, 72, 96 and 120 hours of the culture time (or model simulation time). Viable cell (X_v), ESA cell (X_{ad}), dead cell (X_d) and mAb (Ab) concentrations were primary model variables that the sensitivity indices were estimated based on.

±25% deviation of parameter values in the cell growth sub-model (Table 7.2.1) often caused the simulations to be terminated before the time points that the sensitivity indices were collected, especially during the stationary and death phases. Consequently, the effect of parameters in the other sub-models on the model variables could not be truly investigated during these periods of the culture. In addition, values of the parameters in metabolism and

apoptosis sub-models were relatively uncertain as compared to the cell growth sub-model since some of them were herein estimated with very limited clues from previous studies. Further evaluation of parameter sensitivities, therefore, were conducted specifically to pinpoint the effect of parameters in these sub-models on the model variables of interest.

GSA was further performed with the range/space of parameter variation in the metabolism and apoptosis sub-models being relatively larger than those in other sub-models. ±25% and ±50% deviation from the nominal values of parameters in the metabolism and apoptosis sub-models, respectively, were implemented while the range/space of parameter variation of the remaining parameters was set at ±5%. The GSA was performed with 60,000 Sobol's sequences and the sensitivity indices were collected at 0, 24, 48, 60, 72, 96 and 120 hours of the culture time. Apart from viable cells (Xv), ESA cells (Xad), dead cells (Xd) and the concentration of mAb (Ab), the effect of these parameter variation on other variables were also explored.

It is worth noting that the global sensitivities obtained from this study, however, were based on the preliminary set of parameter values, which is most likely to be later amended according to the GSA result. Despite taking into account the uncertainty of parameter values used in the model (the preliminary ones), the GSA with the amended parameter values could provide a different result to the one achieved from the preliminary values. This could be because the analysis range of the preliminary parameter values was limited (±25%) and the later amended ones can be outside this range.

Given that parameter values are randomly and simultaneously sampled within the pre-specified range of the parameter values in the GSA, it is possible to determine a set of optimal parameter values that provides the best reproduction of experimental data based on the GSA algorithm. This was performed using the same algorithm as the GSA (Matlab-gPROMS

simulations) as above described. All 80 parameters were randomly and simultaneously sampled in the ±60% deviation from their default values. 100,000 Sobol's sequences were generated to represent the random sampling within the ±60% pre-specified range of parameter values (a random sequence is a set of 80 parameter values that their values were randomly selected within the range). Viable cells (Xv), ESA cells (Xad), viability (Via) and the concentration of mAb (Ab) were used as primary model variables of interest and were simulated in accordance with the sampled sets of parameter values at 0, 24, 48, 60, 72, 96 and 120 hours of the culture time. Simulations using the 100,000 randomly sampled sets of parameter values provided 100,000 different trajectories of the model output. In order to determine the trajectory that showed the best reproduction of the corresponding experimental data, the percentage error for each simulated output trajectory was calculated using Eq. 7.2.42, which represents the percent difference between the simulated output trajectory and the experimental data for a model variable at a culture time point.

Eq. 7.2.42 The percentage error (PE)

$$PE_{i,j} = \frac{|\text{Simulated data}_{i,j} - \text{Experimental data}_{i,j}|}{\text{Experimental data}_{i,j}} \text{;i=model variable, j=time}$$

Eq. 7.2.43 The total percentage error (TPE)

$$TPE = \sum_{j=1}^{M} \sum_{i=1}^{N} PE_{i,j} \text{ ;N=No. of model variables of interest, j=No. of time points}$$

The percentage error was estimated for each model variable (Xv, Xad, Via and Ab) and at the different observed culture time (0, 24, 48, 60, 72, 96 and 120 hours). Therefore, there were 7 percentage errors for each model variable and 28 percentage errors for each simulated output trajectory. The total percentage error is the summation of all 28 percentage errors (Eq. 7.2.43) in order to take into account the errors for all the model variables of interest at all the

observed time points. The simulated output trajectory that provided the minimum total percentage error was selected as the best reproduction of experimental data. Therefore, the sampled set of parameter values that generated the selected output trajectory was treated as the set of optimal parameter values.

7.3 Results & Discussion

7.3.1 Batch and Fed-batch simulations

The data obtained from simulations in gPROMS were compared to the experimental data. The Pearson correlation coefficient (r_p) was determined to indicate whether the simulations could capture the trend of experimental data. If the simulation results can perfectly capture the trend of experimental data, there should be a linear correlation between those types of data, indicated by the r_p being close to 1 with the *p*-value (indicating the likelihood of being wrong in concluding that there is a linear correlation between in the two variables) being less than the significant level (alpha=0.05). In addition, to represent the goodness of fit of, the adjusted R^2 value was calculated through the sum-of-squares of errors generated from 1) deviation between simulated data and observed data and 2) deviation between observed data and the mean of the observed data (based on the assumption of two degrees of freedom can be adjusted to obtain the simulation data of a variable). It represents how well the model simulation reproduces the experimental data. The closer to 1 the adjusted R^2 value is, the better the model can potentially fit the experimental data.

In this study, both the adjusted R^2 value and the r_p were together considered to compare between the simulation and experimental data because 1) in several occasions the adjusted R^2 value being close to 1 is not necessary to ensure the goodness of fit of the model simulation and 2) the r_p can only indicate whether the simulation data and the experimental data are

correlated, in the other words, whether the model simulations can capture the trend of the experimental data, but not exactly how well the model can reproduce the experimental data. The criterion of r_p being larger than 0.8 indicates a very strong correlation (Evans, 1996), which can imply that the model simulation can reasonably capture the trend of experimental data. There is no critical value for the adjusted R^2; however, in this context, if the model can reasonably reproduce the experimental data, the high adjusted R^2 value (close to 1) is expected; otherwise the model might not well represent the experimental data.

Figure 7.3.1 illustrates the agreement of simulation results with the experimental data of cell growth and death-related variables from the batch and fed-batch cultures. Overall, the model provided a reasonably good reproduction of the experimental data especially for the batch culture as can be seen from the r_p and adjusted R^2 values being close to 1, though there were several situations that the experimental data were quantitatively misestimated. The model appeared to overpredict the viable cell concentration during the early-exponential phase (0 to 24 hours) in both batch and fed-batch cultures (Figure 7.3.1-A). The model could also not well capture the viable cell concentration during the death phase of the both cultures (from 96 hours). For the batch data, the underestimation of viable cell concentration during the death phase could be as a consequence of the overprediction of dead cell concentration as can be seen from Figure 7.3.1-B&C. Although the concentration of ESA cells was overestimated during the death phase in the fed-batch culture (Figure 7.3.1-B&C), the model simulation showed the overprediction of viable cell concentration during the same period. The value of R^2 being equal to -0.863 might reflect this overestimation though the model could capture the trend of the ESA cell concentration. This could be because the net growth rate during the death phase in the fed-batch culture was overpredicted as a result of the feeding of glutamate and other amino acids.

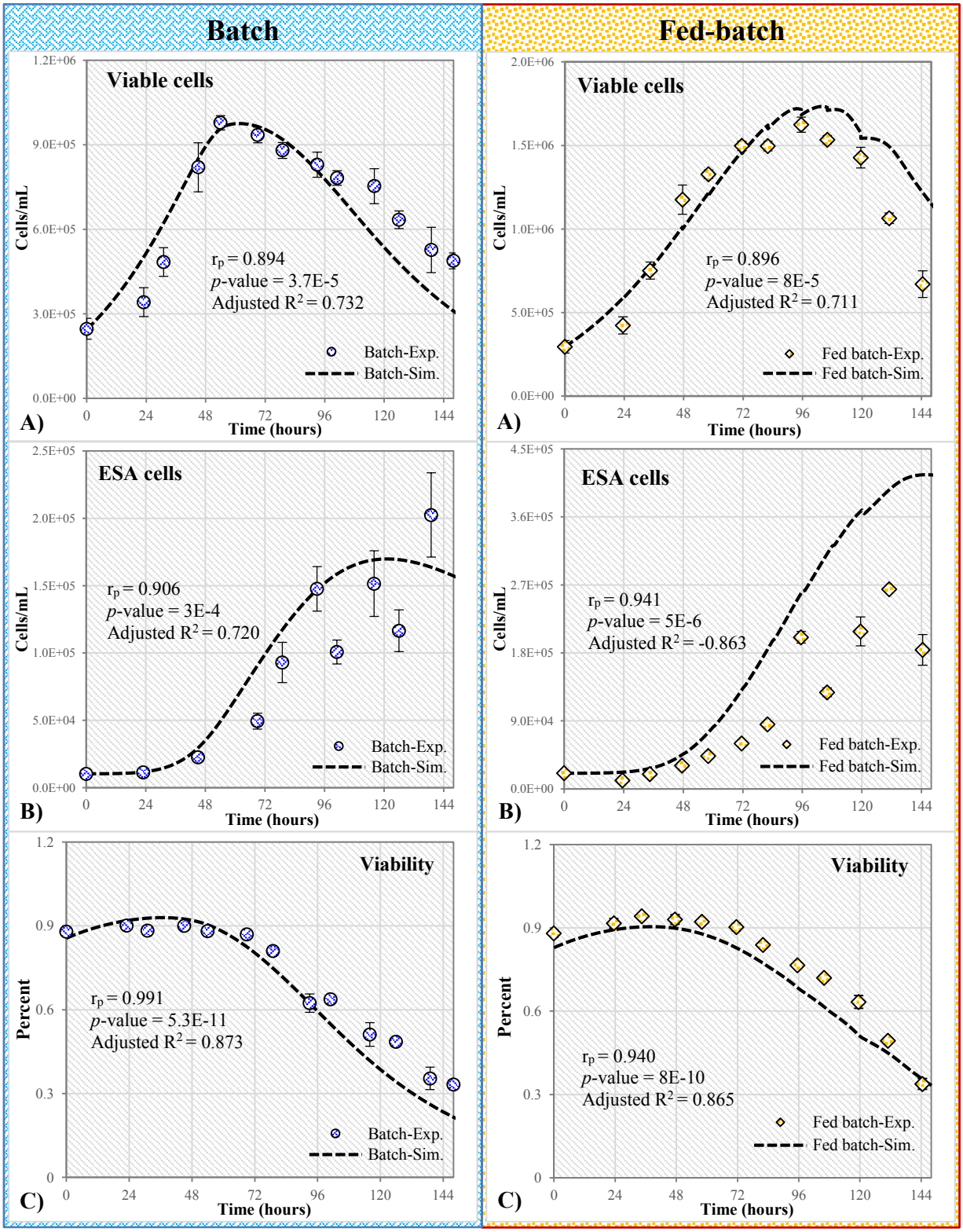


Figure 7.3.1 Model simulation results for (A) viable cell concentration; (B) ESA cell concentration; and (C) viability. The left column represents the batch data and the right column represents the fed-batch data. r_p stands for the Pearson correlation coefficient, *p*-value indicates the probability that the identified correlation might not be existing, and Adjusted R^2 indicates goodness of fit.

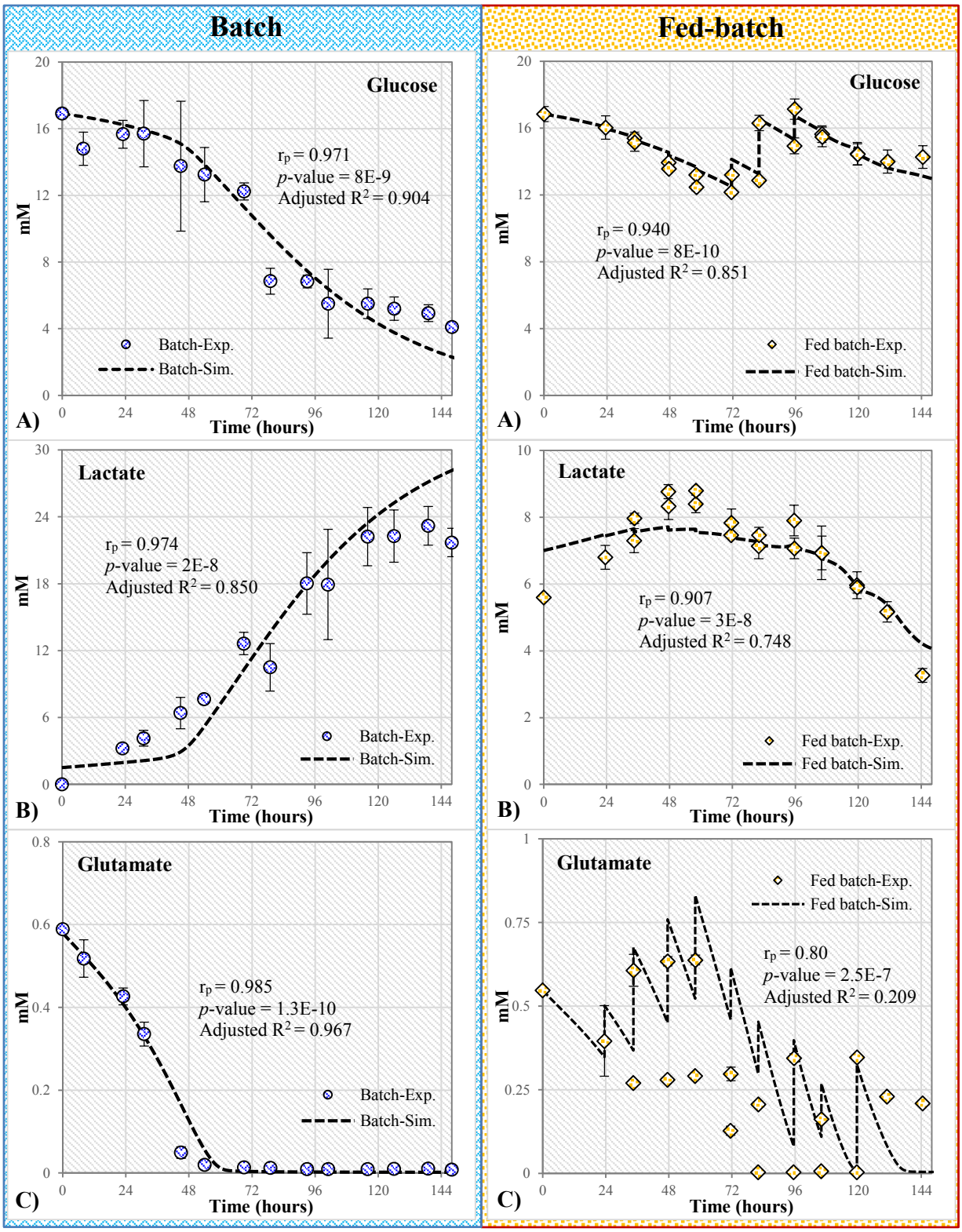


Figure 7.3.2 Model simulation results (A) glucose; (B) lactate; and (C) glutamate concentrations. The left column represents the batch data and the right column represents the fed-batch data. r_p stands for the Pearson correlation coefficient, *p*-value indicates the probability that the identified correlation might not be existing, and Adjusted R^2 indicates goodness of fit.

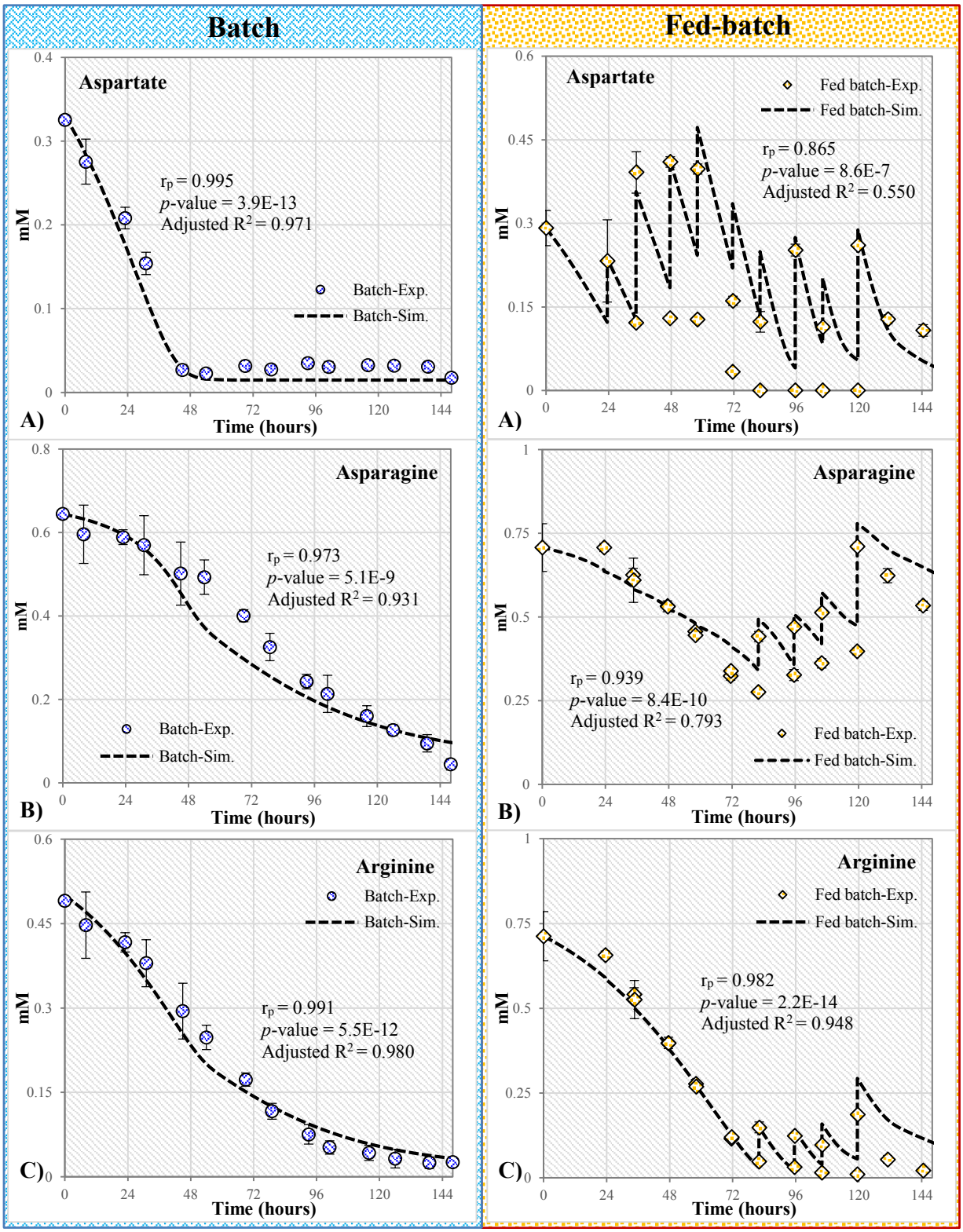


Figure 7.3.3 Model simulation results for (A) aspartate; (B) asparagine; and (C) arginine concentrations. The left column represents the batch data and the right column represents the fed-batch data. r_p stands for the Pearson correlation coefficient, *p*-value indicates the probability that the identified correlation might not be existing, and Adjusted R^2 indicates goodness of fit.

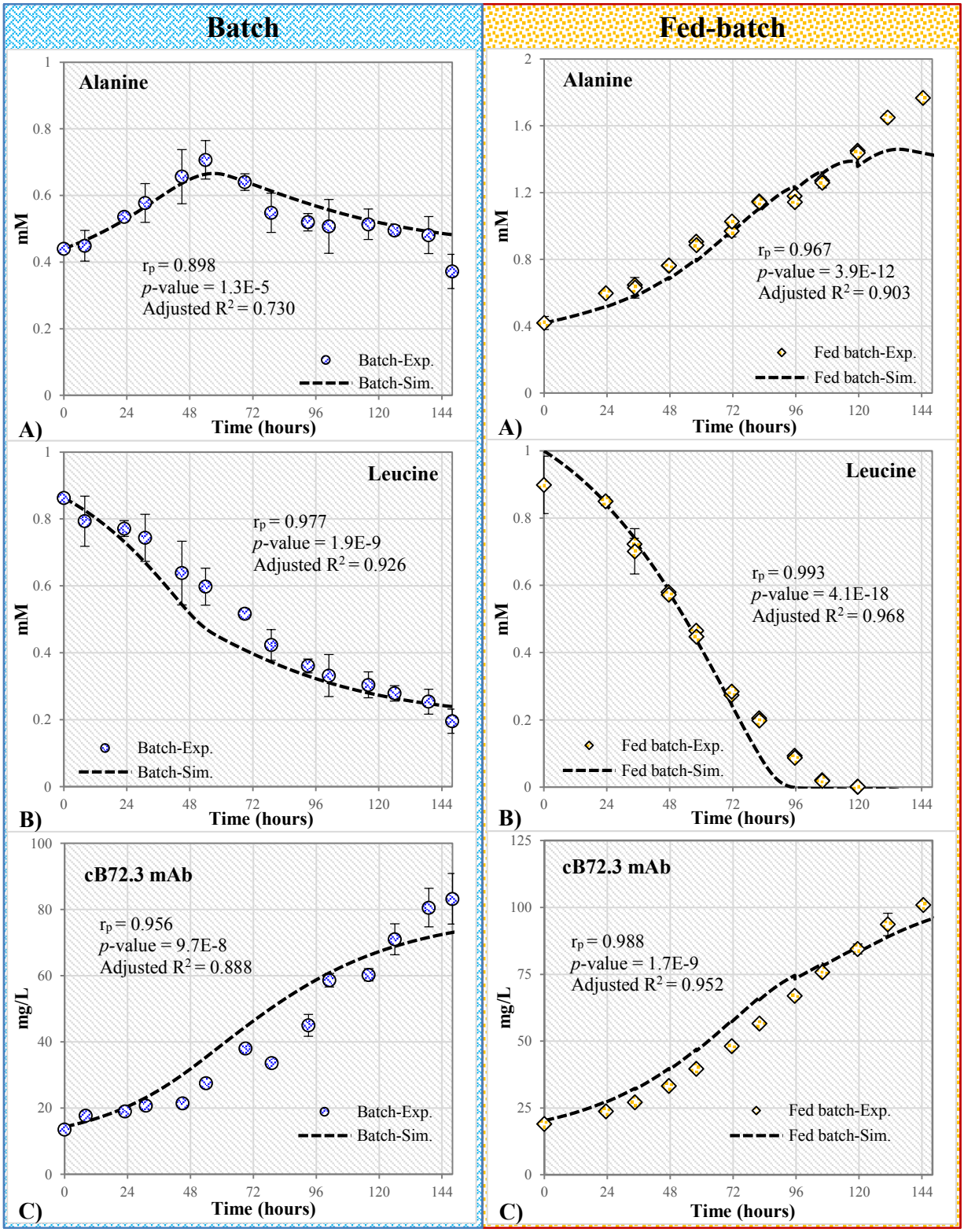


Figure 7.3.4 Model simulation results (A) alanine; (B) leucine; and (C) mAb concentrations. The left column represents the batch data and the right column represents the fed-batch data. r_p stands for the Pearson correlation coefficient, *p*-value indicates the probability that the identified correlation might not be existing, and Adjusted R^2 indicates goodness of fit.

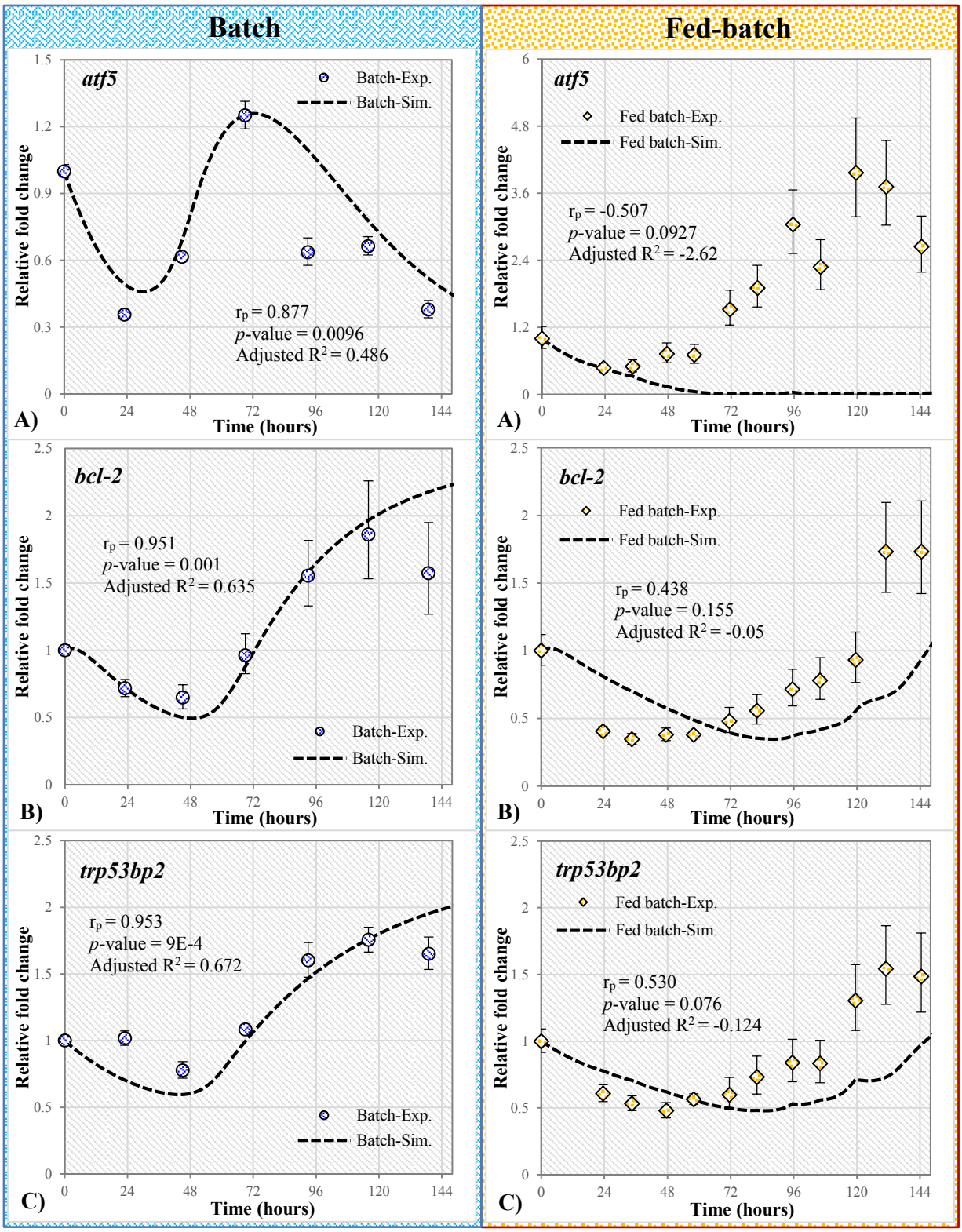


Figure 7.3.5 Model simulation results for (A) *atf5*; (B) *bcl-2*; (C) *trp53bp2*; (D) *casp8*; and (E) *casp3* expressions. The left column represents the batch data and the right column represents the fed-batch data. r_p stands for the Pearson correlation coefficient, *p*-value indicates the probability that the identified correlation might not be existing, and Adjusted R^2 indicates goodness of fit.

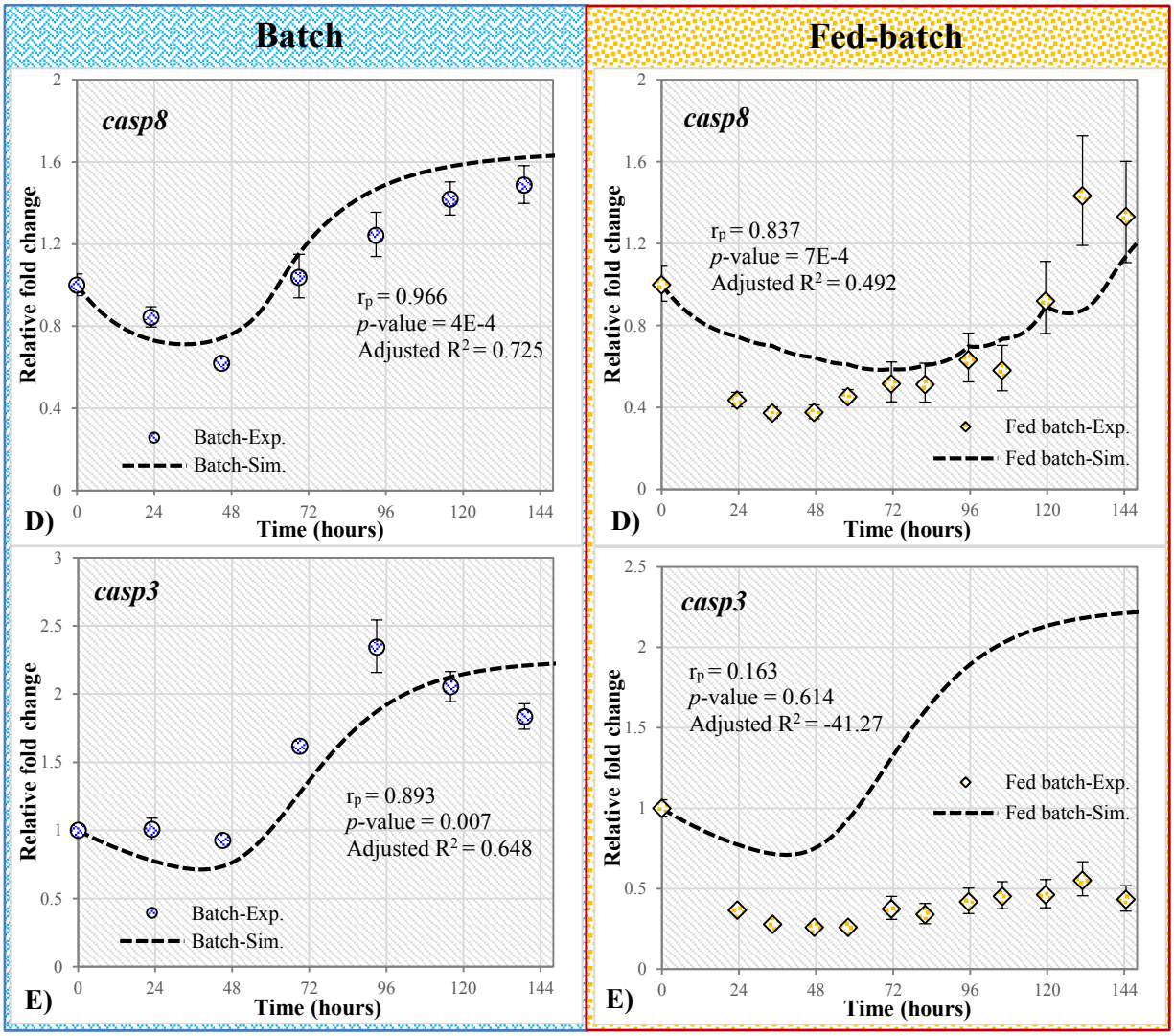


Figure 7.3.5 (continued) Model simulation results for (A) *atf5*; (B) *bcl-2*; (C) *trp53bp2*; (D) *casp8*; and (E) *casp3* expressions. The left column represents the batch data and the right column represents the fed-batch data. r_p stands for the Pearson correlation coefficient, *p*-value indicates the probability that the identified correlation might not be existing, and Adjusted R^2 indicates goodness of fit.

The metabolic profiles in the batch and fed-batch cultures were well reproduced by the model simulations as indicated by the r_p and the adjusted R^2 values being close to 1 as shown in Figure 7.3.2 to 7.3.4. There was a good agreement between the model simulations and the experimental data of glucose and lactate concentrations. It appeared that the concentration profiles of glucose in both batch and fed-batch cultures were well captured (r_p>0.9, Figure

7.3.2-A). In addition, the lactate consumption phase in the fed-batch culture was also reproduced by the model simulation (r_p>0.9, Figure 7.3.2-B). The models' reproduction of glucose and lactate concentrations in the cultures supports the hypothesis that the glucose and lactate consumption were subject to aspartate availability. The simulated profiles of glutamate as well as aspartate concentrations in the fed-batch culture, however, were not quantitatively accurate as reflected by the adjusted R^2 values being relatively lower than those for other metabolites (Figure 7.3.2-C & 7.3.3-A). Compared to the experimental data, they were qualitatively precise (r_p=0.80 for glutamate and r_p=0.865 for aspartate with p<0.05). The underestimation of the net glutamate and aspartate consumption during the fed-batch culture could be further corrected by adjusting the simulated glutamate as well as aspartate fluxes in accordance with the parameter sensitivity data.

As indicated by the r_p and the adjusted R^2 values, the model showed a reasonably good fit for the concentration profiles of asparagine (Figure 7.3.3-B), arginine (Figure 7.3.3-C), alanine (Figure 7.3.4-A) and leucine (Figure 7.3.4-B) in both batch and fed-batch cultures. However, in some circumstance, the simulated data of these amino acid concentration profiles were slightly quantitatively incorrect during the death phase of the fed-batch culture, despite being qualitatively accurate and showing reasonably high values of the adjusted R^2 values. This could be because glutamate consumption was misestimated during the death phase. The simulated concentration profiles of asparagine and leucine appeared to be not quantitatively accurate during the stationary phase of the cultures as a result of the proposed assumptions that 1) the asparagine and leucine consumption rates are enhanced by aspartate exhaustion and leucine availability, respectively. The model provides a good estimation of the cB72.3 mAb concentration profiles in both cultures, indicated by both the r_p and the adjusted R^2 values being very close to 1 (Figure 7.3.4-C).

The profiles of apoptotic gene expression in the batch culture were well captured by the model simulations. However, it appeared that the model relatively failed to reproduce the gene expression profiles in the fed-batch culture. The simulated profile of *atf5* expression (Figure 7.3.4-A) showed a good fit for the batch experimental data ($r_p = 0.88$, the adjusted $R^2 = 0.49$), while it failed to capture the elevated level of the gene expression after the stationary phase of the fed-batch culture. The misestimation in the fed-batch culture was also reflected by the negative values of the r_p and the adjusted R^2 in Figure 7.3.4-A. Given that mathematical expression of the *atf5* expression was assumed to be subject to aspartate deprivation and ER stresses due to mAb synthesis, the simulated *atf5* expression profile was, therefore, down-regulated throughout the culture time as a result of aspartate being excessively fed into the culture.

The simulated expression profiles of *bcl-2*, *trp53bp2* and *casp8* were in good agreement ($r_p>0.9$) with the experimental data of the batch culture (Figure 7.3.4-B, Figure 7.3.4-C and Figure 7.3.5-A, respectively). *bcl-2* and *trp53bp2* might possibly follow the trend of the fed-batch experimental data given their r_p values being between 0.4 and 0.6 (Evans, 1996) as well as the larger than 0.05 *p*-values. In addition, they were not quantitatively accurate as reflected by their adjusted R^2 values being negative. This could be because of the oversimplification of *bcl-2* and *trp53bp2* related interactions/activities for the model construction since these two factors can be also influenced by other cellular signalling pathways. The simulated expression profile of *casp3* showed a relatively good fit for the batch experimental data ($r_p>0.8$ and a high adjusted R^2). However, it did not follow the trend of the experimental data of the fed-batch culture ($r_p=0.163$ and negative adjusted R^2, Figure 7.3.5-B). As discussed in Chapter 6, apoptosis cell death could be triggered independently from the caspase-3 activation under a particular condition probably occurring in the fed-batch culture. Given that apoptosis cell death in this model was assumed to be proportionally correlated with the activation of caspase-3, the

model was therefore not able to represent the circumstance where there was a steady increase in apoptotic cells while there was no caspase-3 activation.

Overall, the simulation results were reasonably acceptable. However, the simulated profiles of apoptotic gene expression were relatively poorer compared to the others, and required to be further refined. GSA was performed in order to provide an insight into model parameter sensitivities, and to allow improving the proposed mathematical model.

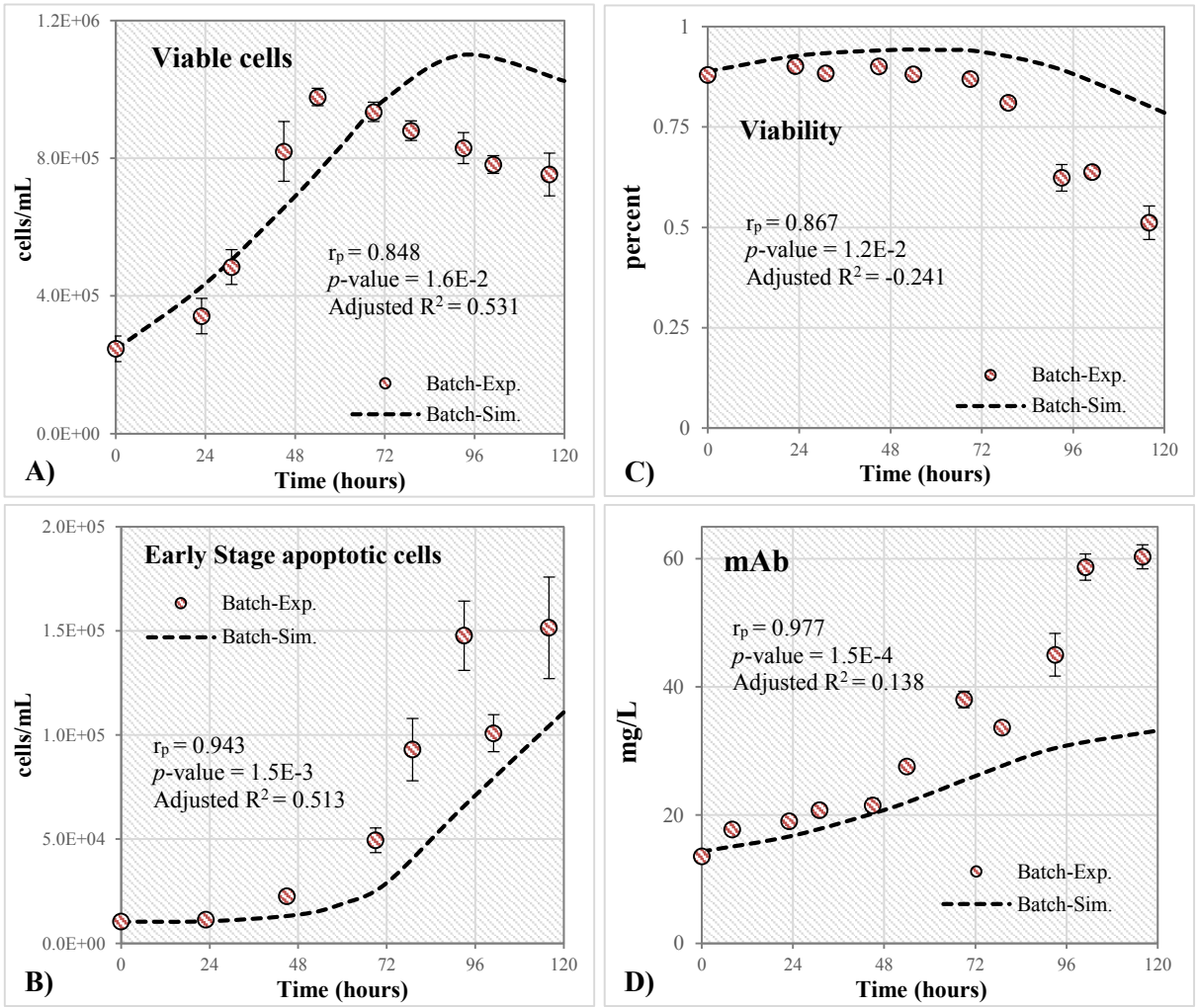


Figure 7.3.6 Model simulation results based on the set of optimal parameter values providing the minimum percentage error for (A) viable cell concentration; (B) ESA cell concentration; (C) viability; and (D) mAb concentration in the batch culture. r_p stands for the Pearson correlation coefficient, *p*-value indicates the probability that the identified correlation might not be existing, and Adjusted R^2 indicates goodness of fit.

Figure 7.3.6 illustrates simulation results from the set of parameter values providing the minimum percent error, which was identified through randomly and simultaneously sampling from the parameter space as described in Section 7.2.4. The values are shown in Table B.4.1 in Appendix B.4 which are within ±60% from the default parameter values. The simulation results for the variables of interest, including viable cells, ESA cells, viability and mAb concentration, capture the trend of the experimental data, as indicated by the correlation coefficient being larger than 0.8. However, it seems that the simulation results show a relatively poorer reproduction of the experimental data given the adjusted R^2. The process of determining the sampled parameter values with the minimum percentage error to the experimental data conducted here was based on only 4 variables and only 7 discrete time points (given the computational expensive and model complexity). This could contribute to the observed misestimation of the experimental data from the simulation with the samples parameter values.

7.3.2 Parameter sensitivities

In order to select significant parameters, a cut-off threshold of total sensitivity (S_{tot}) was pre-specified. The threshold was typically set from 0.01 to 0.1 of S_{tot} (Tang et al., 2007, van Werkhoven et al., 2008, Vanrolleghem et al., 2015). Significant parameters were herein defined as "the ones that contribute to ≥ 10% of total model variability". The following tables show the TSIs of potential parameters with respect to model variables of interest (Table 7.3.1-4), including viable, ESA, and dead cell concentrations, and mAb titre. In addition, the percentage contribution of higher order effects to the S_{tot} of the potential parameters was also included (shown in brackets).

During the exponential phase, it appeared that $\mu_{max,\ glc}$ and $\mu_{max,\ glu}$ are the most significant parameters to the viable cell concentration given these parameter total sensitivities being the highest ones as shown in Table 7.3.1. This was in good agreement with the model

assumption that the cell growth was assumed to be associated with glucose and glutamate. These parameters became less significant over time given the decrease in their S_{tot} while m_{glu} and $Y_{x,\ asp}$ became more significant, suggesting the simulated viable cell density after the exponential phase was also subject to glutamate and aspartate metabolism.

Table 7.3.1 The total sensitivity indices (TSIs) with respect to the viable cell concentration (X_V). The GSA was performed with ±25% simultaneous variation of all parameter values and 100,000 Sobol's sequences. Coloured cells are the parameter sensitivities being over the threshold (≥ 0.1).

S_{tot} (% interaction)		**with respect to viable cell concentration (X_V)**					
Potential significant parameters		**Culture time (hours)**					
		Exponential phase		**Stationary phase**		**Death phase**	
		24	48	60	72	96	120
Cell growth Sub-model	**$\mu_{max,\ glc}$**	**0.42 (0.00)**	**0.29 (0.00)**	**0.17 (0.00)**	**0.10 (0.00)**		
	K_{glc}	0.09 (3.13)	0.09 (2.15)	0.06 (1.22)			
	$\mu_{max,\ glu}$	**0.48 (0.17)**	**0.42 (0.02)**	**0.22 (0.45)**	0.08 (3.89)		
Metabolism Sub-model	**m_{glu}**		0.06 (12.74)	**0.18 (4.26)**	**0.13 (2.37)**		
	$Y_{x,\ asp}$					**0.15 (27.42)**	**0.17 (8.50)**
	$f_{asp,\ asn}$					0.06 (31.19)	0.09 (18.79)
	$Y_{x,\ asn}$						0.05 (69.72)
	$Y_{ala,\ glu}$			0.06 (6.30)			
Apoptosis Sub-model	**$\beta_{mRNA_{trp53bp2}}$**	0.06 (100.0)					

ESA-associated parameters: $\mu_{max,\ ad}$ and K_{casp3}, were found to be sensitive parameters with respect to the ESA cell concentration, as can be seen in Table 7.3.2. These parameters were found significant from the exponential phase until the end of stationary phase, though their sensitivities decreased over time. Parameters that were associated with the activation of

caspase-3: k_{C3} and k_{bax}, were also found significant during the same period. Later, β_{ibax} became significant during the 48 to 72 hours of the culture. At the death phase, the aspartate metabolism-associated parameters, including $Y_{x,\ asp}$ and $f_{asp,\ asn}$, became significant. These results were in agreement with the mathematical model expression for the ESA cell concentration, where the generation rate of ESA cells was assumed to be dependent on caspase-3 activation (Eq. 7.2.9). However, the results suggest that the dependence of ESA cell concentration on the activation of caspase-3 could be at the translational level, rather than the transcriptional level. The significant sensitivities of $Y_{x,\ asp}$ and $f_{asp,\ asn}$ indicate the effect of the aspartate balance on the ESA cell concentration during the death phase, though this effect was greatly contributed by the higher order effects.

The parameters relating to the cell death by other pathways than apoptosis: $\mu_{max,\ nd}$ and K_{lac}, were found significant to the dead cell concentration at 24 hours of the culture (Table 7.3.3). In addition, the lactate production-related parameter, $Y_{lac,\ glc}$, was also a significant parameter. These results were in line with the mathematical expression of the generation of dead cells via other pathways than apoptosis (Eq. 7.2.11), which was assumed to be dependent on lactate concentration. These results also suggest that the generation of dead cells during the beginning of the culture was most likely subject to the cell death via other pathways than apoptosis. However, apoptosis-related parameters, including $\mu_{max,\ ad}$, K_{casp3} and β_{ibax}, became significant after the exponential phase (60 and 72 hours), suggesting the dead cell concentration was later dependent on apoptosis after the exponential phase. $\mu_{max,\ glu}$ was also found significant at the 48 hours of the culture, reflecting that the connection between the dead cell concentration and cell growth.

Table 7.3.2 The total sensitivity indices (TSIs) with respect to the ESA cell concentration (X_{ad}). The GSA was performed with ±25% simultaneous variation of all parameter values and 100,000 Sobol's sequences. Coloured cells are the parameter sensitivities being over the threshold (≥ 0.1).

Stot (% interaction)		**with respect to ESA cell concentration (X_{ad})**					
Potential significant parameters		**Culture time (hours)**					
		Exponential phase		**Stationary phase**		**Death phase**	
		24	48	60	72	96	120
Cell growth Sub-model	**$\mu_{max, glc}$**		0.05 (0.00)	0.07 (0.00)	0.07 (0.00)		
	$\mu_{max, glu}$		0.07 (0.14)	0.09 (0.01)	0.08 (1.66)		
	$\mu_{max, ad}$	**0.25 (0.42)**	**0.17 (1.11)**	**0.14 (1.14)**	**0.10 (0.74)**		
	K_{casp3}	**0.27 (2.40)**	**0.16 (1.85)**	**0.11 (1.38)**	0.07 (0.94)		
	$\mu_{max, d}$				0.07 (2.75)	0.06 (0.34)	
Metabolism Sub-model	**$Y_{x, asp}$**						**0.16 (22.32)**
	$f_{asp, asn}$						**0.10 (39.46)**
	$Y_{x, asn}$						0.09 (83.24)
Apoptosis sub-model	**k_{C3}**	**0.12 (5.06)**	0.09 (3.52)	0.07 (3.10)			
	β_{ibax}	0.08 (15.58)	**0.20 (7.08)**	**0.20 (5.64)**	**0.14 (5.73)**		
	$k_{_bax}$	0.05 (14.13)	0.06 (9.57)				
	k_{bax}	**0.11 (8.59)**	0.08 (6.45)	0.05 (5.20)			

The most significant parameter with respect to the mAb concentration was α_{ab}, which represents the specific rate of mAb synthesis. As can be seen from Table 7.3.4, its sensitivity was the highest since the beginning of the culture until the death phase, though it gradually decreased. In addition, the sensitivities of the growth-related parameters, $\mu_{max, glu}$ and $\mu_{max, glc}$, also contributed to the total variation of mAb concentration during the exponential and stationary phases. $Y_{x, asp}$ was found significant to the mAb titre during the death phase with a

high level of the higher order effects. It is worth noting that the significant sensitivity of $Y_{x,\,asp}$ showed a similar pattern of the TSIs among the observed variables as above shown. This could be inferred that the aspartate balance had a significant effect on these variables as a result of aspartate levels being mathematically linked with the induction of apoptosis as well as glucose and amino acid metabolism.

Table 7.3.3 The total sensitivity indices (TSIs) with respect to the dead cell concentration (X_d). The GSA was performed with ±25% simultaneous variation of all parameter values and 100,000 Sobol's sequences. Coloured cells are the parameter sensitivities being over the threshold (≥ 0.1).

Stot (% interaction)		**with respect to dead cell concentration (X_d)**					
Potential significant parameters		**Culture time (hours)**					
		Exponential phase		**Stationary phase**		**Death phase**	
		24	48	60	72	96	120
Cell growth Sub-model	**$\mu_{max,\,glc}$**	0.06 (0.00)	0.09 (0.00)	0.06 (0.00)			
	$\mu_{max,\,glu}$	0.07 (0.55)	**0.13 (3.46)**	0.09 (0.96)	0.06 (0.32)		
	$\mu_{max,\,ad}$		0.08 (0.68)	**0.12 (0.82)**	**0.14 (0.65)**	**0.11 (0.26)**	
	K_{casp3}		0.08 (6.23)	**0.11 (4.72)**	**0.11 (3.30)**	0.06 (1.46)	
	$\mu_{max,\,nd}$	**0.31 (0.93)**					
	K_{lac}	**0.32 (3.39)**					
Metabolism Sub-model	**$Y_{x,\,glc}$**	0.09 (7.38)					
	$Y_{lac,\,glc}$	**0.16 (7.88)**					
	$Y_{x,\,asp}$		0.06 (22.32)	0.05 (22.32)			**0.11 (36.46)**
	$f_{asp,\,asn}$						0.08 (54.29)
	$Y_{x,\,asn}$						0.09 (84.72)
Apoptosis sub-model	**k_{C3}**		0.05 (14.59)	0.06 (10.66)	0.06 (7.13)		
	β_{ibax}		**0.11 (18.57)**	**0.18 (13.62)**	**0.20 (9.64)**	**0.11 (7.43)**	
	k_{bax}		0.05 (27.70)	0.05 (17.75)			

Table 7.3.4 The total sensitivity indices (TSIs) with respect to the mAb titre (Ab). The GSA was performed with ±25% simultaneous variation of all parameter values and 100,000 Sobol's sequences. Coloured cells are the parameter sensitivities being over the threshold (≥ 0.1).

Stot (% interaction) with respect to mAb concentration (Ab)							
Potential significant parameters		**Culture time (hours)**					
		Exponential phase		**Stationary phase**		**Death phase**	
		24	48	60	72	96	120
Cell growth Sub-model	$\mu_{max,\ glc}$		0.07 (0.00)	0.06 (0.00)			
	$\mu_{max,\ glu}$		**0.10 (0.01)**	0.08 (0.86)			
Metabolism Sub-model	$Y_{x,\ asp}$						**0.12 (21.17)**
	$f_{asp,\ asn}$						0.07 (45.44)
	$Y_{x,\ asn}$						0.08 (82.64)
	α_{ab}	**0.91 (0.17)**	**0.79 (0.52)**	**0.75 (0.56)**	**0.56 (0.49)**	**0.18 (0.13)**	0.07 (13.13)

The further evaluation of parameter sensitivities was performed to take into account the possibilities that the nominal parameter estimates in metabolism and apoptosis sub-models could be containing a relatively higher degree of uncertainty. While keeping the variation degree of the rest of parameters at ±5%, parameters in the metabolism and apoptosis sub-model were varied within ±25% and ±50%, respectively, of their nominal values.

The further analysis showed that $f_{asp,\ asn}$, $Y_{ala,\ glu}$ and $Y_{gln,\ glu}$ were found significant to the viable cell concentration (Table 7.3.5-A), in addition to above discussed ones. The results confirmed that the simulated viable cell concentration was dependent on aspartate and glutamate metabolism in a time-dependent manner, given that these significant parameters were aspartate and glutamate metabolism-associated and they became significant at a different phase of the culture. A number of parameters in apoptosis sub-model were found significant in the further analysis, though their significance was not previously found. It appeared that β_{ibax}

was the most significant parameter with respect to the viable cell concentration given its highest sensitivity over all phases of the culture (Table 7.3.5-B). In addition, $\beta_{iC3,}$ k_{C3} and k_{bax} were also found significant, suggesting that the simulated viable cell concentration during the stationary and death phase was subject to the control of apoptosis at the translational level.

Glutamate metabolism-associated parameters: m_{glu} and $Y_{ala,\ glu}$, were among significant parameters with respect to the ESA cell concentration (Table 7.3.6-A), though they were not previously found significant. This result also indicates the dependence of the ESA cells on the glutamate balance in addition to the aspartate one. Additional significant parameters were found in the apoptosis sub-model, such as β_{iC3} and $k_{_bax}$. Furthermore, their significant sensitivities were observed from the exponential phase until the end of stationary phase or the beginning of dead phase (Table 7.3.6-B), which was different from what was previously showed (Table 7.3.2). These results also confirmed the assumption that the ESA is dependent on the caspase-3 balance. However, it appeared that the Bax-activation was the major route whereby caspase-3 was activated, given the high contribution of Bax activation-related parameters to the model total sensitivities. This might not truly represent the induction of apoptosis in the culture as previously discussed in Chapter 5 and Chapter 6.

The further analysis also showed that $Y_{x,\ glc}$, $Y_{lac,\ glc}$ and $Y_{lac,\ con}$ were among significant parameters to the dead cell concentration during the exponential phase of the culture (Table 7.3.7-A). This complements the above discussed results, suggesting that dead cells were subject to cell death via other pathways than apoptosis (which was assumed to be governed by lactate concentration). In addition, aspartate and glutamate metabolism-related parameters: m_{glu} and $Y_{x,\ asp}$, were also found significant, suggesting the dependence of the dead cell concentration on aspartate and glutamate levels. In addition to β_{ibax}, additional apoptosis-related parameters: β_{iC3}, k_{C3}, $k_{_bax}$, k_{bax} and kb_{ibax}, were found significant (Table 7.3.7-B).

The results from the further evaluation of S_{tot} with respect to the mAb titre was similar to the previous shown result, where α_{ab} was the most significant parameter to the mAb concentration (Table 7.3.8-A). This analysis also showed that β_{iC3}, k_{C3}, k_{bax} and β_{ibax} were significant to the mAb titre (Table 7.3.8-B).

It is worth discussing about the contribution of higher order effects on the S_{tot}. As can be seen from the above shown results, the sensitivities of several significant parameters, such as $Y_{x,\,asp}$, $Y_{x,\,asn}$, $f_{asp,\,asn}$, k_{bax}, k_{bax} and kb_{ibax} contained a large portion of sensitivities contributed by the higher order effects. The parameters with the high percentage parameter interactions (higher order effects) tend to be unidentifiable since the effect of these parameters on a particular model variable can be compensated by the effects of other parameters that these parameters interact with. However, the effect of the parameter interactions must be evaluated based on how significant it is to the model variables. It was suggested that the higher order effects were counted as "significant" if its sensitivities is larger than 0.1 (Vanrolleghem et al., 2015). Therefore, if the higher order effects are found significant, the corresponding parameters will be considered as unidentifiable. In this study, the presented significant parameters, however, contained less than 0.1 total sensitivities of the higher order effects.

Table 7.3.5 The total sensitivity indices (TSIs) with respect to the viable cell concentration: A) ±25% simultaneous variation of metabolism sub-model parameter values while 5% simultaneous variation of the reaming parameter values; and B) ±50% simultaneous variation of apoptosis sub-model parameter values while 5% simultaneous variation of the reaming parameter values. The analysis was performed with 60,000 simulations. Coloured cells are the parameter sensitivities being over the S_{tot} threshold (≥ 0.1).

A)

S_{tot} (% interaction)		**with respect to viable cell concentration (X_V)**					
Potential significant parameters		**Culture time (hours)**					
		Exponential phase		**Stationary phase**		**Death phase**	
		24	48	60	72	96	120
Metabolism Sub-model	$Y_{x,\,glu}$		0.08 (0.62)	0.09 (0.38)	0.07 (0.23)		
	m_{glu}		**0.30 (2.56)**	**0.41 (0.61)**	**0.35 (1.45)**		
	$f_{glu,\,gln}$		0.06 (14.96)	0.07 (3.49)	0.06 (9.65)		
	$Y_{x,\,asp}$					**0.20 (19.20)**	**0.24 (6.76)**
	$Km_{asp,\,asp}$						0.05 (18.18)
	$f_{asp,\,asn}$					**0.10 (28.21)**	**0.13 (18.13)**
	$Y_{x,\,asn}$						0.07 (54.13)
	$Y_{ala,\,glu}$		**0.12 (17.83)**	**0.13 (2.94)**	**0.12 (7.67)**		
	$Y_{gln,\,glu}$		**0.11 (19.55)**	**0.11 (2.12)**	0.09 (6.22)		

B)

S_{tot} (% interaction)		**with respect to viable cell concentration (X_V)**					
Potential significant parameters		**Culture time (hours)**					
		Exponential phase		**Stationary phase**		**Death phase**	
		24	48	60	72	96	120
Apoptosis Sub-model	β_{iC3}			0.07 (3.77)	0.10 (2.63)	**0.14 (1.68)**	**0.19 (1.17)**
	k_{C3}		0.08 (4.61)	**0.11 (4.38)**	**0.13 (4.15)**	**0.11 (1.90)**	0.09 (2.14)
	β_{ibax}		**0.15 (7.09)**	**0.29 (4.87)**	**0.40 (2.85)**	**0.46 (1.03)**	**0.46 (1.97)**
	$k_{_bax}$			0.07 (13.74)	0.08 (10.73)	0.07 (10.96)	0.06 (21.40)
	k_{bax}		0.07 (17.45)	0.09 (13.07)	**0.10 (9.86)**	0.08 (6.04)	0.06 (11.89)
	kb_{ibax}			0.07 (25.24)	0.07 (16.86)	0.08 (6.78)	0.07 (13.54)
	$\beta_{mRNAtrp53\,bp2}$	0.08 (100.0)					

Table 7.3.6 The total sensitivity indices (TSIs) with respect to the ESA cell concentration: A) ±25% simultaneous variation of metabolism sub-model parameter values while 5% simultaneous variation of the reaming parameter values; and B) ±50% simultaneous variation of apoptosis sub-model parameter values while 5% simultaneous variation of the reaming parameter values. The analysis was performed with 60,000 simulations. Coloured cells are the parameter sensitivities being over the S_{tot} threshold (≥ 0.1).

A)

S_{tot} (% interaction)		**with respect to ESA cell concentration (X_{ad})**					
Potential significant parameters		**Culture time (hours)**					
		Exponential phase		**Stationary phase**		**Death phase**	
		24	48	60	72	96	120
Metabolism Sub-model	$Y_{x,\,glu}$			0.06 (0.87)	0.07 (0.36)		
	m_{glu}		0.05 (14.64)	**0.25 (1.80)**	**0.32 (0.77)**		
	$f_{glu,\,ala}$				0.05 (2.03)		
	$Y_{x,\,asp}$						**0.20 (18.86)**
	$Km_{asp,\,asp}$						0.06 (37.98)
	$f_{asp,\,asn}$						**0.13 (18.13)**
	$Y_{x,\,asn}$						0.09 (39.09)
	$Y_{ala,\,glu}$			0.09 (8.34)	**0.11 (2.48)**		
	$Y_{gln,\,glu}$			0.08 (7.99)	0.09 (2.35)		

B)

S_{tot} (% interaction)		**with respect to ESA cell concentration (X_{ad})**					
Potential significant parameters		**Culture time (hours)**					
		Exponential phase		**Stationary phase**		**Death phase**	
		24	48	60	72	96	120
Apoptosis Sub-model	β_{iC3}	0.06 (2.21)	0.09 (2.43)	**0.10 (2.10)**	**0.11 (2.10)**	**0.11 (2.18)**	
	k_{C3}	**0.26 (2.45)**	**0.18 (3.14)**	**0.16 (2.04)**	**0.14 (1.84)**	**0.10 (6.11)**	
	k_{C8}	0.07 (20.31)					
	β_{ibax}	**0.17 (8.79)**	**0.36 (3.41)**	**0.41 (1.15)**	**0.44 (1.00)**	**0.45 (7.54)**	**0.24 (71.64)**
	$k_{_bax}$	**0.13 (21.02)**	**0.11 (12.29)**	**0.10 (9.21)**	0.09 (10.88)	0.08 (32.68)	0.05 (100.0)
	k_{bax}	**0.29 (18.95)**	**0.16 (10.21)**	**0.13 (5.44)**	**0.11 (5.87)**	0.09 (26.02)	0.07 (100.0)
	kb_{ibax}	0.06 (40.70)	0.09 (21.21)	0.08 (10.40)	0.07 (7.15)	0.07 (29.33)	0.07 (100.0)
	$\beta_{mRNAtrp53bp2}$						0.06 (100.0)
	$Km_{atf5,\,bcl2}$	0.06 (99.90)					

Table 7.3.7 The total sensitivity indices (TSIs) with respect to the dead cell concentration: A) ±25% simultaneous variation of metabolism sub-model parameter values while 5% simultaneous variation of the reaming parameter values; and B) ±50% simultaneous variation of apoptosis sub-model parameter values while 5% simultaneous variation of the reaming parameter values. The analysis was performed with 60,000 simulations. Coloured cells are the parameter sensitivities being over the S_{tot} threshold (≥ 0.1).

A)

S_{tot} (% interaction)		**with respect to dead cell concentration (X_d)**					
Potential significant parameters		**Culture time (hours)**					
		Exponential phase		**Stationary phase**		**Death phase**	
		24	48	60	72	96	120
Metabolism Sub-model	$Y_{x,glc}$	**0.35 (0.20)**	**0.17 (0.58)**				
	$Y_{lac,glc}$	**0.35 (1.91)**	**0.23 (1.86)**	**0.10 (2.14)**			
	$Y_{lac,con}$	**0.17 (0.29)**	**0.10 (0.37)**				
	m_{glu}			0.07 (5.47)	**0.15 (2.57)**		
	$Y_{x,asp}$		**0.22 (6.47)**	**0.32 (4.64)**	**0.20 (3.15)**		**0.15 (31.27)**
	$Km_{asp,asp}$						0.05 (51.13)
	$f_{asp,asn}$						**0.12 (53.22)**
	$Y_{x,asn}$						**0.10 (85.76)**
	$Y_{ala,glu}$				0.05 (7.16)		

B)

S_{tot} (% interaction)		**with respect to dead cell concentration (X_d)**					
Potential significant parameters		**Culture time (hours)**					
		Exponential phase		**Stationary phase**		**Death phase**	
		24	48	60	72	96	120
Apoptosis Sub-model	β_{iC3}		0.07 (4.13)	0.09 (3.51)	**0.11 (2.50)**	**0.14 (1.47)**	**0.19 (1.08)**
	k_{C3}	**0.13 (1.18)**	**0.16 (11.05)**	**0.15 (8.80)**	**0.14 (6.26)**	**0.11 (2.88)**	0.09 (2.42)
	β_{ibax}	0.07 (7.06)	**0.33 (15.52)**	**0.39 (10.05)**	**0.43 (5.32)**	**0.47 (1.38)**	**0.46 (1.60)**
	$k_{_bax}$	0.05 (10.59)	**0.13 (31.88)**	**0.11 (23.20)**	0.09 (15.50)	0.07 (11.39)	0.06 (19.32)
	k_{bax}	**0.13 (16.99)**	**0.17 (33.47)**	**0.14 (24.09)**	**0.11 (14.58)**	0.08 (6.20)	0.07 (10.54)
	kb_{ibax}		**0.12 (48.49)**	**0.11 (36.14)**	**0.10 (22.93)**	0.08 (7.51)	0.07 (10.73)

Table 7.3.8 The total sensitivity indices (TSIs) with respect to the mAb concentration: A) ±25% simultaneous variation of metabolism sub-model parameter values while 5% simultaneous variation of the reaming parameter values; and B) ±50% simultaneous variation of apoptosis sub-model parameter values while 5% simultaneous variation of the reaming parameter values. The analysis was performed with 60,000 simulations. Coloured cells are the parameter sensitivities being over the S_{tot} threshold (≥ 0.1).

A)

S_{tot} (% interaction)		**with respect to mAb concentration (mAb)**					
Potential significant parameters		**Culture time (hours)**					
		Exponential phase		**Stationary phase**		**Death phase**	
		24	48	60	72	96	120
Metabolism Sub-model	$Y_{x,asp}$						**0.16 (20.11)**
	$f_{asp,asn}$						**0.10 (46.95)**
	$Y_{x,asn}$						0.08 (86.91)
	α_{ab}	**0.98 (0.01)**	**0.96 (0.03)**	**0.94 (0.08)**	**0.87 (0.13)**	**0.27 (0.34)**	0.09 (16.47)

B)

S_{tot} (% interaction)		**with respect to mAb concentration (mAb)**					
Potential significant parameters		**Culture time (hours)**					
		Exponential phase		**Stationary phase**		**Death phase**	
		24	48	60	72	96	120
Apoptosis Sub-model	β_{iC3}					0.08 (2.91)	**0.12 (1.42)**
	k_{C3}				0.05 (5.86)	**0.10 (3.69)**	**0.10 (2.51)**
	β_{ibax}			0.05 (15.17)	**0.14 (7.52)**	**0.31 (2.73)**	**0.38 (1.29)**
	k_bax					0.06 (9.47)	0.06 (8.82)
	k_{bax}	**0.10 (99.93)**	0.09 (94.06)	**0.10 (80.69)**	**0.10 (61.17)**	**0.10 (33.39)**	0.09 (22.48)
	kb_{ibax}					0.06 (13.40)	0.06 (7.79)

The relation between the other model variables and their corresponding parameters was also revealed. Table 7.3.9 summarises significant and insignificant parameters with respect to corresponding model variables. Generally, most of parameters that were mathematically related to the corresponding variables were found significant as respect to these variables. For example, the yield of cells over glucose ($Y_{x,\,glc}$) and the yield of lactate over glucose ($Y_{lac,\,glc}$) were found significant with respect to glucose and lactate concentrations, respectively. However, there were also parameters that were not found significant to model variables, though they were mathematically associated. For examples, the aspartate and asparagine associated maintenance energy constants (m_{asp} and m_{asn}) were not significant parameters with respect to aspartate and asparagine concentrations, respectively.

The results from GSA pave the way for the further model modification. The identification of significant and insignificant parameters indicate model identifiability. Given that insignificant parameters have minor effect on the model total variation, these parameters tend to be unidentifiable since their estimates can be any values without severely affecting the model output (Ho et al., 2006). Significant parameters are most likely identifiable, nevertheless, some of them could be unidentifiable if they were found to have interactions with other parameters. Further model modifications will be performed in a direction that avoids having unidentifiable parameters in the model. For example, according to the results, the maintenance energy constants (i.e. m_{asp} and m_{asn}) could be considered to be removed or refined. However, this action will have to be justified with the negligible overall effects on the model reproducibility. The GSA will be re-performed for the refined mathematical model.

Table 7.3.9 Significant and insignificant parameters with respect to the corresponding model variables. The parameter significance was judged based on S_{tot} values being larger than 0.1. The S_{tot} was achieved from the further evaluation of parameter sensitivities as discussed earlier.

Model variables		Significant parameters	Insignificant parameters
Metabolism Sub-model	**Glc**	$Y_{x,\,glc}$, $Y_{x,\,asp}$, $Y_{x,\,asn}$, $f_{asp,\,asn}$	$Km_{glc,\,asp}$
	Glu	$Y_{x,\,glu}$, m_{glu}, $Y_{ala,\,glu}$, $Y_{gln,\,glu}$	$f_{glu,\,ala}$, $f_{glu,\,gln}$, $f_{glu,\,asp}$, $f_{glu,\,arg}$, $Km_{glu,\,glu}$
	Gln	m_{glu}, $Y_{ala,\,glu}$, $Y_{x,\,gln}$, $Km_{gln,\,gln}$, $Y_{gln,\,glu}$	$f_{glu,\,gln}$, m_{gln}
	Lac	$Y_{x,\,glc}$, $Y_{lac,\,glc}$, $Y_{lac,\,con}$, $Y_{x,\,asp}$, $Y_{x,\,asn}$, $f_{asp,\,asn}$	$k_{lac,\,con}$
	Asp	$Y_{x,\,asp}$, $Y_{x,\,asn}$, $f_{asp,\,asn}$	$f_{glu,\,asp}$, m_{asp}, $Km_{asp,\,asp}$
	Asn	m_{glu}, $f_{glu,\,gln}$, $Y_{x,\,asp}$, $Y_{x,\,asn}$, $Km_{asn,\,asp}$	m_{asn}
	Arg	m_{glu}, $Y_{x,\,arg}$	$f_{glu,\,arg}$, m_{arg}, $Km_{arg,\,arg}$
	Ala	m_{glu}, $f_{glu,\,gln}$, $Y_{ala,\,glu}$, $Y_{gln,\,glu}$	$Y_{x,\,ala}$, m_{ala}, $Km_{ala,\,glu}$, $f_{glu,\,ala}$
	Leu	$Y_{x,\,leu}$, m_{glu}	m_{leu}, $Km_{leu,\,leu}$
Apoptosis Sub-model	**iCasp3**	β_{iC3}, β_{ibax}, $\beta_{mRNA_{casp3}}$, $Km_{trp53bp2,\,bcl\text{-}2}$	Kb_{iC3}, k_{C3}
	Casp3	β_{iC3}, k_{C3}, β_{ibax}, $k_{_bax}$, k_{bax}, Kb_{ibax}, $\beta_{mRNA_{casp3}}$	Kb_{iC3}
	Casp8	β_{iC8}, Kb_{bcl2}	Kb_{iC8}, k_{C8}
	Bax4	β_{ibax}, $k_{_bax}$, k_{bax}, Kb_{ibax}	-
	iBax	β_{ibax}, k_{bax}, Kb_{ibax}	$k_{_bax}$,
	Bcl2	β_{ibax}, k_{bax}, Kb_{ibax}	β_{bcl2}, Kb_{bcl2}
	$mRNA_{casp3}$	β_{iC3}, β_{ibax}, $\beta_{mRNA_{casp3}}$, $Km_{casp3,\,iC3}$, $\alpha_{mRNA_{casp3}}$	-
	$mRNA_{casp8}$	$\beta_{mRNA_{casp8}}$, $\alpha_{mRNA_{casp8}}$, $Km_{lac,\,trp53bp2}$	$Km_{glu,\,casp8}$
	$mRNA_{bax}$	$\beta_{mRNA_{bax}}$, $Km_{trp53bp2,\,bax}$, $Km_{bcl\text{-}2,\,bax}$, $\alpha_{mRNA_{bax}}$, $\beta_{mRNA_{bcl2}}$	-
	$mRNA_{trp53bp2}$	$\beta_{mRNA_{trp53bp2}}$, $Km_{glu,\,trp53bp2}$ $\alpha_{mRNA_{trp53bp2}}$	$Km_{lac,\,trp53bp2}$
	$mRNA_{bcl2}$	$\beta_{mRNA_{bcl2}}$, $Km_{trp53bp2,\,bcl\text{-}2}$, $\alpha_{mRNA_{bcl2}}$, $\beta_{mRNA_{trp53bp2}}$, $\alpha_{mRNA_{trp53bp2}}$	$Km_{bcl\text{-}2,\,bax}$
	$mRNA_{atf5}$	$\beta_{mRNA_{atf5}}$, $Km_{asp,\,atf5}$, $Km_{ab,\,atf5}$, $\alpha_{mRNA_{atf5}}$	-

7.4 Conclusions

This chapter aims to construct a first-principles and experimentally validated mathematical model for apoptosis in the GS-NS0 cell culture. Apoptosis was, previously and extensively, mathematically modelled; however, its dynamic and mechanistic behaviour as regards relevant cellular processes was not fully described. Our constructed mathematical model demonstrates that the mechanistic understanding of apoptosis and its links to cell growth and metabolism is well incorporated.

The constructed mathematical model consists of three sub-models describing cell growth, metabolism and apoptosis. The cell growth sub-model describes viable, apoptotic, and dead cell balances. Cell growth was assumed to be proportional to glutamate and glucose concentrations while apoptosis cell death was subject to the caspase-3 activation. The cell metabolism sub-model captures glucose and amino acid metabolism. Glucose consumption and the net lactate consumption/production were linked to the amino acid availability. Glutamate was assumed to be converted to glutamine as well as alanine. In the meantime, its production rate was subject to aspartate, alanine, arginine, and glutamine consumption. The synthesis of mAb was assumed to be dependent on asparagine and leucine concentrations. The transcriptional regulation of apoptosis was mathematically described in apoptosis sub-model. The activation of caspase-3 was assumed to be subject to active Bax as well as caspase-8 activation which were also assumed to be governed by their transcriptional activities. The transcription of *casp8*, *trp53bp2* as well as *atf5* with its links to metabolic stresses due to changes in amino acid availability and the mAb synthesis was also included in this sub-model.

The proposed model showed a reasonably good fit for the experimental data from the batch and fed-batch cultures. It reproduced the observed cell growth and death, including viable

cell, ESA cell and dead cell concentrations, as well as glucose and amino acids metabolism over the cultivation period. However, the model provides a relatively pooper reproduction of the transcriptional control of apoptosis in the fed-batch culture given that the fed-batch culture experienced apoptosis in a difference manner to that in the batch culture where the apoptosis mathematical expression was constructed based on. The GSA was performed to reveal relationships between model variables and parameters. Significant parameters were mostly among those corresponding to model variables; $\mu_{max,\ glc}$ and $\mu_{max,\ glu}$ are significant parameters with respect to the viable cell concentration while the ESA and dead cell concentrations are highly dependent on $\mu_{max,\ ad}$, K_{casp3} and μ_{max}. The results from the parameter sensitivity evaluation provide a crucial guide to refine the proposed model structure. Insignificant parameters could be considered to be removed from the mathematical model, though the model reproducibility has to be accordingly evaluated to justify the removal of unnecessary parameters.

Chapter 8

Overall Conclusions and Future Research Directions

8.1 Overall conclusions

8.1.1 Summary of results

In this thesis, a combined computational and experimental approach was adopted to study apoptosis in the culture of GS-NS0 cell line producing cB72.3 mAb. A batch culture experiment was performed in order to pinpoint relationships between the metabolic stresses - which inherently occur in this mode of culture - and apoptosis. Interplay between cell cycle and apoptosis, and its effects on cell growth and metabolism was also explored. In addition, culturing condition studies; temperature shifts and medium content shifts, were conducted in order to investigate effects of these culturing conditions on the induction of apoptosis as well as its association with cell cycle and metabolism. A fed-batch culture experiment was later carried out in accordance with what was observed in the batch cultures. The feeding strategies employed were devised based on the identified limiting nutrients. The fed-batch cultures were aimed to validate experimental phenomena observed in the batch cultures. The fed-batch together with the batch experimental data were then utilised for the development of a mathematical model for apoptosis in mammalian cell cultures. The aim of the mathematical model was to describe the kinetics of growth and metabolism, and its association with the induction of apoptosis at the transcriptional level. Global sensitivity analysis (GSA) was then performed to evaluate model characteristics, and to thus allow further refining the structure of the model.

The observed results from the experiments conducted and the proposed mathematical model are summarised as follows:

- **The batch culture experiment** showed that there was a strong relationship among cell growth (cell cycle), metabolism, and the induction of apoptosis. Aspartate and glutamate were among first nutrients that became exhausted during the culture. It appeared that deprivation of these amino acids triggered metabolic shifts as well as apoptosis, as indicated by the transition from the alanine production phase to the consumption phase, and the simultaneously elevated level of apoptotic gene expressions, respectively. In addition, a relationship between the control of cell cycle and apoptosis was suggested, given that the increase in percentage of G_1/G_0 cells with the elevated *p21* expression level was coincident with the increase in the early stage apoptotic (ESA) cell density. This experiment provides a map of cell proliferation, metabolism and apoptosis for the culture of GS-NS0 cells, indicating metabolic shifts as well as apoptosis and cell cycle-associated events occurring as regards culture phases.
- **The temperature shift experiment** showed that mAb productivity was enhanced in the cultures with the temperature shifts (to both 35°C and 39°C), although there was no significant difference in final mAb titre in the biphasic hypothermic (35°C) culture as compared to the monophasic batch culture at 37°C. It appeared that apoptosis induction and cell growth were delayed by the hypothermic condition, while they were not significantly affected in the biphasic hyperthermic (39°C) culture. In addition, the accumulation of cells at G_2/M cell cycle phase was observed after the temperature shift to the hypothermic condition. Given the delayed apoptosis induction, this supports the hypothesis that cell growth arrest at this phase could be a survival mechanism against apoptosis.
- **The medium content experiment** revealed the effect of medium content variation on the apoptosis induction. It appeared that pro-apoptotic genes, including *trp53bp2*,

casp8 and *casp3*, were up-regulated in the culture using 100% spent medium. The other cultures, which grew cells in the medium containing fractions of fresh medium, showed a higher cell growth and a lower ESA cell fraction, as compared to the 100% conditioned medium culture. The net lactate production was reduced in the culture with the medium containing fractions of conditioned medium, suggesting the presence of possible factors in the conditioned medium that could trigger the metabolic transition from lactate production to consumption. In addition, the observed apoptotic gene expressions and cyclin expression profiles elucidated the relationship between the induction of apoptosis and the control of cell cycle progression in response to the variation in the medium contents.

- **The fed-batch culture experiments** demonstrated that the onset of apoptosis was delayed by the addition of nutrients, including glucose and amino acids. The down-regulated expression of *casp3* was observed in the culture with feeding 4 amino acids: glutamate, aspartate, asparagine and arginine. In addition, *atf5, casp8* and *trp53bp2* expressions were also lower than those in the batch culture especially during the stationary phase of the cultures. Nevertheless, the fed-batch culture eventually underwent apoptosis as indicated by the increase in ESA and drop in viability during the death phase of the culture. This suggests that the addition of these nutrients could help reduce metabolic stresses arising from nutrient deprivation, however it could not completely prevent cells from apoptosis. In addition, the observed apoptosis in the fed-batch culture might progress without caspase-3 activation (as indicated by the down-regulated level of *casp3* expression). It also appeared that the addition of these nutrients triggered lactate consumption, suggesting that changes in the concentration of these nutrients influence the metabolic activities in the TCA cycle.

- **The mathematical model for apoptosis in the GS-NS0 cell culture** captured apoptosis at the transcriptional level with its links to cell growth, death and metabolism. The model was the combination of unstructured and structured sub-models, each of which described 1) cell growth and death, 2) glucose and amino acid metabolism, and 3) the transcriptional control of apoptosis. The model demonstrated a reasonably good reproducibility of the batch and fed-batch experimental data with a preliminary and unoptimised set of parameter estimates. Significant and in significant parameters to model output were identified through GSA. The parameter sensitivity analyses guide further model refinement required for improving model identifiability as well as reproducibility.

8.1.2 Main conclusions

According the results obtained in this study, a number of conclusions can be drawn as follows:

1) The metabolic shifts in the cultures of GS-NS0 cell line are subject to levels of amino acids, especially glutamate and aspartate. The shifts in alanine, lactate and ammonium concentration profiles can be treated as indicators of the change in directions of relevant metabolic fluxes in TCA cycle pathways.
2) The expression level of *atf5* can be treated as an indicator of the presence of metabolic stresses arising from the deprivation of amino acids and cell adaptation. The expression level of *casp3*, in contrast, can partially indicate the activation of apoptosis, given that apoptosis could be observed without the up-regulated level of *caps3*.
3) The delay in apoptosis might not result in enhancing mAb productivity given the observed results in the batch and fed-batch cultures. Nevertheless, the final mAb titre

can be improved because the cultures can achieve a greater number of viable cells and a longer culture period due to the delayed cell death.

4) The temperature shift to a hyperthermic condition can be applied to the culture of GS-NS0 cell line to achieve a higher mAb productivity and final titre. However, the induction of apoptosis can be accelerated as a result of hyperthermia, causing shorter cultivation lifetime and lower viability. Therefore, the multiphasic culture which combines the hyperthermic temperature shift(s) with the hypothermic one(s)-which can prolong culture viability- could help further enhance the final mAb titre as well as mAb productivity.
5) Cells experience adaptation to a lesser degree when they are seeded in the medium that contains a fraction (up to 50% based on the observation) of conditioned medium from previous sub-cultures.
6) Given the observed results in all experiments, a balanced level between apoptosis cell death and cell cycle arrest could be the key to improve mAb productivity. The combination of optimised culture conditions, including culture temperature, medium as well as addition of limiting nutrients, could pave the way for the control of apoptosis in the mammalian cell cultures.
7) The use of GSA can provide model behaviour as well as significance of parameters with respect to model output. Model parameters in the constructed mathematical model are most likely sensitive to their corresponding variables. However, this is not the case for some parameters. These insignificant parameters contribute to unidentifiability of the model and need to be refined.

8.2 Recommendations for future work

Based on the results and conclusions of this thesis, the following suggestions can be made for future research directions.

8.2.1 Experimental investigations

Dynamic profiling of intercellular metabolites involves the quantification of intracellular metabolites of interest over the culture time. The observed results in the batch and fed-batch cultures demonstrated changes in extracellular concentration of glucose and amino acids, and also suggested possible metabolic reactions that could take place intracellularly. Therefore, the dynamic profiles of intracellular nutrient concentrations, such as glucose, lactate, and amino acids, can complement what was experimentally observed in this study, and can also validate the proposed reaction networks, the direction of the reactions, as well as metabolic shifts, as suggested in Chapter 5 & 6. The dynamic profiling of intercellular metabolites can be performed using high-performance liquid chromatography (HPLC) according to the previous studies (Dietmair et al., 2010, Kyriakopoulos et al., 2013).

Quantification of apoptotic proteins is certainly essential for the study of apoptosis given their roles in apoptotic pathways. In this study, transcriptional regulation of apoptosis in response to metabolic stresses was predominantly investigated. Additionally, in the constructed mathematical model, the levels of apoptotic proteins were assumed to be directly dependent on their corresponding gene expressions. Therefore, the quantification of apoptotic proteins can help confirm the effect of metabolic stresses on the induction of apoptosis, and validate the proposed reaction networks among apoptotic genes and proteins as well as the assumptions made for the apoptosis model construction. Apoptotic proteins can be quantified with several analytical techniques, including Flow cytometer, ELISA and Western blotting.

Identification and evaluation of cells death via other pathways than apoptosis can be a major breakthrough in the mammalian cell cultures. This study focused on cell death via apoptosis, however, cells can die via other pathways than apoptosis depending on the culture and physiological conditions. Necrosis is another mode of cell death, which can be recognised by specific morphological and physiological characteristics, such as cell swelling, dilution of cytosols, and loss of cell membrane integrity (Cobb et al., 1996, Lecoeur et al., 2001). It can be induced by non-physiological severe injuries, such as high concentration of toxic metabolites (Singh et al., 1994, Mercille and Massie, 1994a), heat shock, and oxidative stresses (Lecoeur et al., 2001). However, some of its makers are similar to those of late stage apoptosis (LSA), making it difficult to distinguish between them (Darzynkiewicz, 1998, Riccardi and Nicoletti, 2006). In addition, autophagy, which is also considered as a stress-response mechanism, was reported to be induced by glucose and amino acid deprivation (Hwang and Lee, 2008, Glick et al., 2010, Jardon et al., 2012). The role of autophagy still remains inclusive (Ramírez-Peinado et al., 2013, Munoz-Pinedo and Martin, 2014), although it was reported to actually protect cells from apoptosis (Han et al., 2011, Jardon et al., 2012). Previous studies also suggested that there is a strong relationship between cell death (necrosis and apoptosis) and autophagy, and they are actually occurring simultaneously in the culture in order to maintaining systems' homeostasis (Thorburn, 2008). These facts attest the necessity to study, in addition to apoptosis, necrosis and autophagy in the mammalian cell cultures. Given the production of the recombination was enhanced by suppressing autophagy (Jardon et al., 2012), it is interesting to investigate its effect on cell growth and metabolism as well as its association with necrosis and apoptosis.

8.2.2 Mathematical modelling and its applications

Further model refinement is certainly essential for the model development. It will be performed in accordance with the analyses obtained from GSA. The extension of global sensitivity analysis (i.e. identifying higher order terms in details, further exploring parameter sensitivity with respect to all model variables) might be also conducted in order to gain more details of parameter sensitivities and interactions among parameters. The first-principle mathematical model will be refined in a way that 1) unnecessary parameters could be removed, and 2) model identifiability could be improved, while maintaining reasonable model reproducibility.

Model enhancement involves including further relevant cellular processes into the existing mathematical model. In this study, the model focuses on apoptosis and its links to cell growth and metabolism. Cell cycle progression is a basic biological mechanism that underlies cell proliferation. It also has a strong relation to apoptosis, and its regulation has effects on mAb production and mAb quality. The combined cell cycle and apoptosis model can be used for the study of dynamics of interrelation between them, and the investigation of their combined effects on culture viability and productivity.

Parameter estimation and model validation involve iterative steps that are required to assure model validity and predictability. The steps consist of 1) optimal experimental design, 2) experimentation, 3) parameter estimation, and 4) model validity evaluation (Kontoravdi et al., 2010, Kiparissides et al., 2011a). Significant parameters are identified by performing GSA with the refined mathematical model. Based on identified significant parameters and possible variables that can be treated as degrees of freedom (such as feeding volume, feeding time, temperature shift time etc.), an optimally-designed experiment can be computationally generated. The experimentation is conducted in accordance with the designed experiment. The

values of significant parameters are then estimated based on the experimental data obtained from the designed experimentation. The 95% confidence intervals falling within ±10% of the parameter estimates suggest the validity of the model, otherwise the parameter estimates are not considered valid and the whole process will be repeated. The predictability of the validated model can be further checked with independent sets of experiments.

Model-based applications employ the predictive and experimentally-validated mathematical model, which is achieved from the parameter estimation and model validation, to simulate/predict various scenarios in the corresponding biological systems. Process control and optimisation is one of examples of model-based applications. An optimal feeding strategy can be computationally postulated using the model. The model can be also useful for the scale-up of mammalian cell cultures. The information of the difference between lab-scale (250 mL working volume) and large-scale (>10 L working volume) cultures can be achieved through simulations. Finally, automated mammalian cell cultures indeed require optimisation software with a predictive mathematical model in order to real-time generate an optimal strategy to control of culture conditions, such as temperature and feeding schemes, in response to online measurement data.

Bibliography

ABDI, H. & WILLIAMS, L. J. 2010. Newman-Keuls test and Tukey test. *Encyclopedia of Research Design. Thousand Oaks, CA: Sage***,** 1-11.

ABE, T. T. Y. O. A. H. S. K. A. T. O. T. 2001. Accumulation of cell cycle regulatory proteins, p21 and p27, induced after hyperthermia in human glioma cells. *International Journal of Hyperthermia,* 17**,** 499-507.

AGARWAL, M. L., AGARWAL, A., TAYLOR, W. R. & STARK, G. R. 1995. p53 controls both the G2/M and the G1 cell cycle checkpoints and mediates reversible growth arrest in human fibroblasts. *Proceedings of the National Academy of Sciences of the United States of America,* 92**,** 8493-8497.

AGHAMOHSENI, H., OHADI, K., SPEARMAN, M., KRAHN, N., MOO-YOUNG, M., SCHARER, J. M., BUTLER, M. & BUDMAN, H. M. 2014. Effects of nutrient levels and average culture pH on the glycosylation pattern of camelid-humanized monoclonal antibody. *Journal of Biotechnology,* 186**,** 98-109.

AHMAD, I. & HELLEBUST, J. A. 1985. Effects of methionine sulfoximine on growth and nitrogen assimilation of the marine microalga Chlorella autotrophica. *Marine Biology,* 86**,** 85-91.

AL-RUBEAI, M. & EMERY, A. N. 1990. Mechanisms and kinetics of monoclonal antibody synthesis and secretion in synchronous and asynchronous hybridoma cell cultures. *Journal of Biotechnology,* 16**,** 67-85.

AL-RUBEAI, M. & SINGH, R. P. 1998. Apoptosis in cell culture. *Current Opinion in Biotechnology,* 9**,** 152-156.

ALBERTS, B., JOHNSON, A., LEWIS, J., RAFF, M., ROBERTS, K. & WALTER, P. 2002. *Molecular Biology of the Cell,* New York, Garland Science.

ALTAMIRANO, C., BERRIOS, J., VERGARA, M. & BECERRA, S. 2013. Advances in improving mammalian cells metabolism for recombinant protein production. *Electronic Journal of Biotechnology; Vol 16, No 3 (2013)*.

ALVA, N., PALOMEQUE, J., #XFA & CARBONELL, T. 2013. Oxidative Stress and Antioxidant Activity in Hypothermia and Rewarming: Can RONS Modulate the Beneficial Effects of Therapeutic Hypothermia? *Oxidative Medicine and Cellular Longevity,* 2013**,** 10.

AMARAL, J. D., XAVIER, J. M., STEER, C. J. & RODRIGUES, C. M. 2010. The role of p53 in apoptosis. *Discov Med,* 9**,** 145-52.

ANDREWS, J. F. 1968. A mathematical model for the continuous culture of microorganisms utilizing inhibitory substrates. *Biotechnology and Bioengineering,* 10**,** 707-723.

ANTONIEWICZ, M. R. 2013. Dynamic metabolic flux analysis — tools for probing transient states of metabolic networks. *Current Opinion in Biotechnology,* 24**,** 973-978.

ARDEN, N. & BETENBAUGH, M. J. 2004. Life and death in mammalian cell culture: strategies for apoptosis inhibition. *Trends in Biotechnology,* 22**,** 174-180.

ASTLEY, K. & AL-RUBEAI, M. 2008. The role of Bcl-2 and its combined effect with p21CIP1 in adaptation of CHO cells to suspension and protein-free culture. *Applied Microbiology and Biotechnology,* 78**,** 391-399.

ASTLEY, K., NACIRI, M., RACHER, A. & AL-RUBEAI, M. 2007. The role of p21cip1 in adaptation of CHO cells to suspension and protein-free culture. *Journal of Biotechnology,* 130**,** 282-290.

AUGUSTO, E. F. P., BARRAL, M. F. & PICCOLI, R. A. M. 2008. Mathematical models for growth and product synthesis in animal cell culture. *In:* CASTILHO, L. R., MORAES, A. M., AUGUSTO, E. F. P. & BUTLER, M. (eds.) *Animal Cell Technology: From Biopharmaceuticals to Gene Therapy*. Madison Avenue, New York: Taylor & Francis Group.

BAGCI, E. Z., VODOVOTZ, Y., BILLIAR, T. R., ERMENTROUT, G. B. & BAHAR, I. 2006. Bistability in Apoptosis: Roles of Bax, Bcl-2, and Mitochondrial Permeability Transition Pores. *Biophysical Journal,* 90**,** 1546-1559.

BAIK, J. Y., LEE, M. S., AN, S. R., YOON, S. K., JOO, E. J., KIM, Y. H., PARK, H. W. & LEE, G. M. 2006. Initial transcriptome and proteome analyses of low culture temperature-induced expression in CHO cells producing erythropoietin. *Biotechnology and Bioengineering,* 93**,** 361-371.

BALCARCEL, R. R. & STEPHANOPOULOS, G. 2001. Rapamycin reduces hybridoma cell death and enhances monoclonal antibody production. *Biotechnology and Bioengineering,* 76**,** 1-10.

BANIK, G., TODD, P. & KOMPALA, D. 1996. Foreign protein expression from S phase specific promoters in continuous cultures of recombinant CHO cells. *Cytotechnology,* 22**,** 179-184.

BARNABÉ, N. & BUTLER, M. 1994. Effect of temperature on nucleotide pools and monoclonal antibody production in a mouse hybridoma. *Biotechnology and Bioengineering,* 44**,** 1235-1245.

BARNES, L., BENTLEY, C. & DICKSON, A. 2000a. Advances in animal cell recombinant protein production: GS-NS0 expression system. *Cytotechnology,* 32**,** 109-123.

BARNES, L. M., BENTLEY, C. M. & DICKSON, A. J. 2000b. Advances in animal cell recombinant protein production: GS-NS0 expression system. *Cytotechnology,* 32**,** 109-123.

BATT, B. C. & KOMPALA, D. S. 1989. A structured kinetic modeling framework for the dynamics of hybridoma growth and monoclonal antibody production in continuous suspension cultures. *Biotechnology and Bioengineering,* 34**,** 515-531.

BEBBINGTON, C. R., RENNER, G., THOMSON, S., KING, D., ABRAMS, D. & YARRANTON, G. T. 1992. High-Level Expression of a Recombinant Antibody from Myeloma Cells Using a Glutamine Synthetase Gene as an Amplifiable Selectable Marker. *Nat Biotech,* 10**,** 169-175.

BEERE, H. M., WOLF, B. B., CAIN, K., MOSSER, D. D., MAHBOUBI, A., KUWANA, T., TAILOR, P., MORIMOTO, R. I., COHEN, G. M. & GREEN, D. R. 2000. Heat-shock protein 70 inhibits apoptosis by preventing recruitment of procaspase-9 to the Apaf-1 apoptosome. *Nat Cell Biol,* 2**,** 469-475.

BELLMAN, R. & ÅSTRÖM, K. J. 1970. On structural identifiability. *Mathematical Biosciences,* 7**,** 329-339.

BENEDETTI, L., CLAEYS, F., NOPENS, I. & VANROLLEGHEM, P. A. 2011. Assessing the convergence of LHS Monte Carlo simulations of wastewater treatment models. *Water Sci Technol,* 63**,** 2219-24.

BENTELE, M., LAVRIK, I., ULRICH, M., STÖßER, S., HEERMANN, D. W., KALTHOFF, H., KRAMMER, P. H. & EILS, R. 2004. Mathematical modeling reveals threshold mechanism in CD95-induced apoptosis. *The Journal of Cell Biology,* 166**,** 839-851.

BI, J.-X., SHUTTLEWORTH, J. & AL-RUBEAI, M. 2004. Uncoupling of cell growth and proliferation results in enhancement of productivity in p21CIP1-arrested CHO cells. *Biotechnology and Bioengineering,* 85**,** 741-749.

BIBILA, T. & FLICKINGER, M. C. 1991. A structured model for monoclonal antibody synthesis in exponentially growing and stationary phase hybridoma cells. *Biotechnology and Bioengineering,* 37**,** 210-226.

BISSONNETTE, N. & HUNTING, D. J. 1998. p21-induced cycle arrest in G1 protects cells from apoptosis induced by UV-irradiation or RNA polymerase II blockage. *Oncogene,* 16**,** 3461-9.

BLOEMKOLK, J.-W., GRAY, M. R., MERCHANT, F. & MOSMANN, T. R. 1992. Effect of temperature on hybridoma cell cycle and MAb production. *Biotechnology and Bioengineering,* 40**,** 427-431.

BOLLATI-FOGOLÍN, M., FORNO, G., NIMTZ, M., CONRADT, H. S., ETCHEVERRIGARAY, M. & KRATJE, R. 2005. Temperature Reduction in Cultures of hGM-CSF-expressing CHO Cells: Effect on Productivity and Product Quality. *Biotechnology Progress,* 21**,** 17-21.

BOMMIASAMY, H., BACK, S. H., FAGONE, P., LEE, K., MESHINCHI, S., VINK, E., SRIBURI, R., FRANK, M., JACKOWSKI, S., KAUFMAN, R. J. & BREWER, J. W. 2009. ATF6α induces XBP1-independent expansion of the endoplasmic reticulum. *Journal of Cell Science,* 122**,** 1626-1636.

BORYS, M. C., LINZER, D. I. H. & PAPOUTSAKIS, E. T. 1994. Ammonia affects the glycosylation patterns of recombinant mouse placental lactogen-I by chinese hamster ovary cells in a pH-dependent manner. *Biotechnology and Bioengineering,* 43**,** 505-514.

BREE, M. A., DHURJATI, P., GEOGHEGAN, R. F. & ROBNETT, B. 1988. Kinetic modelling of hybridoma cell growth and immunoglobulin production in a large-scale suspension culture. *Biotechnology and Bioengineering,* 32**,** 1067-1072.

BROGNARD, J., CLARK, A. S., NI, Y. & DENNIS, P. A. 2001. Akt/Protein Kinase B Is Constitutively Active in Non-Small Cell Lung Cancer Cells and Promotes Cellular Survival and Resistance to Chemotherapy and Radiation. *Cancer Research,* 61**,** 3986-3997.

BROWN, M., RENNER, G., FIELD, R. & HASSELL, T. 1992. Process development for the production of recombinant antibodies using the glutamine synthetase (GS) system. *Cytotechnology,* 9**,** 231-236.

BROWNE, S. & AL-RUBEAI, M. 2011a. Defining viability in mammalian cell cultures. *Biotechnology Letters,* 33**,** 1745-1749.

BROWNE, S. M. & AL-RUBEAI, M. 2011b. Analysis of an artificially selected GS-NS0 variant with increased resistance to apoptosis. *Biotechnology and Bioengineering,* 108**,** 880-892.

BRUEY, J.-M., DUCASSE, C., BONNIAUD, P., RAVAGNAN, L., SUSIN, S. A., DIAZ-LATOUD, C., GURBUXANI, S., ARRIGO, A.-P., KROEMER, G., SOLARY, E. & GARRIDO, C. 2000. Hsp27 negatively regulates cell death by interacting with cytochrome c. *Nat Cell Biol,* 2**,** 645-652.

BRUGAROLAS, J., MOBERG, K., BOYD, S. D., TAYA, Y., JACKS, T. & LEES, J. A. 1999. Inhibition of cyclin-dependent kinase 2 by p21 is necessary for retinoblastoma protein-mediated G1 arrest after γ-irradiation. *Proceedings of the National Academy of Sciences,* 96**,** 1002-1007.

BUCHER, J., RIEDMAIER, S., SCHNABEL, A., MARCUS, K., VACUN, G., WEISS, T., THASLER, W., NUSSLER, A., ZANGER, U. & REUSS, M. 2011. A systems biology approach to dynamic modeling and inter-subject variability of statin pharmacokinetics in human hepatocytes. *BMC Systems Biology,* 5**,** 66.

BUELL, D. N. & FAHEY, J. L. 1969. Limited periods of gene expression in immunoglobulin-synthesizing cells. *Science,* 164**,** 1524-5.

BUNZ, F., DUTRIAUX, A., LENGAUER, C., WALDMAN, T., ZHOU, S., BROWN, J. P., SEDIVY, J. M., KINZLER, K. W. & VOGELSTEIN, B. 1998. Requirement for p53 and p21 to Sustain G2 Arrest After DNA Damage. *Science,* 282**,** 1497-1501.

BUSS, N. A. P. S., HENDERSON, S. J., MCFARLANE, M., SHENTON, J. M. & DE HAAN, L. 2012. Monoclonal antibody therapeutics: history and future. *Current Opinion in Pharmacology,* 12**,** 615-622.

CARMODY, R. J. & COTTER, T. G. 2000. Oxidative stress induces caspase-independent retinal apoptosis in vitro. *Cell Death Differ,* 7**,** 282-91.

CARRILLO-COCOM, L. M., GENEL-REY, T., ARAÍZ-HERNÁNDEZ, D., LÓPEZ-PACHECO, F., LÓPEZ-MEZA, J., ROCHA-PIZAÑA, M. R., RAMÍREZ-MEDRANO, A. & ALVAREZ, M. M. 2014. Amino acid consumption in naïve and recombinant CHO cell cultures: producers of a monoclonal antibody. *Cytotechnology***,** 1-12.

CATZ, S. D. & JOHNSON, J. L. 2001. Transcriptional regulation of bcl-2 by nuclear factor kappa B and its significance in prostate cancer. *Oncogene,* 20**,** 7342-51.

CAZZALINI, O., SCOVASSI, A. I., SAVIO, M., STIVALA, L. A. & PROSPERI, E. 2010. Multiple roles of the cell cycle inhibitor p21CDKN1A in the DNA damage response. *Mutation Research/Reviews in Mutation Research,* 704**,** 12-20.

CHAN, K., SALTELLI, A. & TARANTOLA, S. 1997. Sensitivity Analysis Of Model Output: Variance-based Methods Make The Difference. *In:* SALTELLI, A. &

TARANTOLA, S., eds., 1997. Proceedings of the 1997 Winter Simulation Conference, 261-268.

CHAPPELL, M. J. & GODFREY, K. R. 1992. Structural identifiability of the parameters of a nonlinear batch reactor model. *Mathematical Biosciences,* 108**,** 241-251.

CHARBONNEAU, J. & GAUTHIER, E. 2000. Prolongation of murine hybridoma cell survival in stationary batch culture by Bcl-xL expression. *Cytotechnology,* 34**,** 131-139.

CHARRIER-SAVOURNIN, F. B., CHÂTEAU, M.-T., GIRE, V., SEDIVY, J., PIETTE, J. & DULIĆ, V. 2004. p21-Mediated Nuclear Retention of Cyclin B1-Cdk1 in Response to Genotoxic Stress. *Molecular Biology of the Cell,* 15**,** 3965-3976.

CHEE FURNG WONG, D., TIN KAM WONG, K., TANG GOH, L., KIAT HENG, C. & GEK SIM YAP, M. 2005. Impact of dynamic online fed-batch strategies on metabolism, productivity and N-glycosylation quality in CHO cell cultures. *Biotechnology and Bioengineering,* 89**,** 164-177.

CHEN, C., CUI, J., LU, H., WANG, R., ZHANG, S. & SHEN, P. 2007. Modeling of the Role of a Bax-Activation Switch in the Mitochondrial Apoptosis Decision. *Biophysical Journal,* 92**,** 4304-4315.

CHEN, P. & HARCUM, S. W. 2006. Effects of elevated ammonium on glycosylation gene expression in CHO cells. *Metabolic Engineering,* 8**,** 123-132.

CHEN, T., ZHOU, Y. & TAN, W.-S. 2009. Influence of lactic acid on the proliferation, metabolism, and differentiation of rabbit mesenchymal stem cells. *Cell Biology and Toxicology,* 25**,** 573-586.

CHEN, W. W., NIEPEL, M. & SORGER, P. K. 2010. Classic and contemporary approaches to modeling biochemical reactions. *Genes & Development,* 24**,** 1861-1875.

CHO, K.-H., SHIN, S.-Y., KOLCH, W. & WOLKENHAUER, O. 2003. Experimental Design in Systems Biology, Based on Parameter Sensitivity Analysis Using a Monte Carlo Method: A Case Study for the TNFα-Mediated NF-κ B Signal Transduction Pathway. *SIMULATION,* 79**,** 726-739.

CHOI, Y., LEE, D., KIM, I., KIM, H., PARK, H., CHOE, T. & KIM, I.-H. 2007. Enhancement of erythropoietin production in recombinant Chinese hamster ovary cells by sodium lactate addition. *Biotechnology and Bioprocess Engineering,* 12**,** 60-72.

CHONG, S. L., MOU, D. G., ALI, A. M., LIM, S. H. & TEY, B. T. 2008. Cell growth, cell-cycle progress, and antibody production in hybridoma cells cultivated under mild hypothermic conditions. *Hybridoma (Larchmt),* 27**,** 107-11.

CHU, L. & ROBINSON, D. K. 2001. Industrial choices for protein production by large-scale cell culture. *Current Opinion in Biotechnology,* 12**,** 180-187.

CLANCY, S. 2008a. DNA transcription. *Nature Education,* 1**,** 41.

CLANCY, S. 2008b. RNA splicing: introns, exons and spliceosome. *Nature Education,* 1**,** 31.

COBB, J. P., HOTCHKISS, R. S., KARL, I. E. & BUCHMAN, T. G. 1996. Mechanisms of cell injury and death. *British Journal of Anaesthesia,* 77**,** 3-10.

COBELLI, C., LEPSCHY, A. & JACUR, G. R. 1979. Identifiability of compartmental systems and related structural properties. *Mathematical Biosciences,* 44**,** 1-18.

COCKETT, M. I., BEBBINGTON, C. R. & YARRANTON, G. T. 1990. High level expression of tissue inhibitor of metalloproteinases in Chinese hamster ovary cells using glutamine synthetase gene amplification. *Biotechnology (N Y),* 8**,** 662-7.

COLCHER, D., MILENIC, D., ROSELLI, M., RAUBITSCHEK, A., YARRANTON, G., KING, D., ADAIR, J., WHITTLE, N., BODMER, M. & SCHLOM, J. 1989. Characterization and Biodistribution of Recombinant and Recombinant/Chimeric Constructs of Monoclonal Antibody B72.3. *Cancer Research,* 49**,** 1738-1745.

COLLINS, J. A., SCHANDL, C. A., YOUNG, K. K., VESELY, J. & WILLINGHAM, M. C. 1997. Major DNA Fragmentation is a Late Event in Apoptosis. *Journal of Histochemistry & Cytochemistry,* 45**,** 923-934.

COLUSSI, P. A., HARVEY, N. L., SHEARWIN-WHYATT, L. M. & KUMAR, S. 1998. Conversion of Procaspase-3 to an Autoactivating Caspase by Fusion to the Caspase-2 Prodomain. *Journal of Biological Chemistry,* 273**,** 26566-26570.

CONTOIS, D. E. 1959. Kinetics of Bacterial Growth: Relationship between Population Density and Specific Growth Rate of Continuous Cultures. *Journal of General Microbiology,* 21**,** 40-50.

COQUERET, O. 2002. Linking cyclins to transcriptional control. *Gene,* 299**,** 35-55.

COTTER, T. G. & MARTIN, S. J. 1996. *Techniques in apoptosis: a user's guide*, Portland.

CRESCENZI, E., SANNINO, M., TONZIELLO, G. & PALUMBO, G. 2002. Association of Bcl-2 with Cyclin A/Cdk-2 Complex and Its Effects on Cdk-2 Activity. *Annals of the New York Academy of Sciences,* 973**,** 268-271.

CRUZ, H. J., FERREIRA, A. S., FREITAS, C. M., MOREIRA, J. L. & CARRONDO, M. J. T. 1999. Metabolic responses to different glucose and glutamine levels in baby hamster kidney cell culture. *Applied Microbiology and Biotechnology,* 51**,** 579-585.

CRUZ, H. J., FREITAS, C. M., ALVES, P. M., MOREIRA, J. L. & CARRONDO, M. J. T. 2000. Effects of ammonia and lactate on growth, metabolism, and productivity of BHK cells. *Enzyme and Microbial Technology,* 27**,** 43-52.

CUDNA, R. E. & DICKSON, A. J. 2006. Engineering responsiveness to cell culture stresses: Growth arrest and DNA damage gene 153 (GADD153) and the unfolded protein response (UPR) in NS0 myeloma cells. *Biotechnology and Bioengineering,* 94**,** 514-521.

CUI, J., CHEN, C., LU, H., SUN, T. & SHEN, P. 2008. Two Independent Positive Feedbacks and Bistability in the Bcl-2 Apoptotic Switch. *PLoS ONE,* 3**,** e1469.

CUMMINGS, B. S., KINSEY, G. R., BOLCHOZ, L. J. C. & SCHNELLMANN, R. G. 2004. Identification of Caspase-Independent Apoptosis in Epithelial and Cancer Cells. *Journal of Pharmacology and Experimental Therapeutics,* 310**,** 126-134.

DADEHBEIGI, N. & DICKSON, A. J. 2015. Chemical manipulation of the mTORC1 pathway in industrially relevant CHOK1 cells enhances production of therapeutic proteins. *Biotechnology Journal,* 10**,** 1041-1050.

DAHIRU, T. 2008. P – VALUE, A TRUE TEST OF STATISTICAL SIGNIFICANCE? A CAUTIONARY NOTE. *Annals of Ibadan Postgraduate Medicine,* 6**,** 21-26.

DALILI, M., SAYLES, G. D. & OLLIS, D. F. 1990. Glutamine-limited batch hybridoma growth and antibody production: Experiment and model. *Biotechnology and Bioengineering,* 36**,** 74-82.

DARZYNKIEWICZ, Z. 1998. Analysis of cell death by flow cytometry. *In:* STUDZINSKI, G. P. (ed.) *Cell growth and apoptosis: a practical approach.* IRL Press at Oxford University Press.

DAVIS, C. G., GALLO, M. L. & CORVALAN, J. R. 1999. Transgenic mice as a source of fully human antibodies for the treatment of cancer. *Cancer Metastasis Rev,* 18**,** 421-5.

DE TREMBLAY, M., PERRIER, M., CHAVARIE, C. & ARCHAMBAULT, J. 1992. Optimization of fed-batch culture of hybridoma cells using dynamic programming: single and multi feed cases. *Bioprocess Engineering,* 7**,** 229-234.

DE WILDE, K., DE BUCK, S., VANNESTE, K. & DEPICKER, A. 2013. Recombinant Antibody Production in Arabidopsis Seeds Triggers an Unfolded Protein Response. *Plant Physiology,* 161**,** 1021-1033.

DEGENRING, D., FROEMEL, C., DIKTA, G. & TAKORS, R. 2004. Sensitivity analysis for the reduction of complex metabolism models. *Journal of Process Control,* 14**,** 729-745.

DEMPSEY, J., RUDDOCK, S., OSBORNE, M., RIDLEY, A., STURT, S. & FIELD, R. 2003. Improved Fermentation Processes for NS0 Cell Lines Expressing Human Antibodies and Glutamine Synthetase. *Biotechnology Progress,* 19**,** 175-178.

DHANASEKARAN, D. N. & REDDY, E. P. 2008. JNK signaling in apoptosis. *Oncogene,* 27**,** 6245-6251.

DI GIACOMO, C., SORRENTI, V., ACQUAVIVA, R., CAMPISI, A., VANELLA, G., PEREZ-POLO, J. R. & VANELLA, A. 1997. Ornithine decarboxylase activity in cerebral post-ischemic reperfusion damage: effect of methionine sulfoximine. *Neurochem Res,* 22**,** 1145-50.

DIETMAIR, S., TIMMINS, N. E., GRAY, P. P., NIELSEN, L. K. & KRÖMER, J. O. 2010. Towards quantitative metabolomics of mammalian cells: Development of a metabolite extraction protocol. *Analytical Biochemistry,* 404**,** 155-164.

DISTEFANO, D. J., MARK, G. E. & ROBINSON, D. K. 1996. Feeding of nutrients delays apoptotic death in fed-batch cultures of recombinant NSO myeloma cells. *Biotechnology Letters,* 18**,** 1067-1072.

DLUZEN, D., LI, G., TACELOSKY, D., MOREAU, M. & LIU, D. X. 2011. BCL-2 Is a Downstream Target of ATF5 That Mediates the Prosurvival Function of ATF5 in a Cell Type-dependent Manner. *Journal of Biological Chemistry,* 286**,** 7705-7713.

DODD, K. M. & TEE, A. R. 2012. Leucine and mTORC1: a complex relationship. *American Journal of Physiology - Endocrinology and Metabolism,* 302**,** E1329-E1342.

DODGE, T. C., JI, G.-Y. & HU, W.-S. 1987. Loss of viability in hybridoma cell culture—A kinetic study. *Enzyme and Microbial Technology,* 9**,** 607-611.

DORAI, H., ELLIS, D., KEUNG, Y. S., CAMPBELL, M., ZHUANG, M., LIN, C. & BETENBAUGH, M. J. 2010. Combining high-throughput screening of caspase activity with anti-apoptosis genes for development of robust CHO production cell lines. *Biotechnology Progress,* 26**,** 1367-1381.

DORAI, H., KYUNG, Y. S., ELLIS, D., KINNEY, C., LIN, C., JAN, D., MOORE, G. & BETENBAUGH, M. J. 2009. Expression of anti-apoptosis genes alters lactate metabolism of Chinese Hamster Ovary cells in culture. *Biotechnology and Bioengineering,* 103**,** 592-608.

DRESIOS, J., ASCHRAFI, A., OWENS, G. C., VANDERKLISH, P. W., EDELMAN, G. M. & MAURO, V. P. 2005. Cold stress-induced protein Rbm3 binds 60S ribosomal subunits, alters microRNA levels, and enhances global protein synthesis. *Proceedings of the National Academy of Sciences of the United States of America,* 102**,** 1865-1870.

DUAN, H., CHINNAIYAN, A. M., HUDSON, P. L., WING, J. P., HE, W.-W. & DIXIT, V. M. 1996. ICE-LAP3, a Novel Mammalian Homologue of the Caenorhabditis elegans Cell Death Protein Ced-3 Is Activated during Fas- and Tumor Necrosis Factor-induced Apoptosis. *Journal of Biological Chemistry,* 271**,** 1621-1625.

DUARTE, T. M., CARINHAS, N., BARREIRO, L. C., CARRONDO, M. J. T., ALVES, P. M. & TEIXEIRA, A. P. 2014. Metabolic responses of CHO cells to limitation of key amino acids. *Biotechnology and Bioengineering,* 111**,** 2095-2106.

DUDGEON, C., QIU, W., SUN, Q., ZHANG, L. & YU, J. 2009. Transcriptional Regulation of Apoptosis. *In:* DONG, Z. & YIN, X.-M. (eds.) *Essentials of Apoptosis.* Humana Press.

DUVAL, D., DEMANGEL, C., MIOSSEC, S. & GEAHEL, I. 1992. Role of Metabolic Waste Products in the Control of Cell Proliferation and Antibody Production by Mouse Hybridoma Cells. *Hybridoma,* 11**,** 311-322.

EARLY, P., ROGERS, J., DAVIS, M., CALAME, K., BOND, M., WALL, R. & HOOD, L. 1980. Two mRNAs can be produced from a single immunoglobulin μ gene by alternative RNA processing pathways. *Cell,* 20**,** 313-319.

EDROS, R., MCDONNELL, S. & AL-RUBEAI, M. 2014. The relationship between mTOR signalling pathway and recombinant antibody productivity in CHO cell lines. *BMC Biotechnology,* 14**,** 1-10.

EISSING, T., CONZELMANN, H., GILLES, E. D., ALLGÖWER, F., BULLINGER, E. & SCHEURICH, P. 2004. Bistability Analyses of a Caspase Activation Model for Receptor-induced Apoptosis. *Journal of Biological Chemistry,* 279**,** 36892-36897.

EL-DEIRY, W. S., HARPER, J. W., O'CONNOR, P. M., VELCULESCU, V. E., CANMAN, C. E., JACKMAN, J., PIETENPOL, J. A., BURRELL, M., HILL, D. E., WANG, Y., WIMAN, K. G., MERCER, W. E., KASTAN, M. B., KOHN, K. W., ELLEDGE, S. J., KINZLER, K. W. & VOGELSTEIN, B. 1994. WAF1/CIP1 Is Induced in p53-mediated G1 Arrest and Apoptosis. *Cancer Research,* 54**,** 1169-1174.

ELVIN, J. G., COUSTON, R. G. & VAN DER WALLE, C. F. 2013. Therapeutic antibodies: Market considerations, disease targets and bioprocessing. *International Journal of Pharmaceutics,* 440**,** 83-98.

ERGULER, K., PIERI, M. & DELTAS, C. 2013. A mathematical model of the unfolded protein stress response reveals the decision mechanism for recovery, adaptation and apoptosis. *BMC Systems Biology,* 7**,** 16-16.

EVANS, J. D. 1996. *Straightforward statistics for the behavioral sciences,* Pacific Grove, Calif., Brooks/Cole Publ. Co : An International Thomson Publ. Co.

FADDA, S., CINCOTTI, A. & CAO, G. 2012. A novel population balance model to investigate the kinetics of in vitro cell proliferation: Part I. model development. *Biotechnology and Bioengineering,* 109**,** 772-781.

FANG, X., WALLQVIST, A. & REIFMAN, J. 2009. A systems biology framework for modeling metabolic enzyme inhibition of Mycobacterium tuberculosis. *BMC Systems Biology,* 3**,** 92.

FIGUEROA, B., CHEN, S., OYLER, G. A., HARDWICK, J. M. & BETENBAUGH, M. J. 2004. Aven and Bcl-xL enhance protection against apoptosis for mammalian cells exposed to various culture conditions. *Biotechnology and Bioengineering,* 85**,** 589-600.

FIGUEROA, B., SAUERWALD, T. M., MASTRANGELO, A. J., HARDWICK, J. M. & BETENBAUGH, M. J. 2001. Comparison of Bcl-2 to a Bcl-2 deletion mutant for mammalian cells exposed to culture insults. *Biotechnology and Bioengineering,* 73**,** 211-222.

FILIPP, F. V., RATNIKOV, B., DE INGENIIS, J., SMITH, J. W., OSTERMAN, A. L. & SCOTT, D. A. 2012. Glutamine-fueled mitochondrial metabolism is decoupled from glycolysis in melanoma. *Pigment Cell & Melanoma Research,* 25**,** 732-739.

FOGOLíN, M. B., WAGNER, R., ETCHEVERRIGARAY, M. & KRATJE, R. 2004. Impact of temperature reduction and expression of yeast pyruvate carboxylase on hGM-CSF-producing CHO cells. *Journal of Biotechnology,* 109**,** 179-191.

FOX, S. R., PATEL, U. A., YAP, M. G. S. & WANG, D. I. C. 2004. Maximizing interferon-γ production by chinese hamster ovary cells through temperature shift optimization: Experimental and modeling. *Biotechnology and Bioengineering,* 85**,** 177-184.

FOX, S. R., TAN, H. K., TAN, M. C., WONG, S. C. N. C., YAP, M. G. S. & WANG, D. I. C. 2005. A detailed understanding of the enhanced hypothermic productivity of interferon-γ by Chinese-hamster ovary cells. *Biotechnology and Applied Biochemistry,* 41**,** 255-264.

FRAME, K. K. & HU, W.-S. 1991. Kinetic study of hybridoma cell growth in continuous culture. I. A model for non-producing cells. *Biotechnology and Bioengineering,* 37**,** 55-64.

FRANCINI, F., DEL ZOTTO, H., MASSA, M. L. & GAGLIARDINO, J. J. 2009. Selective effect of INGAP-PP upon mouse embryonic stem cell differentiation toward islet cells. *Regulatory Peptides,* 153**,** 43-48.

FRANĚK, F., VOMASTEK, T. & DOLNÍKOVÁ, J. 1992. Fragmented DNA and apoptotic bodies document the programmed way of cell death in hybridoma cultures. *Cytotechnology,* 9**,** 117-123.

FREDRICKSON, A. G. 1976. Formulation of structured growth models. *Biotechnology and Bioengineering,* 18**,** 1481-1486.

FURUKAWA, K. & OHSUYE, K. 1998. Effect of culture temperature on a recombinant CHO cell line producing a C-terminal α-amidating enzyme. *Cytotechnology,* 26**,** 153-164.

FURUKAWA, K. & OHSUYE, K. 1999. Enhancement of productivity of recombinant α-amidating enzyme by low temperature culture. *Cytotechnology,* 31**,** 85-94.

FURUKAWA, Y., IWASE, S., KIKUCHI, J., TERUI, Y., NAKAMURA, M., YAMADA, H., KANO, Y. & MATSUDA, M. 2000. Phosphorylation of Bcl-2 Protein by CDC2 Kinase during G2/M Phases and Its Role in Cell Cycle Regulation. *Journal of Biological Chemistry,* 275**,** 21661-21667.

FUSSENEGGER, M. & BAILEY, J. E. 1998. Molecular Regulation of Cell-Cycle Progression and Apoptosis in Mammalian Cells: Implications for Biotechnology. *Biotechnology Progress,* 14**,** 807-833.

FUSSENEGGER, M., BAILEY, J. E. & VARNER, J. 2000. A mathematical model of caspase function in apoptosis. *Nat Biotech,* 18**,** 768-774.

FUSSENEGGER, M., SCHLATTER, S., DATWYLER, D., MAZUR, X. & BAILEY, J. E. 1998a. Controlled proliferation by multigene metabolic engineering enhances the productivity of Chinese hamster ovary cells. *Nat Biotech,* 16**,** 468-472.

FUSSENEGGER, M., SCHLATTER, S., DATWYLER, D., MAZUR, X. & BAILEY, J. E. 1998b. Controlled proliferation by multigene metabolic engineering enhances the productivity of Chinese hamster ovary cells. *Nat Biotechnol,* 16**,** 468-72.

GALVAO, J., DAVIS, B., TILLEY, M., NORMANDO, E., DUCHEN, M. R. & CORDEIRO, M. F. 2014. Unexpected low-dose toxicity of the universal solvent DMSO. *The FASEB Journal,* 28**,** 1317-1330.

GARCÍA MÜNZER, D. G. 2014. *An integrated experimental and modelling approach for the study of cell cycle in GS-NS0 cell culture.* PhD, Imperial College London.

GARCÍA MÜNZER, D. G., IVARSSON, M., USAKU, C., HABICHER, T., SOOS, M., MORBIDELLI, M., PISTIKOPOULOS, E. N. & MANTALARIS, A. 2015. An unstructured model of metabolic and temperature dependent cell cycle arrest in hybridoma batch and fed-batch cultures. *Biochemical Engineering Journal,* 93**,** 260-273.

GARRIDO, C., GURBUXANI, S., RAVAGNAN, L. & KROEMER, G. 2001. Heat Shock Proteins: Endogenous Modulators of Apoptotic Cell Death. *Biochemical and Biophysical Research Communications,* 286**,** 433-442.

GARTEL, A. L. & TYNER, A. L. 2002a. The Role of the Cyclin-dependent Kinase Inhibitor p21 in Apoptosis. *Molecular Cancer Therapeutics,* 1**,** 639-649.

GARTEL, A. L. & TYNER, A. L. 2002b. The Role of the Cyclin-dependent Kinase Inhibitor p21 in Apoptosis 1 Supported in part by NIH Grant R01 DK56283 (to A. L. T.) for the p21 research and Campus Research Board and Illinois Department of Public Health Penny Severns Breast and Cervical Cancer grants (to A. L. G.).1. *Molecular Cancer Therapeutics,* 1**,** 639-649.

GERDES, J., LEMKE, H., BAISCH, H., WACKER, H. H., SCHWAB, U. & STEIN, H. 1984. Cell cycle analysis of a cell proliferation-associated human nuclear antigen defined by the monoclonal antibody Ki-67. *The Journal of Immunology,* 133**,** 1710-1715.

GLACKEN, M., HUANG, C. & SINSKEY, A. 1989. Mathematical descriptions of hybridoma culture kinetics. III. Simulation of fed-batch bioreactors. *Journal of Biotechnology,* 10**,** 39-65.

GLICK, D., BARTH, S. & MACLEOD, K. F. 2010. Autophagy: cellular and molecular mechanisms. *The Journal of Pathology,* 221**,** 3-12.

GONZÁLEZ-LEAL, I. J., CARRILLO-COCOM, L. M., RAMÍREZ-MEDRANO, A., LÓPEZ-PACHECO, F., BULNES-ABUNDIS, D., WEBB-VARGAS, Y. & ALVAREZ, M. M. 2011. Use of a Plackett–Burman statistical design to determine the effect of selected amino acids on monoclonal antibody production in CHO cells. *Biotechnology Progress,* 27**,** 1709-1717.

GOOCHEE, C. F. & MONICA, T. 1990. Environmental Effects on Protein Glycosylation. *Nat Biotech,* 8**,** 421-427.

GOSWAMI, J., SINSKEY, A. J., STELLER, H., STEPHANOPOULOS, G. N. & WANG, D. I. C. 1999. Apoptosis in batch cultures of Chinese Hamster Ovary cells. *Biotechnology and Bioengineering,* 62**,** 632-640.

GOUBIN, F. & DUCOMMUN, B. 1995. Identification of binding domains on the p21Cip1 cyclin-dependent kinase inhibitor. *Oncogene,* 10**,** 2281-7.

GPROMS 2014. *version 4.0.0 (x64),* www.psenterprise.com/gproms, Process Systems Enterprise Ltd. .

GU, Z. T., LI, L., WU, F., ZHAO, P., YANG, H., LIU, Y. S., GENG, Y., ZHAO, M. & SU, L. 2015. Heat stress induced apoptosis is triggered by transcription-independent p53, Ca2+ dyshomeostasis and the subsequent Bax mitochondrial translocation. *Scientific Reports,* 5**,** 11497.

GUO, Y., XIAO, P., LEI, S., DENG, F., XIAO, G. G., LIU, Y., CHEN, X., LI, L., WU, S., CHEN, Y., JIANG, H., TAN, L., XIE, J., ZHU, X., LIANG, S. & DENG, H. 2008. How is mRNA expression predictive for protein expression? A correlation study on human circulating monocytes. *Acta Biochimica et Biophysica Sinica,* 40**,** 426-436.

HA, T. K., JEON, M. K., YU, D. Y. & LEE, G. M. 2013. Effect of Bcl-xL overexpression on lactate metabolism in chinese hamster ovary cells producing antibody. *Biotechnology Progress,* 29**,** 1594-1598.

HALDAR, S., NEGRINI, M., MONNE, M., SABBIONI, S. & CROCE, C. M. 1994. Down-Regulation of bcl-2 by p53 in Breast Cancer Cells. *Cancer Research,* 54**,** 2095-2097.

HAN, S. I., OH, S. Y., JEON, W. J., KIM, J. M., LEE, J. H., CHUNG, H. Y., CHOI, Y. H., YOO, M. A., KIM, H. D. & KANG, H. S. 2002. Mild heat shock induces cyclin D1 synthesis through multiple Ras signal pathways. *FEBS Letters,* 515**,** 141-145.

HAN, Y. K., HA, T. K., LEE, S. J., LEE, J. S. & LEE, G. M. 2011. Autophagy and apoptosis of recombinant Chinese hamster ovary cells during fed-batch culture: Effect of nutrient supplementation. *Biotechnology and Bioengineering,* 108**,** 2182-2192.

HASSELL, T., GLEAVE, S. & BUTLER, M. 1991. Growth inhibition in animal cell culture. *Applied Biochemistry and Biotechnology,* 30**,** 29-41.

HATZIS, C., SRIENC, F. & FREDRICKSON, A. G. 1995. Multistaged corpuscular models of microbial growth: Monte Carlo simulations. *Biosystems,* 36**,** 19-35.

HENDERSON JR, J. W. & BROOKS, A. 2010. Improved Amino Acid Methods using Agilent ZORBAX Eclipse Plus C18 Columns for a Variety of Agilent LC Instrumentation and Separation Goals. USA: Agilent Technologies, Inc.

HENDRICK, V., WINNEPENNINCKX, P., ABDELKAFI, C., VANDEPUTTE, O., CHERLET, M., MARIQUE, T., RENEMANN, G., LOA, A., KRETZMER, G. & WERENNE, J. 2001. Increased productivity of recombinant tissular plasminogen activator (t-PA) by butyrate and shift of temperature: a cell cycle phases analysis. *Cytotechnology,* 36**,** 71-83.

HENGARTNER, M. O. 2000. The biochemistry of apoptosis. *Nature,* 407**,** 770-776.

HILL, A. V. 1913. The Combinations of Haemoglobin with Oxygen and with Carbon Monoxide. I. *Biochemical Journal,* 7**,** 471-480.

HIRAI, I. & WANG, H. G. 2001. Survival-factor-induced phosphorylation of Bad results in its dissociation from Bcl-x(L) but not Bcl-2. *Biochemical Journal,* 359**,** 345-352.

HO, S. C. L., TONG, Y. W. & YANG, Y. 2013. Generation of monoclonal antibody-producing mammalian cell lines. *Pharmaceutical Bioprocessing,* 1**,** 71-87.

HO, Y., KIPARISSIDES, A., PISTIKOPOULOS, E. N. & MANTALARIS, A. 2012. Computational approach for understanding and improving GS-NS0 antibody production under hyperosmotic conditions. *Journal of Bioscience and Bioengineering,* 113**,** 88-98.

HO, Y., VARLEY, J. & MANTALARIS, A. 2006. Development and Analysis of a Mathematical Model for Antibody-Producing GS-NS0 Cells Under Normal and Hyperosmotic Culture Conditions. *Biotechnology Progress,* 22**,** 1560-1569.

HOCKENBERY, D., NUNEZ, G., MILLIMAN, C., SCHREIBER, R. D. & KORSMEYER, S. J. 1990. Bcl-2 is an inner mitochondrial membrane protein that blocks programmed cell death. *Nature,* 348**,** 334-6.

HOMMA, T. & SALTELLI, A. 1996. Importance measures in global sensitivity analysis of nonlinear models. *Reliability Engineering & System Safety,* 52**,** 1-17.

HONG, Y. K., BAIK, S. S., CHUNG, M. S. & YOON, H. S. 2008. Expression of Cyclin D1 and bcl-2 in Infiltrative Ductal Carcinoma of the Breast: Their Correlations and Clinical implications. *J Breast Cancer,* 11**,** 172-179.

HOSHINO, E. 1987. L-serine Enhances the Anaerobic Lactate Metabolism of Veillonella dispar ATCC 177451. *Journal of Dental Research,* 66**,** 1162-1165.

HSU, Y.-L., YU, H.-S., LIN, H.-C., WU, K.-Y., YANG, R.-C. & KUO, P.-L. 2011. Heat shock induces apoptosis through reactive oxygen species involving mitochondrial and death receptor pathways in corneal cells. *Experimental Eye Research,* 93**,** 405-412.

HU, W., ZHANG, C., WU, R., SUN, Y., LEVINE, A., FENG, Z. & LEVINE, A. J. 2010. Glutaminase 2, a novel p53 target gene regulating energy metabolism and antioxidant

function. *Proceedings of the National Academy of Sciences of the United States of America,* 107**,** 7455-7460.

HUA, F., CORNEJO, M. G., CARDONE, M. H., STOKES, C. L. & LAUFFENBURGER, D. A. 2005. Effects of Bcl-2 levels on Fas signaling-induced caspase-3 activation: molecular genetic tests of computational model predictions. *The Journal of Immunology,* 175**,** 6235-6237.

HUSSAIN, H., MALDONADO-AGURTO, R. & DICKSON, A. 2014. The endoplasmic reticulum and unfolded protein response in the control of mammalian recombinant protein production. *Biotechnology Letters,* 36**,** 1581-1593.

HWANG, S. O. & LEE, G. M. 2008. Nutrient deprivation induces autophagy as well as apoptosis in Chinese hamster ovary cell culture. *Biotechnology and Bioengineering,* 99**,** 678-685.

HWANG, S. O. & LEE, G. M. 2009. Effect of Akt overexpression on programmed cell death in antibody-producing Chinese hamster ovary cells. *Journal of Biotechnology,* 139**,** 89-94.

IBARRA, N., WATANABE, S., BI, J.-X., SHUTTLEWORTH, J. & AL-RUBEAI, M. 2003. Modulation of Cell Cycle for Enhancement of Antibody Productivity in Perfusion Culture of NS0 Cells. *Biotechnology Progress,* 19**,** 224-228.

INNOCENTE, S. A., ABRAHAMSON, J. L. A., COGSWELL, J. P. & LEE, J. M. 1999. p53 regulates a G(2) checkpoint through cyclin B1. *Proceedings of the National Academy of Sciences of the United States of America,* 96**,** 2147-2152.

ITOH, Y., UEDA, H. & SUZUKI, E. 1995. Overexpression of bcl-2, apoptosis suppressing gene: Prolonged viable culture period of hybridoma and enhanced antibody production. *Biotechnology and Bioengineering,* 48**,** 118-122.

IZUMI, S., SAITO, A., KANEMOTO, S., KAWASAKI, N., ASADA, R., IWAMOTO, H., OKI, M., MIYAGI, H., OCHI, M. & IMAIZUMI, K. 2012. The Endoplasmic Reticulum Stress Transducer BBF2H7 Suppresses Apoptosis by Activating the ATF5-MCL1 Pathway in Growth Plate Cartilage. *Journal of Biological Chemistry,* 287**,** 36190-36200.

JÄGER, R. & FEARNHEAD, H. O. 2012. "Dead Cells Talking": The Silent Form of Cell Death is Not so Quiet. *Biochemistry Research International,* 2012**,** 8.

JANG, J. D. & BARFORD, J. P. 2000. An unstructured kinetic model of macromolecular metabolism in batch and fed-batch cultures of hybridoma cells producing monoclonal antibody. *Biochemical Engineering Journal,* 4**,** 153-168.

JANG, J. D., SANDERSON, C. S., CHAN, L. C. L., BARFORD, J. P. & REID, S. 2000. Structured modeling of recombinant protein production in batch and fed-batch culture of baculovirus-infected insect cells. *Cytotechnology,* 34**,** 71-82.

JANUMYAN, Y. M., SANSAM, C. G., CHATTOPADHYAY, A., CHENG, N., SOUCIE, E. L., PENN, L. Z., ANDREWS, D., KNUDSON, C. M. & YANG, E. 2003. *Bcl-xL/Bcl-2 coordinately regulates apoptosis, cell cycle arrest and cell cycle entry*.

JARDON, M. A., SATTHA, B., BRAASCH, K., LEUNG, A. O., CÔTÉ, H. C. F., BUTLER, M., GORSKI, S. M. & PIRET, J. M. 2012. Inhibition of glutamine-dependent autophagy increases t-PA production in CHO Cell fed-batch processes. *Biotechnology and Bioengineering,* 109**,** 1228-1238.

JEONG, Y.-H. & WANG, S. S. 1995. Role of glutamine in hybridoma cell culture: Effects on cell growth, antibody production, and cell metabolism. *Enzyme and Microbial Technology,* 17**,** 47-55.

KAIJA, H., PAKANEN, L., KORTELAINEN, M.-L. & PORVARI, K. 2015. Hypothermia and Rewarming Induce Gene Expression and Multiplication of Cells in Healthy Rat Prostate Tissue. *PLoS ONE,* 10**,** e0127854.

KANG, S., REN, D., XIAO, G., DARIS, K., BUCK, L., ENYENIHI, A. A., ZUBAREV, R., BONDARENKO, P. V. & DESHPANDE, R. 2014. Cell line profiling to improve monoclonal antibody production. *Biotechnology and Bioengineering,* 111**,** 748-760.

KARLEN, Y., MCNAIR, A., PERSEGUERS, S., MAZZA, C. & MERMOD, N. 2007. Statistical significance of quantitative PCR. *BMC Bioinformatics,* 8**,** 131.

KASTAN, M., CANMAN, C. & LEONARD, C. 1995. P53, cell cycle control and apoptosis: Implications for cancer. *Cancer and Metastasis Reviews,* 14**,** 3-15.

KAUFMANN, H., MAZUR, X., FUSSENEGGER, M. & BAILEY, J. E. 1999. Influence of low temperature on productivity, proteome and protein phosphorylation of CHO cells. *Biotechnology and Bioengineering,* 63**,** 573-582.

KAUFMANN, H., MAZUR, X., MARONE, R., BAILEY, J. E. & FUSSENEGGER, M. 2001. Comparative analysis of two controlled proliferation strategies regarding product quality, influence on tetracycline-regulated gene expression, and productivity. *Biotechnology and Bioengineering,* 72**,** 592-602.

KAWAMOTO, H., KOIZUMI, H. & UCHIKOSHI, T. 1997. Expression of the G2-M checkpoint regulators cyclin B1 and cdc2 in nonmalignant and malignant human breast lesions: immunocytochemical and quantitative image analyses. *The American journal of pathology,* 150**,** 15-23.

KENT, E., NEUMANN, S., KUMMER, U. & MENDES, P. 2013. What Can We Learn from Global Sensitivity Analysis of Biochemical Systems? *PLoS ONE,* 8**,** e79244.

KHATTAK, S. F., XING, Z., KENTY, B., KOYRAKH, I. & LI, Z. J. 2010. Feed development for fed-batch CHO production process by semisteady state analysis. *Biotechnology Progress,* 26**,** 797-804.

KIM, D.-H., SARBASSOV, D. D., ALI, S. M., KING, J. E., LATEK, R. R., ERDJUMENT-BROMAGE, H., TEMPST, P. & SABATINI, D. M. 2002. mTOR Interacts with Raptor to Form a Nutrient-Sensitive Complex that Signals to the Cell Growth Machinery. *Cell,* 110**,** 163-175.

KIM, Y.-G., KIM, J. Y., MOHAN, C. & LEE, G. M. 2009. Effect of Bcl-xL overexpression on apoptosis and autophagy in recombinant Chinese hamster ovary cells under nutrient-deprived condition. *Biotechnology and Bioengineering,* 103**,** 757-766.

KIM, Y.-G., KIM, J. Y., PARK, B., AHN, J. O., JUNG, J.-K., LEE, H. W., LEE, G. M. & LEE, E. G. 2011. Effect of Bcl-xL overexpression on erythropoietin production in recombinant Chinese hamster ovary cells treated with dimethyl sulfoxide. *Process Biochemistry,* 46**,** 2201-2204.

KIM, Y.-G. & LEE, G. M. 2009. Bcl-xL overexpression does not enhance specific erythropoietin productivity of recombinant CHO cells grown at 33°C and 37°C. *Biotechnology Progress,* 25**,** 252-256.

KIPARISSIDES, A., KOUTINAS, M., KONTORAVDI, C., MANTALARIS, A. & PISTIKOPOULOS, E. N. 2011a. 'Closing the loop' in biological systems modeling — From the in silico to the in vitro. *Automatica,* 47**,** 1147-1155.

KIPARISSIDES, A., KUCHERENKO, S. S., MANTALARIS, A. & PISTIKOPOULOS, E. N. 2009. Global Sensitivity Analysis Challenges in Biological Systems Modeling. *Industrial & Engineering Chemistry Research,* 48**,** 7168-7180.

KIPARISSIDES, A., PISTIKOPOULOS, E. N. & MANTALARIS, A. 2010. Towards energy-based dynamic optimization of monoclonal antibody producing GS-NS0 Cultures. *In:* PIERUCCI, S. & FERRARIS, G. B. (eds.) *Computer Aided Chemical Engineering.* Elsevier.

KIPARISSIDES, A., PISTIKOPOULOS, E. N. & MANTALARIS, A. 2011b. On the model based optimization of secreting mammalian cell cultures via minimal glucose provision. *In:* E.N. PISTIKOPOULOS, M. C. G. & KOKOSSIS, A. C. (eds.) *Computer Aided Chemical Engineering.* Elsevier.

KIPARISSIDES, A., PISTIKOPOULOS, E. N. & MANTALARIS, A. 2014. On the model-based optimization of secreting mammalian cell (GS-NS0) cultures. *Biotechnology and Bioengineering***,** n/a-n/a.

KIPARISSIDES, A., PISTIKOPOULOS, E. N. & MANTALARIS, A. 2015. On the model-based optimization of secreting mammalian cell (GS-NS0) cultures. *Biotechnology and Bioengineering,* 112**,** 536-548.

KITA, H., CARMICHAEL, J., SWARTZ, J., MURO, S., WYTTENBACH, A., MATSUBARA, K., RUBINSZTEIN, D. C. & KATO, K. 2002. Modulation of polyglutamine-induced cell death by genes identified by expression profiling. *Human Molecular Genetics,* 11**,** 2279-2287.

KNOOP, H., GRÜNDEL, M., ZILLIGES, Y., LEHMANN, R., HOFFMANN, S., LOCKAU, W. & STEUER, R. 2013. Flux Balance Analysis of Cyanobacterial Metabolism: The Metabolic Network of Synechocystis sp. PCC 6803. *PLoS Computational Biology,* 9**,** e1003081.

KOBAYASHI, S., KAJINO, S., TAKAHASHI, N., KANAZAWA, S., IMAI, K., HIBI, Y., OHARA, H., ITOH, M. & OKAMOTO, T. 2005. 53BP2 induces apoptosis through the mitochondrial death pathway. *Genes to Cells,* 10**,** 253-260.

KOBER, L., ZEHE, C. & BODE, J. 2012. Development of a novel ER stress based selection system for the isolation of highly productive clones. *Biotechnology and Bioengineering,* 109**,** 2599-2611.

KOHLER, G. & MILSTEIN, C. 1975. Continuous cultures of fused cells secreting antibody of predefined specificity. *Nature,* 256**,** 495-497.

KONTORAVDI, C., ASPREY, S. P., PISTIKOPOULOS, E. N. & MANTALARIS, A. 2005. Application of Global Sensitivity Analysis to Determine Goals for Design of Experiments: An Example Study on Antibody-Producing Cell Cultures. *Biotechnology Progress,* 21**,** 1128-1135.

KONTORAVDI, C., PISTIKOPOULOS, E. N. & MANTALARIS, A. 2010. Systematic development of predictive mathematical models for animal cell cultures. *Computers & Chemical Engineering,* 34**,** 1192-1198.

KONTORAVDI, C., WONG, D., LAM, C., LEE, Y. Y., YAP, M. G. S., PISTIKOPOULOS, E. N. & MANTALARIS, A. 2007. Modeling Amino Acid Metabolism in Mammalian Cells-Toward the Development of a Model Library. *Biotechnology Progress,* 23**,** 1261-1269.

KOUTINAS, M., KIPARISSIDES, A., SILVA-ROCHA, R., LAM, M.-C., MARTINS DOS SANTOS, V. A. P., DE LORENZO, V., PISTIKOPOULOS, E. N. & MANTALARIS, A. 2011. Linking genes to microbial growth kinetics--An integrated biochemical systems engineering approach. *Metabolic Engineering,* In Press, Corrected Proof.

KOUTINAS, M., LAM, M. C., KIPARISSIDES, A., SILVA-ROCHA, R., GODINHO, M., LIVINGSTON, A. G., PISTIKOPOULOS, E. N., DE LORENZO, V., DOS SANTOS, V. A. & MANTALARIS, A. 2010. The regulatory logic of m-xylene biodegradation by Pseudomonas putida mt-2 exposed by dynamic modelling of the principal node Ps/Pr of the TOL plasmid. *Environ Microbiol,* 12**,** 1705-18.

KRACIKOVA, M., AKIRI, G., GEORGE, A., SACHIDANANDAM, R. & AARONSON, S. A. 2013. A threshold mechanism mediates p53 cell fate decision between growth arrest and apoptosis. *Cell Death Differ,* 20**,** 576-588.

KRAMPE, B. & AL-RUBEAI, M. 2010. Cell death in mammalian cell culture: molecular mechanisms and cell line engineering strategies. *Cytotechnology,* 62**,** 175-188.

KROMENAKER, S. J. & SRIENC, F. 1994. Effect of lactic acid on the kinetics of growth and antibody production in a murine hybridoma: secretion patterns during the cell cycle. *Journal of Biotechnology,* 34**,** 13-34.

KUBBIES, M. & STOCKINGER, H. 1990. Cell cycle-dependent DHFR and t-PA production in cotransfected, MTX-amplified CHO cells revealed by dual-laser flow cytometry. *Exp Cell Res,* 188**,** 267-71.

KUMAR, N., GAMMELL, P. & CLYNES, M. 2007. Proliferation control strategies to improve productivity and survival during CHO based production culture. *Cytotechnology,* 53**,** 33-46.

KURANO, N., LEIST, C., MESSI, F., KURANO, S. & FIECHTER, A. 1990. Growth behavior of Chinese hamster ovary cells in a compact loop bioreactor. 2. Effects of medium components and waste products. *Journal of Biotechnology,* 15**,** 113-128.

KUROKAWA, H., PARK, Y. S., IIJIMA, S. & KOBAYASHI, T. 1994. Growth characteristics in fed-batch culture of hybridoma cells with control of glucose and glutamine concentrations. *Biotechnology and Bioengineering,* 44**,** 95-103.

KYPARISSIDIS, A.-D. 2012. *Development of a combined mathematical and experimental framework for the control and optimisation of mammalian cell culture systems.* PhD, Imperial College London.

KYRIAKOPOULOS, S., POLIZZI, K. & KONTORAVDI, C. 2013. Dynamic profiling of amino acid transport and metabolism in Chinese hamster ovary cell culture. *BMC Proceedings,* 7**,** P97.

LAM, C. M., SRIYUDTHSAK, K., KONTORAVDI, C., KOTHARI, K., PARK, H.-H., PISTIKOPOULOS, E. N. & MANTALARIS, A. 2008. Cell cycle modelling for off-line dynamic optimisation of mammalian cultures. *In:* BERTRAND, B. & XAVIER, J. (eds.) *Computer Aided Chemical Engineering.* Elsevier.

LANNEAU, D., BRUNET, M., FRISAN, E., SOLARY, E., FONTENAY, M. & GARRIDO, C. 2008. Heat shock proteins: essential proteins for apoptosis regulation. *Journal of Cellular and Molecular Medicine,* 12**,** 743-761.

LAO, M.-S. & TOTH, D. 1997. Effects of Ammonium and Lactate on Growth and Metabolism of a Recombinant Chinese Hamster Ovary Cell Culture. *Biotechnology Progress,* 13**,** 688-691.

LASUNSKAIA, E. B., FRIDLIANSKAIA, I. I., DARIEVA, Z. A., DA SILVA, M. S. R., KANASHIRO, M. M. & MARGULIS, B. A. 2003. Transfection of NS0 myeloma fusion partner cells with HSP70 gene results in higher hybridoma yield by improving cellular resistance to apoptosis. *Biotechnology and Bioengineering,* 81**,** 496-504.

LECOEUR, H., PRÉVOST, M.-C. & GOUGEON, M.-L. 2001. Oncosis is associated with exposure of phosphatidylserine residues on the outside layer of the plasma membrane: A reconsideration of the specificity of the annexin V/propidium iodide assay. *Cytometry,* 44**,** 65-72.

LEGEWIE, S., BLÜTHGEN, N. & HERZEL, H. 2006. Mathematical Modeling Identifies Inhibitors of Apoptosis as Mediators of Positive Feedback and Bistability. *PLoS Comput Biol,* 2**,** e120.

LENGWEHASATIT, I. & DICKSON, A. J. 2002. Analysis of the role of GADD153 in the control of apoptosis in NS0 myeloma cells. *Biotechnology and Bioengineering,* 80**,** 719-730.

LEUNG-PINEDA, V., PAN, Y., CHEN, H. & KILBERG, M. S. 2004. Induction of p21 and p27 expression by amino acid deprivation of HepG2 human hepatoma cells involves mRNA stabilization. *Biochem J,* 379**,** 79-88.

LI, F., VIJAYASANKARAN, N., SHEN, A., KISS, R. & AMANULLAH, A. 2010. Cell culture processes for monoclonal antibody production. *mAbs,* 2**,** 466-479.

LI, J., WONG, C. L., VIJAYASANKARAN, N., HUDSON, T. & AMANULLAH, A. 2012. Feeding lactate for CHO cell culture processes: Impact on culture metabolism and performance. *Biotechnology and Bioengineering,* 109**,** 1173-1186.

LI, L., TAN, H., GU, Z., LIU, Z., GENG, Y., LIU, Y., TONG, H., TANG, Y., QIU, J. & SU, L. 2014. Heat Stress Induces Apoptosis through a Ca²⁺-Mediated Mitochondrial Apoptotic Pathway in Human Umbilical Vein Endothelial Cells. *PLoS ONE,* 9**,** e111083.

LI, Y., JENKINS, C. W., NICHOLS, M. A. & XIONG, Y. 1994. Cell cycle expression and p53 regulation of the cyclin-dependent kinase inhibitor p21. *Oncogene,* 9**,** 2261-8.

LIEDTKE, C., GRÖGER, N., MANNS, M. P. & TRAUTWEIN, C. 2003. The Human Caspase-8 Promoter Sustains Basal Activity through SP1 and ETS-like Transcription Factors and Can Be Up-regulated by a p53-dependent Mechanism. *Journal of Biological Chemistry,* 278**,** 27593-27604.

LIN, H. M., LEE, Y. J., LI, G., PESTELL, R. G. & KIM, H. R. 2001a. Bcl-2 induces cyclin D1 promoter activity in human breast epithelial cells independent of cell anchorage. *Cell Death Differ,* 8**,** 44-50.

LIN, K. M., LIN, B., LIAN, I. Y., MESTRIL, R., SCHEFFLER, I. E. & DILLMANN, W. H. 2001b. Combined and Individual Mitochondrial HSP60 and HSP10 Expression in Cardiac Myocytes Protects Mitochondrial Function and Prevents Apoptotic Cell Deaths Induced by Simulated Ischemia-Reoxygenation. *Circulation,* 103**,** 1787-1792.

LINARDOS, T. I., KALOGERAKIS, N., BEHIE, L. A. & LAMONTAGNE, L. R. 1991. The effect of specific growth rate and death rate on monoclonal antibody production in hybridoma chemostat cultures. *The Canadian Journal of Chemical Engineering,* 69**,** 429-438.

LIU, Y.-H., BI, J.-X., ZENG, A.-P. & YUAN, J.-Q. 2007. A Population Balance Model Describing the Cell Cycle Dynamics of Myeloma Cell Cultivation. *Biotechnology Progress,* 23**,** 1198-1209.

LIU, Y.-H., BI, J.-X., ZENG, A.-P. & YUAN, J.-Q. 2008. A simple kinetic model for myeloma cell culture with consideration of lysine limitation. *Bioprocess and Biosystems Engineering,* 31**,** 569-577.

LIVAK, K. J. & SCHMITTGEN, T. D. 2001. Analysis of Relative Gene Expression Data Using Real-Time Quantitative PCR and the 2−ΔΔCT Method. *Methods,* 25**,** 402-408.

LODISH H, B. A., ZIPURSKY SL, ET AL. 2000. Section 17.6, Post-Translational Modifications and Quality Control in the Rough ER. *Molecular Cell Biology.* 4th edition ed. New York: W. H. Freeman.

LOGUE, S. E., GORMAN, A. M., CLEARY, P., KEOGH, N. & SAMALI, A. 2013. Current concepts in ER stress-induced apoptosis. *Journal of Carcinogenesis & Mutagenesis*.

LYNCH, C. J. 2001. Role of Leucine in the Regulation of mTOR by Amino Acids: Revelations from Structure–Activity Studies. *The Journal of Nutrition,* 131**,** 861S-865S.

MA, N., ELLET, J., OKEDIADI, C., HERMES, P., MCCORMICK, E. & CASNOCHA, S. 2009. A single nutrient feed supports both chemically defined NS0 and CHO fed-batch processes: Improved productivity and lactate metabolism. *Biotechnology Progress,* 25**,** 1353-1363.

MADDOCKS, O. D., BERKERS, C. R., MASON, S. M., ZHENG, L., BLYTH, K., GOTTLIEB, E. & VOUSDEN, K. H. 2013. Serine starvation induces stress and p53-dependent metabolic remodelling in cancer cells. *Nature,* 493**,** 542-6.

MAIER, T., GÜELL, M. & SERRANO, L. 2009. Correlation of mRNA and protein in complex biological samples. *FEBS Letters,* 583**,** 3966-3973.

MAJID, F. A. A., BUTLER, M. & AL-RUBEAI, M. 2007. Glycosylation of an immunoglobulin produced from a murine hybridoma cell line: The effect of culture mode and the anti-apoptotic gene, bcl-2. *Biotechnology and Bioengineering,* 97**,** 156-169.

MAJORS, B. S., BETENBAUGH, M. J. & CHIANG, G. G. 2007. Links between metabolism and apoptosis in mammalian cells: Applications for anti-apoptosis engineering. *Metabolic Engineering,* 9**,** 317-326.

MARCHANT, R., AL-FAGEEH, M., UNDERHILL, M., RACHER, A. & SMALES, C. M. 2008. Metabolic Rates, Growth Phase, and mRNA Levels Influence Cell-Specific Antibody Production Levels from In Vitro-Cultured Mammalian Cells at Sub-Physiological Temperatures. *Molecular Biotechnology,* 39**,** 69-77.

MASON, E. F. & RATHMELL, J. C. 2011. Cell metabolism: An essential link between cell growth and apoptosis. *Biochimica et Biophysica Acta (BBA) - Molecular Cell Research,* 1813**,** 645-654.

MASTERTON, R. J. & SMALES, C. M. 2014. The impact of process temperature on mammalian cell lines and the implications for the production of recombinant proteins in CHO cells. *Pharmaceutical Bioprocessing,* 2**,** 49-61.

MASTRANGELO, A. J., HARDWICK, J. M., BEX, F. & BETENBAUGH, M. J. 2000a. Part I. Bcl-2 and bcl-xL limit apoptosis upon infection with alphavirus vectors. *Biotechnology and Bioengineering,* 67**,** 544-554.

MASTRANGELO, A. J., HARDWICK, J. M., ZOU, S. & BETENBAUGH, M. J. 2000b. Part II. Overexpression of bcl-2 family members enhances survival of mammalian cells in response to various culture insults. *Biotechnology and Bioengineering,* 67**,** 555-564.

MATLAB 2014. *version 8.3.3 (R2014a),* Natick, Massachusetts, The MathWorks Inc.

MAZEL, S., BURTRUM, D. & PETRIE, H. T. 1996. Regulation of cell division cycle progression by bcl-2 expression: a potential mechanism for inhibition of programmed cell death. *The Journal of Experimental Medicine,* 183**,** 2219-2226.

MAZUMDER, S., DUPREE, E. L. & ALMASAN, A. 2004. A Dual Role of Cyclin E in Cell Proliferation and Apotosis May Provide a Target for Cancer Therapy. *Current cancer drug targets,* 4**,** 65-75.

MCCULLOUGH, K. D., MARTINDALE, J. L., KLOTZ, L.-O., AW, T.-Y. & HOLBROOK, N. J. 2001. Gadd153 Sensitizes Cells to Endoplasmic Reticulum Stress by Down-Regulating Bcl2 and Perturbing the Cellular Redox State. *Molecular and Cellular Biology,* 21**,** 1249-1259.

MCKENNA, S. L. & COTTER, T. G. 2000. Inhibition of caspase activity delays apoptosis in a transfected NS/0 myeloma cell line. *Biotechnology and Bioengineering,* 67**,** 165-176.

MEAD, E. J., CHIVERTON, L. M., SPURGEON, S. K., MARTIN, E. B., MONTAGUE, G. A., SMALES, C. M. & VON DER HAAR, T. 2012. Experimental and In Silico Modelling Analyses of the Gene Expression Pathway for Recombinant Antibody and By-Product Production in NS0 Cell Lines. *PLoS ONE,* 7**,** e47422.

MEENTS, H., ENENKEL, B., WERNER, R. G. & FUSSENEGGER, M. 2002. p27Kip1-mediated controlled proliferation technology increases constitutive sICAM production in CHO-DUKX adapted for growth in suspension and serum-free media. *Biotechnology and Bioengineering,* 79**,** 619-627.

MEGEE III, R. D., DRAKE, J. F., FREDRICKSON, A. G. & TSUCHIYA, H. M. 1972. Studies in intermicrobial symbiosis. Saccharomyces cerevisiae and Lactobacillus casei. *Canadian Journal of Microbiology,* 18**,** 1733-1742.

MENG, X. W., FRASER, M. J., FELLER, J. M. & ZIEGLER, J. B. 2000. Caspase-3-dependent and caspase-3-independent pathways leading to chromatin DNA fragmentation in HL-60 cells. *Apoptosis,* 5**,** 61-7.

MERCILLE, S. & MASSIE, B. 1994a. Induction of apoptosis in nutrient-deprived cultures of hybridoma and myeloma cells. *Biotechnology and Bioengineering,* 44**,** 1140-1154.

MERCILLE, S. & MASSIE, B. 1994b. Induction of apoptosis in oxygen-deprived cultures of hybridoma cells. *Cytotechnology,* 15**,** 117-128.

MESHRAM, M., NADERI, S., MCCONKEY, B., BUDMAN, H., SCHARER, J. & INGALLS, B. 2012. Population-based modeling of the progression of apoptosis in mammalian cell culture. *Biotechnology and Bioengineering,* 109**,** 1193-1204.

MESHRAM, M., NADERI, S., MCCONKEY, B., INGALLS, B., SCHARER, J. & BUDMAN, H. 2013. Modeling the coupled extracellular and intracellular environments in mammalian cell culture. *Metabolic Engineering,* 19**,** 57-68.

MESHRAM, M., NADERI, S., WEI, Y.-Y., MCCONKEY, B., INGALLS, B., BUDMAN, H. & SCHARER, J. 2011. Dynamic Modeling of Apoptosis and its Interaction with Cell Growth in Mammalian Cell Culture. *the 18th IFAC World Congress.* Università Cattolica del Sacro Cuore, Milano, Italy.

MIAO, H., XIA, X., PERELSON, A. & WU, H. 2011. On Identifiability of Nonlinear ODE Models and Applications in Viral Dynamics. *SIAM Review,* 53**,** 3-39.

MILLER, W. M., BLANCH, H. W. & WILKE, C. R. 1988a. A kinetic analysis of hybridoma growth and metabolism in batch and continuous suspension culture: Effect of nutrient concentration, dilution rate, and pH. *Biotechnology and Bioengineering,* 32**,** 947-965.

MILLER, W. M., WILKE, C. R. & BLANCH, H. W. 1988b. Transient responses of hybridoma cells to lactate and ammonia pulse and step changes in continuous culture. *Bioprocess Engineering,* 3**,** 113-122.

MILNER, A. E., WANG, H. & GREGORY, C. D. 1996. Analysis of Apoptosis by Flow Cytometry. *In:* AL-RUBEAI, M. & EMERY, A. N. (eds.) *Flow cytometry applications in cell culture.* Marcel Dekker.

MIYASHITA, T., HARIGAI, M., HANADA, M. & REED, J. C. 1994. Identification of a p53-dependent Negative Response Element in the bcl-2 Gene. *Cancer Research,* 54**,** 3131-3135.

MOLEY, K. H. & MUECKLER, M. M. 2000. Glucose transport and apoptosis. *Apoptosis,* 5**,** 99-105.

MOLL, U. M. & PETRENKO, O. 2003. The MDM2-p53 Interaction. *Molecular Cancer Research,* 1**,** 1001-1008.

MOORE, A., MERCER, J., DUTINA, G., DONAHUE, C., BAUER, K., MATHER, J., ETCHEVERRY, T. & RYLL, T. 1997. Effects of temperature shift on cell cycle, apoptosis and nucleotide pools in CHO cell batch cultues. *Cytotechnology,* 23**,** 47-54.

MORONEY, S. & PLÜCKTHUN, A. 2005. Modern antibody technology: the impact on drug development. *Modern Biopharmaceuticals. Weinheim, Germany: Wiley-VCH Verlag GmbH & Co KGaA***,** 1147-1186.

MOSER, H. 1958. *The dynamics of bacterial populations maintained in the chemostat*, Carnegie Institution of Washington.

MUNOZ-PINEDO, C. & MARTIN, S. J. 2014. Autosis: a new addition to the cell death tower of babel. *Cell Death Dis,* 5**,** e1319.

MURPHY, T. C., WOODS, N. R. & DICKSON, A. J. 2001. Expression of the transcription factor GADD153 is an indicator of apoptosis for recombinant chinese hamster ovary (CHO) cells. *Biotechnology and Bioengineering,* 75**,** 621-629.

NADERI, S., MESHRAM, M., WEI, C., MCCONKEY, B., INGALLS, B., BUDMAN, H. & SCHARER, J. 2011. Development of a mathematical model for evaluating the dynamics of normal and apoptotic Chinese hamster ovary cells. *Biotechnology Progress,* 27**,** 1197-1205.

NADERI, S., NIKDEL, A., MESHRAM, M., MCCONKEY, B., INGALLS, B., BUDMAN, H. & SCHARER, J. 2014. Modeling of cell culture damage and recovery leads to increased antibody and biomass productivity in CHO cell cultures. *Biotechnology Journal,* 9**,** 1152-1163.

NASSERI, S. S., GHAFFARI, N., BRAASCH, K., JARDON, M. A., BUTLER, M., KENNARD, M., GOPALUNI, B. & PIRET, J. M. 2014. Increased CHO cell fed-batch monoclonal antibody production using the autophagy inhibitor 3-MA or gradually increasing osmolality. *Biochemical Engineering Journal,* 91**,** 37-45.

NAUMOVSKI, L. & CLEARY, M. L. 1996. The p53-binding protein 53BP2 also interacts with Bc12 and impedes cell cycle progression at G2/M. *Molecular and Cellular Biology,* 16**,** 3884-3892.

NELSON, D. L. & COX, M. M. 2004. *Lehninger principles of biochemistry* W. H. Freeman.

NEUTELINGS, T., LAMBERT, C. A., NUSGENS, B. V. & COLIGE, A. C. 2013. Effects of Mild Cold Shock (25°C) Followed by Warming Up at 37°C on the Cellular Stress Response. *PLoS ONE,* 8**,** e69687.

NEWLAND, M., KAMAL, M. N., GREENFIELD, P. F. & NIELSEN, L. K. 1994. Ammonia inhibition of hybridomas propagated in batch, fed-batch, and continuous culture. *Biotechnology and Bioengineering,* 43**,** 434-438.

NICULESCU, A. B., 3RD, CHEN, X., SMEETS, M., HENGST, L., PRIVES, C. & REED, S. I. 1998. Effects of p21(Cip1/Waf1) at both the G1/S and the G2/M cell cycle transitions: pRb is a critical determinant in blocking DNA replication and in preventing endoreduplication. *Mol Cell Biol,* 18**,** 629-43.

NIVITCHANYONG, T., MARTINEZ, A., ISHAQUE, A., MURPHY, J. E., KONSTANTINOV, K., BETENBAUGH, M. J. & THRIFT, J. 2007. Anti-apoptotic genes Aven and E1B-19K enhance performance of BHK cells engineered to express recombinant factor VIII in batch and low perfusion cell culture. *Biotechnology and Bioengineering,* 98**,** 825-841.

NOLAN, R. P. & LEE, K. 2011. Dynamic model of CHO cell metabolism. *Metabolic Engineering,* 13**,** 108-124.

NORTON, L. E. & LAYMAN, D. K. 2006. Leucine Regulates Translation Initiation of Protein Synthesis in Skeletal Muscle after Exercise. *The Journal of Nutrition,* 136**,** 533S-537S.

O'CONNOR, C. 2008. Cell Division: Stages of Mitosis. *Nature Education,* 1**,** 188.

O'CONNOR, C. & ADAMS, J. U. 2010. Essentials of Cell Biology. Cambridge, MA: NPG Education.

OGUCHI, S., SAITO, H., TSUKAHARA, M. & TSUMURA, H. 2006. pH Condition in temperature shift cultivation enhances cell longevity and specific hMab productivity in CHO culture. *Cytotechnology,* 52**,** 199-207.

OHTSUBO, T., PARK, H. J., LYONS, J. C., SONG, C. W. & OHNISHI, T. 2000. Effect of acidic environment and p53 on apoptosis induction by hyperthermia. *International Journal of Hyperthermia,* 16**,** 481-491.

OKAZAKI, N., ASANO, R., KINOSHITA, T. & CHUMAN, H. 2008. Simple computational models of type I/type II cells in Fas signaling-induced apoptosis. *Journal of Theoretical Biology,* 250**,** 621-633.

ORMEROD, M. G. 1999. *Flow Cytometer*, Bios Scientific Publishers.

ORMEROD, M. G. 2000. Flow cytometry in the study of apoptosis. *In:* ORMEROD, M. G. (ed.) *Flow Cytometry: A Practical Approach.* 3rd ed.: Oxford University Press.

OZTURK, S. S., RILEY, M. R. & PALSSON, B. O. 1992. Effects of ammonia and lactate on hybridoma growth, metabolism, and antibody production. *Biotechnology and Bioengineering,* 39**,** 418-431.

PANDEY, P., FARBER, R., NAKAZAWA, A., KUMAR, S., BHARTI, A., NALIN, C., WEICHSELBAUM, R., KUFE, D. & KHARBANDA, S. 2000. Hsp27 functions as a negative regulator of cytochrome c-dependent activation of procaspase-3. *Oncogene,* 19**,** 1975-81.

PAPAS, K. K., SUN, L., ROOS, E. S., GOUNARIDES, J. S., SHAPIRO, M. & NALIN, C. M. 1999. Change in lactate production in Myc-transformed cells precedes apoptosis and can be inhibited by Bcl-2 overexpression. *FEBS Letters,* 446**,** 338-342.

PATEL, S., GEORGE, R., AUTORE, F., FRATERNALI, F., LADBURY, J. E. & NIKOLOVA, P. V. 2008. Molecular interactions of ASPP1 and ASPP2 with the p53 protein family and the apoptotic promoters PUMA and Bax. *Nucleic Acids Research,* 36**,** 5139-5151.

PAUL-SAMOJEDNY, M., KOKOCIŃSKA, D., SAMOJEDNY, A., MAZUREK, U., PARTYKA, R., LORENZ, Z. & WILCZOK, T. 2005. Expression of cell survival/death genes: Bcl-2 and Bax at the rate of colon cancer prognosis. *Biochimica et Biophysica Acta (BBA) - Molecular Basis of Disease,* 1741**,** 25-29.

PAVLOSTATHIS, S. G., MARCHANT, R., BANAT, I. M., TERNAN, N. G. & MCMULLAN, G. 2006. High growth rate and substrate exhaustion results in rapid cell death and lysis in the thermophilic bacterium Geobacillus thermoleovorans. *Biotechnology and Bioengineering,* 95**,** 84-95.

PENDEVILLE, H., CARPINO, N., MARINE, J.-C., TAKAHASHI, Y., MULLER, M., MARTIAL, J. A. & CLEVELAND, J. L. 2001. The Ornithine Decarboxylase Gene Is Essential for Cell Survival during Early Murine Development. *Molecular and Cellular Biology,* 21**,** 6549-6558.

PÉREZ-GARIJO, A., FUCHS, Y. & STELLER, H. 2013. Apoptotic cells can induce non-autonomous apoptosis through the TNF pathway. *eLife,* 2**,** e01004.

PERSENGIEV, S. P., DEVIREDDY, L. R. & GREEN, M. R. 2002. Inhibition of apoptosis by ATFx: a novel role for a member of the ATF/CREB family of mammalian bZIP transcription factors. *Genes & Development,* 16**,** 1806-1814.

PESO, L. D., GONZÁLEZ-GARCíA, M., PAGE, C., HERRERA, R. & NUÑEZ, G. 1997. Interleukin-3-Induced Phosphorylation of BAD Through the Protein Kinase Akt. *Science,* 278**,** 687-689.

PIRT, S. J. 1965. The Maintenance Energy of Bacteria in Growing Cultures. *Proceedings of the Royal Society of London. Series B, Biological Sciences,* 163**,** 224-231.

PIRT, S. J. 1982. Maintenance energy: a general model for energy-limited and energy-sufficient growth. *Archives of Microbiology,* 133**,** 300-302.

PÖRTNER, R. & SCHÄFER, T. 1996. Modelling hybridoma cell growth and metabolism — a comparison of selected models and data. *Journal of Biotechnology,* 49**,** 119-135.

PÖRTNER, R., SCHILLING, A., LÜDEMANN, I. & MÄRKL, H. 1996. High density fed-batch cultures for hybridoma cells performed with the aid of a kinetic model. *Bioprocess Engineering,* 15**,** 117-124.

PRASHAD, K. & MEHRA, S. 2015. Dynamics of unfolded protein response in recombinant CHO cells. *Cytotechnology,* 67**,** 237-254.

PROUD, C. G. 2004. mTOR-mediated regulation of translation factors by amino acids. *Biochemical and Biophysical Research Communications,* 313**,** 429-436.

PYBUS, L. P., JAMES, D. C., DEAN, G., SLIDEL, T., HARDMAN, C., SMITH, A., DARAMOLA, O. & FIELD, R. 2014. Predicting the expression of recombinant monoclonal antibodies in Chinese hamster ovary cells based on sequence features of the CDR3 domain. *Biotechnology Progress,* 30**,** 188-197.

QUAISER, T. & MONNIGMANN, M. 2009. Systematic identifiability testing for unambiguous mechanistic modeling - application to JAK-STAT, MAP kinase, and NF-kappaB signaling pathway models. *BMC Systems Biology,* 3**,** 50.

RAJENDRA, Y., KISELJAK, D., BALDI, L., HACKER, D. & WURM, F. 2011. Influence of glutamine on transient and stable recombinant protein production in CHO and HEK-293 cells. *BMC Proceedings,* 5**,** P35.

RAMÍREZ-PEINADO, S., LEÓN-ANNICCHIARICO, C. L., GALINDO-MORENO, J., IURLARO, R., CARO-MALDONADO, A., PREHN, J. H. M., RYAN, K. M. & MUÑOZ-PINEDO, C. 2013. Glucose starved cells do not engage in pro-survival autophagy. *Journal of Biological Chemistry*.

RAMKRISHNA, D. 1979. Statistical models of cell populations. *Advances in Biochemical Engineering, Volume 11.* Springer Berlin Heidelberg.

RAN, R., LU, A., ZHANG, L., TANG, Y., ZHU, H., XU, H., FENG, Y., HAN, C., ZHOU, G., RIGBY, A. C. & SHARP, F. R. 2004. Hsp70 promotes TNF-mediated apoptosis by binding IKKγ and impairing NF-κB survival signaling. *Genes & Development,* 18**,** 1466-1481.

REUVENY, S., VELEZ, D., MACMILLAN, J. D. & MILLER, L. 1986. Factors affecting cell growth and monoclonal antibody production in stirred reactors. *Journal of Immunological Methods,* 86**,** 53-59.

REYNAUD, E. 2010. Protein misfolding and degenerative diseases. *Nature Education,* 3**,** 28.

RICCARDI, C. & NICOLETTI, I. 2006. Analysis of apoptosis by propidium iodide staining and flow cytometry. *Nat. Protocols,* 1**,** 1458-1461.

ROBINSON, D. K., CHAN, C. P., YU LP, C., TSAI, P. K., TUNG, J., SEAMANS, T. C., LENNY, A. B., LEE, D. K., IRWIN, J. & SILBERKLANG, M. 1994. Characterization of a recombinant antibody produced in the course of a high yield fed-batch process. *Biotechnology and Bioengineering,* 44**,** 727-735.

ROBINSON, D. K. & MEMMERT, K. W. 1991. Kinetics of recombinant immunoglobulin production by mammalian cells in continuous culture. *Biotechnology and Bioengineering,* 38**,** 972-976.

RODRIGUES, M. E., COSTA, A. R., HENRIQUES, M., AZEREDO, J. & OLIVEIRA, R. 2010. Technological progresses in monoclonal antibody production systems. *Biotechnology Progress,* 26**,** 332-351.

RODRIGUEZ-FERNANDEZ, M., MENDES, P. & BANGA, J. R. 2006. A hybrid approach for efficient and robust parameter estimation in biochemical pathways. *Biosystems,* 83**,** 248-265.

RODRIGUEZ, J., SPEARMAN, M., HUZEL, N. & BUTLER, M. 2005. Enhanced Production of Monomeric Interferon-β by CHO Cells through the Control of Culture Conditions. *Biotechnology Progress,* 21**,** 22-30.

ROEDERER, M. 2000. *Compensation* [Online]. Available: http://www.drmr.com/compensation/index.html.

SAINI, K. & WALKER, N. 1998. Biochemical and molecular mechanisms regulating apoptosis. *Molecular and Cellular Biochemistry,* 178**,** 9-25.

SAKURAI, T., ITOH, K., HIGASHITSUJI, H., NONOGUCHI, K., LIU, Y., WATANABE, H., NAKANO, T., FUKUMOTO, M., CHIBA, T. & FUJITA, J. 2006. Cirp protects against tumor necrosis factor-α-induced apoptosis via activation of extracellular signal-regulated kinase. *Biochimica et Biophysica Acta (BBA) - Molecular Cell Research,* 1763**,** 290-295.

SALTELLI, A., TARANTOLA, S. & CAMPOLONGO, F. 2000. Sensitivity Analysis as an Ingredient of Modeling. *Statistical Science,* 15**,** 377-395.

SAMUELS-LEV, Y., O'CONNOR, D. J., BERGAMASCHI, D., TRIGIANTE, G., HSIEH, J.-K., ZHONG, S., CAMPARGUE, I., NAUMOVSKI, L., CROOK, T. & LU, X. 2001. ASPP Proteins Specifically Stimulate the Apoptotic Function of p53. *Molecular Cell,* 8**,** 781-794.

SANDERSON, C. S., BARFORD, J. P. & BARTON, G. W. 1999a. A structured, dynamic model for animal cell culture systems. *Biochemical Engineering Journal,* 3**,** 203-211.

SANDERSON, C. S., BARFORD, J. P., BARTON, G. W., WONG, T. K. K. & REID, S. 1999b. A structured, dynamic model for animal cell culture: application to baculovirus/insect cell systems. *Biochemical Engineering Journal,* 3**,** 219-229.

SANDERSON, C. S., JANG, J. D., BARFORD, J. P. & BARTON, G. W. 1999c. A structured, dynamic model for animal cell culture systems: application to murine hybridoma. *Biochemical Engineering Journal,* 3**,** 213-218.

SANFELIU, A., PAREDES, C., CAIRÓ, J. J. & GÒDIA, F. 1997. Identification of key patterns in the metabolism of hybridoma cells in culture. *Enzyme and Microbial Technology,* 21**,** 421-428.

SANFELIU, A. & STEPHANOPOULOS, G. 1999. Effect of glutamine limitation on the death of attached Chinese hamster ovary cells. *Biotechnology and Bioengineering,* 64**,** 46-53.

SANO, R. & REED, J. C. 2013. ER stress-induced cell death mechanisms. *Biochimica et Biophysica Acta (BBA) - Molecular Cell Research,* 1833**,** 3460-3470.

SAUERWALD, T. M., OYLER, G. A. & BETENBAUGH, M. J. 2003. Study of caspase inhibitors for limiting death in mammalian cell culture. *Biotechnology and Bioengineering,* 81**,** 329-340.

SAX, J. K. & EL-DEIRY, W. S. 2003. p53 downstream targets and chemosensitivity. *Cell Death Differ,* 10**,** 413-417.

SCHNEIDER, Y.-J. & LAVOIX, A. 1990. Monoclonal antibody production in semi-continuous serum- and protein-free culture: Effect of glutamine concentration and culture conditions on cell growth and antibody secretion. *Journal of Immunological Methods,* 129**,** 251-268.

SCHULER, M. & GREEN, D. R. 2005. Transcription, apoptosis and p53: catch-22. *Trends in Genetics,* 21**,** 182-187.

SELLICK, C. A., CROXFORD, A. S., MAQSOOD, A. R., STEPHENS, G., WESTERHOFF, H. V., GOODACRE, R. & DICKSON, A. J. 2011. Metabolite profiling of recombinant CHO cells: Designing tailored feeding regimes that enhance

recombinant antibody production. *Biotechnology and Bioengineering,* 108**,** 3025-3031.

SELTMAN, H. J. 2012. Experimental design and analysis. *Online at: http://www. stat. cmu. edu/, hseltman/309/Book/Book. pdf*.

SEO, J., KIM, Y., CHO, J., BAEK, E. & LEE, G. 2013. Effect of culture pH on recombinant antibody production by a new human cell line, F2N78, grown in suspension at 33.0 °C and 37.0 °C. *Applied Microbiology and Biotechnology,* 97**,** 5283-5291.

SHENG, Z., LI, L., ZHU, L. J., SMITH, T. W., DEMERS, A., ROSS, A. H., MOSER, R. P. & GREEN, M. R. 2010. A genome-wide RNA interference screen reveals an essential CREB3L2-ATF5-MCL1 survival pathway in malignant glioma with therapeutic implications. *Nat Med,* 16**,** 671-677.

SHERR, C. J. & ROBERTS, J. M. 1995. Inhibitors of mammalian G1 cyclin-dependent kinases. *Genes & Development,* 9**,** 1149-1163.

SHI, M., XIE, Z., YU, M., SHEN, B. & GUO, N. 2005. Controlled Growth of Chinese Hamster Ovary Cells and High Expression of Antibody-IL-2 Fusion Proteins by Temperature Manipulation. *Biotechnology Letters,* 27**,** 1879-1884.

SHUI, C. & SCUTT, A. 2001. Mild Heat Shock Induces Proliferation, Alkaline Phosphatase Activity, and Mineralization in Human Bone Marrow Stromal Cells and Mg-63 Cells In Vitro. *Journal of Bone and Mineral Research,* 16**,** 731-741.

SHULER, M. L. & KARGI, F. 2002. Chapter 4: How cells works. *Bioprocess Engineering, Basic Concepts.* 2nd ed. Upper Saddle River, NJ 07458: Prentice Hall PTR.

SIDOLI, F. R., MANTALARIS, A. & ASPREY, S. P. 2004. Modelling of Mammalian Cells and Cell Culture Processes. *Cytotechnology,* 44**,** 27-46.

SIGMASTAT 2006a. Manual of SigmaStat 3.5 for Windows. Chapter 8**,** 308-326.

SIGMASTAT 2006b. Manual of SigmaStat 3.5 for Windows. Chapter 11**,** 630-634.

SIMPSON, N. H., SINGH, R. P., EMERY, A. N. & AL-RUBEAI, M. 1999a. Bcl-2 over-expression reduces growth rate and prolongs G1 phase in continuous chemostat cultures of hybridoma cells. *Biotechnol Bioeng,* 64**,** 174-86.

SIMPSON, N. H., SINGH, R. P., EMERY, A. N. & AL-RUBEAI, M. 1999b. Bcl-2 over-expression reduces growth rate and prolongs G1 phase in continuous chemostat cultures of hybridoma cells. *Biotechnology and Bioengineering,* 64**,** 174-186.

SIMPSON, N. H., SINGH, R. P., PERANI, A., GOLDENZON, C. & AL-RUBEAI, M. 1998. In hybridoma cultures, deprivation of any single amino acid leads to apoptotic death,

which is suppressed by the expression of the bcl-2 gene. *Biotechnology and Bioengineering,* 59**,** 90-98.

SINGH, R. P., AL.-RUBEAI, M., GREGORY, C. D. & EMERY, A. N. 1994. Cell death in bioreactors: A role for apoptosis. *Biotechnology and Bioengineering,* 44**,** 720-726.

SMALES, C. M., DINNIS, D. M., STANSFIELD, S. H., ALETE, D., SAGE, E. A., BIRCH, J. R., RACHER, A. J., MARSHALL, C. T. & JAMES, D. C. 2004. Comparative proteomic analysis of GS-NS0 murine myeloma cell lines with varying recombinant monoclonal antibody production rate. *Biotechnology and Bioengineering,* 88**,** 474-488.

SOBOL, I. M. 2001. Global sensitivity indices for nonlinear mathematical models and their Monte Carlo estimates. *Mathematics and Computers in Simulation,* 55**,** 271-280.

SOBOL, I. M., TARANTOLA, S., GATELLI, D., KUCHERENKO, S. S. & MAUNTZ, W. 2007. Estimating the approximation error when fixing unessential factors in global sensitivity analysis. *Reliability Engineering & System Safety,* 92**,** 957-960.

SONNA, L. A., FUJITA, J., GAFFIN, S. L. & LILLY, C. M. 2002. Invited Review: Effects of heat and cold stress on mammalian gene expression. *Journal of Applied Physiology,* 92**,** 1725-1742.

SPEIDEL, D. 2010. Transcription-independent p53 apoptosis: an alternative route to death. *Trends in cell biology,* 20**,** 14-24.

SPRICK, M. R. & WALCZAK, H. 2004. The interplay between the Bcl-2 family and death receptor-mediated apoptosis. *Biochim Biophys Acta,* 1644**,** 125-32.

SRIBURI, R., JACKOWSKI, S., MORI, K. & BREWER, J. W. 2004. XBP1: a link between the unfolded protein response, lipid biosynthesis, and biogenesis of the endoplasmic reticulum. *The Journal of Cell Biology,* 167**,** 35-41.

STANKIEWICZ, A. R., LACHAPELLE, G., FOO, C. P. Z., RADICIONI, S. M. & MOSSER, D. D. 2005. Hsp70 Inhibits Heat-induced Apoptosis Upstream of Mitochondria by Preventing Bax Translocation. *Journal of Biological Chemistry,* 280**,** 38729-38739.

STARK, A. M., PFANNENSCHMIDT, S., TSCHESLOG, H., MAASS, N., RÖSEL, F., MEHDORN, H. M. & HELD-FEINDT, J. 2006. Reduced mRNA and protein expression of BCL-2 versus decreased mRNA and increased protein expression of BAX in breast cancer brain metastases: a real-time PCR and immunohistochemical evaluation. *Neurological Research,* 28**,** 787-793.

STENNICKE, H. R., JÜRGENSMEIER, J. M., SHIN, H., DEVERAUX, Q., WOLF, B. B., YANG, X., ZHOU, Q., ELLERBY, H. M., ELLERBY, L. M., BREDESEN, D., GREEN, D. R., REED, J. C., FROELICH, C. J. & SALVESEN, G. S. 1998. Pro-caspase-3 Is a Major Physiologic Target of Caspase-8. *Journal of Biological Chemistry,* 273**,** 27084-27090.

SUGIMOTO, N., SHIDO, O., MATSUZAKI, K., OHNO-SHOSAKU, T., HITOMI, Y., TANAKA, M., SAWAKI, T., FUJITA, Y., KAWANAMI, T., MASAKI, Y., OKAZAKI, T., NAKAMURA, H., KOIZUMI, S., YACHIE, A. & UMEHARA, H. 2012. Cellular Heat Acclimation Regulates Cell Growth, Cell Morphology, Mitogen-activated Protein Kinase Activation, and Expression of Aquaporins in Mouse Fibroblast Cells. *Cellular Physiology and Biochemistry,* 30**,** 450-457.

SUGIURA, T. 1992. Effects of glucose on the production of recombinant protein C in mammalian cell culture. *Biotechnology and Bioengineering,* 39**,** 953-959.

SURESHKUMAR, G. K. & MUTHARASAN, R. 1991. The influence of temperature on a mouse–mouse hybridoma growth and monoclonal antibody production. *Biotechnology and Bioengineering,* 37**,** 292-295.

SUZUKI, E. & OLLIS, D. F. 1989. Cell cycle model for antibody production kinetics. *Biotechnology and Bioengineering,* 34**,** 1398-1402.

SUZUKI, T., FUJIKURA, K., HIGASHIYAMA, T. & TAKATA, K. 1997. DNA Staining for Fluorescence and Laser Confocal Microscopy. *Journal of Histochemistry & Cytochemistry,* 45**,** 49-53.

SWIDEREK, H. & AL-RUBEAI, M. 2007. Functional genome-wide analysis of antibody producing NS0 cell line cultivated at different temperatures. *Biotechnology and Bioengineering,* 98**,** 616-630.

SZEGEZDI, E., LOGUE, S. E., GORMAN, A. M. & SAMALI, A. 2006. Mediators of endoplasmic reticulum stress-induced apoptosis. *EMBO Reports,* 7**,** 880-885.

TABAS, I. & RON, D. 2011. Integrating the mechanisms of apoptosis induced by endoplasmic reticulum stress. *Nature cell biology,* 13**,** 184-190.

TAKAGI, M., HIA, H. C., JANG, J. H. & YOSHIDA, T. 2001. Effects of high concentrations of energy sources and metabolites on suspension culture of Chinese hamster ovary cells producing tissue plasminogen activator. *Journal of Bioscience and Bioengineering,* 91**,** 515-521.

TAKUMA, S., HIRASHIMA, C. & PIRET, J. M. 2007. Dependence on glucose limitation of the pCO2 influences on CHO cell growth, metabolism and IgG production. *Biotechnology and Bioengineering,* 97**,** 1479-1488.

TANG, Y., REED, P., VAN WERKHOVEN, K. & WAGENER, T. 2007. Advancing the identification and evaluation of distributed rainfall-runoff models using global sensitivity analysis. *Water Resources Research,* 43**,** n/a-n/a.

TEIXEIRA, A., CUNHA, A. E., CLEMENTE, J. J., MOREIRA, J. L., CRUZ, H. J., ALVES, P. M., CARRONDO, M. J. T. & OLIVEIRA, R. 2005. Modelling and optimization of a recombinant BHK-21 cultivation process using hybrid grey-box systems. *Journal of Biotechnology,* 118**,** 290-303.

TEMPLETON, N., LEWIS, A., DORAI, H., QIAN, E. A., CAMPBELL, M. P., SMITH, K. D., LANG, S. E., BETENBAUGH, M. J. & YOUNG, J. D. 2014. The impact of anti-apoptotic gene Bcl-2Δ expression on CHO central metabolism. *Metabolic Engineering,* 25**,** 92-102.

TERADA, S., ITOH, Y., UEDA, H. & SUZUKI, E. 1997. Characterization and fed-batch culture of hybridoma overexpressing apoptosis suppressing gene bcl-2. *Cytotechnology,* 24**,** 135-141.

TEY, B. T. & AL-RUBEAI, M. 2004. Suppression of apoptosis in perfusion culture of Myeloma NS0 cells enhances cell growth but reduces antibody productivity. *Apoptosis,* 9**,** 843-852.

TEY, B. T. & AL-RUBEAI, M. 2005. Effect of Bcl-2 overexpression on cell cycle and antibody productivity in chemostat cultures of myeloma NS0 cells. *Journal of Bioscience and Bioengineering,* 100**,** 303-310.

TEY, B. T., SINGH, R. P., PIREDDA, L., PIACENTINI, M. & AL-RUBEAI, M. 2000a. Bcl-2 mediated suppression of apoptosis in myeloma NS0 cultures. *Journal of Biotechnology,* 79**,** 147-159.

TEY, B. T., SINGH, R. P., PIREDDA, L., PIACENTINI, M. & AL-RUBEAI, M. 2000b. Influence of Bcl-2 on cell death during the cultivation of a Chinese hamster ovary cell line expressing a chimeric antibody. *Biotechnology and Bioengineering,* 68**,** 31-43.

THOMPSON, M., PABELICK, C. & PRAKASH, Y. S. 2009. Role of STIM1 in Regulation of Store-Operated Ca2+ Influx in Pheochromocytoma Cells. *Cellular and Molecular Neurobiology,* 29**,** 193-202.

THORBURN, A. 2008. Apoptosis and Autophagy: regulatory connections between two supposedly different processes. *Apoptosis : an international journal on programmed cell death,* 13**,** 1-9.

TIGGES, M. & FUSSENEGGER, M. 2006. Xbp1-based engineering of secretory capacity enhances the productivity of Chinese hamster ovary cells. *Metabolic Engineering,* 8**,** 264-272.

TINTÓ, A., GABERNET, C., VIVES, J., PRATS, E., CAIRÓ, J. J., CORNUDELLA, L. S. & GÒDIA, F. 2002. The protection of hybridoma cells from apoptosis by caspase inhibition allows culture recovery when exposed to non-inducing conditions. *Journal of Biotechnology,* 95**,** 205-214.

TORKASHVAND, F., VAZIRI, B., MALEKNIA, S., HEYDARI, A., VOSSOUGHI, M., DAVAMI, F. & MAHBOUDI, F. 2015. Designed Amino Acid Feed in Improvement of Production and Quality Targets of a Therapeutic Monoclonal Antibody. *PLoS ONE,* 10**,** e0140597.

TOSHIYUKI, M. & REED, J. C. 1995. Tumor suppressor p53 is a direct transcriptional activator of the human bax gene. *Cell,* 80**,** 293-299.

TRUMMER, E., FAULAND, K., SEIDINGER, S., SCHRIEBL, K., LATTENMAYER, C., KUNERT, R., VORAUER-UHL, K., WEIK, R., BORTH, N., KATINGER, H. & MÜLLER, D. 2006. Process parameter shifting: Part I. Effect of DOT, pH, and temperature on the performance of Epo-Fc expressing CHO cells cultivated in controlled batch bioreactors. *Biotechnology and Bioengineering,* 94**,** 1033-1044.

TURNER, K. J., PLOZZA, T. M. & HOLT, P. G. 1985. Cell cycle-dependent fluctuations in IgE secretion in a human myeloma line. *Clin Immunol Immunopathol,* 36**,** 212-6.

TYSON, J. J., BAUMANN, W. T., CHEN, C., VERDUGO, A., TAVASSOLY, I., WANG, Y., WEINER, L. M. & CLARKE, R. 2011. Dynamic modelling of oestrogen signalling and cell fate in breast cancer cells. *Nat Rev Cancer,* 11**,** 523-532.

TZUR, A., MOORE, J. K., JORGENSEN, P., SHAPIRO, H. M. & KIRSCHNER, M. W. 2011. Optimizing Optical Flow Cytometry for Cell Volume-Based Sorting and Analysis. *PLoS ONE,* 6**,** e16053.

VAJDA, S., GODFREY, K. R. & RABITZ, H. 1989. Similarity transformation approach to identifiability analysis of nonlinear compartmental models. *Mathematical Biosciences,* 93**,** 217-248.

VAN BAKEL, H., NISLOW, C., BLENCOWE, B. J. & HUGHES, T. R. 2010. Most "Dark Matter" Transcripts Are Associated With Known Genes. *PLoS Biology,* 8**,** e1000371.

VAN ENGELAND, M., NIELAND, L. J., RAMAEKERS, F. C., SCHUTTE, B. & REUTELINGSPERGER, C. P. 1998. Annexin V-affinity assay: a review on an apoptosis detection system based on phosphatidylserine exposure. *Cytometry,* 31**,** 1-9.

VAN WERKHOVEN, K., WAGENER, T., REED, P. & TANG, Y. 2008. Characterization of watershed model behavior across a hydroclimatic gradient. *Water Resources Research,* 44**,** n/a-n/a.

VANDER HEIDEN, M. G., CANTLEY, L. C. & THOMPSON, C. B. 2009. Understanding the Warburg Effect: The Metabolic Requirements of Cell Proliferation. *Science,* 324**,** 1029-1033.

VANDER HEIDEN, M. G., PLAS, D. R., RATHMELL, J. C., FOX, C. J., HARRIS, M. H. & THOMPSON, C. B. 2001. Growth Factors Can Influence Cell Growth and Survival through Effects on Glucose Metabolism. *Molecular and Cellular Biology,* 21**,** 5899-5912.

VANROLLEGHEM, P. A., MANNINA, G., COSENZA, A. & NEUMANN, M. B. 2015. Global sensitivity analysis for urban water quality modelling: Terminology, convergence and comparison of different methods. *Journal of Hydrology,* 522**,** 339-352.

VARGAS, F., PIZARRO, F., PEREZ-CORREA, J. R. & AGOSIN, E. 2011. Expanding a dynamic flux balance model of yeast fermentation to genome-scale. *BMC Systems Biology,* 5**,** 75.

VE´LIZ, E. C., RODRı´GUEZ, G. & CARDERO, A. F. 2008. Bioreactors for animal cells. *In:* CASTILHO, L. R., MORAES, A. M., AUGUSTO, E. F. P. & BUTLER, M. (eds.) *Animal Cell Technology: From Biopharmaceuticals to Gene Therapy.* Madison Avenue, New York: Taylor & Francis Group.

VERGARA, M., BECERRA, S., BERRIOS, J., OSSES, N., REYES, J., RODRÍGUEZ-MOYÁ, M., GONZALEZ, R. & ALTAMIRANO, C. 2014. Differential Effect of Culture Temperature and Specific Growth Rate on CHO Cell Behavior in Chemostat Culture. *PLoS ONE,* 9**,** e93865.

VERMES, I., HAANEN, C., STEFFENS-NAKKEN, H. & REUTELLINGSPERGER, C. 1995. A novel assay for apoptosis Flow cytometric detection of phosphatidylserine expression on early apoptotic cells using fluorescein labelled Annexin V. *Journal of Immunological Methods,* 184**,** 39-51.

VOMASTEK, T. & FRANĚK, F. 1993. Kinetics of development of spontaneous apoptosis in B cell hybridoma cultures. *Immunology Letters,* 35**,** 19-24.

WAAGE, P. & GULBERG, C. M. 1986. Studies concerning affinity. *Journal of Chemical Education,* 63**,** 1044.

WALTER, E. & LECOURTIER, Y. 1981. Unidentifiable compartmental models: what to do? *Mathematical Biosciences,* 56**,** 1-25.

WANG, D., MA, J., SUN, D., LI, H., JIANG, C. & LI, X. 2015. Expression of bioactive anti-CD20 antibody fragments and induction of ER stress response in Arabidopsis seeds. *Applied Microbiology and Biotechnology,* 99**,** 6753-6764.

WANG, X., SPANDIDOS, A., WANG, H. & SEED, B. 2012. PrimerBank: a PCR primer database for quantitative gene expression analysis, 2012 update. *Nucleic Acids Research,* 40**,** D1144-D1149.

WARBURG, O., WIND, F. & NEGELEIN, E. 1927. The metabolism of tumors in the body. *The Journal of General Physiology,* 8**,** 519-530.

WATANABE, S., SHUTTLEWORTH, J. & AL-RUBEAI, M. 2001. Regulation of Cell Cycle and Productivity in NS0 Cells by the Over-Expression of p21CIP1. *In:* LINDNER-OLSSON, E., CHATZISSAVIDOU, N. & LÜLLAU, E. (eds.) *Animal Cell Technology: From Target to Market.* Springer Netherlands.

WATANABE, S., SHUTTLEWORTH, J. & AL-RUBEAI, M. 2002. Regulation of cell cycle and productivity in NS0 cells by the over-expression of p21CIP1. *Biotechnology and Bioengineering,* 77**,** 1-7.

WATATANI, Y., KIMURA, N., SHIMIZU, Y. I., AKIYAMA, I., TONAKI, D., HIROSE, H., TAKAHASHI, S. & TAKAHASHI, Y. 2007. Amino acid limitation induces expression of ATF5 mRNA at the post-transcriptional level. *Life Sciences,* 80**,** 879-885.

WATSON, J. V., CHAMBERS, S. H. & SMITH, P. J. 1987. A pragmatic approach to the analysis of DNA histograms with a definable G1 peak. *Cytometry,* 8**,** 1-8.

WEIDEMANN, R., LUDWIG, A. & KRETZMER, G. 1994. Low temperature cultivation — A step towards process optimisation. *Cytotechnology,* 15**,** 111-116.

WEISSTEIN, E. W. 2016. F-Distribution. From MathWorld--A Wolfram Web Resource.

WERNER, R. G., NOE, W., KOPP, K. & SCHLUTER, M. 1998. Appropriate mammalian expression systems for biopharmaceuticals. *Arzneimittelforschung,* 48**,** 870-80.

WERSTO, R. P., CHREST, F. J., LEARY, J. F., MORRIS, C., STETLER-STEVENSON, M. & GABRIELSON, E. 2001. Doublet discrimination in DNA cell-cycle analysis. *Cytometry,* 46**,** 296-306.

WHITFORD, W. G. 2006. Fed-Batch Mammalian Cell Culture in Bioproduction. *BioProcess International,* 4**,** pp. 30-40.

WIDLAK, P. 2000. The DFF40/CAD endonuclease and its role in apoptosis. *Acta Biochim Pol,* 47**,** 1037-44.

WONG, D. C. F., WONG, K. T. K., NISSOM, P. M., HENG, C. K. & YAP, M. G. S. 2006. Targeting early apoptotic genes in batch and fed-batch CHO cell cultures. *Biotechnology and Bioengineering,* 95**,** 350-361.

WOODWARD, C., HENDERSON JR., J. W. & WIELGOS, T. 2007. High-Speed Amino Acid Analysis (AAA) on 1.8 μm Reversed-Phase (RP) Columns. USA: Agilent Technologies, Inc. .

XANTHOUDAKIS, S., ROY, S., RASPER, D., HENNESSEY, T., AUBIN, Y., CASSADY, R., TAWA, P., RUEL, R., ROSEN, A. & NICHOLSON, D. W. 1999. Hsp60 accelerates the maturation of pro-caspase-3 by upstream activator proteases during apoptosis. *The EMBO Journal,* 18**,** 2049-2056.

XIAO, B., COSTE, B., MATHUR, J. & PATAPOUTIAN, A. 2011. Temperature-dependent STIM1 activation induces Ca2+ influx and modulates gene expression. *Nat Chem Biol,* 7**,** 351-358.

XIE, L. & WANG, D. I. C. 1994. Fed-batch cultivation of animal cells using different medium design concepts and feeding strategies. *Biotechnology and Bioengineering,* 43**,** 1175-1189.

XING, J. Z., YANG, X., XU, P., ANG, W. T. & CHEN, J. 2012. Ultrasound-Enhanced Monoclonal Antibody Production. *Ultrasound in Medicine & Biology,* 38**,** 1949-1957.

XU, G., KWON, G., CRUZ, W. S., MARSHALL, C. A. & MCDANIEL, M. L. 2001. Metabolic Regulation by Leucine of Translation Initiation Through the mTOR-Signaling Pathway by Pancreatic β-Cells. *Diabetes,* 50**,** 353-360.

XU, P., DAI, X.-P., GRAF, E., MARTEL, R. & RUSSELL, R. 2014. Effects of glutamine and asparagine on recombinant antibody production using CHO-GS cell lines. *Biotechnology Progress***,** n/a-n/a.

YANG, J., CHI, Y., BURKHARDT, B. R., GUAN, Y. & WOLF, B. A. 2010. Leucine metabolism in regulation of insulin secretion from pancreatic beta cells. *Nutrition reviews,* 68**,** 270-279.

YANG, M. & BUTLER, M. 2000. Effects of ammonia on CHO cell growth, erythropoietin production, and glycosylation. *Biotechnology and Bioengineering,* 68**,** 370-380.

YOON, S. K., HONG, J. K., CHOO, S. H., SONG, J. Y., PARK, H. W. & LEE, G. M. 2006. Adaptation of Chinese hamster ovary cells to low culture temperature: Cell growth and recombinant protein production. *Journal of Biotechnology,* 122**,** 463-472.

YOON, S. K., KIM, S. H. & LEE, G. M. 2003a. Effect of Low Culture Temperature on Specific Productivity and Transcription Level of Anti-4–1BB Antibody in Recombinant Chinese Hamster Ovary Cells. *Biotechnology Progress,* 19**,** 1383-1386.

YOON, S. K., SONG, J. Y. & LEE, G. M. 2003b. Effect of low culture temperature on specific productivity, transcription level, and heterogeneity of erythropoietin in Chinese hamster ovary cells. *Biotechnology and Bioengineering,* 82**,** 289-298.

YOUNG, J. D. 2013. Metabolic flux rewiring in mammalian cell cultures. *Current Opinion in Biotechnology,* 24**,** 1108-1115.

YU, J. & ZHANG, L. 2005. The transcriptional targets of p53 in apoptosis control. *Biochem Biophys Res Commun,* 331**,** 851-8.

YUE, H., BROWN, M., KNOWLES, J., WANG, H., BROOMHEAD, D. S. & KELL, D. B. 2006. Insights into the behaviour of systems biology models from dynamic sensitivity and identifiability analysis: a case study of an NF-[small kappa]B signalling pathway. *Molecular BioSystems,* 2**,** 640-649.

YUGI, K., NAKAYAMA, Y., KINOSHITA, A. & TOMITA, M. 2005. Hybrid dynamic/static method for large-scale simulation of metabolism. *Theoretical Biology and Medical Modelling,* 2**,** 42.

ZAGARI, F., JORDAN, M., STETTLER, M., BROLY, H. & WURM, F. M. 2013. Lactate metabolism shift in CHO cell culture: the role of mitochondrial oxidative activity. *New Biotechnology,* 30**,** 238-245.

ZHANG, T., BRAZHNIK, P. & TYSON, J. J. 2009. Computational Analysis of Dynamical Responses to the Intrinsic Pathway of Programmed Cell Death. *Biophysical Journal,* 97**,** 415-434.

ZHOU, D., PALAM, L. R., JIANG, L., NARASIMHAN, J., STASCHKE, K. A. & WEK, R. C. 2008. Phosphorylation of eIF2 Directs ATF5 Translational Control in Response to Diverse Stress Conditions. *Journal of Biological Chemistry,* 283**,** 7064-7073.

ZHOU, F., BI, J.-X., ZENG, A.-P. & YUAN, J.-Q. 2006. A macrokinetic and regulator model for myeloma cell culture based on metabolic balance of pathways. *Process Biochemistry,* 41**,** 2207-2217.

ZHOU, M., CRAWFORD, Y., NG, D., TUNG, J., PYNN, A. F. J., MEIER, A., YUK, I. H., VIJAYASANKARAN, N., LEACH, K., JOLY, J., SNEDECOR, B. & SHEN, A.

2011. Decreasing lactate level and increasing antibody production in Chinese Hamster Ovary cells (CHO) by reducing the expression of lactate dehydrogenase and pyruvate dehydrogenase kinases. *Journal of Biotechnology,* 153**,** 27-34.

ZHOU, W., CHEN, C.-C., BUCKLAND, B. & AUNINS, J. 1997a. Fed-batch culture of recombinant NS0 myeloma cells with high monoclonal antibody production. *Biotechnology and Bioengineering,* 55**,** 783-792.

ZHOU, W., REHM, J., EUROPA, A. & HU, W.-S. 1997b. Alteration of mammalian cell metabolism by dynamic nutrient feeding. *Cytotechnology,* 24**,** 99-108.

ZHU, W., CHEN, J., CONG, X., HU, S. & CHEN, X. 2006. Hypoxia and Serum Deprivation-Induced Apoptosis in Mesenchymal Stem Cells. *STEM CELLS,* 24**,** 416-425.

ZIEHN, T. & TOMLIN, A. S. 2009. GUI–HDMR – A software tool for global sensitivity analysis of complex models. *Environmental Modelling & Software,* 24**,** 775-785.

ZUSTIAK, M. P., JOSE, L., XIE, Y., ZHU, J. & BETENBAUGH, M. J. 2014. Enhanced transient recombinant protein production in CHO cells through the co-transfection of the product gene with Bcl-xL. *Biotechnology Journal,* 9**,** 1164-1174.

Appendix A: Supplementary Materials for Chapter 4

A.1 Apoptotic cell population quantification

For the data acquisition in LSRFortessa cell analyser, the fluorescent laser configuration was set as follows: an excitation wavelength of 488 nm for Annexin-V-FITC and of 561 nm for PI and with a 530/30 nm and a 610/20 nm collection filters, respectively. In this study, the fluorescence compensation is required since there are more than two staining colours in the assay. It helps cancel out the "spillover", caused by that one colour has the fluorescence emission range overlapping with the fluorescent detection range of another staining colour (Roederer, 2000). Therefore, the single colour stained cells together with unstained cells were treated as controls and used for the compensation.

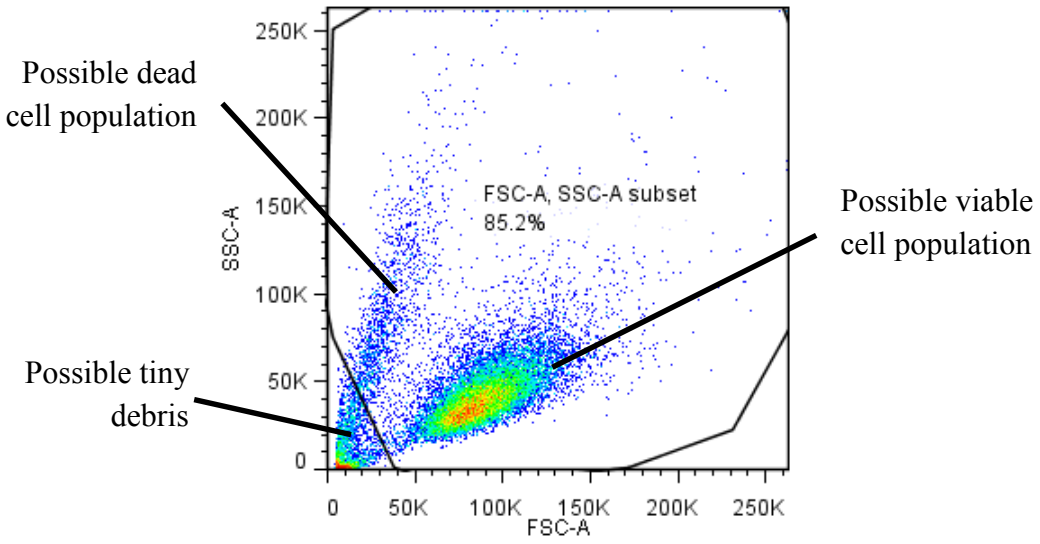
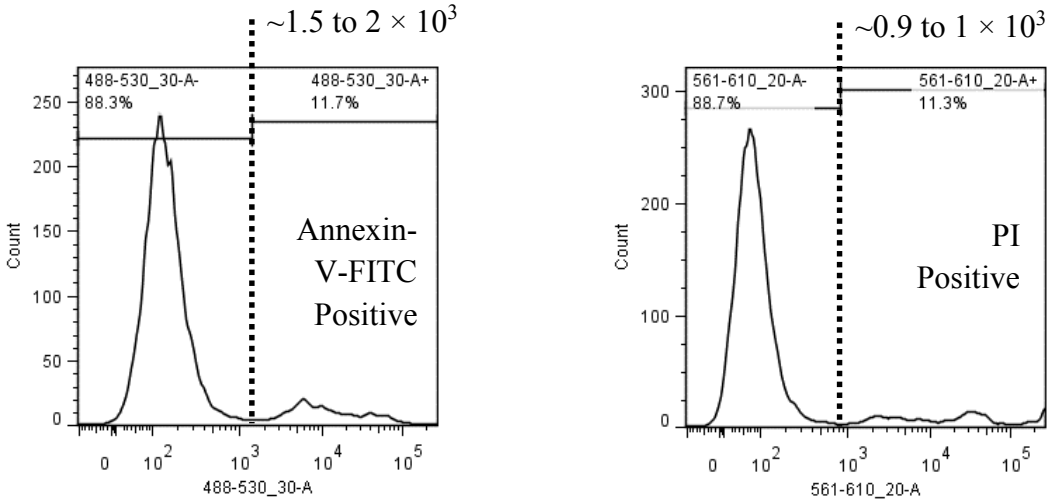


Figure A.1.1 Side scatter (SSC) VS. Forward scatter (FSC) diagram of an unstained sample with a gate to include viable and dead cell populations.

Forward scatter (FSC) and side scatter (SSC) were exploited to generally distinguish (viable and dead) cells from tiny debris, as shown in Figure A.1.1. The signal level of FSC is

proportional to the size of cell, while the SSC refers to the intracellular structure (Milner et al., 1996). This gate was applied to all samples and controls.



(A) (B)

Figure A.1.2 The histograms of the single stained samples, (A) Annexin V FITC and (B) PI.

The single stained samples; Annexin-V-FITC and PI, were analysed through their histograms, where the frequency of counts (cells) was plotted against the intensity of the specific fluorescence according to the staining colour. As can be seen in Figure A.1.2, there is a clear separation between the two populations; Annexin-V-FITC (A) and PI (B) positive, and Annexin-V-FITC negative and PI negative populations, respectively. The intensity value of the florescence, where the two populations were separated, was used to locate the gate to separate viable cells, apoptotic cells, and damaged cells in the next step. The compensation was computationally created using Flowjo with the data obtained from unstrained and single stained samples. The compensation was then applied to all unknown samples to avoid the possible false-positive/negative results caused by the "spillover" of the emission and collection fluorescence wavelengths.

It is worth mentioning here that flow cytometry records pulse signals when particles pass through the laser light. This signals can be collected by three options: height (the peak),

area (the integral of the pulse signal) and width (the duration). It is believed that the dot plot of FSC width versus FSC area helps discriminate among cell populations by the difference in their size, such as doublets from singlets (Wersto et al., 2001), because the width signal can be directly proportional to the particle diameter (Tzur et al., 2011).

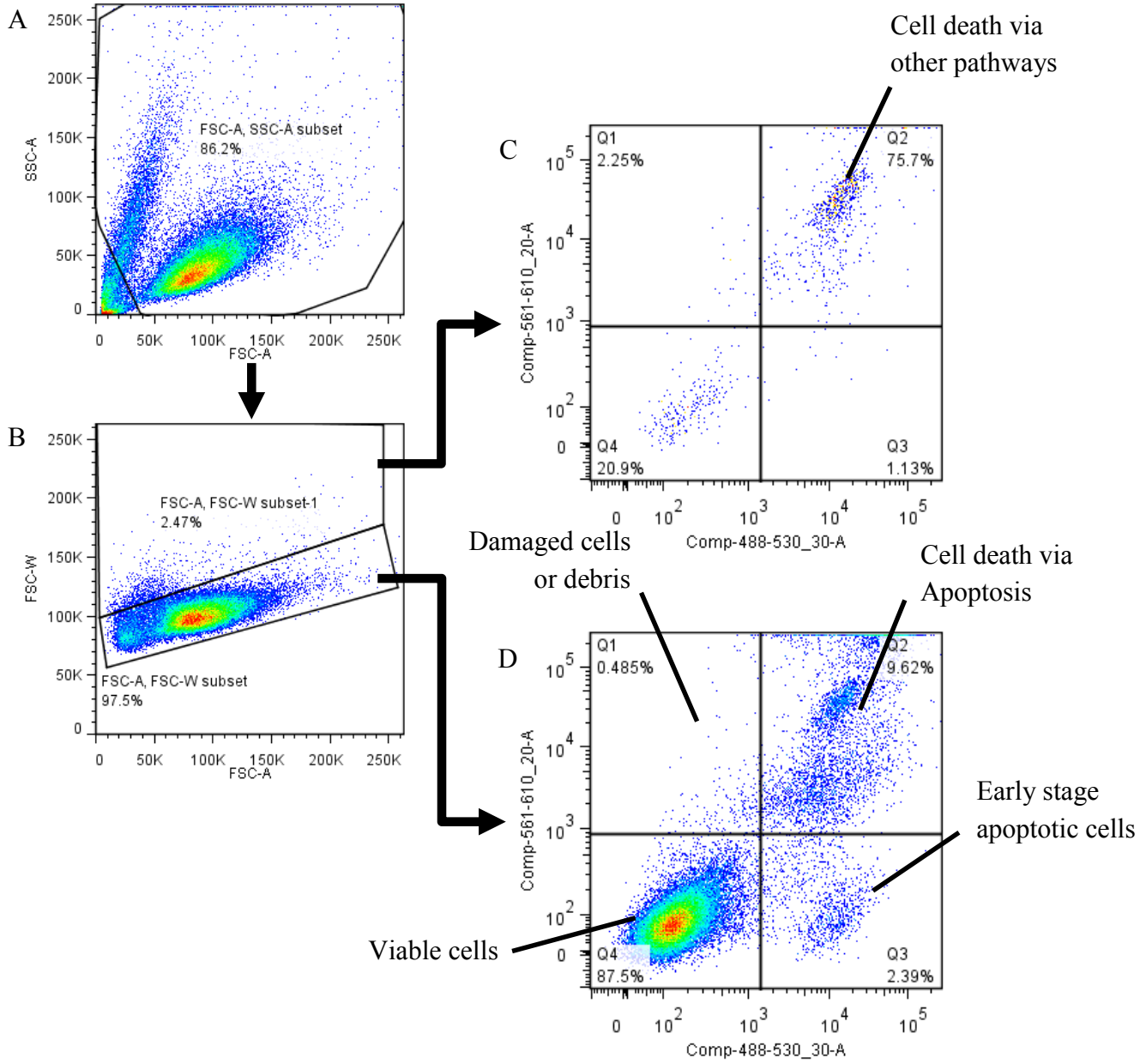


Figure A.1.3 The workflow of the quantification of apoptotic population fractions; (A) the first gate applied to the double stained sample; (B) the dot pot of FSC width versus FSC area to differentiate between populations by the diameter size; (C) and (D) quad gates used to separate the four populations.

In this analysis, the dot plot of FSC width versus FSC area was applied to separate potential swollen cells from normal and shrunk cells (Figure A.1.3-B). Then, both separated sub-populations were gated into four populations (Figure A.1.3-B&C); 1) Annexin-V-FITC and PI negative, or viable cells; 2) Annexin-V-FITC positive and PI negative, or ESA cells; 3) Annexin-V-FITC and PI positive, or dead cells; 4) Annexin-V-FITC negative and PI positive, or damaged cells. The quad gate was placed at the intensity values obtained from the single stained samples as previously shown; around 1.5×10^3 of 488 nm wavelength for Annexin-V-FITC and 0.9×10^3 561 nm wavelength for PI. The difference between the two sub-populations is that the swollen cells with both Annexin-V-FITC and PI positive (Figure A.1.3-C) was treated as "cell death by other pathways than apoptosis", since, for example, cell swelling is one of key morphological changes of necrotic cells (Cobb et al., 1996, Meshram et al., 2012). The normal size and shrunk cells with both staining positive were treated as cell death via apoptosis.

A.2 Cell cycle analysis

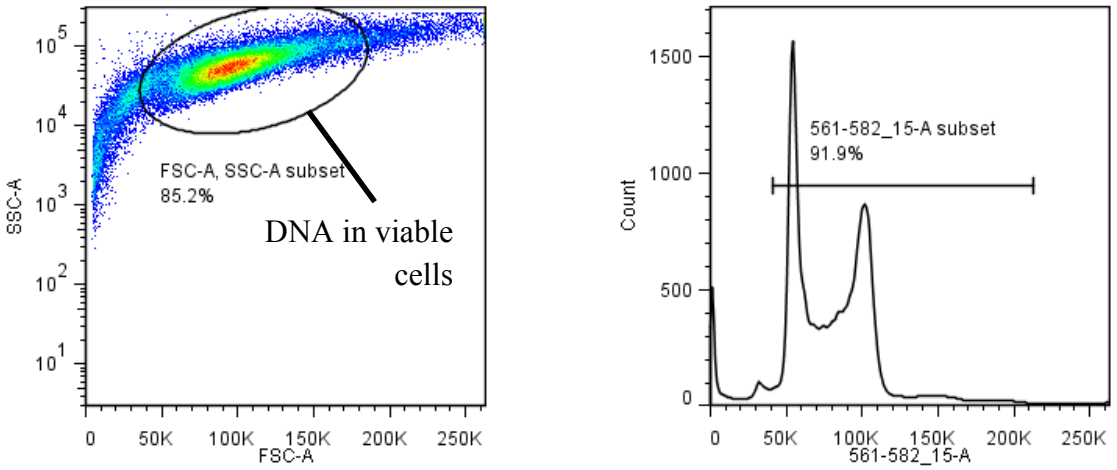


Figure A.2.1 DNA analysis with gates: (A) the dot plot of SSC versus FSC; and (B) the histogram showing the events against 561 nm fluorescence intensity.

The wavelength used for the data acquisition in the LSRFortessa cell analyser was at 561nm for excitation with a 582/15 nm collection filter, when PI solution was used to stained DNA. The data obtained were then analysed in Flowjo. The first gate introduced to the dot plot of SSC versus FSC, aims to include mostly DNA in viable cells as cell cycle is a proliferation process, as shown in Figure A.2.1-A. Figure A.2.1-B shows a histogram of the sup-population obtained from the first gate. Another gate was allocated to the histogram in order to crop-out possible debris and dead cell populations, as can be seen in Figure A.2.1-B.

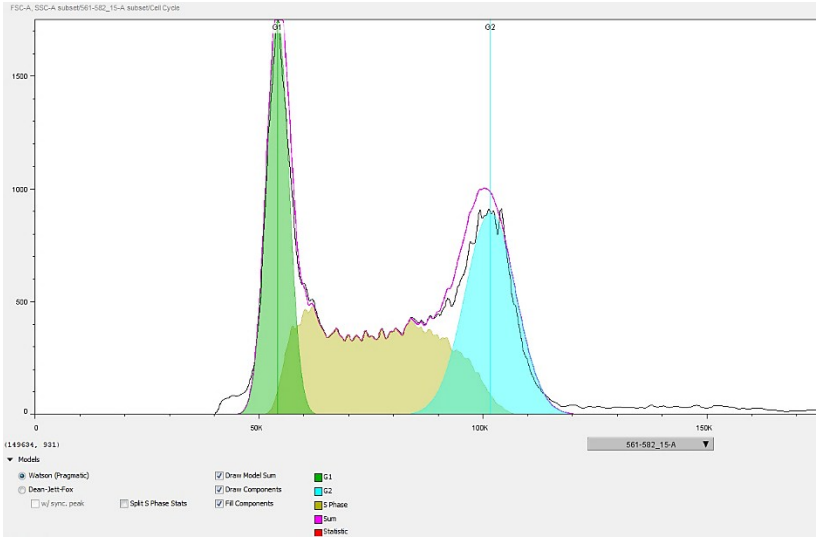


Figure A.2.2 Watson Algorithm (Watson et al., 1987) used to quantify the fraction of each sub-populations; G_1/G_0, S and G_2/M.

To identify each cell cycle phase sub-population, the gated DNA histogram was analysed using a well-established algorithm provided by Flowjo. There are two choices of the algorithms: 1) Watson and 2) Dean-Jett-Fox. The latter comes with a mathematical model to estimate the S phase population while the former has no assumption, but replicate the histogram curve. In this study, Watson algorithms was selected as it realistically capture the s phase population (Figure A.2.2). The G_1/G_0 phase population was identified as the first peak of the histogram. Given that cells at G_2/M have theoretically double amount of DNA to the G_1/G_0, the G_2/M population in the histogram can be also estimated when the G_1/G_0 one is identified.

In this analysis, a constraint of G_2 = approx.1.9 times of G_1 was used estimate the G_2/M population.

A.3 Cyclin quantification

The stained samples were analysed using the LSRFortessa flow cytometer (BD Biosciences). Data acquisition was performed using an excitation wavelength and emission filters for data collection as shown in Table A.3.1.

Table A.3.1 Flow cytometers configurations.

Stains	Excitation wavelength (nm)	Emission filters (nm/nm)
PI (DNA)	561	582/15
FITC (cyclins)	488	530/30
FxCycle (DNA)	405	450/50
FITC (cyclins)	488	530/30
PE (Ki-67)	561	582/15

Once cell cycle was analysed, the bivariate plot between DNA content and cyclin fluorescence was then generated, as shown in Figure A.3.1. There are two gates: one is around the isotype-stained area indicating non-specific binding; the other is above the isotype area indicating the positive expression of cyclins (Figure A.3.1). These gates were then applied to the DNA content of each phase of cell cycle. The expression of both isotype and cyclin-positive in each phase of cell cycle was compared. The cyclin that has the lowest expression at a corresponding phase was used as a reference expression; cyclin D1, E1 and B1 expressions were assumed to be minimal in the S, G_2/M and G_1/G_0, respectively. The expression of cyclins at a specific phase was normalised to the reference, enabling the cyclin quantification by comparison.

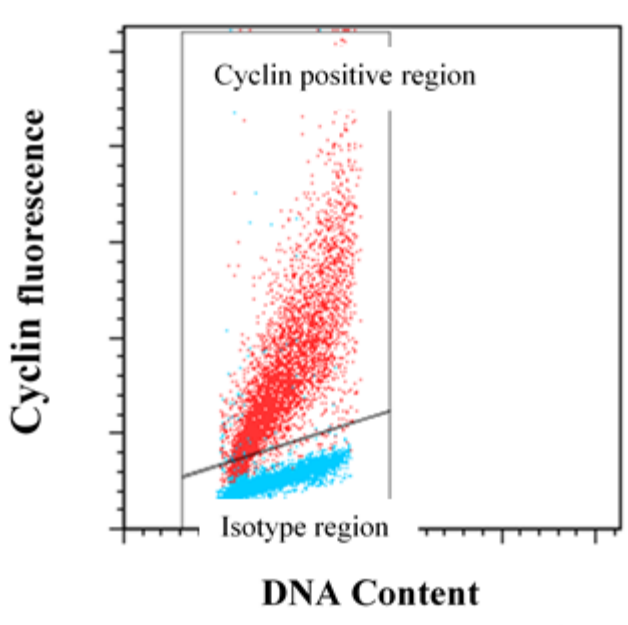


Figure A.3.1 Data analysis for cyclin quantification. Adapted from (García Münzer, 2014).

A.4 The estimation of gene expression using $\Delta\Delta C_T$ approach

As described earlier, the data were collected at the end of each thermal or PCR reaction cycle. The highly fluorescent marker (SYBR®), which is attached to the PCR product during the reactions, enables us to "real-time" monitor the quantity of the PCR product (in the form of fluorescence intensity) as respect to the increasing number of cycles. The plot between the cycle number and the net fluorescence intensity (ΔRn) is called "amplification plot", as shown in Figure A.4.1-A&B. There are three main phases of the plots: 1) linear-ground or lag phase (I), 2) exponential phase (II), and 3) linear or plateau phase (III). A threshold value of the fluorescence intensity was manually set in the region of the exponential phase (II), as previously reported (Karlen et al., 2007). Setting the threshold value enables us to obtain the threshold cycle (C_T), which is the number of cycle required to achieve the threshold value of the PCR product quantity. The logarithm plot of the amplification curve is preferable since the exponential phase is easier to be identified (Figure A.4.1-B). The C_T value is used for the estimation of gene expressions using the $\Delta\Delta C_T$ comparative method.

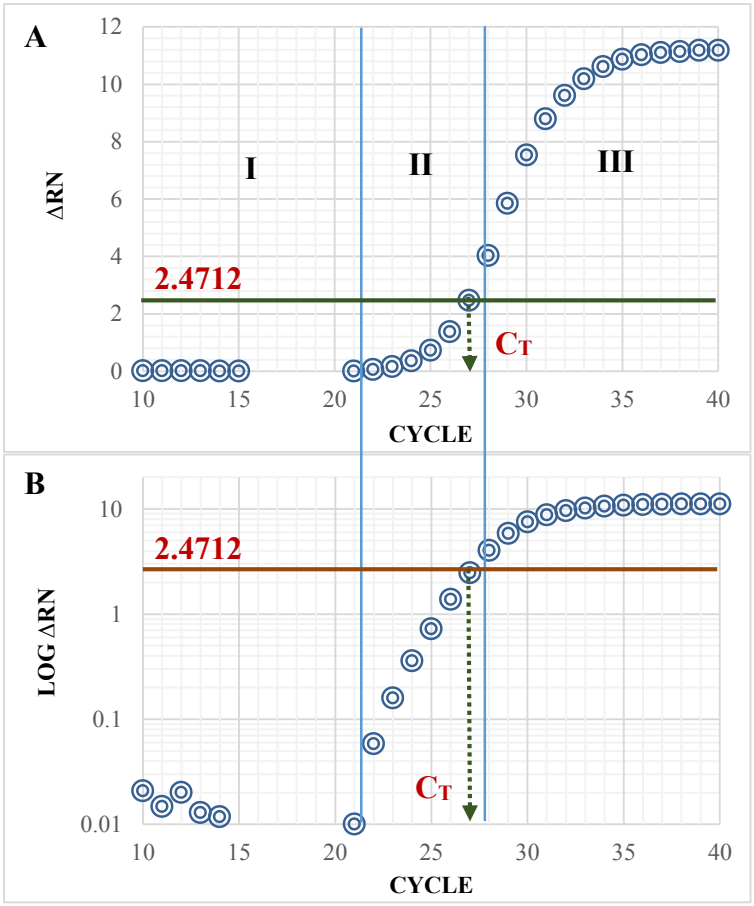


Figure A.4.1 The amplification plot and the threshold cycle (C_T) value; (A) the linear scale, and (B) the logarithm scale of the net fluorescence intensity. For example, The C_T value is around 27 cycles at the threshold value = 2.4712.

The $\Delta\Delta C_T$ comparative approach presents the gene expression in the form of relative fold change, which takes into account 1) the internal control expression (i.e. a housekeeping gene such as *gapdh*) and the reference sample expression (i.e. the sample at the beginning of the culture). After C_T values were obtained, the following equations were employed to estimate the relative fold change of unknown samples (Livak and Schmittgen, 2001).

Eq. A.4.1 The estimation of ΔC_T

$$\Delta C_{T,\, g=i,\, t=j} = C_{T,\, g=i,\, t=j} - C_{T,\, gapdh,\, t=j}$$

Where, "g" is gene and "t" is time point ($C_{T,i,j}$ is C_T value of gene "i" at time "j").

Eq. A.4.2 The estimation of $\Delta\Delta C_T$

$$\Delta\Delta C_{T,\, g=i,\, t=j} = \Delta C_{T,\, g=i,\, t=j} - \Delta C_{T,\, g=i,\, t=0}$$

Eq. A.4.3 The estimation of relative fold change

$$\text{Relative fold change*} = 2^{-\Delta\Delta C_T}$$

*The calculation assumed that all PCR reactions exhibited equally efficient DNA amplification.

The estimation of standard deviation (SD) of the expression was also performed along with the relative fold change of gene expression calculation. Since the real-time PCR was carried out in duplicate for each replicate, two C_T values were averaged for a C_T value of a gene at a time point of each culture replicate (Table A.4.1). The calculation of ΔC_T and $\Delta\Delta C_T$ involves the number with SD. Therefore, the SD of the outputs was estimated using Equation A.4.4. Table A.4.1 shows an example of the calculation of $\Delta\Delta C_T$ of *atf5* expression at 23 hour with its deviation.

Eq. A.4.4 The summation of number with standard deviation

$$(C \pm dC) = (A \pm dA) \pm (B \pm dB) \rightarrow C = A \pm B,\ dC \approx \sqrt{dA^2 + dB^2}$$

Table A.4.1 The estimation of $\Delta\Delta C_T$ value of *atf5* gene at time = 23 hours of a culture replicate.

Time (hr)	Gene	duplicate	C_T	Mean C_T	SD C_T	Mean ΔC_T	SD ΔC_T	Mean $\Delta\Delta C_T$	SD $\Delta\Delta C_T$
0	***atf5***	1	26.95	26.93	0.025	7.939	0.0432	0.00	0.0611
		2	26.91		0.018				
	gapdh	1	19.02	18.99	0.035	-	-	-	-
		2	18.97						
23	***atf5***	1	27.99	27.97	0.020	9.423	0.0693	**1.485**	**0.0816**
		2	27.96						
	gapdh	1	18.60	18.55	0.066	-	-	-	-
		2	18.50						

The $\Delta\Delta C_T$ values from each culture replicate were averaged (Table A.4.2). The SDs of the $\Delta\Delta C_T$ replicate averages were determined in the same way as Eq. A.4.4. Then, the relative

fold change of a gene expression at a time point was estimated using Equation A.4.3 with the $\Delta\Delta C_T$ replicate means. The deviation of the resulting relative fold change arises from the value of $2^{-\Delta\Delta C_T+SD_{\Delta\Delta C_T}}$ and $2^{-\Delta\Delta C_T-SD_{\Delta\Delta C_T}}$. Table A.4.2 shows an example of the calculation of the relative fold change of *atf5* expression at 23 hour with its deviation.

Table A.4.2 The estimation of average *atf5* expression relative fold changes for all culture replicates at time = 23 hours.

Time (hr)	Flask	Mean $\Delta\Delta C_T$	SD $\Delta\Delta C_T$	Mean of Mean $\Delta\Delta C_T$	SD of SD $\Delta\Delta C_T$	Mean $2^{-\Delta\Delta C_T}$	Max. $2^{-\Delta\Delta C_T-SD}$	Min. $2^{-\Delta\Delta C_T+SD}$
0	**A**	0.000	0.0446	0.000	0.121	**1.00**	**1.087**	**0.920**
	B	0.000	0.0943					
	C	0.000	0.0611					
23	**A**	1.706	0.1368	1.624	0.198	**0.33**	**0.372**	**0.283**
	B	1.680	0.1179					
	C	1.485	0.0816					

A.5 Calibration curve construction for amino acid quantification

Free amino acids in samples from the cultures were analysed using the HPLC system with the pre-column derivatization as described earlier in Chapter 4. To quantify the amino acids in the samples, a series of amino acid standard dilutions was constructed. It was analysed using the same procedure as that for the unknown samples. Table A.5.1 shows a series of amino acid standard dilutions where the concentrations of amino acid standards were consecutively diluted (by 50% from the 3rd dilution). The amino acid standard (Sigma-Aldrich, AAS18-10X1ML) do not include several amino acids: L-asparagine (Sigma-Aldrich, 51363), L-tryptophan (Sigma-Aldrich, 51145) and L-glutamine (Sigma-Aldrich, 76523). The solution form of these amino acids is not relatively stable at room temperature. They were, therefore,

prepared in a high concentration (22.5 mM in dH2O) and then mixed with the standard, as shown in Table A.5.1. Then, the dilution was conducted by adding 0.1 N HCl as indicated in Table A.5.1.

Given that the concentration of amino acids in fresh medium is not greater than 1.0 mM, calibration curves were constructed based on the data of up to the 3rd dilution. The injection of the standard dilutions was performed at least two times; before and after the analysis, to confirm the reproducibility. The absorbance data was recorded as the form of multiple-peak curves or chromatograms. Each peak represents each derivative, or implicitly each amino acid corresponding to its derivative. Areas under each peak were determined using OpenLAB Chromatography Data System C.01.04 (Agilent Technologies). Then, the plot between the area and concentration was created. Figure A.5.1 shows a plot between four key amino acid standards, glutamate, aspartate, asparagine and arginine, at different dilutions, and the area under corresponding peaks. Linear regression was applied to the data to relate the concentration of amino acid standards with the areas. Table A.5.2 summarises the linear correlations between the areas under the peaks and the concentrations of all the amino acids of interest.

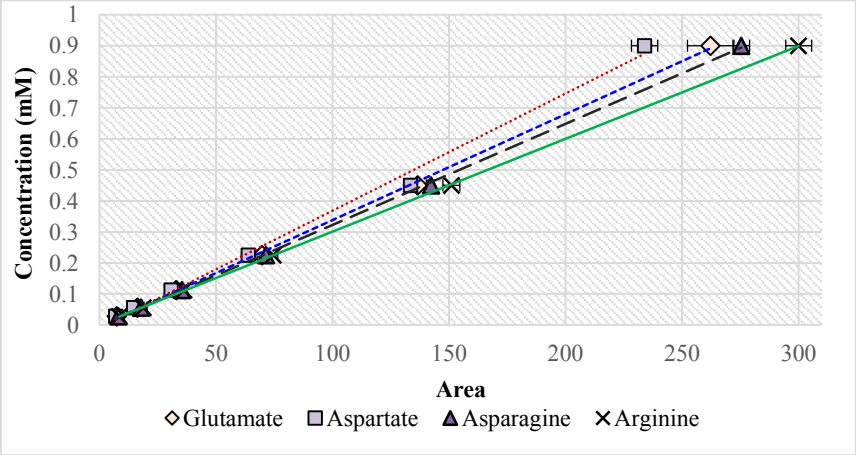


Figure A.5.1 The plot of the amino acid concentrations versus the corresponding areas under peaks. The linear lines represent the correlations between the concentrations and the areas.

Table A.5.1 A series of amino acid standard dilutions.

Dilutions		*take (µL)*	*1st Dil.*	*take (µL)*	*2nd Dil.*	*take (µL)*	*3rd Dil.*	*take (µL)*	*4th Dil.*	*take (µL)*	*5th Dil.*	*take (µL)*	*6th Dil.*	*take (µL)*	*7th Dil.*	*take (µL)*	*8th Dil.*
Amino acids Concentration	**(mM)**		**(mM)**		(mM)		(mM)		(mM)		**(mM)**		**(mM)**		**(mM)**		**(mM)**
L-Alanine	2.5		1.875		1.5		0.9		0.45		0.225		0.113		0.0563		0.028
NH_4Cl	2.5		1.875		1.5		0.9		0.45		0.225		0.113		0.0563		0.028
L-Arginine	2.5		1.875		1.5		0.9		0.45		0.225		0.113		0.0563		0.028
L-Aspartic Acid	2.5		1.875		1.5		0.9		0.45		0.225		0.113		0.0563		0.028
L-Cystine	1.25		0.9375		0.75		0.45		0.225		0.113		0.056		0.0281		0.014
L-Glutamic Acid	2.5		1.875		1.5		0.9		0.45		0.225		0.113		0.0563		0.028
Glycine	2.5		1.875		1.5		0.9		0.45		0.225		0.113		0.0563		0.028
L-Histidine	2.5		1.875		1.5		0.9		0.45		0.225		0.113		0.0563		0.028
L-Isoleucine	2.5		1.875		1.5		0.9		0.45		0.225		0.113		0.0563		0.028
L-Leucine	2.5	**900**	1.875		1.5		0.9		0.45		0.225		0.113		0.0563		0.028
L-Lysine	2.5		1.875		1.5		0.9		0.45		0.225		0.113		0.0563		0.028
L-Methionine	2.5		1.875	**800**	1.5	**600**	0.9	**500**	0.45	**500**	0.225	**500**	0.113	**500**	0.0563	**500**	0.028
L-Phenylalanine	2.5		1.875		1.5		0.9		0.45		0.225		0.113		0.0563		0.028
L-Proline	2.5		1.875		1.5		0.9		0.45		0.225		0.113		0.0563		0.028
L-Serine	2.5		1.875		1.5		0.9		0.45		0.225		0.113		0.0563		0.028
L-Threonine	2.5		1.875		1.5		0.9		0.45		0.225		0.113		0.0563		0.028
L-Tyrosine	2.5		1.875		1.5		0.9		0.45		0.225		0.113		0.0563		0.028
L-Valine	2.5		1.875		1.5		0.9		0.45		0.225		0.113		0.0563		0.028
(add) L-asparagine	22.5	**100**	1.875		1.5		0.9		0.45		0.225		0.113		0.0563		0.028
(add) L-tryptophan	22.5	**100**	1.875		1.5		0.9		0.45		0.225		0.113		0.0563		0.028
(add) L-glutamine	22.5	**100**	1.875		1.5		0.9		0.45		0.225		0.113		0.0563		0.028
Adding 0.1 N HCl		**0**	**add**	**200**	**add**	**400**		**500**		**500**		**500**		**500**		**500**	
total		**1200**		**1000**		**1000**		**1000**		**1000**		**1000**		**1000**		**1000**	
remaining		**400**		**400**		**500**		**500**		**500**		**500**		**500**		**1000**	

Table A.5.2 The linear correlations between the areas under the peaks and the concentrations of corresponding amino acids, where [Amino acid Conc.] = A × [Peak area] + B.

Amino acid	A	B	R^2	Amino acid	A	B	R^2
Aspartate	0.0038	-0.0093	0.9947	**Tyrosine**	0.0033	-0.0041	0.9999
Glutamate	0.0034	-0.0037	0.9993	**Cystine**	0.0019	-0.0033	0.9998
Asparagine	0.0033	-0.0040	0.9997	**Valine**	0.0032	-0.0095	0.9996
Serine	0.0032	-0.0003	1.0000	**Methionine**	0.0031	-0.0045	0.9999
glutamine	0.0032	-0.0023	0.9999	**Tryptophan**	0.0032	-0.0027	0.9999
Histidine	0.0038	0.0037	0.9999	**Phenylalanine**	0.0032	-0.0040	0.9998
Glycine	0.0031	0.0057	0.9999	**Isoleucine**	0.0031	-0.0059	0.9997
Threonine	0.0033	-0.0046	0.9999	**Leucine**	0.0031	-0.0061	0.9997
Arginine	0.0030	0.0018	0.9999	**Lysine**	0.0017	0.0118	0.9982
Alanine	0.0031	-0.0048	0.9997				

A.6 Calibration curve construction for mAb quantification

A series of mAb standard dilutions is required to construct a calibration curve for the mAb quantification. The mAb standard (8.76 mg/mL) was kindly provided by Lonza Biologics (Slough, UK). It was consecutively diluted by a factor of 2 as shown in Table A.6.1; from 8.76 mg/mL or 8760 mg/L to 8.554688 mg/L. PBS was used to dilute the standard. Since the concentration of mAb in samples ranges from around 15 mg/L possibly up to 300 mg/L, the dilutions used to construct the calibration curve were from the 4^{th} (D4) to the 10^{th} dilution (D10). The dilutions were injected, detected and analysed using the same procedure/method to that of samples, as described earlier in Chapter 4. The injection of the dilutions was performed twice to confirm its reproducibility. The area under peak was estimated using OpenLAB Chromatography Data System C.01.04 (Agilent Technologies). Figure A.6.1 shows the linear correlation between the area under the peak and the concentration of mAb. The linear regression shows an excellent fit for the measure data ($R^2 > 0.99$). The linear correlation was used to estimate the concentration of mAb in samples.

Table A.6.1 A series of mAb standard dilutions.

Dilutions	mg/mL	mg/L	
D0	8.76	8760	
D1	4.38	4380	
D2	2.19	2190	
D3	1.095	1095	
D4	0.5475	547.5	Working dilutions
D5	0.27375	273.75	
D6	0.136875	136.875	
D7	0.068438	68.4375	
D8	0.034219	34.21875	
D9	0.017109	17.10938	
D10	0.008555	8.554688	

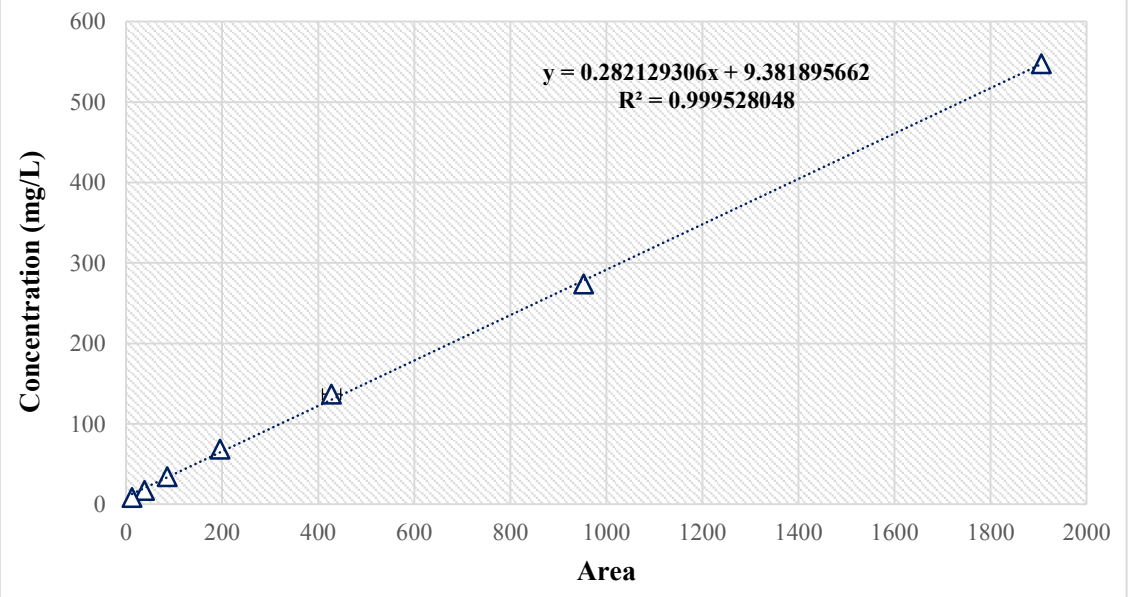
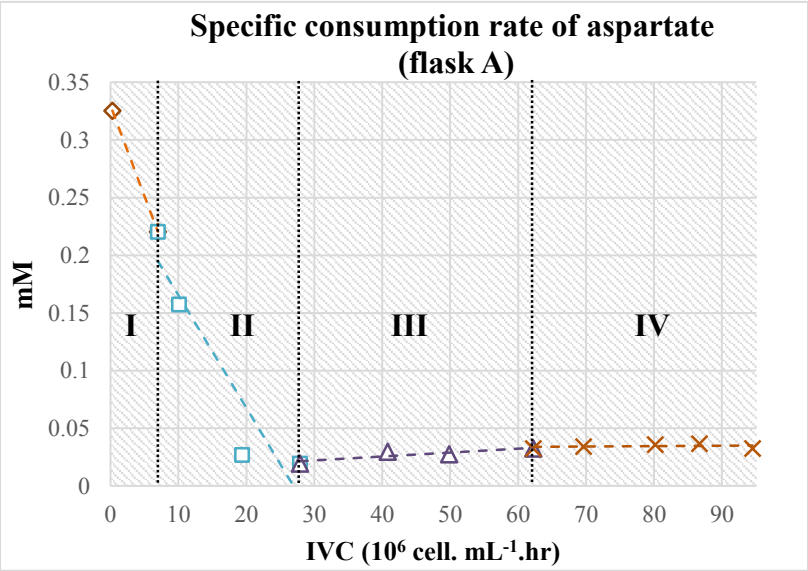


Figure A.6.1 The calibration curve for mAb quantification.

A.7 Examples of cell culture descriptive parameter estimation

The integral of viable cells (IVC) and the specific cell growth rate were determined according to Eq. 4.4.1 as previously described in Chapter 4. IVC was used to estimate other cell culture parameters, including specific consumption/production rates of extracellular

nutrients, metabolites and mAb. To determine these parameters, plots between IVC (x-axis) and the extracellular concentration of nutrients, mAb and metabolites (y-axis) were created. As can be seen in Figure A.7.1, the specific consumption rate of aspartate were obtained from the linear regression line for the data. The slope of the line represents the specific consumption rate, where the unit of the slope is the unit of Y-axis; µmole.mL^{-1}, over the unit of x-axis; 10^6 cell.mL^{-1}.hr = µmole.10^{-6} cell.hr^{-1}.



Culture phase	Slope
Early exponential (I)	-0.0174
Exponential (II)	-0.0093
Stationary (III)	0.0004
Death (IV)	-8.00E-5

Figure A.7.1 The estimation of specific consumption rates (slope) of aspartate in each phase of a culture replicate: (I) early exponential, (II) exponential, (III) stationary and (IV) death phases.

The data were divided into culture phases: early exponential (I), exponential (II), stationary (III) and death phases (IV). The slope of the linear regression line in each phase, therefore, represents the specific consumption/production rate in each culture phase, as can be seen in Figure A.7.1. The mean value of the culture parameters and their SD were estimated from the culture parameter of each culture replicate. Table A.7.1 shows an example of the estimation of the mean specific consumption rate of aspartate and the SD from all culture replicates.

Table A.7.1 The average value of the specific consumption rate of aspartate (μmol.10^{-6} cell. day^{-1}) from all culture replicates and its standard deviation.

Culture phase	Specific consumption rate (μmol.10^{-6} cell. day^{-1})				
	Flask A	Flask B	Flask C	Average	SD
Early exponential (I)	-0.6505	-0.6969	-0.8219	-0.4165	0.0511
Exponential (II)	-0.4070	-0.3641	-0.3953	-0.2239	0.0128
Stationary (III)	0.0142	0.0147	0.0209	0.0095	0.0022
Death (IV)	0.0013	-0.0058	-0.0052	-0.0019	0.0022

The yield of lactate over glucose was also determined using the graphical method. Instead plotting against IVC, the concentration of lactate produced (y-axis) was plotted against the glucose consumed (x-axis). The slope of the linear regression line in the plot stands for the yield of lactate over glucose. This was performed for all culture replicate (flask A, B and C) to determine the mean yield and its SD, as similar to the one for the specific consumption/production rates.

A.8 F-statistic calculation

Degrees of freedom can be simply estimated from the data size. Table A.8.1 shows the data of p21 expression in the batch culture.

Table A.8.1 p21 expression in the batch culture.

Time (hr)	Group	Mean	SD	Size
0	1	1.00	0.03	3.00
23	2	1.03	0.06	3.00
45	3	1.18	0.03	3.00
69	4	0.93	0.26	3.00
93	5	3.17	0.27	3.00
116	6	3.74	0.28	3.00
139	7	2.40	0.17	3.00

As you can see from Table A.8.1, there are 7 groups (k) and the total sample size is equal to 7×3 = 21.

Therefore, the degrees of freedom between groups = k-1 = 7-1 = 6, while the degrees of freedom within groups = N-k = 21-7 = 14. (Note that the total degrees of freedom = N-1 = 20).

The mean squares (MS) are calculated from the degrees of freedom (DF) and the sum of squares (SS) of both one between groups and one within the groups. The overall mean is calculated from the sum of the group means divided by the number of groups, which is equal to 1.92 as can be seen from Table A.8.2. The SS within the groups is estimated from the sum of sample variances, or the square of the samples SDs multiplied by the DF of the corresponding groups. The MS within the groups is the SS within the groups divided by the DF within the groups, as can be seen at the column 3 in Table A.8.2. The MS between groups is estimated according to Eq. 4.4.3 which is based on the variance among sample means from the overall mean, as you can see from the column 4. The F-statistic is shown in the column 5 which is the MS between groups over MS within groups.

Table A.8.2 F-statistic calculation.

Group	Mean	SS within	SS between	F
1	1.00	0.00	2.54	**116.07**
2	1.03	0.01	2.40	
3	1.18	0.00	1.63	
4	0.93	0.14	2.93	
5	3.17	0.14	4.65	
6	3.74	0.15	9.89	
7	2.40	0.06	0.69	
Total		**0.50**	**24.73**	
	Overall mean	MS within	MS between	
	1.92	**0.04**	**4.12**	

Appendix B: Supplementary Materials for Chapter 5, 6&7

B.1 Raw data of batch and fed-batch mAb quantification

Table B.1.1 Batch culture raw data of mAb quantification.

Time (hours)	Flask A (mg/L)	Flask B (mg/L)	Flask C (mg/L)	Mean (mg/L)	SD (mg/L)
0	N/A	14.03	13.05	13.54	0.69
8	16.77	19.10	17.43	17.77	1.20
23	18.68	19.15	19.22	19.02	0.29
31	20.10	21.14	21.07	20.77	0.59
45	20.71	N/A	22.26	21.49	1.10
54	27.07	N/A	28.07	27.57	0.70
69	37.10	N/A	38.93	38.01	1.29
79	33.24	N/A	34.01	33.63	0.54
93	42.66	N/A	47.36	45.01	3.32
101	56.91	60.92	58.20	58.68	2.05
116	58.95	N/A	61.60	60.27	1.87
126	67.73	N/A	74.33	71.03	4.67
139	73.87	84.25	83.66	80.59	5.83
148	75.21	84.13	90.39	83.24	7.63

N/A indicates that samples were not available due to missing during storage.

Table B.1.2 F1 Fed-Batch culture raw data of mAb quantification.

Time (hours)	Flask A (mg/L)	Flask B (mg/L)	Flask C (mg/L)	Mean (mg/L)	SD (mg/L)
0	19.04	19.42	18.74	19.07	0.34
23.5	24.08	23.64	23.69	23.80	0.24
34.5	26.15	27.91	27.44	27.17	0.91
47.5	33.41	33.19	33.22	33.27	0.12
58	40.13	39.88	39.06	39.69	0.56
71.5	48.62	47.47	48.29	48.13	0.59
82	56.68	56.43	56.82	56.64	0.20
95.5	67.57	65.49	67.77	66.94	1.26
106	76.45	75.83	75.10	75.79	0.68
119.5	83.62	83.20	86.58	84.47	1.84
131	95.61	88.88	96.48	93.66	4.16
144.5	100.83	100.70	101.26	100.93	0.30

Table B.1.3 F2 Fed-Batch culture raw data of mAb quantification.

Time (hours)	Flask A (mg/L)	Flask B (mg/L)	Flask C (mg/L)	Mean (mg/L)	SD (mg/L)
0	18.84	18.55	18.55	18.64	0.17
23	23.79	23.25	24.20	23.75	0.48
35.5	30.90	29.93	29.54	30.13	0.70
47	37.31	36.55	36.38	36.75	0.49
58.5	48.38	48.57	47.99	48.32	0.30
71	56.91	59.02	59.37	58.43	1.33
83.5	69.93	75.50	70.30	71.91	3.11
95	76.99	77.28	77.18	77.15	0.15
108	80.91	81.87	82.92	81.90	1.01
119	77.31	85.35	86.10	82.92	4.87
131.5	85.10	86.41	85.29	85.60	0.71

B.2 Supplementary figures

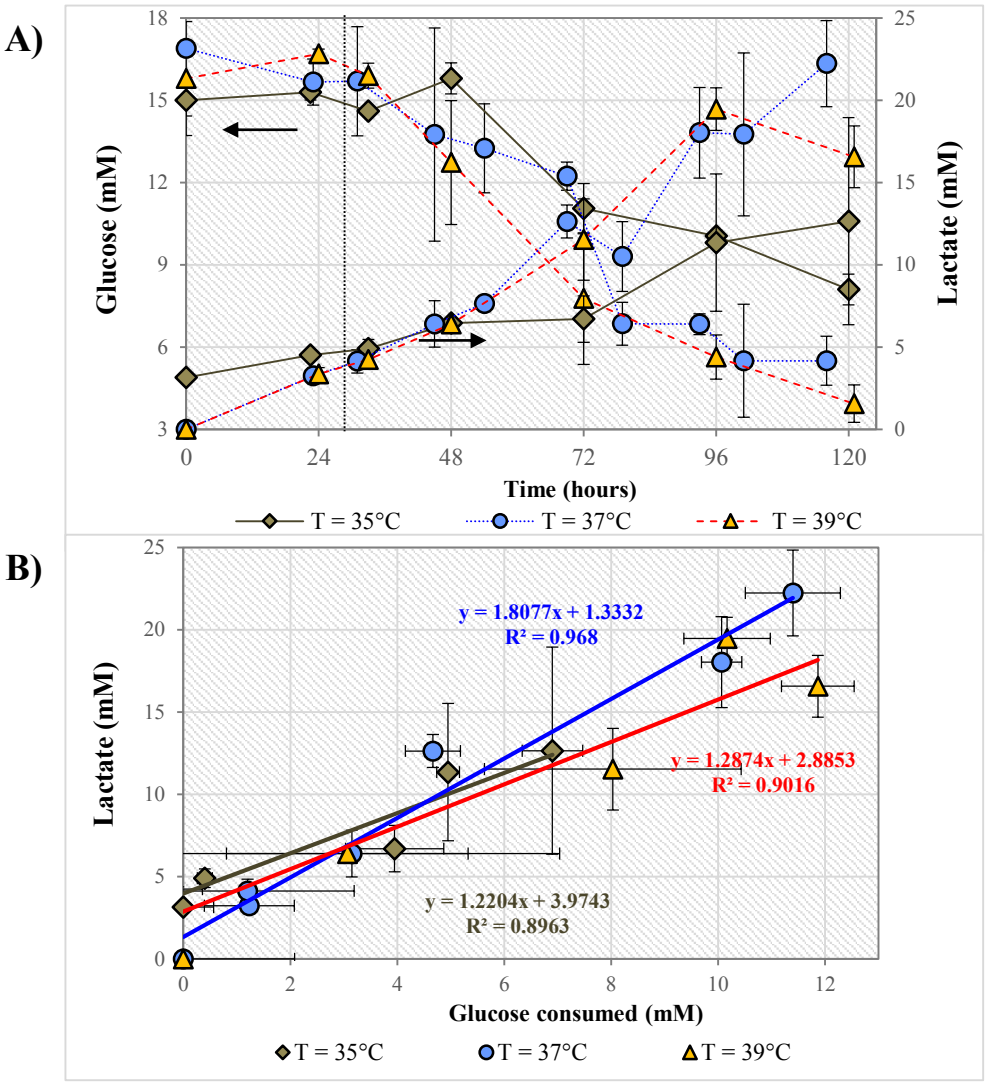


Figure B.2.1 Lactate and glucose metabolism in the temperature shift experiment: A) lactate and glucose concentration profiles; and B) lactate yields over glucose. The vertical dot line represents the temperature shifts, the arrows indicate the corresponding axes to the data (n=3, error bar = SD).

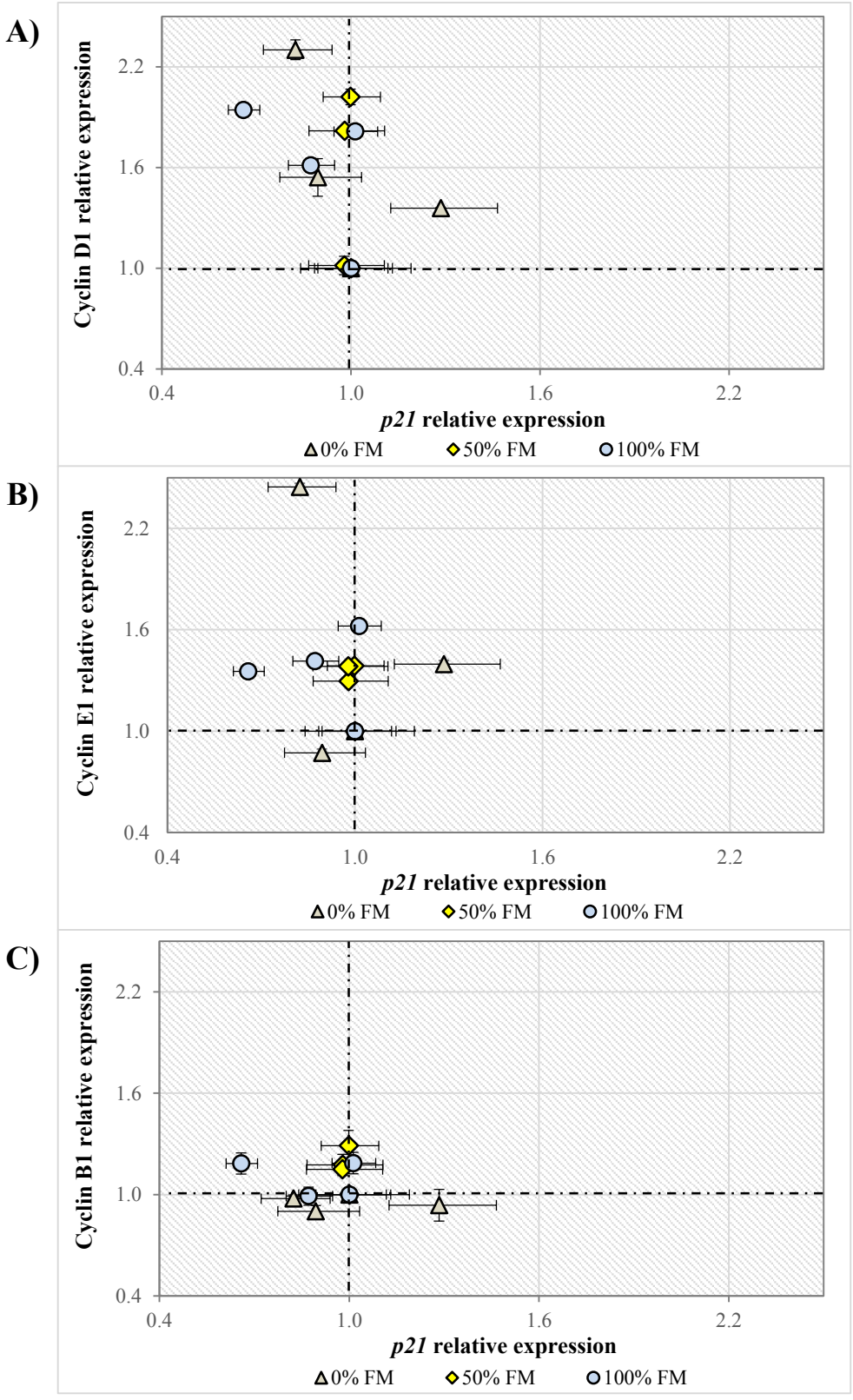


Figure B.2.2 Scatter plots between *p21* and cyclins in the medium shift experiment: A) *p21* and cyclin D1 expressions; B) *p21* and cyclin E1 expressions; and C) *p21* and cyclin B1 expressions. FM is fresh medium and the dash dot lines represent the basal expressions. All relative expressions were normalised to time 0 hour (n=3, error bar = SD).

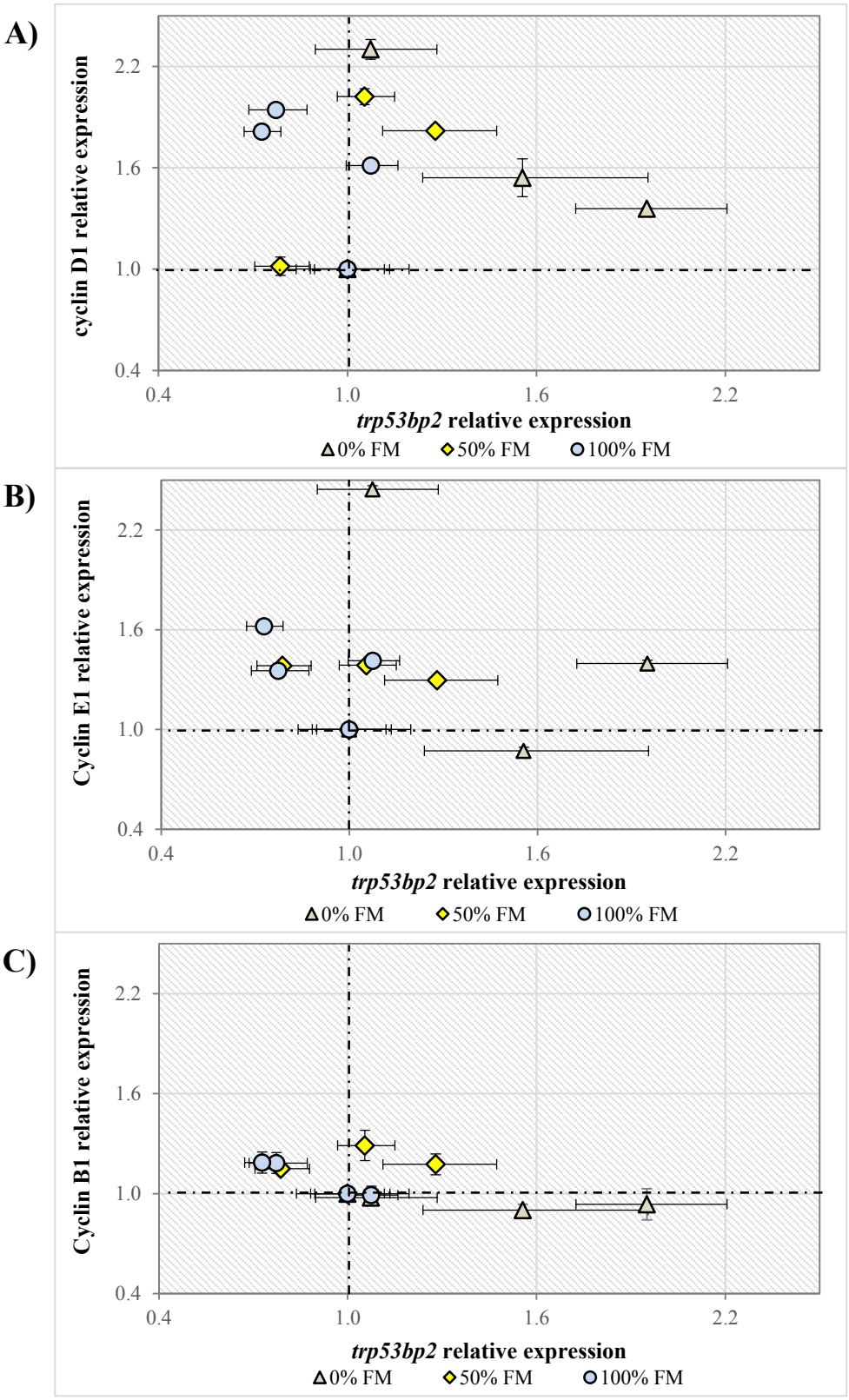


Figure B.2.3 Scatter plots between *trp53bp2* and cyclins in the medium shift experiment: A) *trp53bp2* and cyclin D1 expressions; B) *trp53bp2* and cyclin E1 expressions; and C) *trp53bp2* and cyclin B1 expressions. FM is fresh medium and the dash dot lines represent the basal expressions. All relative expressions were normalised to time 0 hour (n=3, error bar = SD).

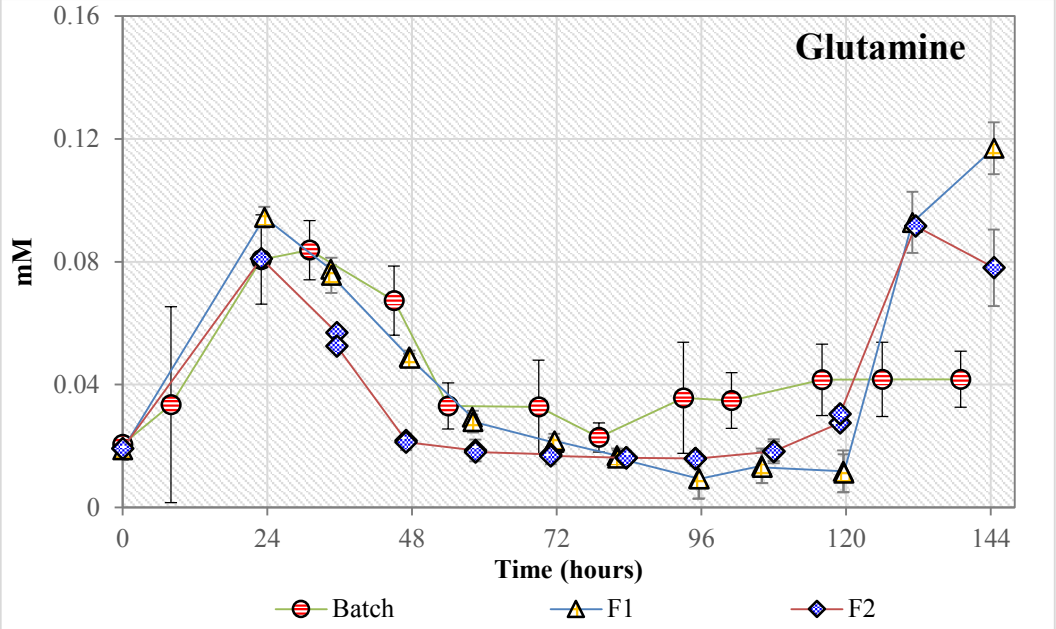


Figure B.2.4 The concentration profiles of glutamine in the batch & fed-batch cultures. F1 and F2 represent the feeding strategies as described in section 6.2.3. (n=3, error bar = SD).

B.3 The statistical analysis results

Table B.3.1 *p*-values from the statistical analysis in Figure 6.3.6.

Figure		*p*-values
6.3.6-A	*[1]	0.047
	*[2]	<0.001
	*[3]	0.003
	*[4]	0.023
6.3.6-B	*[1]	0.014
	*[2]	0.005
	*[3]	-
	*[4]	0.001
6.3.6-C		0.440(0%) 0.993(50%) 0.226(100%)
6.3.6-D	*[1]	0.013
	*[2]	0.05
	*[3]	0.023
	*[4]	0.009

Figure		*p*-values
6.3.6-E	*[1]	0.031
	*[2]	0.001
	*[3]	0.007
	*[4]	0.001
6.3.6-F	*[1]	0.018
	*[2]	0.003
	*[3]	<0.001
	*[4]	<0.001

Table B.3.2 *p*-values from the statistical analysis in Figure 6.3.11.

Figure		*p*-values
6.3.11-A	*[1]	<0.001
	*[2]	0.001
	*[3]	<0.001
	*[4]	<0.001
6.3.11-B	*[1]	0.025
	*[2]	0.01
	*[3]	0.011
	*[4]	<0.001
	*[5]	0.023
6.3.11-C	*[1]	<0.001
	*[2]	<0.001
	*[3]	<0.001
6.3.11-D	*[1]	<0.001
	*[2]	0.004
	*[3]	<0.001

Figure		*p*-values
6.3.11-E	*[1]	0.007
	*[2]	0.028
	*[3]	0.018
	*[4]	0.004
	*[5]	0.022
	*[6]	<0.001
6.3.11-F	*[1]	0.034
	*[2]	0.003
	*[3]	<0.001
	*[4]	<0.001
	*[5]	0.03
	*[6]	<0.001
6.3.11-G	*[1]	<0.001
	*[2]	<0.001
	*[3]	0.018
	*[4]	<0.001

B.4 The optimal set of parameter values

Table B.4.1 An optimal values of model parameters determined using the quasi-Monte Carlo algorithm with the minimisation of the total percentage error.

	No	Parameters (unit)	Old values	Optimised values
Cell growth sub-model	1	$\mu_{max,\ glc}$ (hr^{-1})	2.80E-02	4.77E-02
	2	K_{glc} (mM)	3.90E+01	2.25E+01
	3	$\mu_{max,\ glu}$ (hr^{-1})	1.70E-02	1.85E-02
	4	K_{glu} (mM)	1.00E-01	1.61E-01
	5	$\mu_{max,\ ad}$ (hr^{-1})	3.83E-02	4.26E-02
	6	K_{casp3} (mM)	1.01E+00	1.86E+00
	7	$\mu_{max,\ nd}$ (hr^{-1})	1.13E-02	2.31E-02
	8	K_{lac} (mM)	1.03E+02	1.48E+02
	9	$\mu_{max,\ d}$ (hr^{-1})	1.57E+01	3.14E+01
	10	k_d (hr^{-1})	6.26E-05	1.31E-04
Metabolism sub-model	11	$Y_{x,\ glc}$ (cells/mmol)	4.00E+05	5.47E+05
	12	m_{glc} ($mmol.cells^{-1}.hr^{-1}$)	5.14E-07	8.01E-07
	13	$Km_{glc,\ asp}$(mM)	1.00E-02	1.64E-02
	14	$Y_{lac,\ glc}$ (mmol/mmol)	2.50E+00	4.50E+00
	15	$k_{lac,\ con}$ ($mmol.cells^{-1}.hr^{-1}$)	1.50E-07	1.77E-07
	16	$Km_{lac,\ asp}$(mM)	1.00E-02	2.15E-02
	17	$Y_{x,\ glu}$ (cells/mmol)	6.05E+06	8.58E+06
	18	m_{glu}($mmol.cells^{-1}.hr^{-1}$)	8.87E-09	1.32E-08
	19	$Km_{glu,\ glu}$(mM)	1.00E-01	2.11E-01
	20	$f_{glu,\ ala}$ (mmol/mmol)	5.00E-01	7.36E-01
	21	$f_{glu,\ gln}$ (mmol/mmol)	5.00E-01	8.91E-01
	22	$f_{glu,\ asp}$ (mmol/mmol)	5.00E-01	1.00E+00
	23	$f_{glu,\ arg}$ (mmol/mmol)	5.00E-01	7.69E-01
	24	$Y_{x,\ asp}$ (cells/mmol)	1.40E+06	2.60E+06
	25	m_{asp}($mmol.cells^{-1}.hr^{-1}$)	8.00E-10	1.64E-09
	26	$Km_{asp,\ asp}$ (mM)	2.00E-02	2.23E-02
	27	$f_{asp,\ asn}$ (mmol/mmol)	5.00E-01	9.21E-01
	28	$Y_{x,\ asn}$ (cells/mmol)	1.50E+06	2.20E+06
	29	m_{asn}($mmol.cells^{-1}.hr^{-1}$)	1.00E-09	1.36E-09
	30	$Km_{asn,\ asp}$ (mM)	9.00E-02	1.21E-01
	31	$Y_{x,\ arg}$ (cells/mmol)	2.50E+06	2.89E+06
	32	m_{arg}($mmol.cells^{-1}.hr^{-1}$)	1.00E-09	1.49E-09
	33	$Km_{arg,\ arg}$(mM)	5.00E-02	8.30E-02
	34	$Y_{x,\ ala}$ (cells/mmol)	3.00E+06	6.43E+06
	35	m_{ala}($mmol.cells^{-1}.hr^{-1}$)	3.50E-09	6.50E-09
	36	$Km_{ala,\ glu}$ (mM)	9.00E-02	1.46E-01
	37	$Y_{ala,\ glu}$ (mmol/mmol)	1.60E+00	2.10E+00
	38	$Y_{x,\ gln}$ (cells/mmol)	7.00E+05	1.45E+06
	39	m_{gln}($mmol.cells^{-1}.hr^{-1}$)	2.00E-09	4.06E-09

	40	$Km_{gln,\ gln}$(mM)	7.00E-02	1.19E-01
	41	$Y_{gln,\ glu}$ (mmol/mmol)	2.50E+00	4.17E+00
	42	$Y_{x,\ leu}$ (cells/mmol)	2.00E+06	2.21E+06
	43	m_{leu}(mmol.cells^{-1}.hr^{-1})	1.00E-09	1.55E-09
	44	$Km_{leu,\ leu}$(mM)	5.00E-02	7.49E-02
	45	α_{ab} (mg cells^{-1} hr^{-1})	3.96E-07	4.20E-07
	46	$Km_{mab,\ aa}$ (mM)	1.00E-01	1.87E-01
Apoptosis sub-model	47	β_{iC3} (mmol.hr^{-1})	9.08E-03	1.67E-02
	48	Kb_{iC3} (-)	2.00E-03	3.86E-03
	49	k_{C3} (L.mmol^{-1}.hr^{-1})	3.58E+00	4.30E+00
	50	β_{iC8} (mmol.hr^{-1})	1.02E-03	1.53E-03
	51	Kb_{iC8} (-)	1.45E-01	2.28E-01
	52	k_{C8} (L.mmol^{-1}.hr^{-1})	1.12E-02	1.22E-02
	53	β_{ibax} (mmol.hr^{-1})	2.97E-03	3.82E-03
	54	$k_{_bax}$ (L.mmol^{-1}.hr^{-1})	2.96E+00	5.55E+00
	55	k_{bax} (L^{3}.mmol^{-3}.hr^{-1})	1.82E+00	2.89E+00
	56	Kb_{ibax} (-)	8.47E-01	1.26E+00
	57	β_{bcl2} (mmol.hr^{-1})	2.38E-04	4.98E-04
	58	Kb_{bcl2} (-)	1.30E+01	2.18E+01
	59	$\beta_{mRNA_{casp3}}$ (hr^{-1})	6.36E-02	8.54E-02
	60	$Km_{casp3,\ iC3}$ (mM)	1.41E-01	2.37E-01
	61	$\alpha_{mRNA_{casp3}}$ (hr^{-1})	1.25E-02	2.23E-02
	62	$\beta_{mRNA_{bax}}$ (hr^{-1})	1.11E-01	1.39E-01
	63	$Km_{trp53bp2,\ bax}$ (-)	6.27E-01	8.95E-01
	64	$Km_{bcl\text{-}2,\ bax}$ (-)	7.00E-01	9.15E-01
	65	$\alpha_{mRNA_{bax}}$ (hr^{-1})	1.81E-02	3.82E-02
	66	$\beta_{mRNA_{bcl2}}$ (hr^{-1})	6.83E-01	1.31E+00
	67	$Km_{trp53bp2,\ bcl\text{-}2}$ (-)	2.10E+00	2.65E+00
	68	$Km_{atf5,\ bcl\text{-}2}$ (-)	6.98E+00	9.78E+00
	69	$\alpha_{mRNA_{bcl2}}$ (hr^{-1})	1.97E-01	4.14E-01
	70	$\beta_{mRNA_{trp53bp2}}$ (hr^{-1})	4.68E-02	8.49E-02
	71	$Km_{lac,\ trp53bp2}$ (mM)	1.73E+00	2.93E+00
	72	$Km_{glu,\ trp53bp2}$ (mM)	1.00E-01	1.48E-01
	73	$\alpha_{mRNA_{trp53bp2}}$ (hr^{-1})	2.01E-02	2.55E-02
	74	$\beta_{mRNA_{atf5}}$ (hr^{-1})	3.82E-01	4.15E-01
	75	$Km_{asp,\ atf5}$ (mM)	2.29E-02	2.50E-02
	76	$Km_{ab,\ atf5}$ (mg/L)	2.77E+01	5.26E+01
	77	$\alpha_{mRNA_{atf5}}$ (hr^{-1})	5.42E-02	9.43E-02
	78	$\beta_{mRNA_{casp8}}$ (hr^{-1})	9.46E-02	1.18E-01
	79	$Km_{glu,\ casp8}$ (mM)	1.21E-01	1.90E-01
	80	$\alpha_{mRNA_{casp8}}$ (hr^{-1})	5.13E-02	8.20E-02